

**Novel methods for scoping water  
harvesting sites using remote sensing  
products and geospatial tools.**

**Robert Geoffrey Delaney**

This thesis is submitted in partial fulfilment of the requirement for the award of the  
degree of

**Doctor of Philosophy**



May 2025

IN MEMORY OF PROFESSOR G. ALAN BLACKBURN

*“Small showers last long, but sudden storms are short;”*

WILLIAM SHAKESPEARE

John of Gaunt: Richard II, Act 2, Scene 1

# Abstract

Water harvesting, the collection of precipitation runoff for productive purposes, offers a wide range of benefits depending on the techniques employed. It can supplement domestic water supply, recharge groundwater, enhance plant production, and mitigate erosion, among other advantages. As a result of advances in the nature and availability of remote sensing data sets, there has been significant recent growth in novel methods and tools for identifying optimal locations for specific water harvesting technologies. The work reported in this thesis makes original contributions to this ongoing growth. The substantive contributions are threefold: the ‘SiteFinder’ tool, ‘HRRTLE’ model, and a Port Sudan case study.

The SiteFinder tool addresses the issue of site selection for water harvesting dams via analysis of topography. Existing approaches to site selection often emphasise slope as the primary criterion. However, such approaches tend to overlook the broader topographical context of a site, which limits their effectiveness in identifying suitable locations. SiteFinder tackles this by utilising Digital Elevation Models (DEMs) to automatically assess thousands of sites, computing parameters characterising potential dams, their catchments and impoundment reservoirs. Innovatively, SiteFinder works within a GIS environment. Thus, it allows the possibility of combining its outputs with wider multi-criteria decision-making processes.

The HRRTLE (High Resolution Runoff and Transmission Loss Estimator) model is concerned with hydrological (rainfall-runoff) aspects of water harvesting prediction and site selection. Quantifying the volume of catchment runoff reaching a potential water harvesting site is crucial for assessing whether the site may face water shortages or risk its storage capacity being exceeded. Existing approaches to predicting runoff at potential sites often use curve numbers to generate runoff maps. However, they do

not account for transmission losses that occur as runoff travels to a potential harvesting site across its catchment. These losses can be significant in arid and semi-arid regions where water harvesting is most common. HRRTLE addresses this issue, adding transmission loss estimates to curve number-based runoff models.

The Port Sudan case study demonstrates how SiteFinder and HRRTLE can be used in combination to identify potential water harvesting sites across an area of interest. Moreover, it also introduces a novel method for optimising against the impact of sedimentation rates on storage loss in potential dam-impounded reservoirs for selected schemes.

Overall, the novel tools and methodologies whose development and testing is reported in this thesis provide potential to streamline the process of water harvesting site identification, reducing the need for, and cost of, extensive ground-based work. They address topographic, hydrological and sedimentological aspects of water harvesting site selection, and provide a more comprehensive and detailed evaluation of potential water harvesting sites than existing approaches. As such, they represent novel contributions to the science of arid zone runoff prediction, and have the potential to support improved decision-making, leading to better outcomes and more efficient allocation of resources, specifically at the scoping stage of water harvesting projects.

# Contents

<b>Abstract.....</b>	<b>i</b>
<b>Contents .....</b>	<b>iii</b>
<b>List of tables.....</b>	<b>vi</b>
<b>List of figures.....</b>	<b>x</b>
<b>List of abbreviations and acronyms .....</b>	<b>xiv</b>
<b>Acknowledgements .....</b>	<b>xvii</b>
<b>Declaration.....</b>	<b>xviii</b>
<b>Statement of authorship for multi-authored chapters .....</b>	<b>xix</b>
<b>1 Introduction.....</b>	<b>1</b>
1.1 Thesis aim and objectives	1
1.2 Thesis structure	3
<b>2 An overview of water harvesting .....</b>	<b>6</b>
2.1 Definitions of water harvesting	6
2.2 Sustainability and benefits	7
2.3 Water harvesting classification	14
2.4 Technologies	16
2.5 History of water harvesting	20
2.6 Stakeholders	21
2.7 Mechanisms of Runoff and Associated Processes	23
2.8 Siting – biophysical parameters	25
2.9 Summary	33
<b>3 A literature review of remote sensing products used in water harvesting studies.....</b>	<b>35</b>
3.1 Introduction	35
3.2 Materials and methods	38

3.3 Results	40
3.4 Discussion and evidence-based recommendations	54
3.5 Summary and conclusions	70
<b>4 SiteFinder: A geospatial scoping tool to assist the siting of external water harvesting structures .....</b>	<b>74</b>
4.1 Abstract	74
4.2 Introduction	75
4.3 Materials and methods	80
4.4 Results	92
4.5 Discussion	99
4.6 Conclusions	105
<b>5 HRRTLE (High Resolution Runoff and Transmission Loss Estimator): a novel tool for mapping connectivity of runoff in ephemeral stream networks to aid the siting of water harvesting structures.....</b>	<b>106</b>
5.1 Abstract	106
5.2 Introduction	107
5.3 Materials and methods	113
5.4 Results	127
5.5 Discussion	134
5.6 Conclusion	144
<b>6 Utilising remote sensing products to scope dam locations factoring topographical characteristics, annual runoff, and storage loss due to sedimentation — Port Sudan case study .....</b>	<b>146</b>
6.1 Abstract	146
6.2 Introduction	147
6.3 Materials and methods	152
6.4 Results	171
6.5 Discussion	180

6.6 Conclusions	188
<b>7 Synopsis and recommendations</b> .....	<b>190</b>
7.1 Synopsis	190
7.2 Future research recommendations	199
<b>References</b> .....	<b>206</b>
<b>Appendix A. Supplementary material for Chapter 3</b> .....	<b>271</b>
<b>Appendix B. Supplementary material for Chapter 4</b> .....	<b>275</b>
<b>Appendix C. Supplementary material for Chapter 5</b> .....	<b>279</b>
<b>Appendix D. Supplementary material for Chapter 6</b> .....	<b>283</b>

# List of tables

Table 2.1. Various definitions of water harvesting.....	6
Table 2.2. A variety of water harvesting technologies and their associated benefits. ....	9
Table 2.3 Summary of how different water harvesting technologies support development goals. ...	11
Table 2.4. Details of historic dams, including location, construction timeline, dam height, and dam length (Bretas et al., 2012).....	21
Table 2.5. Water harvesting technologies and the biophysical criteria used in site selection. ....	26
Table 3.1. Search commands used with bibliographic databases (search undertaken in January 2024). ....	38
Table 3.2. Journal titles publishing five or more articles from the review literature.....	43
Table 3.3. Remote sensing products used in more than five different studies from the review literature. ....	45
Table 3.4. Most frequency utilised remote sensing products used in the review literature studies, classified into five groups of elevation, climatic, multi-spectral, RGB and composite [# indicates number of studies]. ....	45
Table 3.5. The bands of Landsat satellites and descriptions of use (U.S. Geological Survey, 2015) [OLI, Operational Land Imager; TIRS, Thermal Infrared Sensor; ETM+, Enhanced Thematic Mapper Plus; TM, Thematic Mapper; MSS, Multispectral Scanner; --, not applicable].....	50
Table 3.6. List of factors relating to DEM selection.....	56
Table 3.7. Summary of open access land cover data features based on product information (from Gutierrez Caloir et al., 2023) .....	63

Table 4.1. Analysis of results from all case study scenarios comparing barrier length (L), polygon area (A), and storage volume (V) using Shuttle Radar Topography Mission (SRTM) elevation data against high-resolution Airborne Research and Survey Facility LiDAR data. ....	93
Table 4.2. Case study Scenario 1: desired parameters, search parameters, tool output parameters, filter limits and parameter range of filtered barriers. ....	94
Table 4.3. Case study Scenario 2: desired parameters, search parameters, tool output parameters, filter limits and parameter range of filtered barriers. ....	97
Table 4.4. Case study Scenario 3: desired parameters, search parameters, tool output parameters, filter limits and parameter range of filtered barriers. ....	99
Table 5.1. Selection of antecedent moisture condition (AMC) using antecedent precipitation (PΣ5) and season. ....	118
Table 5.2. Values of the Nash-Sutcliffe efficiency (NSE) and percentage of average tendency (Pbias) for calibration (cal) and validation (val) runs of the runoff-only (ro) and runoff-and-transferral-ratio (tr) versions of the model, for each of the 28 test catchments. The first two letters of the catchment code indicate country: Australia (AU), Brazil (BR), Israel (IR), USA (US) or South Africa (ZA). ....	129
Table 5.3. Number (out of 28) catchments which show satisfactory values ( $NSE > 0$ ; $-50 \% < Pbias < 50 \%$ ) for the NSE and Pbias performance metrics at the calibration (cal) and validation (val) stage of model development. ....	130
Table 5.4. Catchments with $NSE > 0$ and absolute Pbias values $< 50 \%$ for validation models with transferral ratio effects incorporated, with the predominant land cover characteristics. ....	131
Table 5.5. Proportion of catchments of different dominant landcover type for which the model performed satisfactorily in the validation stage with transferral ratios incorporated. ....	131
Table 6.1. Details of datasets. ....	156

Table 6.2. Number of raster cells within the AOI assigned each stream order (Strahler method), derived from elevation data with a spatial resolution of 90 m × 90 m. ....	158
Table 6.3. The fundamental scale (Saaty, 1987).....	160
Table 6.4. Final pairwise comparison matrix used to compute weights for five main criteria [BH, barrier height (m); BV, barrier volume (m <sup>3</sup> ); AI, area of influence (m <sup>2</sup> ); SV, storage volume (m <sup>3</sup> ); SBVR, storage volume to barrier volume ratio (-)]......	161
Table 6.5. Criterion weights and sub-criterion weights used to calculate local topographic characteristics (LTC) scores [“max” sub-script refers to the maximum corresponding criterion value outputted from all SiteFinder runs]. ....	163
Table 6.6. Summary of SiteFinder results. [BV, barrier volume; AI, area of influence; SV, storage volume; SBVR, storage volume to barrier volume ratio; LTC, local topographic characteristic]. ....	172
Table 6.7. SiteFinder results showing the scheme with the maximum LTCscore and the four schemes with the minimum LTCscore, together with respective metrics [SBVR, storage volume to barrier volume ratio; LTC, local topographic characteristic]. ....	172
Table 6.8. All schemes outputted by SiteFinder with a storage volume greater than the Khor Arbaat main dam immediately after construction and before storage loss to sedimentation (i.e. 16 million cubic metres), along with their corresponding local topographic characteristics score (LTCscore) and stream order. ....	174
Table 6.9. Results showing breakdown of schemes based on annual runoff (2-yr return period) to storage volume ratio. Schemes removed due to under-filling ratio (column “<1”), schemes removed due to over-filling ratio (column “>10”), & schemes passing the filter (column “1–10”). Schemes grouped by local topographic characteristics score (LTC <sub>score</sub> ). ....	176
Table 6.10. Number of potential schemes grouped by local topographic characteristic score (LTCscore). Columns “a” refers to all schemes found using SiteFinder while columns “b” excludes schemes with a predicted annual runoff (50 % probability) to storage volume ratio	

below parity and greater than 10. Columns “c” excludes schemes with sedimentation loss greater or equal to 2 %. Results segregated by stream order. .... 178

# List of figures

Figure 2.1. Ball and cup conceptualisation in sub-Saharan Africa farming livelihood system illustrating the existence of several stable states, with the ball representing the farming system, and the resilience of each state being defined by the depth of the cup. The bold line represents a situation without water harvesting, while the light line represents a situation with water harvesting. The resilience of each state is represented by the depth of each cup, meaning the greater the depth, the harder it is for the ball (representing, for example, a farmer) to move from one state to another. (Dile et al., 2013). .....	13
Figure 2.2. Water harvesting groups, types of catchments and examples of technologies (adapted from Mekdaschi-Studer and Liniger, 2013). .....	16
Figure 2.3. Examples of water harvesting technologies from WOCAT database — (a): floodwater harvesting - diversion canal [© D. Danano]; (b): rooftop harvesting [© A. Amon]; (c): microcatchment water harvesting - Vallerani system [© A. Boureima]; (d): macrocatchment water harvesting - small earth dam [© M. Malesu]. .....	17
Figure 2.4. Illustration from the Keyline Plan showing ridge cultivation. Slightly off contour ploughing is shown in green (Yeomans, 2008, permission granted by Ken Yeomans). .....	18
Figure 2.5. Sub-Saharan water balance (from Rockström and Falkenmark, 2015).....	24
Figure 2.6. Biophysical criteria used in water harvesting site selection. ....	27
Figure 2.7. Drylands of the world based on Global Aridity Index (Zomer and Trabucco, 2022), with drylands defined by encompassing ‘arid’, ‘semi-arid’, and ‘dry sub-humid’ climate classifications. ....	29
Figure 3.1. Diagram illustrating the progression of refining the literature review and the count of references associated with different stages in the process. ....	39
Figure 3.2. A word cloud generated using ‘Keywords’ from the review literature articles. ....	41

Figure 3.3. Chart showing the annual publication count for review literature and the count of those that used remote sensing. ....	42
Figure 3.4. Flow chart showing sources of data to create thematic layers prior to fusion (from Abdekareem et al., 2022) [GWPZs, groundwater prospective zones].....	68
Figure 3.5. Examples of remote sensing product utilisation, with name of product and group classification. ....	72
Figure 4.1. Overview explaining how a DEM is used to obtain script outputs of polygons and volumes.....	82
Figure 4.2. Schematic showing the principal components of barrier creation.....	84
Figure 4.3. Validation of the geometrical process: (a) country map with inset of basin extent, (b) Shuttle Radar Topography Mission (SRTM) 3 arc-second elevation of basin, (c) script outputs of barrier at 854 m based on SRTM DSM input, (d) barrier and polygon created manually using differential Global Positioning System (dGPS) ground survey. ....	88
Figure 4.4. Ethiopia: area of interest (AOI) showing Shuttle Radar Topography Mission (SRTM) elevation data with country level map (inset). ....	90
Figure 4.5. Scenario 1 (Large Dam) results using Shuttle Radar Topography Mission (SRTM) elevation data. ....	94
Figure 4.6. (a) Scenario 2 (Gully Check Dam) results using Shuttle Radar Topography Mission (SRTM) elevation data with inset box, (b) inset of two filtered barriers with their respective area of influence and catchment area.....	96
Figure 4.7. Scenario 3 (Earth Embankment) results using Shuttle Radar Topography Mission (SRTM) elevation data.....	98
Figure 5.1. Schematic of the main stages of the HRRTLE process [CN = Curve Number; TR = Transferral Ratio].....	115

Figure 5.2. Map showing locations of runoff gauging stations used. Each station represents the outlet of a modelled catchment. Basemap of Global Aridity Index (Zomer and Trabucco, 2022). ..... 116

Figure 5.3. (a) location of AUNP catchment; (b) runoff connectivity map (RCM) for the catchment of a gauging station located on the Shaw River, showing mean annual runoff reaching catchment outlet taking transmission losses into account, created using validation data..... 128

Figure 5.4. Sensitivity of Nash-Sutcliffe efficiency (NSE) to variation in transmission loss parameters (catchment code AULT) for calibration data. .... 130

Figure 5.5. Range of values of seven biophysical catchment parameters for 9 catchments with NSE > 0 and absolute Pbias < 50 %, in the context of the full range of values for all 28 catchments for each parameter. Size: catchment area; CFF: catchment form factor; HAND: height above nearest drainage; Rainfall: mean annual rainfall; Aridity: mean aridity index; Baseflow: % of runoff from baseflow; Efficiency: runoff efficiency ..... 133

Figure 6.1. Map of area of interest (AOI) showing significant watercourses together with locations of Khor Arbaat main dam and Moj dam. Study area = 7,385 km<sup>2</sup>. ..... 153

Figure 6.2. Image of Moj dam reservoir. Stone-armoured upstream dam batter wall can be observed in the bottom-right. The presence of vegetation in the reservoir is attributed to sedimentation [Photographed by Mohammed M. Salih in 2024]. ..... 155

Figure 6.3. Schematic of input datasets and processing chain [AOI, area of interest; AHP, Analytical Hierarchy Process; LTC, local topographic characteristics]. ..... 157

Figure 6.4. SiteFinder results: (a) scheme with the highest LTCscore (0.3609) and one of four schemes with the lowest LTCscore (0.0574), (b) higher resolution details of low LTCscore scheme, (c) higher resolution details of highest LTCscore scheme [LTC, local topographic characteristic]..... 173

Figure 6.5. Results, (a) LTCscore, (b) filtered by ‘filling’, (c) filtered by storage loss due to sedimentation, (d) highest LTC<sub>score</sub> schemes from final filter stage, segregated by storage volume. .... 177

Figure 6.6. (a) Location of the scheme with the largest storage volume among the 55 favoured schemes found within the area of interest (AOI), and (b) HRRTLE model connectivity map showing the mean annual runoff reaching the scheme. .... 179

# List of abbreviations and acronyms

AHP	analytical hierarchy process
AOI	area of interest
BH	barrier height
BV	barrier volume
CGIAR	Consultative Group on International Agricultural Research
CI	consistency index
DEM	digital elevation model
dGPS	differential Global Positioning System
DSM	digital surface model
DTM	digital terrain model
FAO	Food and Agriculture Organization of the United Nations
GIS	geographic information system
GPCC	Global Precipitation Climatology Centre
GPS	Global Positioning System
HEC-HMS	Hydrologic Modeling System
HM	hydrological modelling
HRRTLE	high resolution runoff and transmission loss estimator
ICARDA	International Center for Agricultural Research in the Dry Areas
ICOLD	International Commission on Large Dams
InSAR	interferometric synthetic aperture radar
IWMI	International Water Management Institute

LiDAR	light detection and ranging
LTC	local topographic characteristics
LULC	land use / land cover
MCA	multi-criteria analysis
MFD	multi-flow-direction
NASA	National Aeronautics and Space Administration
NDVI	normalised difference vegetation index
NDWI	normalised difference water index
NGO	non-governmental organisation
NSE	Nash-Sutcliffe efficiency
Pbias	percentage bias
RAF	runoff attenuation feature
RL	review literature
RMSE	root mean square error
RS	remote sensing
SBVR	storage volume to barrier volume ratio
SLM	sustainable land management
SOC	soil organic carbon
SPOT	Satellite pour l'Observation de la Terre
SRTM	Shuttle Radar Topography Mission
SWAT	Soil and Water Assessment Tool
SWIR	short wave infrared
TIN	triangulated irregular network

TPI	topographic position index
TRMM	Tropical Rainfall Measurement Mission
TWI	topographic wetness index
UAV	unmanned aerial vehicle
UNEP	United Nations Environment Programme
USDA	U.S. Department of Agriculture
USGS	U.S. Geological Survey
WH	water harvesting
WMO	World Metrological Organization
WOCAT	World Overview of Conservation Approaches and Technologies

# Acknowledgements

I am deeply grateful for the support, guidance, and patience of my supervisors, Andrew Folkard, Duncan Whyatt, and the late Alan Blackburn. It has been a privilege to benefit from their expertise and knowledge, and I owe them a significant debt of gratitude. In particular, I would like to thank Andrew Folkard for encouraging me to enrol as a research candidate at the initial stage of this programme.

I would like to express my gratitude to Dr. Jamila Bargach and her colleagues at Dar Si Hmad Foundation (Morocco) for facilitating a field trip to Agadir, which enabled me to conduct a topographic survey and visit a fog-harvesting installation.

I wish to thank Hatim Ahmed for his invaluable assistance in establishing contacts in Sudan for water harvesting initiatives and coordinating in-country activities.

I am also thankful to Prof. Siddig Eissa Ahmed from the UNESCO Chair in Water Resources at Omdurman Islamic University, Sudan, for facilitating a study on highway flooding in Sudan and providing me with the opportunity to train students in water harvesting, GIS, and remote sensing.

Finally, I would like to express my gratitude to my family and friends for their unwavering support over the past years, with a special thank you to Lama Ranjous.

# Declaration

I declare that, other than where the contribution of others is specified, this thesis is entirely my own work and has not been submitted for the award of any other degree, either at Lancaster University or elsewhere.

Robert Geoffrey Delaney

# Statement of authorship for multi-authored chapters

**Chapter 4: SiteFinder: A geospatial scoping tool to assist the siting of external water harvesting structures**

**Delaney, R. G., Blackburn, G. A., Whyatt, J. D., and Folkard, A. M.: SiteFinder: A geospatial scoping tool to assist the siting of external water harvesting structures, *Agric. Water Manag.*, 272, 107836, <https://doi.org/10.1016/j.agwat.2022.107836>, 2022. Published.**

I was responsible for the conceptualisation, developing the methodology, data curation, preparation of visualisation effects (e.g. figures), software coding, results validation (part), and writing the original draft.

Supervision, writing (review and editing), validation (part) was provided by GAB, AMF, and JDW. AMF was responsible for project administration.

**Chapter 5: HRRTLE (High Resolution Runoff and Transmission Loss Estimator): a novel tool for mapping connectivity of runoff in ephemeral stream networks to aid the siting of water harvesting structures**

**Delaney, R. G., Blackburn, G. A., Folkard, A. M., and Whyatt, J. D.: HRRTLE (High Resolution Runoff and Transmission Loss Estimator): a novel tool for mapping connectivity of runoff in ephemeral stream networks to aid the siting of water harvesting structures, *Hydrol. Earth Syst.***

**Sci. Discuss. [preprint], <https://doi.org/https://doi.org/10.5194/hess-2024-97>, 2024. Preprint published and is under review.**

I was responsible for the conceptualisation, developing the methodology, data curation, preparation of visualisation effects (e.g. figures), software coding, results validation, and writing the original draft.

Supervision, writing (review and editing), validation (part) was provided by AMF, and JDW. AMF was responsible for project administration. GAB provided supervision in the initial stages of the manuscript development.

**Chapter 6: Utilising remote sensing products to scope dam locations factoring topographical characteristics, annual runoff, and storage loss due to sedimentation — Port Sudan case study**

**Delaney, R. G., Ahmed, H., Folkard, A. M., Salih, M. M., and Whyatt, J. D.: Scoping potential dams: Utilising remote sensing products to analyse topographic characteristics, runoff-to-storage ratio, and sedimentation — a Port Sudan case study. Submitted to the Sustainable Water Resources Management journal and is under review.**

I was responsible for the conceptualisation, developing the methodology, data curation, preparation of visualisation effects, software development and use, data curation, results validation, and writing the original draft.

HA and MMS were responsible for project administration in Sudan, provision of Sudan-related resources, and contributions to the methodology.

Supervision, writing (review and editing) and validation was provided by AMF, and JDW. AMF was responsible for UK-related project administration.

I confirm that the above information on the authorship of these chapters and the contribution of Robert G. Delaney is accurate.

Name: Robert G. Delaney

Signature:

**Co-authors:**

Name: Andrew M. Folkard

Signature:

Name: J. Duncan Whyatt

Signature:

Name: Hatim Ahmed

Signature:

Name: Mohammed M. Salih

Signature:

# 1 Introduction

## 1.1 Thesis aim and objectives

The overarching aim of this thesis is to develop, test, and assess novel methods for extracting hydro-morphological information from remote sensing products, with the goal of supporting more effective site selection for large-scale water harvesting technologies. Before the advent of remote sensing, scoping studies largely depended on field visits to evaluate the suitability of locations for deploying specific types of water harvesting technology. However, conducting field surveys can be costly and challenging, depending on the context, which limits the number of locations that can be assessed. Field surveys also present additional concerns. For instance, carrying out a survey at a particular location may raise local stakeholders' expectations that a project will be implemented, even when planners conclude, based on the survey, that the location is technically unsuitable for water harvesting. Additionally, local stakeholders who are eager to see a water harvesting project implemented in a particular location may attempt to influence the planners responsible for conducting field assessments. This can result in more suitable sites being overlooked during the assessment process.

The availability of remote sensing products, combined with the ever-increasing computing power for data analysis, has transformed studies on water harvesting site selection. By utilising remote sensing products, planners can now evaluate multiple locations over large areas and make informed decisions about the suitability of individual sites before conducting field visits. This scoping method allows planners to subsequently examine a more manageable subset of sites in greater detail, using various techniques, including field surveys.

Slope is the most widely used biophysical criterion in water harvesting site selection studies (Adham et al., 2016a). However, since slope is determined based on a small cluster of pixels, it only accounts for a limited portion of the surrounding topography at a given location, which restricts its overall usefulness. Of greater relevance to planners is information related to the actual size of the water harvesting structure and details of the storage zone that would be created as a result of the barrier's construction. This is particularly important for planners working with large-scale water harvesting systems (e.g. embankment dams) rather than in-field water harvesting systems (e.g. contour bunds). Therefore, the first objective of this thesis is to develop and evaluate an automated tool designed to provide more comprehensive and practical information on potential large-scale water harvesting schemes, extending beyond the biophysical criterion of slope.

Runoff is fundamental to water harvesting and is another challenging subject for planners undertaking water harvesting site selection studies in arid and semi-arid environments. Runoff models capable of estimating runoff volumes at various locations, such as potential water harvesting sites, would be valuable. However, researchers tend to rely on runoff maps (e.g. Asmar et al., 2021, Karimi and Zeinivand, 2021, Gavhane et al., 2023) that do not account for transmission losses from the point of runoff generation to a downstream water storage location (which can be considerable). Transmission losses are more relevant to large-scale water harvesting systems than to small-scale ones, as there is often a considerable distance between the points of runoff generation and the actual water storage location. While more sophisticated rainfall-runoff models are available, they are often too cumbersome to apply to numerous large-scale catchment outlets. Therefore, the second objective of this thesis is to improve traditional runoff mapping by accounting for transmission losses, thereby providing more accurate estimates of runoff at catchment outlets, and to quantitatively evaluate model performance.

Sedimentation affects certain water harvesting technologies, posing a significant challenge for water resource planners worldwide, particularly in the context of large-scale reservoirs, as it results in a considerable loss of storage capacity. Schleiss et al. (2016) report that the volume of storage lost due to sedimentation exceeds the storage volume gained from newly constructed facilities. Although a substantial literature on sedimentation and various modelling approaches exists, limited research has been conducted on predicting reservoir sedimentation rates using remote sensing products, especially when analysing multiple potential sites in a single process. The third objective of this thesis is to address the issue of reservoir sedimentation by creating and assessing an automated method for evaluating the susceptibility of potential reservoirs to future storage loss.

The fourth and final objective of this thesis is to devise a site selection methodology that incorporates the tools developed in relation to the previously stated objectives and to test its usability through a case study in a drylands region. The case study should be situated in an area with a demand for enhanced water resources and a need for a study relating to the site selection of large-scale water harvesting technologies (e.g. dams). Furthermore, the methodology should have global applicability.

## **1.2 Thesis structure**

**Chapter 1** outlines the overarching aim and objectives of the thesis, along with its structure.

**Chapter 2** provides an overview of water harvesting, including a brief history of water harvesting and various definitions of the term. This chapter categorises different water harvesting technologies into different groups and examines how these practices contribute to sustainability and development, particularly in the context of the United Nations' Sustainable Development Goals. The chapter also outlines the biophysical criteria used to identify suitable sites for water harvesting.

**Chapter 3** provides a literature review that focuses on identifying the most influential remote sensing products used in water harvesting studies. It offers insights into the processes involved in generating these products, outlines their potential advantages and disadvantages, and highlights emerging trends in their usage. Additionally, it explores best practices for the effective application of these products and provides evidence-based recommendations.

**Chapter 4** introduces a novel automated tool designed to aid in the scoping of potential water harvesting sites. This tool operates within a geographic information system (GIS) environment and uses a digital elevation model (DEM) to generate virtual barriers across riverbeds, simulating the types of structures used in large-scale water harvesting systems, such as embankment dams. It then calculates the characteristics of these barriers and estimates the potential storage capacity that would be available if such large-scale structures were to be constructed in reality.

**Chapter 5** describes a rainfall-runoff model specifically designed for intermittent rivers and ephemeral streams. This parsimonious model utilises three global remote sensing products to compute the annual discharge at a catchment outlet, which could potentially be the site of a large-scale water harvesting structure. Unlike small-scale water harvesting techniques that focus on localised runoff collection, this model is suited to larger catchments, where runoff must travel significant distances before reaching a storage location. The modelling methodology combines an established procedure for calculating runoff using curve numbers with an innovative approach for estimating transmission losses across expansive catchment areas.

**Chapter 6** demonstrates the real-world application of techniques from **Chapters 4** and **5** in Port Sudan. Using satellite-derived terrain data, over 25,000 potential water harvesting sites for reservoirs are identified and evaluated via an automated tool (**Chapter 4**). Sites are then ranked using five

topographic features and a rainfall-runoff model is used to estimate runoff (**Chapter 5**). Further filtering ensured adequate runoff and low sedimentation risk for selected schemes.

**Chapter 7** provides a synopsis of the thesis findings and reflects on the achievements relative to the research objectives outlined in this chapter. It also offers recommendations for future research.

## 2 An overview of water harvesting

### 2.1 Definitions of water harvesting

According to Mekdaschi-Studer and Liniger (2013, p. VII) the principle of water harvesting is to “... capture potentially damaging rainfall runoff and translate this into plant growth or water supply. This makes clear sense where rainfall is limited, uneven or unreliable with pronounced dry spells”. Bossio et al., (2010) states that water harvesting in drylands maximises the use of scarce rainfall by capturing runoff (and sediments) for productive purposes and at the same time reduces unproductive losses of water, reduces runoff and reduces erosion. Various definitions of water harvesting presented by different authors are compiled in **Table 2.1**.

**Table 2.1. Various definitions of water harvesting.**

definition of ‘water harvesting’	reference
“The collection and management of floodwater or rainwater runoff to increase water availability for domestic and agricultural use as well as ecosystem sustenance.”	Mekdaschi-Studer and Liniger, 2013, p. 4
“...maximizes the use of scarce rainfall by capturing runoff (and sediments) for productive purposes.”	Bossio et al., 2010, p. 540
“...the process of concentrating precipitation through runoff and storing it for beneficial use.”	Oweis and Hachum, 2006, p. 67
“...the process of concentrating rainfall as runoff from a larger area for use in a smaller target area.”	Oweis et al., 1999, p. v
“...the collection of runoff for productive purposes.”	Critchley and Siebert, 1991, p. 9

Runoff is central to water harvesting and is included in all five definitions in **Table 2.1**. Runoff is defined as “that part of precipitation, snow or ice melt, or irrigation water which flows across the land to streams or other waterbodies” (Park and Allaby, 2017, p. 395). Runoff occurs naturally and can lead to positive outcomes, such as the growth of riparian vegetation along riverbeds. However, this process cannot be classified as water harvesting, as it lacks human intervention. While runoff is fundamental

to water harvesting, it is the deliberate anthropogenic modification of the landscape to collect, store, and use runoff that defines water harvesting. Therefore, in addition to published definitions (e.g. **Table 2.1**), an alternative definition is provided: 'water harvesting is the deliberate act of collecting, storing, and utilising runoff.'

## **2.2 Sustainability and benefits**

Adopted by all United Nations Member States in 2015, the Sustainable Development Goals (SDGs) provide a "blueprint to achieve a better and more sustainable future for all" (United Nations, 2024). Central to this initiative are 17 Goals aimed at addressing issues such as violent conflict, human rights abuses, climate change, and environmental degradation. Water plays a crucial role, either directly or indirectly, in many of these Goals. As Rockström and Falkenmark (2015, p. 284) note, "Water flows across the SDGs — from improving water, sanitation, and health to ending hunger and poverty”.

While the Sustainable Development Goals (SDGs) clearly emphasise the importance of water in development, the term ‘water harvesting’ is explicitly mentioned in connection with only one SDG (Goal 6) which is to “Ensure availability and sustainable management of water and sanitation for all”. The target relating to this Goal (i.e. Target 6A) states “By 2030, expand international cooperation and capacity-building support to developing countries in water- and sanitation-related activities and programmes, including water harvesting, desalination, water efficiency, wastewater treatment, recycling and reuse technologies” (United Nations, 2020). There are many different types of water harvesting technology, but given the phrasing of Goal 6 and the other types of water-related approaches listed in Target 6A, it could be inferred that water harvesting relates solely to the collection of rainwater from rooftops.

This ambiguity regarding the nature of water harvesting technologies promoted through the SDGs represents a missed opportunity to highlight the need for improved utilisation of runoff, particularly from natural landscapes rather than artificial surfaces (e.g. rooftop water harvesting). However, it could also be argued that the targets are flexible enough to accommodate various technologies to achieve the Goals. Prior to the adoption of the SDGs by the United Nations in September 2015, some experts advocated for changes to the water-related SDGs. An essay published in *Nature* six months before the SDGs were adopted by Rockström and Falkenmark (2015, p. 284) noted, "The goals are vague and assume — as have global water policies for decades — that water for all needs can be drawn from rivers, lakes and groundwater." The authors specifically endorsed water harvesting, advocating for the collection of runoff to increase the availability of "green water" for food and biomass production. They concluded that "Hiding the African Achilles' heel of water scarcity behind unclear wording in the SDGs is a grave mistake. Without connecting water, food, growth, and poverty, the sustainable development framework will not deliver on its promise to Africa" (Rockström and Falkenmark, 2015, p. 285).

**Table 2.2** outlines the intended benefits associated with a range of water harvesting technologies. An overview of the different types of these technologies, as well as an explanation of runoff, is provided in **Section 2.4** and **2.7**, respectively.

**Table 2.2. A variety of water harvesting technologies and their associated benefits.**

<b>technology</b>	<b>benefit</b>	<b>reference</b>
floodwater harvesting	crop cultivation	Babker et al., 2020
rooftop runoff	supplement domestic water supply; reduced household electricity bills	Traboulsi and Traboulsi, 2017
grass strips & planting pits	increased soil moisture through runoff reduction	Tuinhof et al., 2012
warping dams	reduced erosion by gully control; reduced sediment loading in lower basin	Li et al., 2018
check dams	sediment trapping and carbon sequestration	Fang et al., 2023
sand dams & subsurface dams	increased groundwater storage through riverbed infiltration	Tuinhof et al., 2012

By considering water harvesting technologies more comprehensively, it becomes clear that water harvesting can support multiple SDG targets, beyond just Target 6A associated with rooftop harvesting technologies. For example, Target 6.1 (see Goal 6, **Table 2.3**) focuses on access to safe drinking water. The construction of sand dams is one such water harvesting technology that can be utilised to support this target. Sand dams are simple structures built across ephemeral riverbeds, with water stored within the sand's pores (Piemontese et al., 2023). The sand provides filtration and protection from contamination; thus, water extracted from sand dams is generally safer than that from open water sources.

Target 6.5 (Goal 6) introduces the concept of integrated water resources management, including transboundary cooperation. This target is particularly relevant for water harvesting technologies that collect runoff from large catchment areas. For instance, water harvesting technologies like artificial groundwater recharge can contribute to an integrated water management plan by transferring runoff to water stored within an aquifer. If the affected catchment area and aquifer cross international or other significant boundaries, then transboundary cooperation between stakeholders will be necessary.

Consequently, water harvesting technologies designed to promote artificial groundwater recharge could aid in achieving SDG Target 6.5 (see **Table 2.3**).

The aim of SDG Goal 2 is to “End hunger, achieve food security and improved nutrition and promote sustainable agriculture”. Microcatchment water harvesting techniques, characterised by overland flow harvested from short catchment lengths, are particularly well-suited to small-scale food producers (Critchley and Siegert, 1991). Additionally, project implementation is improved by considering the knowledge of indigenous peoples with experience in water harvesting and plant production (Tumbo et al., 2014). The microcatchment water harvesting technique of ‘planting pits’ therefore is an example of water harvesting that can support Goal 2, specifically via Target 2.3 (see **Table 2.3**).

Also associated with Goal 2 is Target 2.4, which seeks to promote practices that “...help maintain ecosystems, strengthen capacity for adaptation to climate change, extreme weather, drought, flooding...”. Water harvesting strengthens adaptation to climate change, such as changes in mean rainfall and extreme events, through what is referred to as ‘water buffering’ or the storage of water. Depending on the water harvesting techniques employed, there is an increase in water storage. Water may be stored in aquifers through groundwater recharge, in the root zone by increasing soil moisture, in tanks filled by rooftop rainwater runoff, and in surface and sub-surface reserves created by dams, embankments, or barrages (Tuinhof et al., 2012). Retention dams lessen the impact of flooding by reducing flood peaks (Parsaie et al., 2018), making such dams an example of a water harvesting technology that can be used in realising Target 2.4 (see **Table 2.3**).

**Table 2.3 Summary of how different water harvesting technologies support development goals.**

<b>Sustainable Development Goals and Targets (United Nations, 2020)</b>	<b>water harvesting technology</b>	<b>water harvesting group</b>
<b>Goal 2. End hunger, achieve food security and improved nutrition and promote sustainable agriculture</b>		
<b>Target 2.3</b> By 2030, double the agricultural productivity and incomes of small-scale food producers, in particular women, indigenous peoples, family farmers, pastoralists and fishers, including through secure and equal access to land, other productive resources and inputs, knowledge, financial services, markets and opportunities for value addition and non-farm employment	planting pits	microcatchment water harvesting
<b>Target 2.4</b> By 2030, ensure sustainable food production systems and implement resilient agricultural practices that increase productivity and production, that help maintain ecosystems, that strengthen capacity for adaptation to climate change, extreme weather, drought, flooding and other disasters and that progressively improve land and soil quality	retention dams	macrocatchment water harvesting
<b>Goal 6. Ensure availability and sustainable management of water and sanitation for all</b>		
<b>Target 6.1</b> By 2030, achieve universal and equitable access to safe and affordable drinking water for all	sand dams	macrocatchment water harvesting
<b>Target 6.5</b> By 2030, implement integrated water resources management at all levels, including through transboundary cooperation as appropriate	artificial groundwater recharge	macrocatchment water harvesting
<b>Target 6A</b> By 2030, expand international cooperation and capacity-building support to developing countries in water and sanitation-related activities and programmes, including water harvesting, desalination, water efficiency, wastewater treatment, recycling and reuse technologies	rooftop & courtyard rainwater WH	rooftop harvesting
<b>Goal 13. Take urgent action to combat climate change and its impacts</b>		
<b>Target 13.2</b> Integrate climate change measures into national policies, strategies and planning	check dams	macrocatchment water harvesting
<b>Goal 15. Protect, restore and promote sustainable use of terrestrial ecosystems, sustainably manage forests, combat desertification, and halt and reverse land degradation and halt biodiversity loss</b>		
<b>Target 15.2</b> By 2020, promote the implementation of sustainable management of all types of forests, halt deforestation, restore degraded forests and substantially increase afforestation and reforestation globally	floodwater spreading	floodwater harvesting
<b>Target 15.3</b> By 2030, combat desertification, restore degraded land and soil, including land affected by desertification, drought and floods, and strive to achieve a land degradation neutral world	contour stone lines	microcatchment water harvesting

Climate change exacerbates variability and uncertainty in natural resources, with detrimental consequences for local communities (Piemontese et al., 2023). Şen et al. (2013) proposed that runoff water harvesting can help mitigate some of the impacts of climate change. In drylands, national policies could include the use of water harvesting technologies as part of a wider strategy to combat the impact of climate change. Hence water harvesting can support SDG Goal 13 since this goal aims to “Take urgent action to combat climate change and its impacts”. A check dam is a specific example of a water harvesting technology that can support SDG Goal 13 with reference to Target 13.2 (see **Table 2.3**).

Addisu and Mekonnen (2019) found that check dams trap soil organic carbon (SOC) at levels ranging from 20 to 290 g kg<sup>-1</sup>, with the considerable variation in SOC levels attributed to differing spatial sources of carbon. In addition, check dams reduce soil erosion. One consequence of climate change will be an increase in soil erosion in many parts of the world, with the highest increase projected to be in semi-arid regions (Eekhout and de Vente, 2022). Hence check dams can play a role in climate change mitigation by trapping SOC, and in climate change adaptation by reducing soil erosion.

SDG Goal 15 relates to the sustainable use of terrestrial ecosystems with Target 15.2 providing a specific focus on forests. Channelling storm flood caused by runoff to agricultural land is an example of floodwater harvesting and an example of how water harvesting technology can be used to support the growth of trees. Target 15.3 focuses on actions to achieve a ‘land degradation neutral world’ and hence the construction of contour stones bunds is an example of a water harvesting technology that can play a role in delivering SDG Goal 15. Gebrenerichael et al., (2005) found that use of this technology resulted in a 68 % reduction in annual soil loss due to water erosion, based on a study located in northern Ethiopia. See **Table 2.3** for descriptions of SDG Goal 15, Targets 15.2, and Target 15.3.

When smallholder farmers implement water harvesting techniques, they can better manage rainfall variability by increasing water storage (e.g. soil moisture), thereby enhancing their resilience to shocks. Ali et al. (2007) argues that water harvesting, if implemented appropriately, is a viable option to improve productivity and conserve natural resources. Dile et al. (2013) illustrated this benefit for subsistence farmers in sub-Saharan Africa with a schematic (**Figure 2.1**). Without water harvesting, the farmer is more vulnerable to being forced to seek a living from ‘other livelihoods’ (threshold ‘a’, **Figure 2.1**) rather than being able to transition to commercial farming, assuming a starting point of subsistence farming. However, with water harvesting, the situation is reversed, with the farmer now

less vulnerable to a forced transition to ‘other livelihoods’, while the barrier to transitioning to ‘commercial’ farming is lowered, as represented by the reduced height between the ball and the light line at threshold ‘b’ (**Figure 2.1**). Hence, water harvesting not only helps farmers avoid abandoning their land to seek alternative livelihoods but also increases the likelihood of transitioning from subsistence to commercial farming.

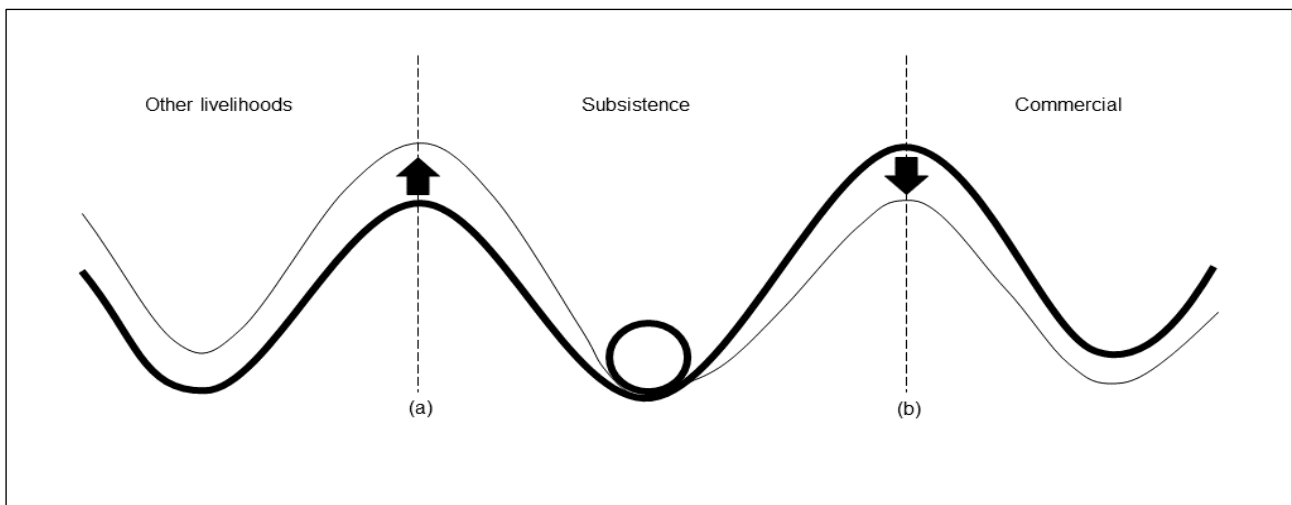


**Figure 2.1. Ball and cup conceptualisation in sub-Saharan Africa farming livelihood system illustrating the existence of several stable states, with the ball representing the farming system, and the resilience of each state being defined by the depth of the cup. The bold line represents a situation without water harvesting, while the light line represents a situation with water harvesting. The resilience of each state is represented by the depth of each cup, meaning the greater the depth, the harder it is for the ball (representing, for example, a farmer) to move from one state to another. (Dile et al., 2013).**

Despite the many benefits of water harvesting technologies, they can have negative side effects. Kibret et al. (2021) found that in Africa both small and large dams can become hotspots for malaria transmission, highlighting the need for integrated disease control efforts alongside these kinds of water harvesting interventions. Ali et al. (2007) also report that other researchers have indicated that improper use of water harvesting projects can result in inequitable access to water resources, and in some cases, may even compromise the reliability of potable water supplies.

Water harvesting is often implemented in drylands, where populations are among the poorest globally (White et al., 2002, cited in Koochafkan and Stewart, 2012). Furthermore, the construction of water harvesting structures in these regions can boost rural infrastructure development, offering support to some of the world's most impoverished communities. Mati et al. (2006) argue that rainwater resources must be managed through water harvesting to "drought-proof" African communities exposed to regular climatic variability and uncertainty.

A review of water harvesting at a national level conducted by Kiggundu et al. (2018) found that water harvesting technologies offered benefits at community and national scales, but that systems had failed due to poor management and vandalism. Şen (2021), after concluding that the literature is rich in studies on climate change impacts on hydro-meteorological records but lacks similar research on reservoirs, reviewed the impact of climate change on runoff harvesting and reservoirs (both surface and underground). In this review, Şen (2021) noted that reservoir structures provide mitigation and adaptation opportunities against the effects of climate change. Wang et al. (2021) reviewed 25 papers spanning two decades on dam siting and found that site selection factors vary depending on the dam's primary purpose. For dams used for irrigation and water supply, site selection focuses more on evaluating water quality. For those intended for power generation, hydrological factors determining power generation potential are the most significant. Meanwhile, for dams designed for flood control, topography and geological conditions play a more crucial role.

## **2.3 Water harvesting classification**

Under the umbrella term of 'water harvesting' there are different technologies, and these technologies can be classified or grouped based on shared characteristics. Critchley and Siegert (1991) divide water

harvesting technologies into two categories ('rainwater harvesting' and 'floodwater harvesting') along with respective sub-categories and sub-divisions.

Mekdaschi-Studer and Liniger (2013) address this issue in a similar manner, stating that water harvesting can be divided into two categories: 'floodwater' and 'rainwater runoff'. The 'floodwater' category consists of a single water harvesting group termed 'floodwater harvesting', while the 'rainwater runoff' category is divided into three groups: 'rooftop harvesting', 'microcatchment water harvesting', and 'macrocatchment water harvesting'. This results in a total of four water harvesting groups (**Figure 2.2**). The first of these groups, 'floodwater harvesting', applies to large catchments with runoff along well-defined channels. Water is stored as soil moisture in the root zone or as groundwater. Examples of floodwater harvesting include flood recession farming, spate irrigation and permeable rock dams. The second group is 'rooftop harvesting' and involves capturing runoff from rooftops and courtyards. The third group is 'microcatchment water harvesting', in which runoff is sourced from 'in-field' catchments, allowing the technology system to be replicated multiple times within the application zone. 'In-field' catchments capture runoff directly within the field itself and therefore do not rely on a collection system of rills, streams, or rivers. Microcatchment water harvesting technologies typically support plant production (e.g. crop, fodder, tree) with examples including small planting pits, mechanised Vallerani basins, and contour bunds. The final group is 'macrocatchment water harvesting' with technologies distinguishable through the utilisation of external catchments with the catchment clearly separate from the application area. Runoff is characterised by sheet and rill flow as well as short channel flow. Examples of macrocatchment water harvesting technologies include ponds for groundwater recharge, small earth dams, and sand dams.

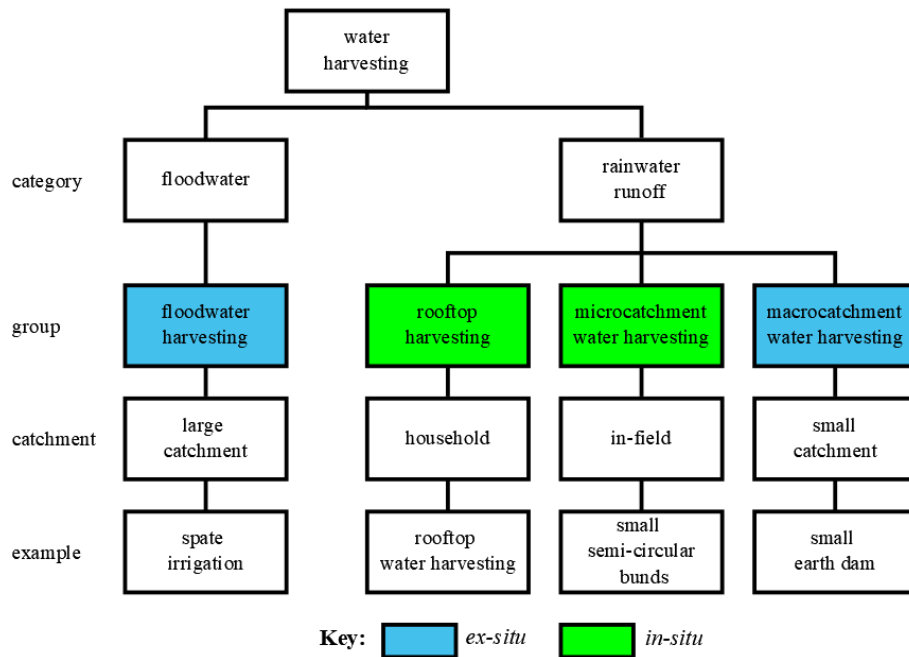


Figure 2.2. Water harvesting groups, types of catchments and examples of technologies (adapted from Mekdaschi-Studer and Liniger, 2013).

An alternative approach to water harvesting classification is to divide technologies into one of two groups: *in situ* or *ex situ*. Dabiri et al. (2016) state that *in situ* water harvesting technologies store water close to the collection area, while *ex situ* water harvesting technologies require a transmission system to transfer water from the collection area to the point of storage. It can be argued then that ‘rooftop harvesting’ and ‘microcatchment harvesting’ technologies can be categorised as *in situ* technologies, while ‘floodwater harvesting’ and ‘macrocatchment water harvesting’ technologies can be categorised as *ex situ* technologies.

## 2.4 Technologies

While there are many kinds of water harvesting technology, **Figure 2.3** provides examples of water harvesting technologies from each group shown in **Figure 2.2**. Using the *in situ/ex situ* method to categorise these four technologies the rooftop harvesting (**Figure 2.3b**) and Vallerani system (**Figure**

2.3c) can be classed as *in situ* forms of water harvesting, while the diversion canal (Figure 2.3a) and small earth dam (Figure 2.3d) can be classed as *ex situ* forms of water harvesting.

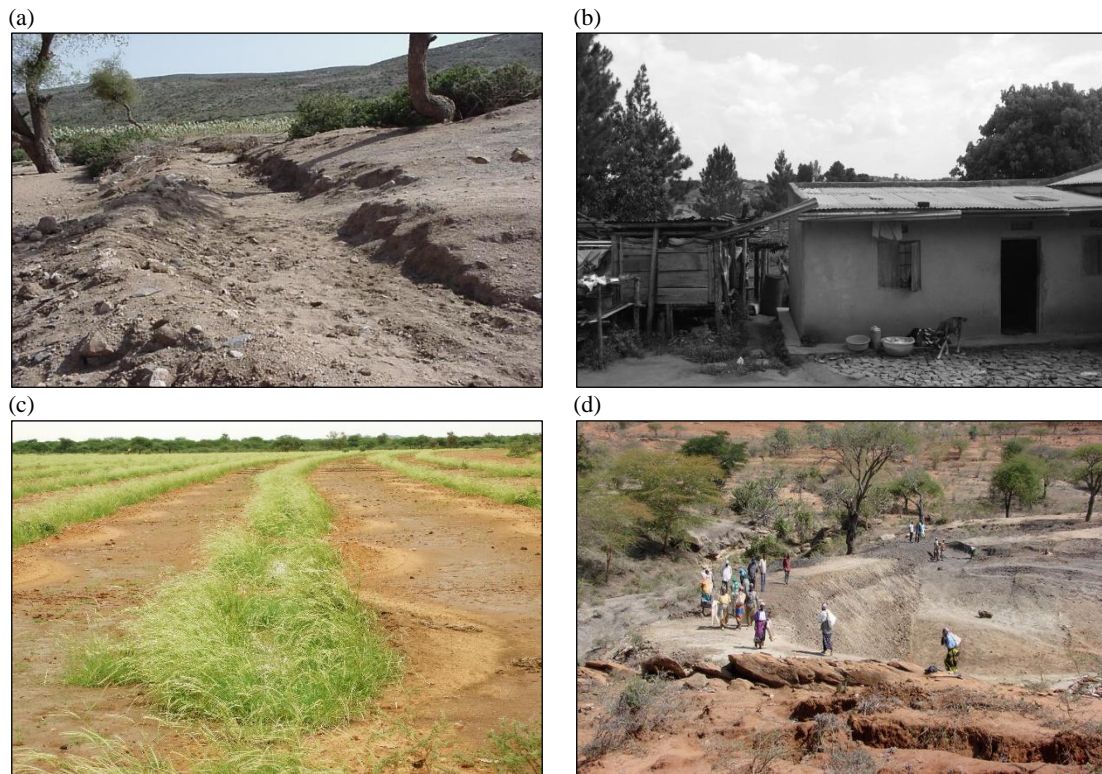


Figure 2.3. Examples of water harvesting technologies from WOCAT database — (a): floodwater harvesting - diversion canal [© D. Danano]; (b): rooftop harvesting [© A. Amon]; (c): microcatchment water harvesting - Vallerani system [© A. Boureima]; (d): macrocatchment water harvesting - small earth dam [© M. Malesu].

Yeomans (1954) developed the concept of the Keyline Plan, with the primary aim of improving soil structure and increasing soil fertility. The plan introduces the concept of 'Keylines', which serve as guides for working the land. Above the Keyline, the valley tends to be narrower and steeper than adjacent areas, while below it, the valley becomes wider and flatter relative to the surrounding topography. By utilising Keylines (illustrated in Figure 2.4), the Keyline Plan offers a straightforward method for conserving all the rainfall that falls on the land by directing it into the soil (Yeomans, 2008). In practice, this is achieved through slightly off-contour ploughing (Ferguson, 2015).

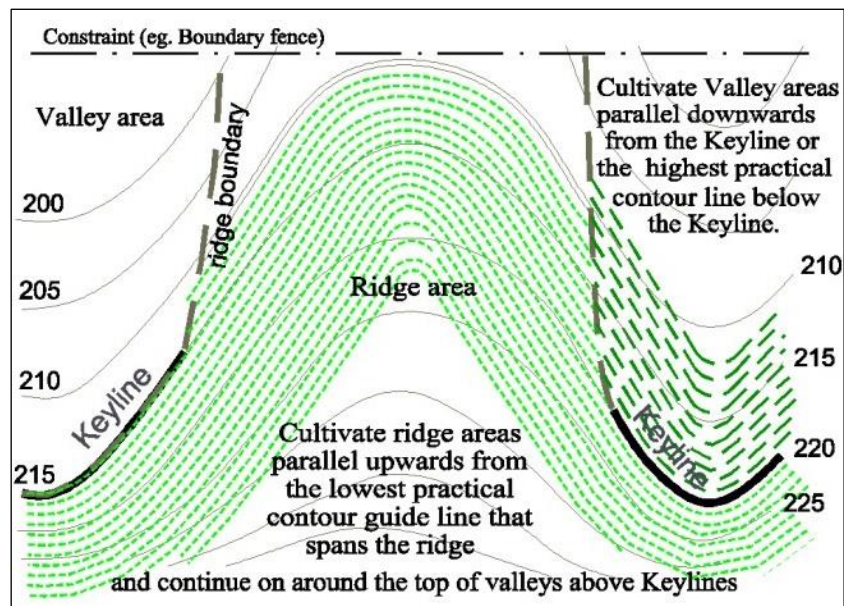


Figure 2.4. Illustration from the Keyline Plan showing ridge cultivation. Slightly off contour ploughing is shown in green (Yeomans, 2008, permission granted by Ken Yeomans).

Water harvesting dam projects, classified under the macrocatchment group (**Figure 2.2**), are often used as part of water supply schemes to enhance access to drinking water (Forzieri et al., 2008; Zaidi et al., 2015; Salih and Al-Tarif, 2012). Warping dams are known to reduce erosion (Li et al., 2018) and can therefore contribute to efforts to conserve and restore ecosystems in mountainous and dryland areas. In low-income countries, small dam failures are common (Pisaniello et al., 2015), often resulting in significant damage and loss of life (Sampson, 2024). In a case study in Vietnam, Pisaniello et al. (2015) reviewed 22 small dams and identified safety issues in each case. Of these, 13 dams had safety issues specifically related to the spillway.

Water harvesting can increase afforestation in drylands. Microcatchment water harvesting structures can be designed to sustain trees by storing enough water runoff in the soil profile during the rainy season to cover the water requirements of the trees during the growing season (Boers et al., 1986).

Aside from runoff there are other commonalities between different types of water harvesting technology. All approaches involve a ‘catchment’ of some description, which can be an artificial

surface (as in the case of rooftop and courtyard water harvesting), a small plot of agricultural land (as in the case for many microcatchment water harvesting schemes), or a drainage basin consisting of rills, streams and rivers (as in the case of floodwater harvesting and macrocatchment water harvesting technologies). The size of catchment differs significantly depending on local characteristics and type of water harvesting technology employed. Anschuetz (2003) states that for small planting pits (microcatchment water harvesting) there can be as many as 10,000 to 25,000 pits per hectare, resulting in a catchment area of 0.4 m<sup>2</sup> for each pit. Small earth dams, which as classified as macrocatchment water harvesting structures are considered to have relatively small catchments (**Figure 2.2**), which can exceed 25 km<sup>2</sup> (Stephens, 2010). Floodwater harvesting structures, in contrast, have “large catchments” (**Figure 2.2**), covering hundreds of square kilometres, with Almasalmeh et al. (2022) researching a floodwater harvesting scheme with a catchment area of almost 900 km<sup>2</sup>. Floodwater systems often include a diversion structure within the riverbed, which is susceptible to damage. This risk stems from uncertainties caused by the variable nature of floodwaters and changes in riverbed morphology (Mekdaschi-Studer and Liniger, 2013).

Another common feature amongst differing water harvesting technologies is storage. The type and proximity of storage to the catchment area vary depending on the technique. Water can be stored above ground in an open reservoir or in an underground cistern designed to collect rooftop rainwater runoff. Some water harvesting techniques store water by increasing soil moisture content. The location of the storage relative to the catchment area varies depending on the technology. For *in situ* water harvesting technologies the storage zone is always close to the entire catchment. Conversely, for *ex situ* technologies the zone of water storage is typically far from the outermost parts of the catchment, with runoff reaching the storage zone via a network of rills, streams, and channelised river flows.

Cherlet et al. (2018) identified nine sustainable land management practices — agroforestry, conservation agriculture, integrated soil fertility management, cross-slope measures, water harvesting, irrigation management, pastoralism and grazing management, integrated crop-livestock management, and forest management — that play a role in combating desertification. Water harvesting technologies, referred to as ‘structural measures’, which form part of the solution to desertification, include terraces, bunds, dams, pans, and barriers. Furthermore, water harvesting structures, such as dams, can be incorporated into systems for combating forest fires (Terêncio et al., 2018).

Bench terraces are suitable for drylands, especially where there are steep slopes, and are effective at controlling erosion by reducing overall runoff (Koochafkan and Stewart, 2012). Some bench terraces are designed with a runoff collection area close to where crops are planted. However, certain types of bench terraces lack runoff collection areas, with crops being irrigated directly by rainfall, leaving no runoff water to supplement irrigation. Since runoff is not part of the technology, such systems cannot strictly be considered as water harvesting.

## **2.5 History of water harvesting**

Historical evidence indicates that water harvesting techniques have been practised for millennia, ranging from small-scale methods such as terracing to retain soil moisture to larger-scale structures like dams. In the Negev Desert, water harvesting systems dating back 4,000 years or more have been discovered (Evanari et al., 1971 cited in Critchley and Siegert, 1991).

While the water harvesting examples shown in **Figure 2.3** are from relatively recent times, large water harvesting structures are known to have been built thousands of years ago. Details of some of the oldest known historic dams are provided in **Table 2.4**. One of oldest known dams was built around 3,000 BC

in present-day Jordan in a place called Jawa (Bretas et al., 2012). This earth embankment dam is believed to have a height of 4.5 m and a length of 80 m.

**Table 2.4. Details of historic dams, including location, construction timeline, dam height, and dam length (Bretas et al., 2012).**

timeline	location	country (present-day)	height (m)	length (m)
3000BC	Jawa	Jordan	5	80
2000BC	Saad-el-Kafara	Egypt	14	113
2nd century	Alcantarilla	Spain	17	557
2nd century	Proserpina	Spain	22	426
2nd century	Cornalbo	Spain	24	220
3rd century	Olisipo	Portugal	8	64
1595	Tibi	Spain	46	65
1640	Elche	Spain	23	95
1653	Relleu	Spain	29	34

## 2.6 Stakeholders

Water harvesting involves a diverse range of stakeholders. These stakeholders play a crucial role in defining the requirements of the systems, and it is essential to ensure timely and effective consultation with them throughout both the planning and implementation stages.

The Food and Agriculture Organization of the United Nations (FAO) has published a manual offering practical guidance for technicians and extension workers on implementing water harvesting schemes (Critchley and Siegert, 1991). Additionally, the International Center for Agricultural Research in the Dry Areas (ICARDA) is actively engaged in water harvesting initiatives. Although not part of the UN system, ICARDA provides "innovative, science-based solutions for countries across the non-tropical

dry areas" (ICARDA, 2023). ICARDA staff have co-authored numerous scientific articles directly related to water harvesting in drylands (e.g. Oweis et al., 2001; Mechlia et al., 2009; Ziadat et al., 2012). The World Overview of Conservation Approaches and Technologies (WOCAT) was founded in 1992 to enhance knowledge in sustainable land management (SLM). Since its inception, it has evolved into a global network and institution (Hurni, 2008). WOCAT manages a portal featuring a database on SLM, including examples of water harvesting technologies implemented worldwide. Established in 1971 to address concerns about famine, the Consultative Group on International Agricultural Research (CGIAR) is the world's largest consortium of internationally publicly funded agricultural research institutes focused on food, land, and water systems (Thornton et al., 2022). Among its sixteen centres, the International Water Management Institute (IWMI) specifically addresses water issues and has published works promoting water harvesting (e.g. Oweis et al., 1999).

A range of donors support water harvesting efforts, either directly or indirectly. For instance, ICARDA receives funding from over sixty different sources, including universities, state governments, the European Commission, and the World Bank (ICARDA, 2023). National research bodies and universities also contribute significantly to water harvesting projects. In Jordan, the National Center for Agricultural Research and Technology Transfer and the University of Jordan collaborated on a study to assess the suitability of water harvesting sites (Ziadat et al., 2006). Governments are key stakeholders. For instance, Jordan's Department of Land and Irrigation, which is part of the Ministry of Agriculture, has been involved in water harvesting initiatives (Ziadat et al., 2012). Non-governmental organisations (NGOs) are also recognised for their role in water harvesting projects, offering financial assistance or direct support (Chunhong et al., 2004; Prinz and Malik, 2002). Tuinhof et al. (2012) argue that capital costs represent a significant component of water harvesting —

particularly in contexts where the banking sector is underdeveloped and where inflation and economic uncertainty are high.

In addition to international and national organisations, local stakeholders are involved in water harvesting. These include households, smallholder farmers, agro-pastoralists, communities, community leaders, and user committees (Chunhong et al., 2004; Prinz and Malik, 2002; Tuinhof et al., 2012; Kiggundu et al., 2018).

## **2.7 Mechanisms of Runoff and Associated Processes**

Given the significance of runoff in water harvesting systems and technologies, as highlighted earlier in this chapter, it is valuable to examine the processes responsible for its generation, as well as other climatic and hydrological processes strongly associated with it. While runoff is a result of rain, not all rainfall events produce runoff. The study of the infiltration is necessary to understand the process of runoff generation and associated flooding and related geomorphic processes (Thomas, 2011). Only when rainfall exceeds the “infiltration capacity” — defined as the maximum rate at which a given soil can absorb rainfall when in a specified condition (Horton, 1933), can runoff occur. Infiltration provides the only source of soil-moisture and hence it is essential for vegetation growth. It is also the source of water for groundwater recharge necessary for water supplies from wells for example. Groundwater may emerge at springs and rivers thus becoming surface water.

Water that adds to soil-moisture following infiltration and is taken up by the root systems of vegetation is returned to the atmosphere through a process called transpiration. Rain that falls on the Earth’s surface and similarly returns to the atmosphere but without first undergoing infiltration is known as evaporation. Together, transpiration and evaporation are known as ‘evapotranspiration’.

Rockström and Falkenmark (2015) presented a water balance, in terms of what becomes of rain, in a Sub-Saharan context (**Figure 2.5**). Transpiration and evaporation account for 15–30 % and 30–50 % respectively. Collectively, evapotranspiration processes can be described as *green water*. Groundwater ranges from 10–30 %, while runoff accounts for 10–25 %. Rain, groundwater and runoff can be grouped and referred to as *blue water*.

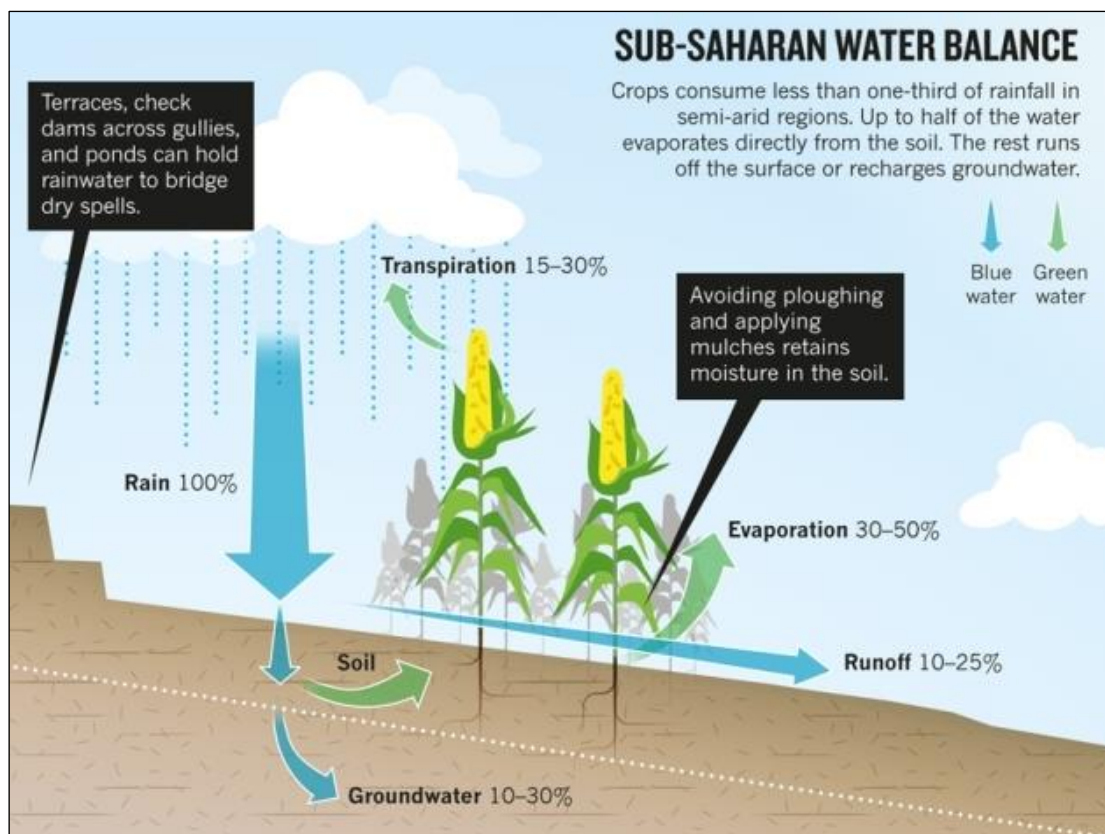


Figure 2.5. Sub-Saharan water balance (from Rockström and Falkenmark, 2015)

For small-scale water harvesting systems, runoff, as shown in **Figure 2.5**, travels over relatively short distances since the catchment area is close to the water harvesting structure (e.g. contour bund). For large-scale water harvesting systems — the primary focus of this thesis — there is often a significant distance between the location where rain makes contact with the Earth’s surface and the actual water harvesting structure. As runoff is generated where rain falls and moves overland through a drainage

network (i.e. rills, streams, rivers), some water volume is ‘lost’ due to evaporation and infiltration. This reduction in runoff volume is collectively referred to as *transmission losses*. Compared to other climatic regions, catchments in arid and semi-arid regions experience high levels of transmission losses. Hence, transmission losses are an important consideration when planning a large-scale system (e.g. macrocatchment water harvesting), due to the long distances runoff must travel to reach the structure and the arid nature of the environments where water harvesting is typically implemented.

As runoff transits from the point of its original generation (i.e. where rain contacts with the soil) to a downstream location — such as an existing or potential water harvesting scheme — it incorporates nutrients, rocks, and sediments. Conceptually, such processes form part of the catchment’s *hydrologic connectivity*, which can be defined as “the water-mediated transport of matter, energy and organisms within or between elements of the hydrological cycle” (Freeman et al., 2007, p. 5). The transport of “matter” in the form of sediments can be problematic for some water harvesting technologies. Sediment deposits in reservoirs are detrimental to the operation and maintenance of such water harvesting systems, especially those primarily intended for water supply. The issue of reservoir sedimentation, specifically in the context of dam planning in dryland environments, is covered later in this thesis (see **Chapter 6**).

## **2.8 Siting – biophysical parameters**

When evaluating the potential for water harvesting in a specific area, various biophysical parameters are selected and utilised within a methodology to determine the suitability of a particular water harvesting technology at a specific location. The following sub-sections highlight biophysical parameters, categorised under common headings, used to assess whether a location is suitable for water

harvesting. The actual biophysical parameters used in any water harvesting study vary and depend on the available resources and the methodology adopted by researchers.

**Table 2.5** lists various types of water harvesting technologies and the biophysical criteria used in site selection studies. However, it should be noted that the table is not exhaustive and significant variations exist in how site selection studies are conducted. Additionally, **Figure 2.6** provides a schematic showing a range of biophysical parameters used in water harvesting site selection studies.

**Table 2.5. Water harvesting technologies and the biophysical criteria used in site selection.**

<b>technology</b>	<b>biophysical criteria</b>	<b>reference</b>
micro dams ( <i>Ndiva</i> ); stone terraces; bench terraces; borders	rainfall; slope; soil texture; soil depth; drainage; land use / land cover	Mbilinyi et al., 2007
high potential surface runoff sites	soil characteristics; land use; rainfall; slope	de Winnaar et al., 2007
in-field and ex-field rainwater harvesting catchment surfaces	aridity zones; rainfall (annual, with 80 % probability of exceedance); soil texture; soil depth; land use / land cover; rivers; dams; lakes	Kahinda et al., 2008
ponds	rainfall; slope	Mati et al., 2006
dams	narrows; influence area of barrage; stream length; catchment area; faults; bedrock depth; substrate porosity	Forzieri et al., 2008
check dams	hydrogeomorphic unit; soil; land use	Padmavathy et al., 1993
<i>Jessours</i> and <i>Tabias</i>	slope; size of watershed	Mechlia et al., 2009
check dam; percolation pond; subsurface dyke	land use / land cover; lithology; soil; slope; rainfall; drainage	Ramakrishnan et al., 2009
artificial aquifer recharge	geological setup; groundwater (level & electrical conductivity)	Abdalla and Al-Rawahi, 2013
sand dams	slope; salinity; stream order	Piemontese et al., 2023

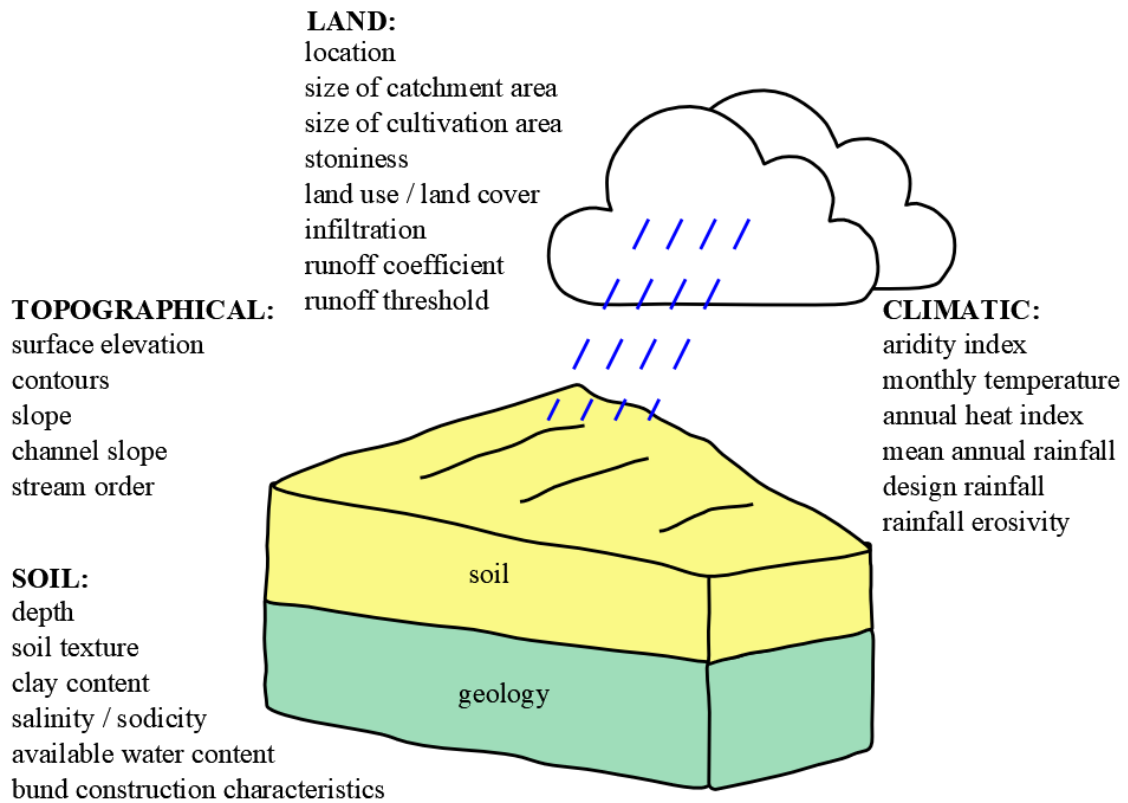


Figure 2.6. Biophysical criteria used in water harvesting site selection.

## 2.8.1 Climate

There is a strong association between water harvesting and drylands. Rainfall alone is often insufficient to determine whether a region can be characterised as drylands. Drylands, which make up about 40 % of the world’s total land area (Koochafkan and Stewart, 2012), can be identified based on the length of the growing season and their susceptibility to desertification. According to Bot et al. (2000), arid, semi-arid, and dry sub-humid zones, which have a growing period of 1–179 days, fall under the ‘drylands’ classification. Moisture availability, rather than just rainfall, is the primary factor defining aridity, as it reflects the balance between precipitation and evapotranspiration (Nicholson, 2011).

To determine the aridity zone (e.g. semi-arid) of a particular location, the aridity index, which is the ratio of precipitation to potential evapotranspiration, can be used. Potential evaporation is the

“maximum quantity of water capable of being lost, as water vapour, in a given climate, by a continuous stretch of vegetation covering the whole ground and well supplied with water. It thus includes evaporation from the soil and transpiration from the vegetation from a specified region in a given time interval; it is expressed as a depth like precipitation” (WMO, 1990, p. 162). The potential evapotranspiration is the amount of water that could be lost through evaporation or transpiration if it was available, as opposed the actual amount of water lost, which is usually less (Park and Allaby, 2017).

Zomer and Trabucco (2022) provide a global aridity index raster (at a spatial resolution of 30 arc-seconds) for the period 1970–2000 period, based on the FAO-56 Penman-Monteith equation. The FAO-56 Penman-Monteith is one of several equations that measure the atmosphere's ability to remove water through evapotranspiration processes. Using the drylands classification approach proposed by Bot et al. (2000), which excludes hyper-arid regions from the definition of ‘drylands’, and applying the Zomer and Trabucco (2022) methodology to define regions based on a Global Aridity Index, dryland regions can be categorised as arid, semi-arid, and dry sub-humid, with Global Aridity Index values of 0.03–0.2, 0.2–0.5, and 0.5–0.65, respectively. **Figure 2.7** presents a world map of drylands. Although 'hyper-arid' regions can technically be included within drylands, they are shown separately here, in accordance with Bot et al. (2000). This distinction is made because hyper-arid regions are not vulnerable to desertification and therefore are not included in the Bot et al. (2000) definition of drylands. Using this approach, drylands cover 31.5 % of the Earth’s land surface and are home to 33.8 % of the world’s population (Wang et al., 2022a).

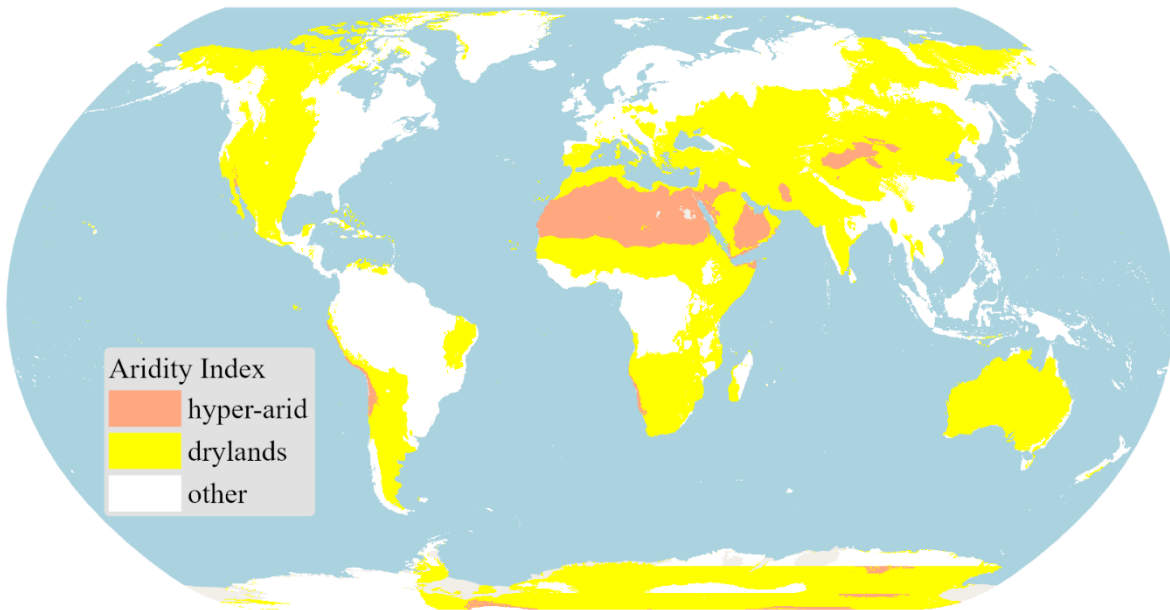


**Figure 2.7. Drylands of the world based on Global Aridity Index (Zomer and Trabucco, 2022), with drylands defined by encompassing ‘arid’, ‘semi-arid’, and ‘dry sub-humid’ climate classifications.**

The frequency of rainfall distribution in drylands is often skewed, with a predominance of subnormal years offset by occasional years of exceptionally high rainfall, which inflate the long-term average. Local factors, such as topography, significantly influence rainfall, creating substantial spatial gradients in mean rainfall. Annual totals are largely determined by a few high-intensity, short-duration rain events. While these events generate high runoff, the overall proportion of rainfall contributing to runoff remains low (Nicholson, 2011). In semi-arid regions, 10–25 % of all rainfall typically becomes surface runoff (Koochafkan and Stewart, 2012) which either moves over the land as surface flow or is channelled into drainage networks of rills, streams, and rivers.

Mean annual rainfall alone can be used to design rooftop water harvesting systems (Traboulsi and Traboulsi, 2017). However, due to the significant temporal variability in rainfall, especially in regions with low precipitation, relying solely on mean annual rainfall means that the water harvesting system will frequently underperform. Kahinda et al. (2008) contend that small-scale farmers dependent on

rainfed agriculture face significant challenges due to aridity and climatic uncertainty, with low crop yields stemming more from erratic temporal and spatial rainfall patterns than from actual water scarcity. To enhance agricultural productivity through water harvesting, Critchley and Siegert (1991, p. 32) recommend considering annual rainfall variability and using a Design Rainfall which they define as "the total amount of rain during the cropping season at which or above which the catchment area will provide sufficient runoff to satisfy the crop water needs". By conducting a probability analysis, which involves ranking years of historical annual rainfall data, the probability of occurrence can be calculated using Return Periods (in years) for different levels of annual rainfall.

Most non-perennial rivers are located in drylands. Rainfall is typically seasonal in such regions, and streams flow intermittently during the wet season, with flow continuing into the dry season only if there are baseflow contributions from groundwater (Shanafield et al., 2021). When implementing water harvesting projects in drylands, planners are likely to deal with ephemeral streams and rivers, which flow for only brief periods and remain dry for most of the year.

### **2.8.2 Topography**

Kadam et al. (2012) used a slope map to identify potential water harvesting sites. Critchley and Siegert (1991) emphasised the critical importance of slope in the success of water harvesting schemes for plant production. They identified ground slope as a key limiting factor, recommending the avoidance of slopes greater than 5 % due to the "uneven distribution of runoff." Additionally, sites with slopes greater than 5 % become uneconomical because of the large volumes of earthworks required.

Moreno-Mateos et al. (2010) conducted a catchment-wide study to identify suitable sites for wetlands and concluded that the tools they developed would be effective for environmental planning purposes. Their study incorporated slope as a factor in the development of these tools. Slope is a common

criterion in site selection for water harvesting studies. A review of water harvesting studies by Adham et al. (2016a) found that slope is the most frequently utilised biophysical selection criterion.

### **2.8.3 Land**

Along with catchment characteristics such as the relationship between rainfall and runoff, the actual size of the catchment is a key parameter in designing or selecting a water harvesting technique. For instance, when estimating the annual catchment runoff for an earth dam, Doherty (2000) noted that the volume of water flowing into the (dam) reservoir could be calculated using just three parameters, one of which was the catchment area (the others being the depth of average annual rainfall and the runoff as a percentage of annual rainfall). Within dryland landscapes, there is considerable uncertainty regarding the nature of runoff, as most research has been conducted on small plots. Consequently, there is scant information on fundamental issues such as how runoff varies with catchment scale (Nicholson, 2011). For water harvesting techniques that promote crop growth, the ratio of the catchment area to the cultivated area should also be considered (Critchley and Siegert, 1991). This ratio can vary with the aridity of the site. For example, in areas with a higher Aridity Index, the land area generating runoff needs to be larger relative to the cultivated area, resulting in an increased catchment-to-cultivated area ratio (Prinz and Malik, 2002).

Specialists typically consider land use and land cover during initial assessments for potential water harvesting sites. Ziadat et al. (2006) assessed the surface cover of the land and quantified “stoniness percent”. They also studied not only the type of vegetation at sample locations but the percentage of coverage.

Critchley and Siegert (1991) note that specific soil properties are particularly relevant to the placement of water harvesting structures for plant production. These properties include soil texture, soil structure,

soil depth, fertility, salinity/sodicity, infiltration rate, and available water content. Ziadat et al. (2006) explain how researchers assessed the texture of the soil surface horizon through tactile analysis (i.e. by feeling it with their hands). Furthermore, the soil's construction characteristics, though often overlooked, are crucial. For water harvesting structures requiring a water-retaining barrier, the soil must be capable of forming a resilient earth bund.

The ideal soil properties of the catchment area differ from those of the cultivated area concerning the runoff coefficient. The catchment area should have a high runoff coefficient to ensure sufficient water is conveyed overland to the cultivation or storage zone. Not all rainfall events generate runoff, as initial raindrops are intercepted by vegetation, and infiltration processes must also be considered. For artificial catchments, the initiation of the runoff process can be determined using a threshold parameter. Designing artificial water harvesting systems involves using different threshold values for various catchment surfaces. For instance, a design standard for an artificial catchment might require a daily rainfall total greater than 10 mm to effectively harvest rainfall. This means that a rainfall-runoff threshold of 10 mm/day will produce runoff only when the daily rainfall exceeds 10 mm (Baek and Coles, 2013).

#### **2.8.4 Geology**

It is a well-established fact that geological composition of an area plays a vital role in the distribution and occurrence of groundwater (Krishnamurthy and Srinivas, 1995 cited in Şen et al., 2013). It follows that when the purpose of a water harvesting structure is to artificially recharge a groundwater aquifer then the geology of the location should be considered at the site selection stage. Şen et al. (2013) actively investigated Quaternary deposits along ephemeral riverbeds in Saudi Arabia when

determining optimal locations for water harvesting structures aimed at enhancing groundwater recharge.

## 2.9 Summary

This chapter has outlined the connection between water harvesting and the Sustainable Development Goals (SDGs). It is anticipated that this thesis could contribute to four SDGs: Goals 2, 6, 13, and 15. This chapter also recognises that water harvesting involves the storage and productive use of runoff, which can be collected from a nearby catchment area (*in situ*) or from a distant one (*ex situ*). Various definitions of water harvesting, gathered from published literature, have been presented, alongside a novel definition: 'water harvesting is the deliberate act of collecting, storing, and utilising runoff.'

The chapter offers the reader an overview of a wide range of water harvesting technologies, describing the regions where water harvesting is most commonly practised, such as drylands, and outlines the typical climatic conditions of these regions. It provides a brief overview of the ancient history of water harvesting and identifies contemporary stakeholders involved in the practice. Additionally, the biophysical characteristics that make a location suitable for water harvesting are examined, along with a brief summary of the various site selection methodologies used by researchers.

An established method for classifying water harvesting techniques is presented (**Figure 2.2**). While the chapter references all four classification groups — including technologies that collect runoff from artificial surfaces, such as rooftop harvesting — this thesis places less emphasis on small-scale techniques, although these are briefly referenced to provide a comprehensive overview of water harvesting. Instead, the primary focus of this thesis is on relatively large-scale water harvesting, particularly macro-catchment systems, with some relevance to floodwater harvesting and micro-

catchment water harvesting. The intention of this chapter, however, is to provide the reader with a broad understanding of the diversity of water harvesting technologies, both past and present.

This chapter presents evidence (e.g. **Table 2.4**) of the ancient origins of certain water harvesting technologies. For example, in Jawa (present-day Jordan), the remains of a water harvesting dam built over 5,000 years ago are still visible today. These sites were selected without the advantages of modern datasets and tools. In the past 50 years, however, the advent of remote sensing products, computational modelling, and GIS has revolutionised how planners select sites for water harvesting techniques. The following chapters of this thesis examine the relationship between water harvesting site selection and the application of innovative geospatial techniques and diverse remote sensing products, with a focus on large-scale systems in sub-national drylands. This research aims to support multiple Sustainable Development Goals.

# **3 A literature review of remote sensing products used in water harvesting studies**

## **3.1 Introduction**

Remote sensing predominantly focuses on gathering and interpreting data about an object or terrain from a remote vantage point. Examples of remote sensing include aerial photography, satellite imagery, radar altimetry and laser bathymetry (Purkis and Klemas, 2011). The sensors used in remote sensing can be described as active or passive. Passive sensors detect natural radiation that is emitted or reflected, while active sensors emit energy to scan objects and then detect the radiation that is reflected or backscattered from objects (Tang et al., 2009).

A pivotal moment in the history of remote sensing came with the launch of the first Landsat satellite in 1972. This event marked the beginning of a continuous stream of space-based information of the Earth, providing invaluable data for research on land use and land cover changes (U.S. Geological Survey, 2015). However, remote sensing is not limited to satellite-based sensors. Airborne remote sensing, conducted by equipping sensors on aircraft or uncrewed aerial vehicles (UAVs), also plays a significant role in capturing spatial data.

Remote sensing provides an approach to observing hydrologic variables across extensive regions. This includes deriving land surface temperature from thermal infrared data, measuring surface soil moisture using passive microwave data, assessing water quality with visible and near-infrared data, and estimating landscape surface roughness through synthetic aperture radar. These techniques are

essential for estimating hydrometeorological fluxes, such as evapotranspiration (Schmugge et al., 2002). Many key factors in the land surface water balance, such as precipitation, evapotranspiration, snow and ice, soil moisture, and changes in terrestrial water storage, can be observed through remote sensing methods with different levels of spatial and temporal resolution and accuracy (Tang et al., 2009). In recent years, remote sensing (RS) technology has advanced significantly, enabling the acquisition of extensive data on hydrological variables such as precipitation, temperature, soil moisture, water levels, evapotranspiration, flood extent, flow velocity, river discharge, and land water storage across regional and global scales. Remote sensing serves as valuable input for integrated hydrodynamics, hydrological, and hydrometeorological models (Duan et al., 2021). This advancement is particularly crucial in remote areas where traditional measurements are impractical or costly.

Remote sensing can assist in selecting sites for water harvesting. Adham et al. (2016a) reviewed 48 studies focused on site selection for water harvesting technologies in arid and semi-arid regions, categorising them into four methodological groups. The first group uses GIS and remote sensing. The second combines hydrological modelling (HM) with GIS and remote sensing. The third integrates multi-criteria analysis (MCA) with HM, GIS, and remote sensing. The last group uses MCA and GIS. The Adham et al. (2016a) review confirms that most studies on water harvesting site selection use remote sensing in their search to identify suitable locations.

There is no recognised standardised method for conducting site selection studies for specific types of water harvesting technologies. Authors of peer-reviewed articles use a variety of data sources (including remote sensing). If HM is utilised, the modelling approaches may vary, and if MCA is employed, the methodologies can differ. Additionally, the functions of GIS used in these studies also vary widely. However, most water harvesting site selection studies do use GIS in combination with HM and MCA (Adham et al., 2016a).

The subject of water harvesting has merited the publication of a number of reviews. Boers and Ben-Asher (1982) examined some 170 articles published from 1970 to 1980 related to rainwater harvesting. While this review highlighted a growing awareness of rainwater harvesting, it made no mention of 'remote sensing'. This suggests that the water harvesting sector did not immediately begin utilising remote sensing datasets, since, as mentioned earlier, the Landsat satellite programme was launched in 1972. Adham et al. (2016a) examined 48 studies related to water harvesting site selection in arid and semi-arid regions, and noted extensive use of remote sensing products by researchers, with three out of four study categories featuring 'remote sensing'. The growing fusion of remote sensing and water harvesting forms the basis of this literature review, as there is a notable gap in existing research that specifically explores remote sensing within the context of water harvesting. Here, this review aims to address this research gap by studying how remote sensing products are utilised in water harvesting (and closely affiliated subject matter) studies. This review also aims to explore emerging patterns and trends in relation to remote sensing and water harvesting.

For regions such as the drylands of Africa there has been a resurgence of interest in water harvesting in recent years, driven by the intersection of three pressing issues: the potential consequences of climate change in arid regions, the decreasing availability of water for agriculture, and the urgent need to sustain a growing population (Critchley et al., 2012). Acknowledging these challenges and recognising the existing research gaps, the primary objective of this review is to identify the most significant remote sensing products employed in relation to water harvesting studies. It seeks to provide insights into the process of generating these products, offer specific examples of their applications, outline potential advantages and disadvantages associated with each product, and pinpoint current trends in their usage. Furthermore, this review strives to explore potential best practices and offer evidence-based recommendations.

Utilising specific search terms, a systematic review (described in the **Materials and Methods** section) was conducted using two prominent search engines. Subsequently, a manual screening process was employed to eliminate non-relevant and inaccessible papers, leading to the identification of 290 peer-reviewed articles all related to water harvesting (or a closely related subject) and collectively referred to as the review literature. In the **Results** section the most frequently used remote sensing products are categorised and presented. In the **Discussion and Evidence-based Recommendations** section issues are discussed with a focus on the strengths and weaknesses of different remote sensing products. Recommendations are made regarding remote sensing and its use within the water harvesting sector.

### **3.2 Materials and methods**

The first stage of the process began with the identification of relevant articles using two bibliographic databases, namely Web of Science (WoS) and Scopus. Details of the search input text and parameters are provided in **Table 3.1**. The citation search was completed in January 2024. Since the outputs of WoS and Scopus produced many identical references, the search results were combined, and duplicate entries were removed. Following this, any result without a Digital Object Identifier (DOI) or accessible only behind a paywall to which Lancaster University does not subscribe was removed from further consideration. The remaining documents were examined, and those unrelated to the primary topic were excluded. Specifically, documents written in languages other than English, documents not originating from journals (e.g. conference proceedings, book chapters, review articles), and results discussing subjects beyond the scope of this work (e.g. rooftop rainwater harvesting) were identified as off-topic and subsequently removed. All results that successfully passed through these preliminary screening steps were included in this literature review and hereafter referred to as ‘review literature’ (RL). **Figure 3.1** provides a visual representation of the process for selecting the RL.

**Table 3.1. Search commands used with bibliographic databases (search undertaken in January 2024).**

A literature review of remote sensing products used in water harvesting studies

search engine	search within	search command
Web of Science	abstract	("water harvesting" OR "runoff harvesting" OR "rain water harvesting" OR "rainwater harvesting")
Scopus	article title, abstract and keywords	AND ("GIS")

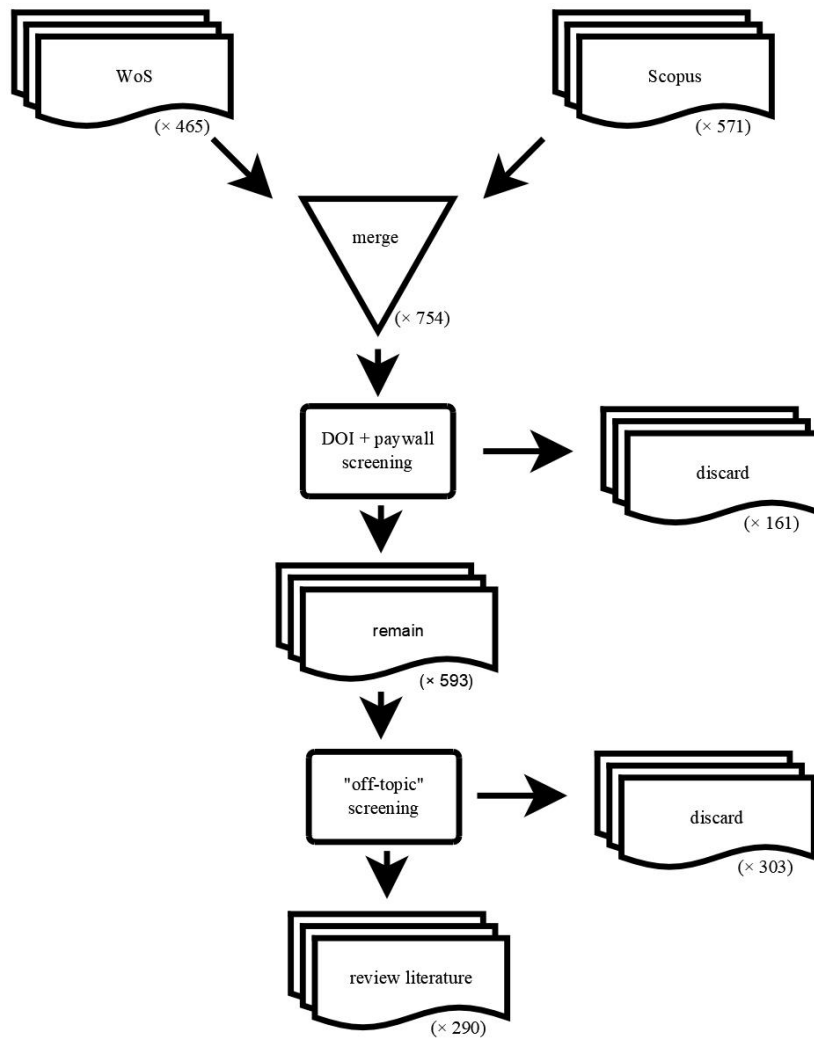


Figure 3.1. Diagram illustrating the progression of refining the literature review and the count of references associated with different stages in the process.

Following the selection of the research literature, each paper was examined to determine whether the study had utilised any type of remote sensing (RS) product. Notes were taken on the type of RS product used and the primary purpose of using the product.

## **3.3 Results**

### **3.3.1 Classification of remote sensing products**

The DOI of each article is provided in **Appendix A** in tabular format (**Table A1**) while details of articles cited in the body of text are provided in full within the **References** section. All the 290 references that comprise the RL were found to be articles published in peer-reviewed journals. ‘Keywords’ from all 290 articles in the research literature were compiled and used to create a word cloud, which was generated using the web-based tool WordCloud.com. The resulting visualisation is presented in **Figure 3.2**.

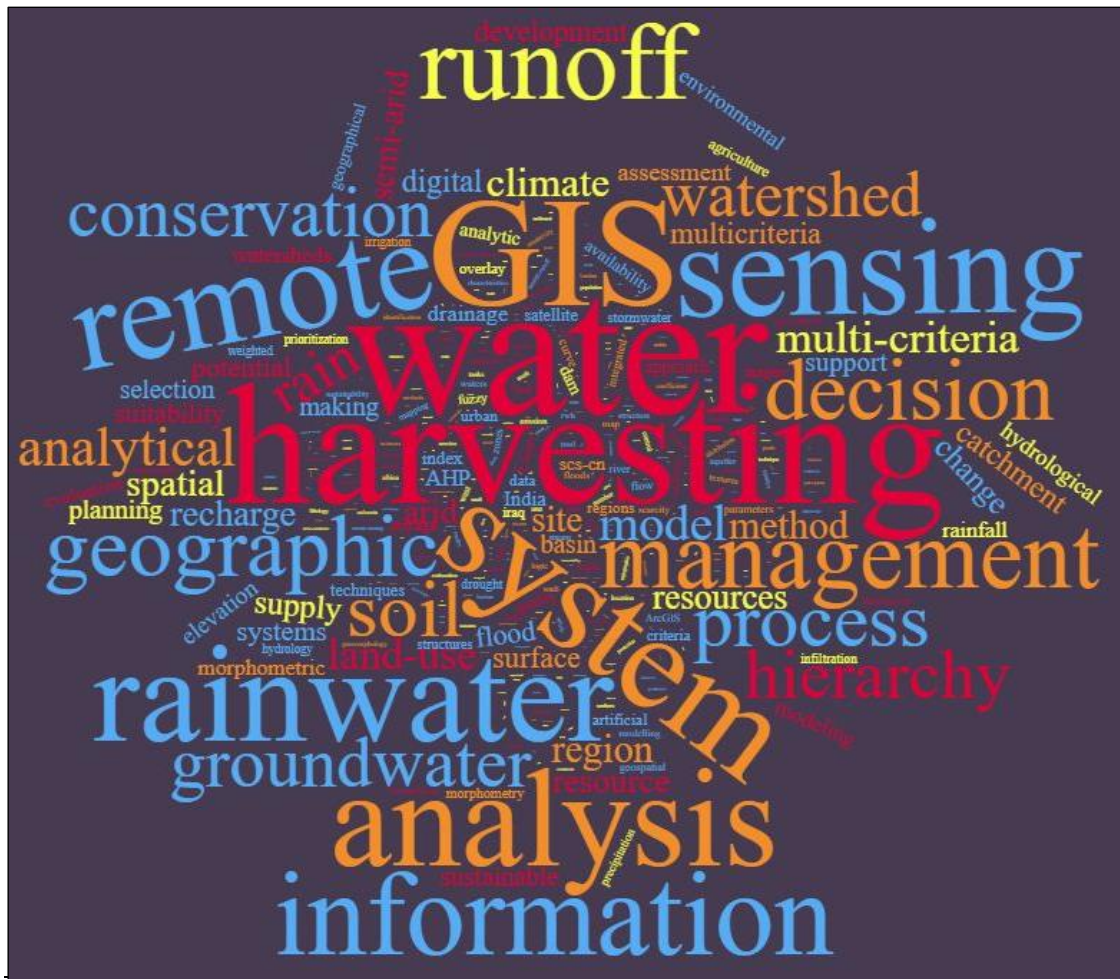
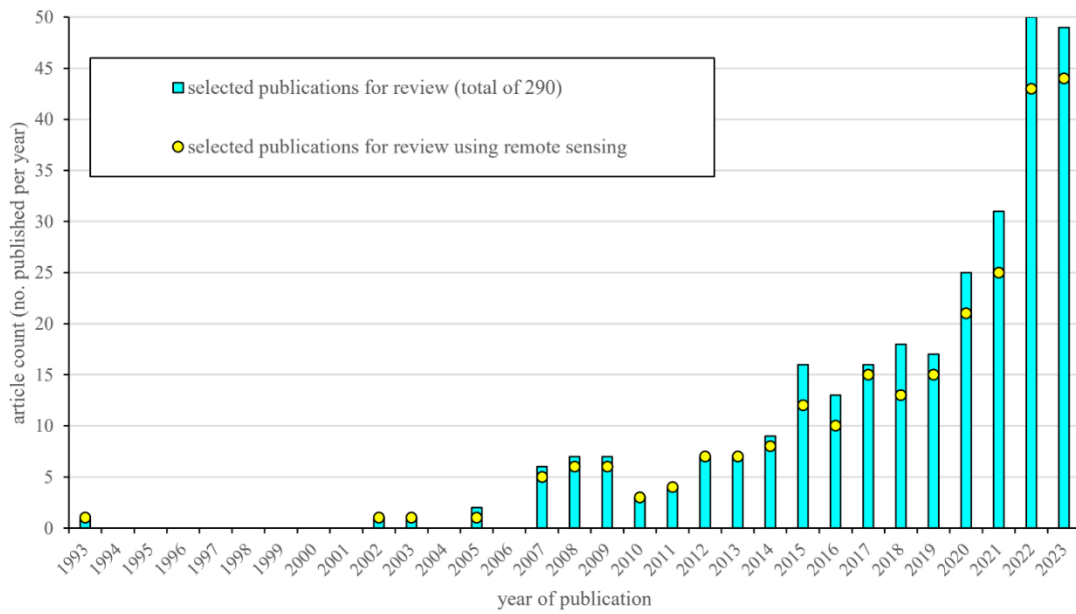


Figure 3.2. A word cloud generated using ‘Keywords’ from the review literature articles.

The RL articles were published over a period spanning 1993 to 2023. **Figure 3.3** illustrates the yearly distribution of the RL and shows a significant surge in annual publication count over time.



**Figure 3.3.** Chart showing the annual publication count for review literature and the count of those that used remote sensing.

The RL literature was published across 108 different journals. The journal ‘Water’ was the most prolific in terms of publishing the greatest number of RL articles with a total of 28, while at the other end of the spectrum 59 journals published only a single RL article. **Table 3.2** presents a list of journals that published five or more RL articles. Among these articles, the most frequently cited (as of March 2024) is the manuscript by Sreedevi et al. (2009), with 159 citations in WoS and 202 citations in Scopus. This highly cited study used a DEM from the Shuttle Radar Topography Mission (SRTM) to compute 14 morphometric watershed parameters related to linear, areal, and relief characteristics.

**Table 3.2. Journal titles publishing five or more articles from the review literature.**

<b>journal</b>	<b>count</b>
Water	28
Arabian Journal of Geosciences	23
Environmental Earth Sciences	12
Geocarto International	12
Water Resources Management	12
Sustainability	11
Physics and Chemistry of the Earth, Parts A/B/C	8
Agricultural Water Management	6
Journal of the Indian Society of Remote Sensing	6
Sustainable Water Resources Management	6
Applied Water Science	5
Environmental Monitoring and Assessment	5
IOP Conference Series: Earth and Environmental Science	5

Before classifying remote sensing products, it is important for the purposes of this review to define what constitutes a 'remote sensing product.' In this context, a 'remote sensing product' refers to the processed data or imagery acquired through remote sensing technologies, such as satellites, UAVs, or aircraft. These products encompass a wide range of outputs, including satellite images, vegetation indices, land use maps, and climatic profiles. A remote sensing product can be relatively simple, comprising a single image or data array, or it can be more complex, consisting of multiple images or arrays.

All 290 RL articles were examined, and any mention of remote sensing products was recorded. Identifying the names of these remote sensing products proved to be uncomplicated in cases where the details were presented clearly in a tabular format, as demonstrated by Patil and Gupta (2023). However, some articles presented a difficulty, as it was not possible to extract details of the remote sensing product(s) utilised from the methodology. In some instances, ambiguous phrasing in the text indicated that a remote sensing product has been utilised without explicitly naming the product, such as merely mentioning the use of 'satellite imagery'. Another observation noted from reading the RL was that

tendency to provide details of the source of the remote sensing product without giving details of the actual remote sensing product acquired. For example, a remote sensing product may have been “downloaded from the USGS website” leaving the reader to speculate on the details of the product used. In other cases, the text in RL articles attributed the source of data to a third party, often a national agency or another study, without clearly identifying if the data originated from a RS product.

In searching and documenting articles that had utilised remote sensing a broad definition of 'remote sensing' was employed, including LiDAR, aerial photography, and satellite imagery (e.g. Google Earth). In total 248 of the 290 RL articles utilised at least one remote sensing product in some way. Since the primary objective of this review is to identify remote sensing applications in water harvesting studies, only articles explicitly detailing the remote sensing product(s) used have been included in this count. However, the actual number is likely to be higher due to vague or unclear descriptions of methodologies, as outlined previously. **Figure 3.3** illustrates both the number of RL articles published in each year and the number of these articles that utilised at least one remote sensing product as part of the study's methodology. This chart reveals a longstanding utilisation of remote sensing products, dating back to 1993 (Padmavathy et al., 1993). With the exception of 2005, the results show that the majority of articles published per year utilised a minimum of one remote sensing product. In 2005 only half the articles used remote sensing while in 2023 approximately 90 % of all published articles indicated using at least one remote sensing product.

The most frequently used remote sensing product was Landsat, with (out of a total of 290) stating that Landsat had been used in their studies. The name of each remote sensing product along with the number of RL studies that employed the product is provided in **Table 3.3**. As previously stated, due to the vagueness in the way some articles are presented **Table 3.3** may not capture the entirety of remote sensing product utilisation. For instance, a number of articles indicated the use of a DEM from

the USGS portal without specifying the actual DEM product, so the actual occurrences of SRTM DEM and ASTER DEM used throughout the RL is likely to exceed the count totals presented in **Table 3.3**.

While QuickBird does appear in **Table 3.3**, its imagery comprises the bulk of Google Earth’s (ranked fifth in **Table 3.3**) imagery where available. If QuickBird imagery is unavailable for certain locations, Google Earth defaults to medium-high resolution Landsat imagery (Potere, 2008). **Table 3.3** is not exhaustive as it contains only remote sensing products that were determined to have been used in more than five different RL article methodologies.

**Table 3.3. Remote sensing products used in more than five different studies from the review literature.**

remote sensing product	count
Landsat	117
SRTM DEM	91
ASTER GDEM	60
IRS LISS	30
Google Earth	23
TRMM	20
Sentinel-2	22
ALOS PALSAR DEM	10
SPOT	10
INDIA CartoDEM	9
QuickBird	9

**Table 3.4. Most frequency utilised remote sensing products used in the review literature studies, classified into five groups of elevation, climatic, multi-spectral, RGB and composite [# indicates number of studies].**

elevation models		climatic		multi-spectral		RGB		composite	
product name	#	product name	#	product name	#	product name	#	product name	#
SRTM DEM	91	TRMM	20	Landsat	117	IRS LISS	30	Google Earth	23
ASTER GDEM	60			Sentinel-2	22	SPOT	10		
ALOS PALSAR DEM	10					QuickBird	9		
INDIA CartoDEM	9								
<b>total</b>	<b>170</b>		<b>20</b>		<b>139</b>		<b>49</b>		<b>23</b>

### 3.3.2 Digital elevation models (DEMs)

#### Description of DEMs

The Shuttle Radar Topography Mission (SRTM), flown aboard the Space Shuttle Endeavour in 2000, used a technique called ‘radar interferometry’ to produce digital topographic data (surface elevation) from two separate radar images captured from slightly different locations (EROS, 2018b). In **Table 3.4** ‘SRTM DEM’ refers to two distinct SRTM DEM products. One is the SRTM X-band DEM product at a spatial resolution of 1 arc-second (~30 m) and the other the SRTM C-band DEM product at spatial resolution of 3 arc-second (~90 m) (Büyüksalih et al., 2005).

The Advanced Spaceborne Thermal Emission and Reflection Radiometer Global Digital Elevation Model (ASTER GDEM) was derived from stereo image data captured between 2000 and 2010 by satellite telescopes (launched onboard NASA's Terra spacecraft) in the near-infrared spectral band. These data were then processed to calculate Earth's elevation, resulting in DEM with a spatial resolution of 30 m (Tachikawa et al., 2011).

The ALOS-PALSAR DEM is an elevation product, covering a temporal span from 2006 to 2011, at a stated spatial resolution of 12.5 m, that is available for download from the ASF Data Search Vertex portal (Alaska Satellite Facility, 2023). This high-resolution DEM is ‘upsampled’ and is “...**not generated from the PALSAR data itself**. It is a copy of an existing DEM that was modified and then used for the radiometric terrain correction process. **The pixel spacing of the source DEM was adjusted to match that of the Terrain Corrected image it is packaged with and is not an indication of the resolution of the DEM.**” (Alaska Satellite Facility, 2023, emphasis in original).

The INDIA CartoDEM, or Cartosat-1 Digital Elevation Model, was created from stereo image data obtained from a pair of panchromatic cameras on the Cartosat-1 satellite, which was launched in 2005

(Muralikrishnan et al., 2011). DEM datasets are available at spatial resolutions of 30 m and 90 m, covering the entirety of India.

### **DEMs and water harvesting**

The majority of RL articles utilised a remote sensing DEM product (some 156 of the 290 articles reviewed, equivalent to 53.8 %) in some way. Pawattana and Tripathi (2008) used an SRTM DEM raster to create a slope raster as part of an Analytical Hierarchical Process (AHP) decision-making process. Forzieri et al. (2008) used the ASTER GDEM product to compute the size of a catchment. Nadhim Al-neama et al. (2022) computed linear parameters (e.g. bifurcation ratio), areal parameters (e.g. compactness coefficient) and relief parameters (e.g. ruggedness number) from the ALOS PALSAR DEM to evaluate surface water runoff potential. Balasubramanian et al. (2017) used the INDIA CartoDEM to compute 16 morphometric parameters with regard to subwatersheds within a basin located in Tamil Nadu, India.

Spatial resolution varies amongst the digital elevation models used throughout the review. A total of 20 studies used the 3 arc-second SRTM DEM product, with a spatial resolution of approximately 90 m (e.g. Sreedevi et al., 2009; Jha et al., 2014; Abdekareem et al., 2022), 41 studies used the 1 arc-second SRTM DEM product with a spatial resolution of approximately 30 m (e.g. Pawattana and Tripathi, 2008; Bajabaa et al., 2014; Waghaye et al., 2023), while for the remainder the resolution of the SRTM DEM product could not be determined from the manuscript. Like the SRTM DEM products the INDIA CartoDEM datasets are available at 1 and 3 arc-second, generated by sub-sampling the original 1/3 arc-second data (Muralikrishnan, 2011). None of the studies in the review literature confirmed that the 3 arc-second (i.e. 90 m) INDIA CartoDEM was used. A number of studies from the review literature stated that the ALOS PALSAR DEM was utilised with a spatial resolution of 12.5 m (Asmar et al., 2021; Nadhim Al-neama et al., 2022; Ouali et al., 2022; Nabit et al., 2023). Dwiatmojo

et al. (2021) employed a DEM derived from remote sensing data with a spatial resolution 8 m obtained from DEMNAS (Badan Informasi Geospasial, 2018). Bruins et al. (2019) employed a LiDAR-derived DEM with an even finer spatial resolution of 0.5 m., while Tiwari et al. (2023) merged high-resolution colour orthophoto with LiDAR-derived topographic variables. Delaney et al. (2022) used a LiDAR-derived DEM data to substantiate results from a global (lower spatial resolution) SRTM DEM and other studies also utilised LiDAR data (Bañados and Quijano, 2022; Wang et al., 2023) created a topographic dataset from LiDAR data. From the RL studies a total of 20 used a DEM with a spatial resolution of 90 m but only five of these articles were published after 2018 (Abdekareem et al., 2022; Debebe et al., 2022; Delaney et al., 2022; Mallick et al., 2022; Elewa et al., 2023).

### **3.3.3 Climatic products**

#### **Description of climatic products**

Tropical Rainfall Measurement Mission (TRMM) datasets consist of products generated for studying precipitation in the tropics and include observations of radiances, microwave temperature, radar reflectivity, rainfall rate, vertical rainfall profile, and convective and stratiform heating (GES DISC, 2017).

#### **Climatic products and water harvesting**

Moawad (2013) used TRMM data in conjunction with averaged six hourly data obtained from a precipitation mapping server to analyse a single specific flooding event. Salar et al. (2018) used TRMM monthly precipitation data to find the mean annual precipitation which was then used to create a weighting map to identify a suitable site for groundwater recharge. Abdekareem et al. (2022) analysed TRMM data as part of a methodology to assess sites for groundwater potential by employing a pairwise matrix with the criteria of runoff and physical catchment characteristics. The ArcGIS ‘Multidimensional Make NetCDF Raster Layer’ tool has been utilised to extract TRMM data, in

network common data form (netCDF) format, into the GIS environment (Mugo and Odera, 2019). Mahmoud and Tang (2015) showed how remotely sensed precipitation data, including TRMM data, could be used with the Inverse Distance Weighted interpolation method to obtain rainfall data for areas where *in situ* climate stations are sparse. Alwan et al. (2020) selected seven criteria to identify water harvesting sites, with one criterion developed from TRMM precipitation data.

Of the 290 review literature articles, 20 used TRMM (**Table 3.4**) however two authors (Mahmoud and Yousif) co-authored half of these articles (Mahmoud, 2014; Mahmoud et al., 2014; Mahmoud and Alazba, 2015; Mahmoud et al., 2015a; Mahmoud et al., 2015b; Mahmoud and Tang, 2015; Yousif and Bubenzer, 2015; Mahmoud et al., 2016; Mahmoud and Alazba, 2016; Yousif and Sracek, 2016).

### **3.3.4 Multi-spectral products**

#### **Description of multi-spectral products**

As previously stated, the Landsat satellite programme commenced in 1972. The first Landsat satellite captured data across four spectral bands. However, over the years the mission has evolved, and the current satellites provide 11 bands of earth observation data. Although the original satellites are no longer operational, newer satellites have entered service to ensure continuous coverage. Consequently, from 1972 to the present day, an uninterrupted dataset is available for certain spectral bands, such as green, red, and near-infrared (U.S. Geological Survey, 2015). Landsat band information and descriptions of use are presented in **Table 3.5**.

The acronym IRS LISS is the combination of Indian Remote Sensing Satellites (IRS) and Linear Imaging Self-Scanning Sensor (LISS) in acknowledgement of the type of multi-spectral radiometer fitted to satellites (eoPortal, 2012). Both LISS-I and LISS-II capture data in the blue, green, red, and near-infrared spectral bands. Sentinel-2 is a multi-spectral imaging satellite mission that has 13 spectral

bands, including four 10 m bands (three RGB bands and one near-infrared), six 20 m bands (narrow bands for vegetation and wider SWIR bands), and three 60 m bands for cloud screening and atmospheric correction (The European Space Agency, 2023).

**Table 3.5. The bands of Landsat satellites and descriptions of use (U.S. Geological Survey, 2015) [OLI, Operational Land Imager; TIRS, Thermal Infrared Sensor; ETM+, Enhanced Thematic Mapper Plus; TM, Thematic Mapper; MSS, Multispectral Scanner; --, not applicable].**

timeline	2013–	1999–	1982–	1982–	1972–	
band name	L8–9 OLI/TIRS	L7 ETM+	L4–5 TM	L4–5 MSS	L1–3 MSS	description of use
Coastal/Aerosol	Band 1	--	--	--	--	Coastal areas and shallow water observations; aerosol, dust, smoke detection studies.
Blue (B)	Band 2	Band 1	Band 1	--	--	Bathymetric mapping; soil/vegetation discrimination, forest type mapping, and identifying manmade features.
Green (G)	Band 3	Band 2	Band 2	Band 1	Band 4	Peak vegetation; plant vigor assessments.
Red (R)	Band 4	Band 3	Band 3	Band 2	Band 5	Vegetation type identification; soils and urban features.
Near-Infrared (NIR)	Band 5	Band 4	Band 4	Band 3	Band 6	Vegetation detection and analysis; shoreline mapping and biomass content.
	--	--	--	Band 4	Band 7	
Shortwave Infrared-1 (SWIR-1)	Band 6	Band 5	Band 5	--	--	Vegetation moisture content/drought analysis; burned and fire- affected areas; detection of active fires.
Shortwave Infrared-2 (SWIR-2)	Band 7	Band 7	Band 7	--	--	Additional detection of active fires (especially at night); plant moisture/drought analysis.
Panchromatic (PAN)	Band 8	Band 8	--	--	--	Sharpening multispectral imagery to higher resolution.
Cirrus	Band 9	--	--	--	--	Cirrus cloud detection.
Thermal (T)	Band 10					
	Band 11	Band 6	Band 6	--	--	Ground temperature mapping and soil moisture estimations.

### Multi-spectral products and water harvesting

Durga Rao and Bhaumik (2003) collected ground data to use as training sets in the supervised classification of Landsat 5 TM satellite data to gain information on land use / land cover (LULC). Ramakrishnan et al. (2008) used a Landsat product (specifically Landsat TM) with image ratios and principal component analysis to upgrade the spatial resolution of an existing database on lithology and soil. Yousif and Bubenzer (2015) used a Landsat product compressed to a colour image (spatial

resolution of 14.25 m) together with a geologic map and field investigations to identify the geological features within the study area. Ahirwar et al. (2020) used a Landsat-8 product with different software (ArcGIS, ENVI, PCI Geomatica and Rockworks 16) to map lineaments while using the same Landsat product to map LULC (verified with visual interpretation of Google Earth imagery and field visits). Ray (2023) used the Landsat-8 remote sensing imagery as part of method to identify groundwater potential zones using 14 thematic layers or maps, two of which were derived from Landsat bands, namely a land use / land cover map and a lineament map.

Behera et al. (2019) exploited the high temporal resolution (5-day revisit) and spatial resolution (10 m) of Sentinel-2 data and computed spectral indices of Normalized Difference Vegetation Index (NDVI) and Normalised Difference Water Index (NDWI) for three seasons to classify LULC in the study area. Rather than manipulate remote sensing directly Sacolo and Mkhandi (2021) utilised a land LULC layer that had been created using Sentinel-2 data and downloaded from a portal run by an organisation disseminating open geospatial datasets for Eastern and Southern Africa. In a study targeting locations for rainwater harvesting structures Gavhane et al. (2023) used ERDAS Imagine 15 software to perform radiometric correction, layer stacking, and mosaicking Sentinel-2 images to create a LULC map.

### **3.3.5 RGB (red-green-blue) imagery products**

#### **Description of RGB products**

SPOT 1, SPOT 2 and SPOT 3 captured multi-spectral bands of green, red, and near-infrared at a spatial resolution of 20 m, and panchromatic at a spatial resolution of 10 m, with products freely available for download via the USGS EarthExplorer portal (EROS, 2018c). SPOT 4 was equipped with a High-Resolution Visible and InfraRed (HRVIR) sensor capturing multi-spectral images at 20 m spatial resolution. SPOT 5 was additionally equipped with an instrument capable to acquiring near-

simultaneous stereopair imagery (CNES, 2023). QuickBird refers to an earth observation satellite which, while no longer operational, provided remote sensing products that remain available through an archive in the form of panchromatic and multi-spectral bands (Maxar, 2019).

### **RGB products and water harvesting**

Biswas (2009) used an IRS LISS satellite image to detect trends in the depletion of water bodies. Jha et al. (2014) obtained an IRS LISS product at a spatial resolution of 5.4 m as part of a process to create a land cover / land use map which subsequently was used to in the production of a curve number map and the computation of runoff. The 'curve number' is a key component of a conceptual model used to analyse how rainfall is converted into runoff. Its purpose is to calculate the depth of direct runoff resulting from a storm event (Ponce and Hawkins, 1996). Sahu and Siddha (2022) used visual interpretation and digitisation to classify land use / land cover including rivers, lakes, waterbodies, villages, agricultural land, barren land, and forests from IRS LISS multi-spectral data in a study to select suitable sites for water harvesting.

Ouessar et al. (2009) created a DEM with a spatial resolution of 30 m using SPOT stereo pair images and a 'TOPOGRIDTOOL' routine in a process that utilised the SPOT image to adjust the DEM to correct modelled stream channels. Setiawan and Nandini (2022) used SPOT images to classify LULC into six types and verified the analysis with direct measurements finding the classification process had an overall accuracy of 95 % and a Kappa coefficient of 0.85. The Kappa statistic is commonly used to assess inter-rater reliability, which measures the degree to which raters consistently assign the same scores to the same variables, verifying the accuracy of the data collected in a study (McHugh, 2012).

In a study to find appropriate locations and capacities of on-farm ponds, Khetkratok et al. (2010) interpreted a QuickBird panchromatic image to assess land tenure, pond capacity, and land use. The

interpretation of this imagery led to the creation of GIS datasets encompassing these factors. To identify narrow valleys best suited to locate water harvesting structures Adham et al. (2018) used a combination of digital elevation data and QuickBird satellite images. Liu et al. (2022) used visual interpretation of QuickBird imagery to identify seven types of LULC (i.e. natural forest land; urban green space; farmland; buildings; bare land; roads; river systems).

### **3.3.6 Composite products**

#### **Description of composite products**

Google Earth is a software program that displays satellite or aerial images of the Earth's surface (Miller, 2011) and offers the option for users to extract the ground elevation for points of interest.

#### **Composite products and water harvesting**

From the review literature of 290 articles a total of 23 (**Table 3.4**) cited the use of Google Earth, published between 2016 and 2023. Adham et al. (2016b) used Google Earth imagery and GIS to measure distances from water harvesting structures to points of interest (e.g. settlements). Rai et al. (2018) used Google Earth images in part of a process to cross verify outcomes produced using multi-spectral data. Salem et al. (2020) used Google Earth images to digitise the Meskat system, a traditional micro-catchment water harvesting technique for olive tree groves, in the Sahel of Tunisia. Soni et al. (2022) used the colour of each Google Earth satellite image pixel to estimate (using MATLAB software) the equivalent runoff coefficient which in turn was used to calculate an estimation of runoff volume. Okeola et al. (2023) obtained rainfall data from the Nigerian Meteorological Agency and using analytical tools including Google Earth, ArcGIS, and Global Positioning System (GPS) computed runoff using the USDA SCS-CN model.

## **3.4 Discussion and evidence-based recommendations**

### **3.4.1 DEM products**

#### **Evidence**

The two most utilised remote sensing products, SRTM DEM and ASTER GDEM, are freely available and offer global coverage. The highest spatial resolution of SRTM DEM products is 1 arc-second (i.e. ~30 m at the equator), the other being 3 arc-second, while the spatial resolution of ASTER GDEM is also 1 arc-second. It is interesting to explore why researchers favour one particular DEM product over another when there is no difference in spatial resolution. Several researchers (e.g. Murphy et al., 2008; Bajabaa et al., 2014; Sayl et al., 2020a; Elewa et al., 2023) used both SRTM DEM and ASTER GDEM products. Murphy et al. (2008) highlighted an issue with both products in that both are based on reflected surface elevations at canopy instead of ground level noting that for forested areas this issue needs to be addressed for proper channel-flow analysis. However, Mallick et al. (2022) assessed the merits of a SRTM DEM product against ASTER GDEM and considered the SRTM DEM (3 arc-second spatial resolution) product to be more accurate than the ASTER GDEM product as the SRTM radar beam penetrates the tree canopy to get accurate topographic measurements whereas the ASTER gets reflections of sun radiation from the tree canopy which are then photogrammetrically processed to derive the elevation model. Thus, the difference in DEM assessments may be due to the fact that the SRTM C-band has some vegetation penetration. However, in heavily forested areas, it is insufficient to reach the ground, instead providing surface estimates that are more similar to the ASTER GDEM methodology. Three different DEM products were evaluated by Yousif and Bubenzer (2015), who used hydrology tools to create a drainage network within a GIS environment and compared these modelled representations against the drainage network observed through a combination of field visits and satellite imagery. They found (perhaps surprisingly) that the SRTM DEM product at a lower spatial

resolution of 3 arc-second produced superior drainage lines compared to that of a higher spatial resolution 1 arc-second SRTM DEM product and the ASTER GDEM 1 arc-second product. Similarly, Mugo and Odera (2019) assessed the merits of the SRTM DEM product against ASTER GDEM by comparing model elevations against precisely levelled data and concluded the SRTM DEM provided superior data and therefore decided to use the SRTM product for their site selection study.

Although SRTM DEM products and the ASTER GDEM product are used extensively throughout the RL articles, the technology used to capture data ultimately used to compute elevation data is different. While SRTM products are made using a technique called radar interferometry with C-band (wavelength 5.6 cm), as previously stated in this chapter, ASTER utilises stereo image data in the near-infrared wavelength region from 0.78 to 0.86  $\mu\text{m}$  (Hirano et al., 2003). This difference in techniques produces respective challenges with Tachikawa et al. (2011) stating that missing data in the ASTER dataset due to constant cloud cover must be filled by DEMs from other sources while for SRTM issues with data are linked to topographically steep areas that create radar shadow and layover.

Of the RL articles several studies utilised DEMs with a higher spatial resolution than 30 m. Notable examples include the ALOS PALSAR DEM, as demonstrated by Asmar et al. (2021), Mamin and Majeed (2022), and Ray (2023), featuring a spatial resolution of 12.5 m. Additionally, Sahu and Siddha (2022) employed the CartoSat-1 DEM, with a spatial resolution of 10 m, while Dwiatmojo et al. (2021) utilised the DEMNAS DEM, which provides an 8 m spatial resolution. Of the review literature the article stating the use of a DEM with the highest spatial resolution was Bruins et al. (2019) who used a procured LiDAR derived DEM with a spatial resolution of 0.5 m.

DEM coverage over the study area is factor when opting to select a particular DEM for research purposes. In the context of this review both SRTM DEM and ASTER GDEM can be considered as

‘global’ as both offer coverage of all regions where water harvesting takes place but the spatial resolution of either product is no higher than 1 arc-second (~30 m). From the RL there are examples of national institutions/organisations supporting research through the provision of DEMs with a higher spatial resolution than that offered by SRTM DEM and ASTER GDEM. Dwiatmojo et al. (2021) obtained a DEM with a spatial resolution of 8 m from DEMNAS (Badan Informasi Geospasial, 2018). Inamdar et al. (2013) obtained a 10 m spatial resolution DEM in raster format (ERSI grid) from Land Victoria. Sahu and Siddha (2022) utilised a Cartosat-1 DEM with a spatial resolution of 10 m downloaded from the Bhuvan portal (Bhuvan: ISRO/NRSC, 2023) for a study in India which is an online archive database of the National Remote Sensing Centre (Mukherjee and Singh, 2020).

Using a DEM with a higher spatial resolution increases the computational demands. From the review literature Bera and Mukhopadhyay (2023) undertook a study area covering almost 2,000 km<sup>2</sup> and concluded that using the SRTM DEM with a spatial resolution of 30 m struck a balance between data availability and computational efficiency, while higher-resolution datasets were more challenging to process and analyse.

**Table 3.6. List of factors relating to DEM selection.**

<b>attribute</b>	<b>ASTER GDEM</b>	<b>reference(s)</b>
spatial resolution (X–Y)	30 m	Hirano et al., 2003
vertical resolution (Z)	1 m (smallest increment)	Hirano et al., 2003
geolocation error	-0.57 to +0.22 arc-seconds	Tachikawa et al., 2011
vertical accuracy - absolute	RMSE 18 to 19 m	Reuter et al., 2009
vertical accuracy – relative*	mean -9.6 m	Reuter et al., 2009
surface / terrain model	surface	Tachikawa et al., 2011
missing or erroneous data	areas under constant cloud cover	Tachikawa et al., 2011
coverage	83° N to 83° S	Tachikawa et al., 2011
availably	freely	Hirt et al., 2010

\* GDEM versus SRTM

A list of factors that may be considered when choosing a DEM for a particular body of research are presented (**Table 3.6**) together with the attributes associated with a commonly utilised DEM product (ASTER GDEM).

### **Evidence-based recommendation**

SRTM DEM and ASTER GDEM are widely used global DEM products with similar spatial resolution (1 arc-second), but their data acquisition methods result in different accuracy and limitations. Studies suggest that SRTM DEM generally provides more accurate elevation data due to its radar-based vegetation penetration capabilities, whereas ASTER GDEM relies on optical data, which can be affected by canopy cover. However, in steep terrain, SRTM DEM may suffer from radar shadow effects. Higher-resolution DEMs ( $\leq 12.5$  m spatial resolution) are available but require greater computational resources. Researchers should select a DEM based on study area characteristics, data accuracy needs, and computational feasibility.

### **Evidence**

In this review 'DEM' refers to elevation models encompassing both digital surface models (DSMs) and digital terrain models (DTMs). Depending on the technique used to create the DEM, the elevation data may represent the Earth's surface (i.e. topmost surface, including buildings, trees, and other objects) or the Earth's terrain (i.e. bare-earth surface, excluding buildings, vegetation, and other surface objects). Typically, researchers working in the field of water harvesting or a closely related subject have an interest in hydrologic characteristics or how water flows overland so terrain data (i.e. DTM) would be preferable over surface data (i.e. DSM) assuming other attributes (e.g. spatial resolution) are equivalent. The appropriateness of DEMs was highlighted in the review literature by Murphy et al. (2008) with respect to a heavily forested study area. DEMs created from laser scanning (i.e. LiDAR) measurements have the advantage of not only offering superior spatial resolution and vertical resolution to that of satellite radar DEMs (e.g. SRTM DEM) (Schumann and Bates, 2018) but can provide terrain elevation data together with vegetation cover measurements (Kukko et al. 2019).

While the spatial resolution remains a vital specification for every DEM and conceivably holds the utmost significance, it is important to consider other features or limitations depending on the given circumstances. The vertical resolution, which denotes the smallest elevation increment along the Z-axis of a DEM, influences its effectiveness in modelling hydrology-related tasks. The vertical resolution of the ASTER GDEM for example is 1 m (Hirano et al., 2003). Gyasi-Agyei et al. (1995) proposed that for most hydrological applications, the ratio of the average drop per pixel (i.e. the elevation difference between a pixel and its neighbouring pixel in the direction of steepest descent) to vertical resolution should exceed one to ensure reliable modelling outputs. They also suggested that this ratio could be used to determine the minimum pixel area for reliable channel network definition for any given vertical resolution.

From the review literature a single study (López-Ramos et al., 2022) utilised freely available HydroSHEDS DEM as part of a methodology to construct a climate model at a spatial resolution of  $460\text{ m} \times 460\text{ m}$ . The HydroSHEDS DEM is created primarily from SRTM DEM data and a void-filling procedure is applied that removes spurious sinks (depressions) while keeping naturally occurring ones creating a continuous elevation surface (Lehner et al., 2008). As of 2008 HydroSHEDS data was available at spatial resolutions of 3, 15, and 30 arc-seconds (Lehner et al., 2008) while as of 2024 there are plans to release a newer version of HydroSHEDS at a spatial resolution of 1 arc-second with improved 'stream-burning' and improved delineation of drainage pathways (HydroSHEDS, 2024). A HydroSHEDS DEM at 1 arc-second (approximately 30 m at the equator) may be of interest to researchers working in the water harvesting sector as it should offer improved mapping of in-stream networks compared to other commonly used DEMs also having a spatial resolution of 30 m (e.g. ASTER GDEM).

### **Evidence-based recommendation**

For hydrology and water harvesting research, DTMs are generally preferable over DSMs as they provide bare-earth elevation data, enhancing overland flow modelling. LiDAR-based DEMs offer superior spatial and vertical resolution, capturing both terrain and vegetation data. Researchers should consider not only spatial resolution but also vertical resolution, ensuring the elevation drop per pixel is sufficient for reliable hydrological modelling. HydroSHEDS, derived from SRTM DEM with enhanced drainage representation, is a valuable alternative, with a planned 1 arc-second update potentially offering improved stream network delineation for water-related studies.

### **3.4.2 Climatic products**

#### **Evidence**

Climatic data, obtained from both remote sensing and non-remote sensing sources, were utilised throughout the review literature articles. A total of 166 studies utilised rainfall data to some degree. However, only a relatively small number of studies used climatic data derived from remote sensing data with the TRMM dataset product being the most widely utilised (**Table 3.3**). Frequently rainfall data, from *in situ* gauge observations, was obtained from a national body. In this literature review 64.6 % studies used rainfall data, comparable to a review carried out by Adham et al. (2016a) who found 27 of 48 studies (56.3 %) used rainfall data. From the review literature an example of rainfall data obtained from a national body is provided by Ibrahim et al. (2019) who gathered monthly rainfall data from the Ministry of Agriculture and Water Resources of the Kurdistan Region spanning 16 years measured at 15 meteorological stations and then used Inverse Distance Weighting (IDW) to interpolate the rainfall data across the study area in raster format.

Runoff is central to water harvesting and it is dependent on rainfall so it perhaps surprising that more review literature studies did not use rainfall data. Indeed, Adham et al. (2016a) stated that rainfall is

one of the three basic criteria for the technical suitability of water harvesting, along with slope and soil type. Researchers may wish to consider several issues prior to opting to use gauge-based rainfall data. Water harvesting commonly takes places in regions where there is a relatively low coverage of rainfall gauges. Should rainfall gauges exist there may be issues with missing or erroneous data or measurements have been discontinued after a period of station operation. Acquiring rainfall data from a national body might not be straightforward and may require obtaining the correct authorisations and making payments, which could lead to a complex and time-consuming process.

Satellite-derived rainfall datasets (e.g. TRMM) on the other hand offer extensive global coverage and are freely accessible. Even though rainfall is one of the three basic site suitability criteria (Adham et al., 2016a) this literature review shows that satellite-derived rainfall data is used less frequently than DEMs. An area for future research would be to explore the reasons why the take up and utilisation of climatic products (e.g. TRMM) is not more widespread in the water harvesting sector. Manipulating and analysing a climatic dataset is more involved compared to a digital elevation model (DEM). As an illustration, SRTM DEM can be acquired as a single GeoTIFF raster tile, while obtaining TRMM data necessitates the handling of Network Common Data Form (netCDF) file format (Mugo and Odera, 2019). Additionally, managing TRMM data is further complicated by the presence of multiple data arrays, stemming from the varying temporal resolutions, such as monthly, daily, and hourly intervals. Furthermore, there is often a significant disparity between the spatial resolutions of climatic products and other remote sensing products utilised in water harvesting studies. For instance, Al-Kakey et al. (2023) state that the spatial resolutions of the TRMM and DEM products used in the same study are  $0.25^\circ$  (approximately 27.75 km at the Earth's great circle) and 30 m, respectively. Consequently, the areal spatial coverage of the DEM product is 855,625 times higher in resolution than that of the climatic

product. Dealing with products of differing specifications, such as spatial resolution, is covered later in **Section 3.4.5**).

### **Evidence-based recommendation**

To enhance the uptake and utilisation of satellite-derived rainfall datasets (e.g. TRMM) for water harvesting studies, researchers should prioritise their adoption due to their global coverage, free accessibility, and suitability for regions with sparse or unreliable ground-based rainfall gauges. While gauge-based data may offer higher local accuracy, issues such as low gauge density, missing data, and bureaucratic challenges can limit their availability. The complexity of handling netCDF files and reconciling differences in spatial resolution between climatic and other remote sensing products may discourage researchers from using satellite-derived rainfall data. Future efforts should focus on improving data accessibility, developing user-friendly processing tools, and implementing capacity-building initiatives to encourage wider adoption in water harvesting studies.

### **3.4.3 Multi-spectral products**

#### **Evidence**

From the review literature articles, multi-spectral remote sensing products are commonly used to create LULC thematic layers. Examples include LULC layers created from Landsat multi-spectral products (e.g. Mahmoud et al., 2014; Mugo and Odera, 2019; Singhai et al., 2019) and Sentinel-2 multi-spectral products (e.g. Mahmood et al., 2020; Sutradhar et al., 2021; Gavhane et al., 2023). In essence procedures to create LULC thematic layers involve processing several bands from a multi-spectral product to create a map differentiating the land based on its use and cover.

However, an alternative to creating bespoke land cover map from a multi-spectral product for a particular study is use an existing land cover product. Gilić et al. (2023) undertook a review of six land

cover products (CGLS-LC100; ESA WorldCover; ELC10; S2GLC; ODSE-LULC; Dynamic World), while Congalton et al. (2014) undertook a review of four global land cover mapping products (GLC 2000; Glob Cover 2009; IGBP; UMD). Of the ten land cover products listed, only the ESA WorldCover product was employed in the 290 review literature articles, and just for one study (Forzini et al., 2022). This observation suggests that researchers prefer generating land use and land cover (LULC) maps from multi-spectral remote sensing products such as Landsat or Sentinel-2, rather than relying on pre-existing "off-the-shelf" land cover products. One a possible explanation could be the multi-faceted utilisation of multi-spectral remote sensing products. A multi-spectral RS product can be used to create not just LULC information but also other pertinent layers. For example, Singhai et al. (2019) in a study to locate rainwater harvesting zones, applied with a supervised classification methodology to a Landsat multi-spectral product to prepare a LULC layer as well as using the same Landsat product to identity lineaments.

Creating a localised LULC layer from a multi-spectral product can result in a map with a higher spatial resolution compared to some global land cover products. The global land cover products GLC 2000, GlobCover 2009, IGBP, and UMD have spatial resolutions of 1 km, 1 km, 1 km, and 300 m, respectively (Congalton et al., 2014). Meanwhile, Mohammad and Adamowski (2015) produced a land cover map from a multi-spectral Landsat product with a spatial resolution of 15 m. Also from the review literature, Forzini et al. (2022) adopted a different approach, using the ESA WorldCover global land cover resource at a spatial resolution of 10 m without the burden of processing, validating, and assessing the product accuracy — tasks that are associated with developing a bespoke LULC map directly from a multi-spectral product.

The choice of creating a bespoke (and typically localised) LULC layer from a multi-spectral remote sensing product over using an existing global land cover mapping product raises a debate about the

appropriateness of one method over the other. Both methods require validation via ground-truthing, but their accuracies vary. Congalton et al. (2014) concluded that the total accuracies of the global land cover products IGBP, GLC 2000, and GlobCover 2009 are 66.9 %, 68.6 %, and 67.5 %, respectively. Gutierrez Caloir et al. (2023), in a study with an aim similar to that of this thesis — to develop new toolboxes and enhance an existing methodology by creating spatial analysis tools within a geographic information system environment for the allocation of large-scale nature-based solutions (e.g. rainwater harvesting, wetland restoration, and natural riverbank stabilisation) — utilised several global land cover datasets (**Table 3.7**), detailing their spatial resolution, availability, source imagery, and accuracy.

**Table 3.7. Summary of open access land cover data features based on product information (from Gutierrez Caloir et al., 2023)**

description	spatial resolution (m)	global cover	source imagery	availability	accuracy (%)
Copernicus Global Land Cover	100	yes	Prova-V and Sentinel 2	2015–2019	75.43
ESRI 2020 Global Land Cover Map	10	yes	Sentinel 2	2020	86.0
ESA WorldCover (2020)	10	yes	Sentinel 2 and Sentinel 1	2020	74.4

Creating LULC maps from multi-spectral products gives researchers more control in terms of temporal analysis compared to global land cover maps. The repeat coverage provided by satellites acquiring multi-spectral data allows seasonal land cover analysis to be undertaken — a point highlighted by Gontia and Patil (2012) in the RL. Growing and dormant seasons are characterised by canopy variations (Tedela et al., 2007), and hence multi-spectral products can be used to determine the timeframe of either season.

Not all global land cover maps have a low spatial resolution. As previously mentioned, the ESA WorldCover global land cover mapping product offers a spatial resolution of 10 m, which matches the resolution that can be achieved when creating a LULC map using Sentinel-2 data (Debebe et al., 2023). Despite the convenience of using a global land cover product, even those with high spatial resolution (e.g. 10 m), the reviewed literature demonstrates a clear preference among researchers for generating bespoke LULC maps. Examples from the literature show that researchers frequently develop

customised LULC maps tailored to their specific study areas, achieving accuracies often superior to those of global datasets. With sufficient resources for ground-truthing, it is possible to accurately estimate a localised land cover map produced from a multi-spectral remote sensing product. For instance, Rai et al. (2018), Behera et al. (2019), Karmakar and Ghosh (2022), Mamin and Majeed (2022), and Odeh et al. (2023) reported overall accuracies for their bespoke LULC maps of 82.50–90.00 %, >83 %, 86.36 %, 89.6 %, and 80 %, respectively.

The thematic accuracy of global land cover products (despite gradually improving over time) is often lower compared to bespoke land cover products developed for smaller, region-specific areas. This disparity largely arises because global land cover products are designed to provide broad classifications across diverse environments, which can result in oversimplifications, especially in heterogeneous landscapes. Their thematic classes are typically more generalised to ensure global applicability, making them less effective at capturing finer details and local variations in land cover. In contrast, bespoke land cover products, created for smaller areas, are tailored with higher-resolution imagery and often incorporate local knowledge, resulting in greater thematic accuracy. These customised LULC maps are more adept at distinguishing between similar land cover types and capturing subtle landscape features, as they can utilise detailed ground-truth data. Nevertheless, the creation of such customised products can be resource intensive.

Global LULC products may therefore be more suited to regional and worldwide studies, at least until global land cover products improve further. Using multi-spectral remote sensing products also provides researchers with the flexibility to examine temporal changes in land cover within the study area and enables customised land cover classification to address specific requirements.

### **Evidence-based recommendation**

Before generating a study-specific Land Use and Land Cover (LULC) map from multi-spectral products, researchers should evaluate the suitability of pre-existing global land cover mapping resources (e.g. ESA WorldCover, ESRI 2020 Global Land Cover Map). These resources, particularly those with high spatial resolutions (e.g. 10 m), offer convenience, global coverage, and acceptable accuracy (e.g. 74.4–86 %), reducing the need for resource-intensive processing and validation. However, for studies requiring finer thematic detail, temporal analysis, or higher accuracy (>80 %), bespoke LULC maps derived from multi-spectral products (e.g. Landsat, Sentinel-2) may be preferable, despite the additional effort. Researchers should weigh factors such as spatial resolution, thematic accuracy, temporal flexibility, and resource availability when deciding between pre-existing global products and bespoke LULC maps.

### **3.4.4 Single-band / Panchromatic / Dual-band / Minimal-band products**

#### **Evidence**

The review of the literature provides numerous examples of more than one thematic layer being created from the same remote sensing product. For instance, Othman et al. (2020) used 23 high spatial resolution QuickBird scenes, captured by satellite over a five-day period, to ascertain the stream width for discharge estimation. They also used the same remote sensing product for training and validating datasets for the purpose of land cover classification. Similarly, Mukherjee and Singh (2020) created five separate thematic layers, all from the same DEM: roughness, curvature, drainage density, slope, topographic wetness index (TWI), and topographic position index (TPI). The TPI compares the elevation of each DEM pixel to the mean elevation of a specified selection of neighbouring pixels (Weiss, 2001).

As previously mentioned, DEMs are often used to model in-stream flow. However, the accuracy of the modelled stream network depends on the suitability of the DEM used. Some techniques used to produce DEMs simultaneously obtain geo-referenced imagery, which can be used to assess the accuracy of the modelled stream channels and allow adjustments to the DEM to improve how well the modelled stream network represents the real world. While SPOT can be used simply as satellite imagery (Elewa et al., 2023), Ouessar et al. (2009) used a SPOT stereo pair to create a DEM and then removed some modelled channels to match the actual occurrence of streams as observed on the SPOT image.

Of the 290 review literature articles, the authors of 17 stated that Google Earth played a role in their research methodology. While this is a relatively small number compared to other remote sensing products used in the reviewed literature (**Table 3.4**), its applications are diverse. Kar et al. (2021) generated random points across Google Earth images, extracted elevation data for each point, and then applied Inverse Distance Weighting (IDW) to generate a continuous elevation surface, enabling the creation of a digital elevation model. Google Earth imagery was utilised to refine stream networks that had been created through the digitisation of topographic maps (Rejani et al., 2017). Soni et al. (2022) introduced a “simple and novel” approach to estimating runoff. They devised a methodology that utilises the colour of individual pixels in Google Earth satellite images to estimate a corresponding runoff coefficient. Soomro et al. (2022) employed Google Earth to delineate the boundaries of the study area by generating shapefiles. Rai et al. (2018) intentionally depended exclusively on satellite-based remote sensing products, which included utilising Google Earth, in a watershed study to showcase the effectiveness of satellite technology. Nine studies from the review literature were noted to have incorporated Google Earth as a component of their land use and land cover (LULC) classification methodology (Grum et al., 2016; Rai et al., 2018; Mahato and Pal, 2019; Roy et al.,

2019; Ahirwar et al., 2020; Pathak et al., 2020; Abdelkebir et al., 2021; Kar et al., 2021; Alem et al., 2022), frequently during the validation phase of the process.

In the reviewed literature, particularly studies focused on site suitability, thematic layers are frequently used (e.g. Buraihi and Shariff, 2015; Mugo and Odera, 2019; Ajibade et al., 2020; Mamin and Majeed, 2022). There are many instances where researchers have created more than one thematic layer from a single remote sensing product. There are a number of advantages of creating different thematic layer from a single remote sensing product as opposed to creating each thematic layer from a different remote sensing product.

One key advantage of creating multiple thematic layers from a single remote sensing product is the consistency in resolution and coverage. Since these layers originate from the same data source, they maintain uniform spatial resolution, temporal coverage, and data quality. This uniformity ensures that the layers are directly comparable, minimising discrepancies and reducing the risk of errors or biases in the analysis. Also, if the remote sensing product is a time-series dataset, creating multiple thematic layers over time allows for change detection and trend analysis. This can be critical for understanding how site conditions have evolved, aiding in predicting future suitability. In summary therefore the capacity to generate multiple thematic layers, relevant to the aim of the study, from a single remote sensing product is advantageous and should be carefully considered when developing the research methodologies.

### **Evidence-based recommendation**

To optimise the number of useful thematic layers generated from a single remote sensing product, researchers should prioritise extracting multiple relevant layers from the same dataset. This approach ensures consistency in spatial resolution, temporal coverage, and data quality, reducing discrepancies

and minimising errors in analysis. Additionally, leveraging a single remote sensing product for multiple layers enhances efficiency, facilitates change detection, and supports trend analysis, making it a valuable methodological consideration in remote sensing studies.

### 3.4.5 Fusion of products

#### Evidence

While it can be advantageous to create multiple thematic layers from the same remote sensing product, as outlined in the previous section, researchers often need to use several sources of information, including different remote sensing products, to generate the thematic layers required to meet the study’s objectives. A review literature provides numerous examples of this practice.

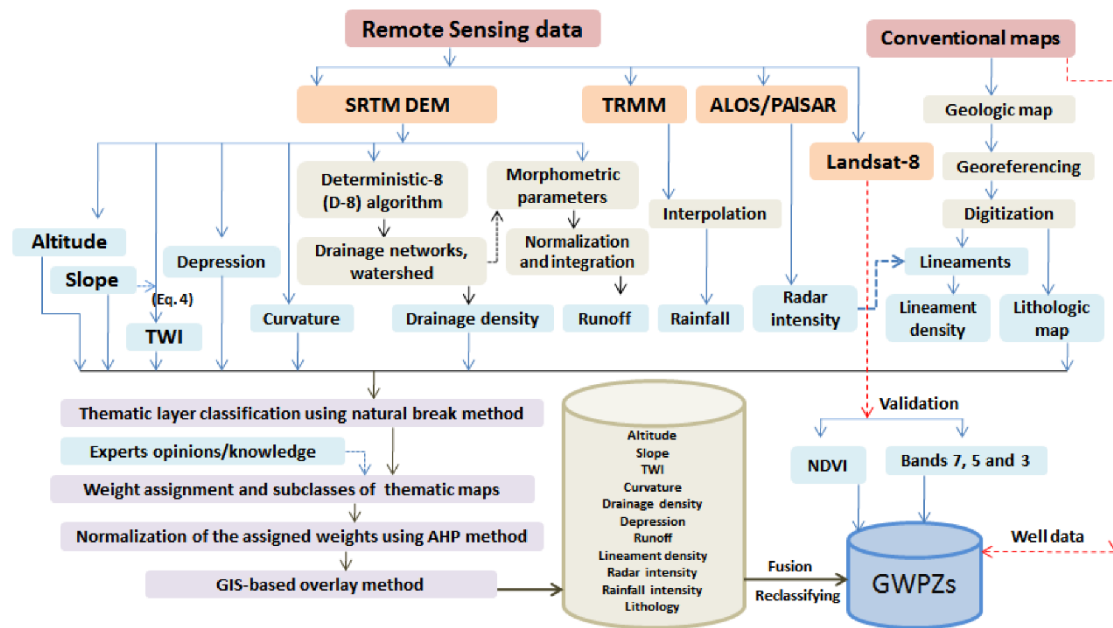


Figure 3.4. Flow chart showing sources of data to create thematic layers prior to fusion (from Abdekareem et al., 2022) [GWPZs, groundwater prospective zones].

Al-Hasani et al. (2023) utilised several data sources, including an SRTM DEM product with a spatial resolution of 30 m, a conventional soil map, precipitation data from the Long Ashton Research Station Weather Generator, and annual land cover maps derived from Sentinel-2 imagery with a 10 m spatial

resolution. From these datasets, six thematic layers were created: rainfall, runoff depth, slope, soil texture, drainage density, and land use/land cover (LULC). Fusion of these layers was necessary before applying a weighting methodology.

The examples provided by Abdekareem et al. (2022) and Al-Hasani et al. (2023) are representative of many studies in the RL. Typically, thematic layers are created from various sources. Some layers originate from the same source, while others come from different sources. In some cases, layers rely on more than one source. **Figure 3.4** illustrates this point. This figure, provided by Abdekareem et al. (2022), shows through a flow diagram, how eleven thematic layers were generated from four different remote sensing products (SRTM DEM, TRMM, ALOS/PALSAR, Landsat) and conventional sources (geology map and well data). To aid analysis, these thematic layers must be integrated — a process known as 'fusion' — which produces more consistent, accurate, and valuable information than analysing each layer separately.

The fusion process may involve integrating data with different resolutions (both spatial and temporal) and spectral bands. The more remote sensing products used to create the thematic layers, the more challenging fusion becomes, given the greater variety of resolutions and spectral bands. There are numerous fusion techniques available, and this number is likely to expand given the ever-increasing range of sensors being deployed. However, the RL details some specific fusion techniques used by authors. Al-Ghobari et al. (2020) used a pan-sharpening technique to produce high-resolution multispectral images (with a spatial resolution of 15 m) by combining images of different spatial resolutions. Mamin and Majeed (2022) also applied a pan-sharpening technique to change the spatial resolution of images. Moawad (2013) applied the cubic convolution method to enhance edges and improve stream extraction. Cubic convolution resamples discrete data using an interpolation technique (Keys, 1981).

### **Evidence-based recommendation**

When merging multiple thematic layers from different remote sensing products, researchers should carefully assess the implications of variations in spatial resolution, temporal coverage, and spectral characteristics. Selecting appropriate fusion methodologies, such as pan-sharpening or cubic convolution, can enhance data consistency and improve analytical accuracy. Given the growing diversity of remote sensing sensors, researchers should evaluate the suitability of available fusion techniques to ensure the optimal integration of multi-source data for their specific study objective.

## **3.5 Summary and conclusions**

This chapter reviewed 290 peer-reviewed articles related to the subject of 'water harvesting', focussing on the adoption and utilisation of remote sensing products. It found that remote sensing products are extensively used, particularly in more recent academic studies. For example, in studies published in 2023, approximately 92 % of all reported methodologies utilized remote sensing products to some degree.

The approach researchers take in their utilisation of remote sensing products varies, with some combining remote sensing data with more traditional sources of information, while others rely solely on remote sensing (e.g. Rai et al., 2018). The degree of manipulation of the remote sensing data by researchers also differs. In some cases, the remote sensing product does not require any processing, such as in the visualisation of satellite imagery, while in other cases, researchers extensively manipulate the data to create a specific product. An example of this is Ouessar et al. (2009) building a DEM from a remote sensing product consisting of stereo pair images.

It was found that the remote sensing products used across the 290 studies could be classified into the following groups: 'elevation models,' 'climatic,' 'multi-spectral,' 'RGB,' and 'composite' groups. **Figure**

**3.5** provides examples from the 290 studies, featuring one from each of these groups, and illustrates how the products were utilised by the respective researchers. Notably, this review demonstrates a strong demand for DEMs among researchers, with globally and freely available DEMs being particularly popular (e.g. SRTM DEM and ASTER GDEM).

Evidence suggests a demand among researchers for DEMs with higher spatial resolution than these global DEM products (i.e. 30 m). While higher spatial resolution DEM products offer greater detail, they have the drawbacks of requiring increased computational resources and often entail additional expenditure for acquisition.

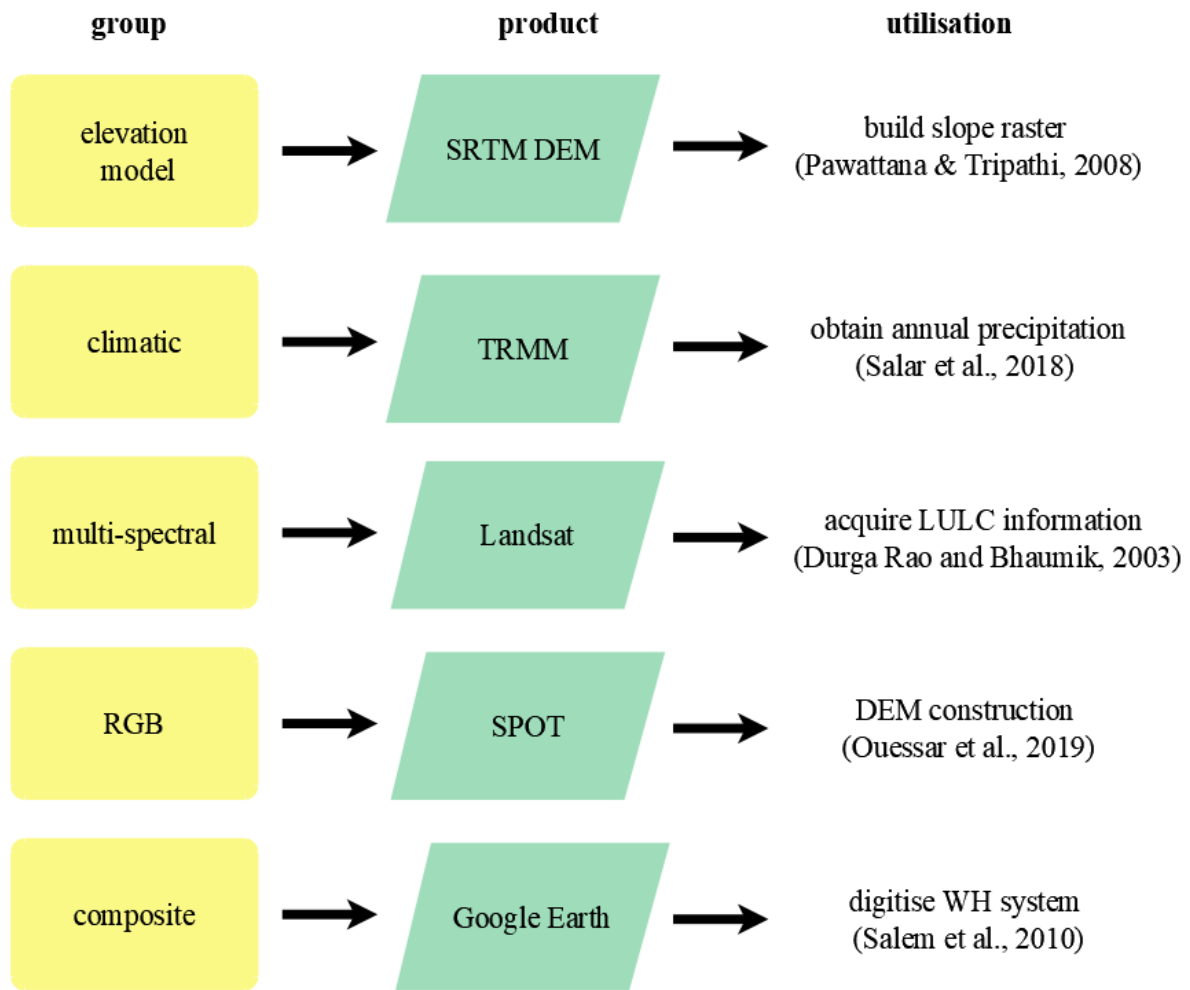


Figure 3.5. Examples of remote sensing product utilisation, with name of product and group classification.

In dryland regions, where water harvesting is widely practised, obtaining rainfall data is often challenging. While this review found examples of researchers using climatic datasets derived from remote sensing (e.g. Yousif and Bubenzer, 2015; Mugo and Odera, 2019; Alwan et al., 2020), it did not find evidence of significant adoption of such datasets. Instead, researchers typically rely on *in situ* gauge-based measurements or do not incorporate rainfall data into their methodologies. Given the importance of rainfall in relation to water harvesting, this suggests a need for greater adoption of climate-related remote sensing products by researchers.

This review found that multi-spectral remote sensing products are popular for creating bespoke land LULC maps. Scant evidence was found for the uptake of global and regional LULC datasets, suggesting that bespoke LULC maps made from multi-spectral remote sensing products offer advantages in terms of greater flexibility and superior pixel differentiation compared to global and regional land cover products.

Some of the remote sensing datasets identified among the 290 articles that comprised the RL, are also used in this thesis. The most obvious example is the utilisation of SRTM DEM products, used 91 times in the RL (see **Table 3.4**). The 1 arc-second SRTM DEM (~30 m spatial resolution) product is used in **Chapter 4** while the SRTM DEM 3 arc-second (~90 m spatial resolution) at global coverage is utilised in **Chapter 4**, **Chapter 5**, and **Chapter 6**. Global climate datasets, notably TRMM, have been utilised by researchers in the RL. Although TRMM is not used for any original research in this thesis, another climate dataset, GPCC, is employed in **Chapter 5**, and **Chapter 6** for the purpose of acquiring precipitation data. The RL also provides examples of LiDAR data usage. **Chapter 4** details how LiDAR was utilised to produce a high-resolution DEM.

Finally, water harvesting studies typically utilise thematic (or predictive) layers to differentiate between low-interest and high-interest zones. These layers often originate from various sources, including different remote sensing products and conventional sources (e.g. maps). The fusion of these layers to facilitate the decision-making process is, therefore, an important topic — one that may gain even greater significance as spatial and temporal resolutions continue to improve. An inference from this is that researchers should aim to maximise the number of relevant thematic layers extracted from a single remote sensing product, while minimising the total number of remote sensing products used in a study, to achieve satisfactory results in line with the study's aims.

# 4 SiteFinder: A geospatial scoping tool to assist the siting of external water harvesting structures

## 4.1 Abstract

Water harvesting has a long history, but still plays an important role today by increasing crop productivity, combatting erosion, and improving water supplies. Geographical information systems (GIS) are used extensively to assess the suitability of sites for water harvesting but available tools fail to consider the synoptic topography of sites. Here, we report the creation of a novel, automated tool – “SiteFinder” – that evaluates potential locations by automatically calculating site-specific information, including parameters of the harvesting structure (height, length, and volume) and descriptors of the zone affected by the structure (storage capacity and area of influence) and the catchment area. Innovatively, compared to existing tools of this kind, SiteFinder works within a GIS environment. Thus, it facilitates combining its outputs with larger Multi-Criteria Decision-Making processes to consider other bio-physical, socio-economic, and environmental factors. It utilises a Digital Elevation Model (DEM) and automatically analyses thousands of potential sites, computing site characteristics for different barrier heights that are dependent on the surrounding topography. It outputs values of parameters related to the water harvesting structure and the zone flooded upstream of the structure, to aid planners in assessing the characteristics of sites as to their suitability for water harvesting. We conducted case studies using 30 m × 30 m gridded DEMs to automatically evaluate several thousand sites and, by filtering the tool outputs, successfully identified sites with characteristics appropriate for scenarios at three spatial scales: nationally significant water supply reservoirs (383 sites analysed; 5

filtered sites for potential large dams, with barriers up to 30 m in height); erosion control structures for regional-scale interventions (4,586 sites analysed; 6 filtered sites for potential large gully erosion dams, with barriers up to 3.6 m in height); and local, community-based projects (801 sites analysed; 6 filtered sites for potential earth embankment dams, with barriers up to 2 m in height). A higher resolution (1 m x 1 m) terrain elevation model, derived from open-source airborne survey LiDAR data, was used to assess the veracity of these results. Correlations between the barrier length, impounded area and storage volume capacity derived from the two different resolution data sets were all strongly significant (Spearman's rank correlation,  $p < 0.001$ ); and normalised root mean square errors were 9 %, 15 % and 16 % for these parameters, respectively.

## 4.2 Introduction

There is evidence that civilisations constructed water harvesting structures over four millennia ago (Evanari et al., 1971 cited in Critchley and Siegert, 1991), yet water harvesting continues to be widely used and the focus of ongoing research (Abdullah et al., 2020; Adham et al., 2019; Farswan et al., 2019; Haile and Suryabhagavan, 2019). It is practised primarily in arid and semi-arid regions (Bruins et al., 1986; Boers, 1994; Wang et al., 2008) where it is valuable as a way of bridging dry spells (Rockström and Falkenmark, 2015) and has been estimated to have the potential to increase crop production by up to 100 % (Piemontese et al., 2020). Depending on the location and design, water harvesting structures can serve different purposes, for example for the promotion of tree or crop cultivation (Mekdaschi-Studer and Liniger, 2013), artificial recharge of aquifers (Abdalla and Al-Rawahi, 2013; Şen et al., 2013), erosion control (Li et al., 2018), surface water storage (Sayl et al., 2019), or sub-surface water storage (Forzieri et al., 2008). Some form of water treatment (AWWA, 2006; Logsdon, 2008; Siabi, 2008; Panagopoulos, 2021) will probably be required when harvested

water is intended for domestic/industrial use, with the type of treatment dependent on the water quality problem (Cairncross and Feachem, 1993; Binnie et al., 2018).

Water harvesting structures vary from small pits or soil bunds made using hand tools, to earth embankments over a kilometre in length built with the aid of machinery. All water harvesting structures aim to reduce runoff and thus increase water storage. Depending on the technique implemented, water storage may take place in the soil, below the surface within introduced material such as sand, in surface water reservoirs or in storage tanks. Water harvesting techniques are described as ‘external’ when they collect water originating from rainfall that has fallen elsewhere, while ‘*in situ*’ water harvesting involves collecting rainfall on the surface where it falls (Helmreich and Horn, 2009).

Many previous studies have used geographical information systems to find potential locations for water harvesting structures without the need for field visits (e.g. Padmavathy et al., 1993; Al-Adamat, 2008; Ziadat et al., 2012; Kadam et al., 2012; Krois and Schulte, 2014; Al-Khuzai et al., 2020). These methods invariably bring together different datasets, from remote sensing and digitised maps, often combined with hydrological modelling, and explore the decision-making space within the GIS environment.

When deciding if a location is appropriate for water harvesting there are numerous biophysical and socio-economic criteria to consider. In a review of 48 studies, Adham et al. (2016a) identified nine biophysical criteria and nine socio-economic criteria that can be used to help assess the suitability of potential sites for water harvesting. Examples of biophysical criteria include rainfall (Adham et al., 2016a), and drainage network metrics (Salih and Al-Tarif, 2012), while examples of socio-economic criteria include population density (Mati et al., 2006), and distance to crops (de Winnaar et al., 2007). Adham et al. (2016a) found that slope was the most common biophysical criterion used to identify

water harvesting sites with 79 % of all studies using slope as a criterion while only 55 % of all studies used rainfall as a criterion. In all studies the slope data used is defined on a point-by-point basis, with flatter locations being identified as preferential for water harvesting locations. However, slope defined on a point-by-point basis does not consider the ‘synoptic topography’, or surrounding relief, which is crucial for identifying the potential of water harvesting locations. Moreover, while it may offer relevant information on the suitability of potential sites, it fails to provide the dimensions of necessary impounding structures (bunds or embankments) and the storage geometry they would create.

Automated tools working outside a GIS environment have been developed that consider the synoptic topography of potential sites and provide details of impounding structures and storage zones. For example, Petheram et al. (2017) developed a novel set of algorithms, named 'DamSite', to aid dam site selection by simulating virtual dam walls at each pixel along a river network within a catchment. The algorithm iterates through incremental dam heights to calculate storage capacity, yield, and cost, identifying optimal dam locations and heights. It relies on a DEM to extract geometric parameters, a D8 flow network, and gridded time-series runoff data to estimate water availability. However, its accuracy is limited by DEM artefacts and errors in the drainage network. Moreover, it can only evaluate dams individually, preventing the identification of optimal dam site combinations, and is unsuitable for very small basins (Teschmacher et al., 2020). The method proposed by Wimmer et al. (2019) automates the identification of potential reservoir sites by analysing contour lines to detect terrain features suitable for dam construction. It uses parallel shifts to identify self-intersecting contour segments that enclose retention areas and relies on a DTM with predefined dam length constraints. The approach assumes a single vertical dam per polygon, disregards terrain stability and hydrological factors, and requires careful selection of input parameters to ensure suitability for the given project scope. They used the point cloud processing software OPALS, storing outputs in a GIS vector dataset;

however, their results do not include details of barrier volume and catchment area. Teschemacher et al. (2020) describe an open-source MATLAB tool that automates the detection, characterisation, and evaluation of retention and detention basin locations using numerical DEM analysis to determine optimal dam orientation, geometry, and basin volume. The tool requires DEM raster data, user-defined dam and basin characteristics (e.g. length, height, volume), and additional input data (e.g. land use, hydraulic conductivity, groundwater levels). It employs a flexible methodology adaptable to different site demands but currently lacks integrated environmental, social, and economic assessment criteria. Users must manually incorporate all relevant criteria (e.g. settlement areas) to identify the most suitable sites. Wang et al. (2021) reviewed dam siting methods and found that the majority were GIS-based, so it is argued that the siting tool introduced in this paper, which operates entirely within a GIS environment, will be of value to those involved in water harvesting site selection.

Open-source Digital Elevation Models (DEMs) are commonly used in selecting water harvesting sites. Typically, those used have a gridded resolution no finer than  $30\text{ m} \times 30\text{ m}$ . Higher resolution DEMs are available, but usually at a significant cost, which can often be prohibitive. Schumann and Bates (2018) argued for freely available DEMs with global coverage, higher resolution and increased accuracy, as open source DEMs are poorly suited for many local-scale hydrologic applications. However, higher spatial resolution brings with it a problem for methods based on point-by-point defined variables in that the higher the resolution, the smaller each pixel becomes in relation to the land affected by a water harvesting structure. Thus, while there is an incentive to use higher resolution DEMs for enhanced hydrologic modelling this reduces the appropriateness of methods that rely on parameters defined on a point-by-point basis, such as the slope variable identified by Adham et al. (2016a), that have been widely used hitherto.

The aim of the present study has been to provide a bridge between the point-based slope criteria calculated in a GIS environment adopted by many researchers for water harvesting site selection and the automated methods that consider the surrounding topography of potential sites but work outside a GIS environment (Petheram et al., 2017; Wimmer et al., 2019; Teschemacher et al., 2020). This was approached by creating a GIS tool – “SiteFinder” – that can aid the siting of water harvesting structures by considering the synoptic topography of potential sites. The intended output of this approach is information about the length and height of potential impounding structures (barriers, hereinafter), and details of the areas of water storage they could create upstream of themselves. In essence, this is a similar approach to existing methods used to estimate the storage capacity of ponds (USDA, 1997) and small dams (Stephens, 2010) in so much as the area of water storage and the barrier height are used to compute predicted storage volume. The tool was designed to calculate the catchment area of each water harvesting structure since there is a correlation between catchment area and runoff efficiency (Karnieli et al., 1988; Boers and Ben-Asher, 1982), and the catchment area to cultivation area ratio is important for water harvesting sites designed for crop production (Critchley and Siegert, 1991). Finally, the tool was developed such that for every location analysed as a potential site for water harvesting, several barrier heights could be considered, up to a user-defined maximum height.

In summary the aim was to create an automated process capable of providing information on barrier size and water storage volumes for potential water harvesting sites that is not at present readily available within the convenient and widely used context of a GIS environment. The intention is that this could assist with scoping out potential sites, with an accuracy sufficient for the pre-feasibility stage of a project cycle. It is envisaged that this would need to be used alongside other biophysical, socio-economic and environmental information as part of decision-making processes.

## 4.3 Materials and methods

### 4.3.1 Tool development

The basic premise of SiteFinder is to take a basin elevation model and for each site of interest, compute the catchment area, create an imaginary axis perpendicular to the flow direction and perform analysis based on how the axis intersects with the model surface for varying heights above the elevation of the site. Tool outputs were compared against those derived manually using a dam site ground survey, and in addition, the tool was used to evaluate thousands of sites and rank them based on relevant parameters. The starting point for the developed tool is a raster-based Digital Elevation Model (DEM), which provides the primary source of elevation data. Clearly, the capability of the tool is in part dependent on the quality and resolution of the DEM used. This is considered further below, but it is described here with reference to a generic DEM, of no specific quality or resolution. SiteFinder is enacted using an ArcPy script within ArcGIS Pro. Through a series of steps, described below, it processes the DEM and creates outputs comprising information on the barrier (length, height, location, and orientation), the storage area the barrier would create, and the volume of the storage created.

Firstly, since the DEM may contain imperfections, a fill tool is used to remove any ‘sinks’ (spurious regions of lower elevation). The next step creates a flow direction raster (**Figure 4.1**, “flow direction”) using the ‘filled’ DEM as the input. Flow direction is defined as the direction from each cell to the steepest downslope neighbouring cell. The flow direction raster is then used to produce a flow accumulation raster (**Figure 4.1**, “flow accumulation”), where flow accumulation is defined as the number of cells that flow into each downstream cell. Subsequently, only cells in the flow accumulation raster with values that fall within a range defined by the user prior to running the tool (based on the minimum and maximum catchment areas) are kept, while other cells are set to ‘no data’. The amended flow accumulation raster, which effectively represents a stream network, is then used, together with

the flow direction raster, to create a stream order raster (**Figure 4.1**, “stream network / stream order”), which classifies each cell using Strahler stream ordering, whereby the uppermost, headwater channels in a network are denoted first order, second order streams are those that result from the confluence of two or more first order streams; third order streams are those that result from the confluence of two or more second order streams, and so on, such that the largest, trunk channels in a network have the highest order (Strahler, 1957). The next step is to create siting points (**Figure 4.1**, “siting points”) by creating a point located at the centre of every cell in the stream order raster. By default, all cells in the stream order raster become siting points but it is possible for the user to control which stream order cells become siting points.

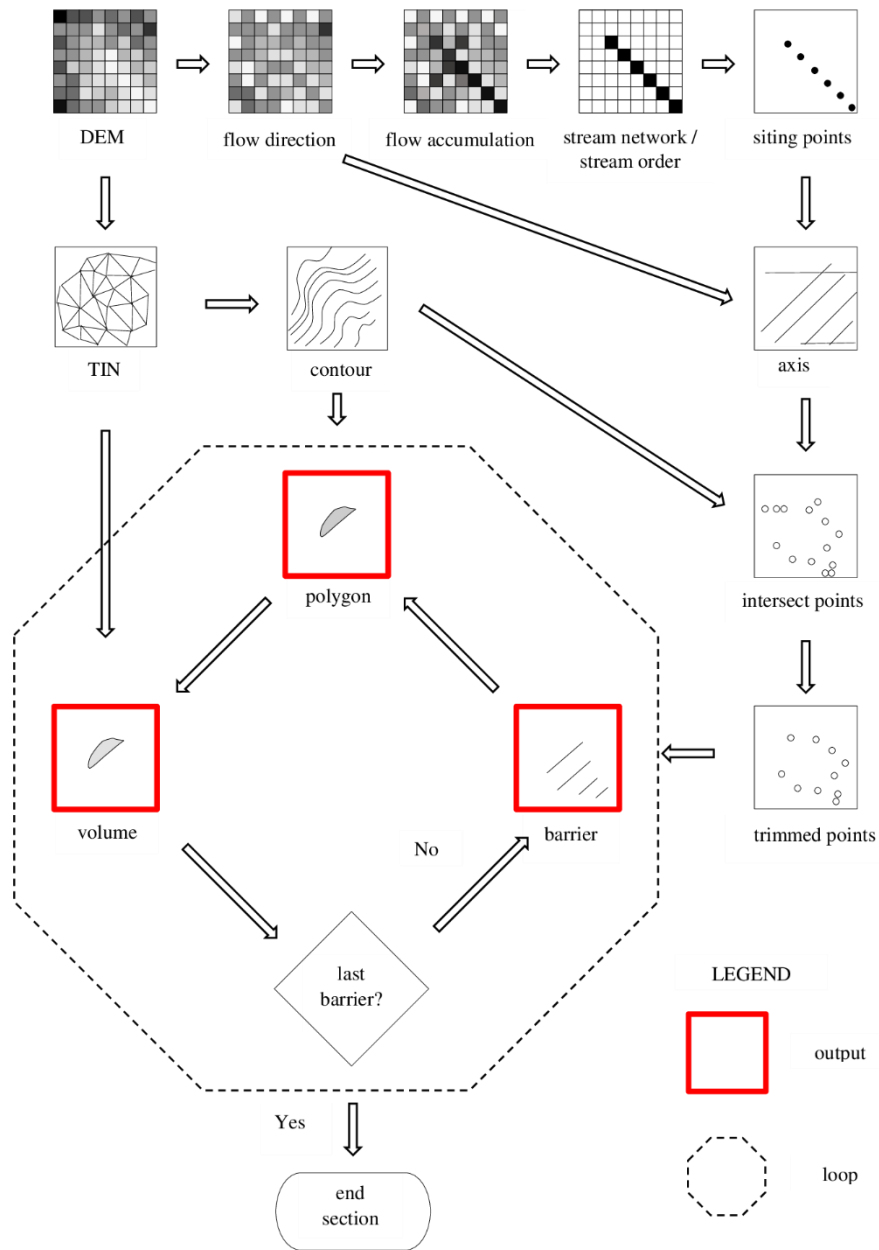
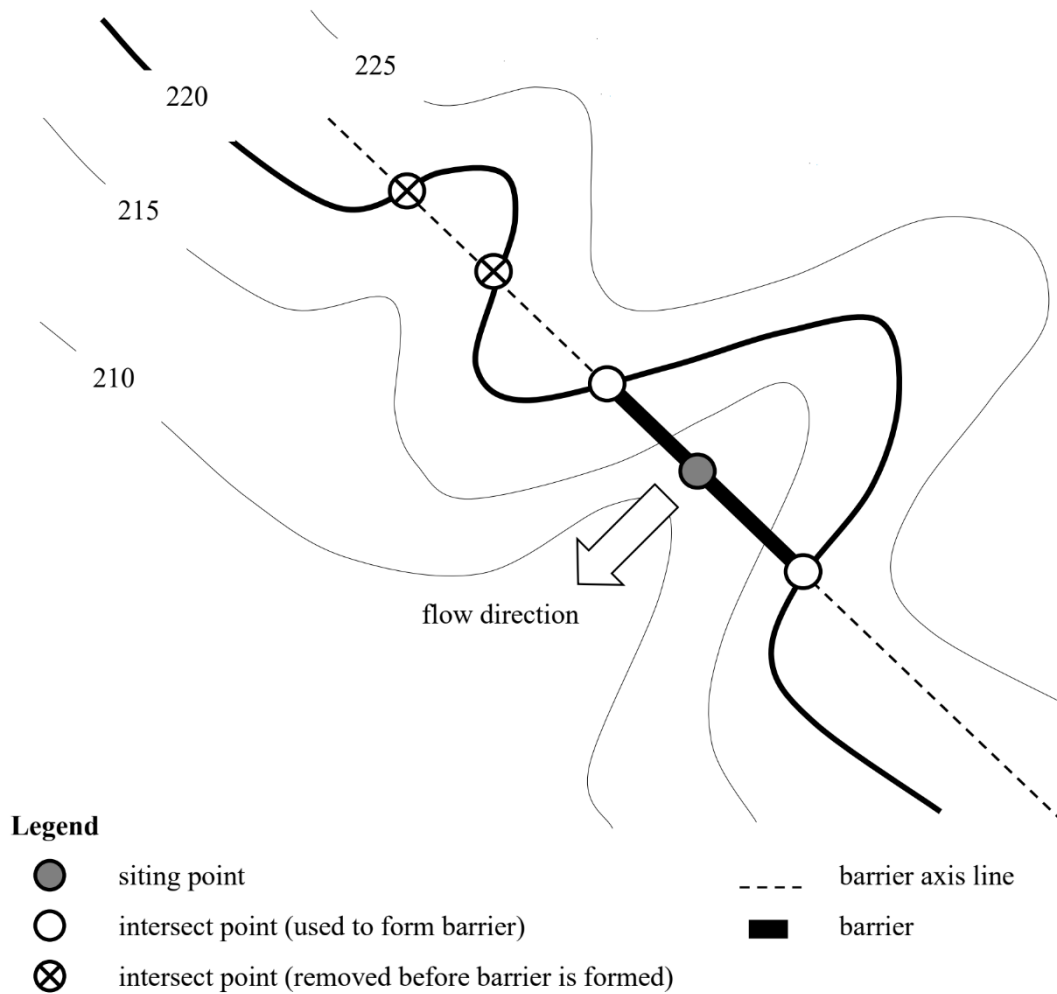


Figure 4.1. Overview explaining how a DEM is used to obtain script outputs of polygons and volumes.

Barrier information is then calculated and added to the siting points database. At every siting point, the SiteFinder script will, if the topography allows, create three barriers at different elevations, labelled A, B and C in order of increasing elevation. The user-defined maximum barrier height is used to calculate the barrier elevations. First, the maximum height is divided by three, and the result is rounded to the nearest integer. This integer, measured in units of the DEM elevation dataset, represents the step change in elevation between each barrier. Barrier elevations are then calculated by rounding up the DEM elevation at the siting point and adding the step change. For example, if the user enters a maximum barrier height of 10 m and the elevation at the siting point is 576.9 m then the first barrier (Contour A) elevation will be 580 m ( $577 + 3$ ), the second barrier (Contour B) elevation will be 583 m ( $577 + 6$ ) and third barrier (Contour C) elevation will be 586 m ( $577 + 9$ ).

The barrier axes pass through the siting point, with their direction set perpendicular to the siting point cell's flow direction and their length equal to half the (user-defined) maximum barrier length on each side of the siting point (**Figure 4.2**).



**Figure 4.2. Schematic showing the principal components of barrier creation.**

To determine the length of the top of each barrier, and subsequently the area of water they could impound, the points at which the barrier meets the ground needs to be determined. This requires putting the barrier axis direction into the context of the ground’s topographic contours. To achieve this, the DEM is used to create a Triangulated Irregular Network (TIN) (Figure 4.1, “TIN”) elevation surface, from which a surface contour (Figure 4.1, “contour”) shapefile is derived. The points at which the top of each barrier intersects the ground are then determined by intersecting the axis shapefile with the contour shapefile, producing intersect points (Figure 4.1, “intersect points”) that are taken as the start and end points of the barrier. Each intersect point is linked with its associated siting point and barrier

elevation (A, B or C) by a ‘contour label - siting point’ reference that is added to the intersect points database. Creation of barrier lines then requires locating two intersect points with identical ‘contour label - siting point’ references on either side of a given siting point (**Figure 4.2**).

The first of several scenarios that may be encountered in this process is that there is no intersect point created for a siting point at an elevation corresponding to any of the barriers A, B or C. This will occur if the land is too planar and the top of the proposed barrier would not meet the surrounding land within half of the user-defined maximum barrier length from the siting point. The second scenario is that an intersect point is unique in that there is no other intersect point with the same ‘contour label - siting point’ reference. This case corresponds to the situation where the barrier top meets the ground as the latter rises up on one side of the siting point, but the land is too planar, or descending, for this to happen within the maximum barrier length on the other side. If either of these two scenarios occur, the site is rejected. The third scenario is that exactly two intersect points with the same ‘contour label – siting point’ reference are found, one on each side of the siting point and the site is identified as a potential water harvesting site. The final scenario is that more than two intersect points exist each having the same ‘contour label - siting point’ reference. In these final cases, SiteFinder identifies multiple intersect points (with identical ‘contour label – siting point’ references) on the same side of the siting point and deletes the more distant ones. The remaining intersect points are referred to as ‘trimmed points’ (**Figure 4.1**, “trimmed points”), and these sites are also thus identified as potential water harvesting sites.

The next step is to create a line representing the top of each barrier. This is done using a points-to-line tool, which uses the ‘contour label - siting point’ references to create a straight line running from one intersect point, through the siting point to the corresponding intersect point on the other side. If for any siting point there is no intersect point or just a single intersect point at an elevation corresponding to

A, B, or C then no barrier is formed since to create a line requires two identical ‘contour label -siting point’ references. Since any more distant intersect points have been deleted, barrier lines can only be formed using the two trimmed intersect points, one on either side of each siting point. These lines are stored as barrier shapefiles (**Figure 4.1**, “barrier”).

Once the barrier lines have been created, SiteFinder then begins a loop, processing one barrier at a time. A polygon (**Figure 4.1**, “polygon”) shapefile, representing the area of potential water storage that each barrier would impound, is created by combining the barrier line with a contour line that has the same contour identification reference as held in the barrier attribute field. This polygon is intersected with the TIN surface (**Figure 4.1**, “TIN”) to obtain the volume (**Figure 4.1**, “volume”) impounded by each barrier. For this to work, each polygon is assigned an elevation value set to the elevation of the top of the barrier with which it is associated.

The loop process ends once every barrier has been analysed. The polygons are then checked for artefacts created by closed contour lines, which result in more than one polygon per barrier. Artefacts are removed by calculating the distance of each polygon centroid to the barrier and removing all polygons except the nearest. The barrier shapefile is updated with the correct storage area and volume, and secondary raster information from the polygon feature class. Each row in the barrier feature class represents a unique barrier and is linked to a unique polygon by a barrier reference.

An estimation of the height of each water harvesting structure is carried out by taking the elevation of the barrier and subtracting the lowest elevation under the barrier profile on the TIN surface. In a similar manner the flow accumulation for each structure is found by extracting the maximum flow accumulation value along the barrier line. Elementary information contained within the barrier feature class is used to calculate additional parameters (for example, catchment area to storage volume ratio)

useful for water harvesting site selection. **Equation 4.1** is used to calculate the barrier volume (i.e. the volume of material that makes up the barrier) based on the geometry of a small earth dam (Nissen-Petersen, 2006), where  $V$  is the barrier volume ( $m^3$ );  $H$  is the maximum height (m) of the barrier before settling;  $L$  is the length (m) of the barrier crest;  $C$  is the width (m) of the crest; and  $S$  is the sum of the upstream and downstream slope. To simplify the comparison of results the crest width was fixed at 0.25 m and the sum of upstream and downstream slopes fixed at 5.5 (aligning with a Nissen-Petersen (2006) worked example of dam design) for all case study scenarios.

$$V = 0.216 HL(2C + HS) \quad (4.1)$$

### 4.3.2 Geometric validation of SiteFinder

To check that the fundamental geometrical aspects of the process described above were functioning as intended, results produced by SiteFinder from a Shuttle Radar Topographic Mission (SRTM) void-filled, 3 arc-seconds (approximately 92 m grid resolution) DEM of an area in Sudan (**Figure 4.3a**) were compared against results obtained manually using elevation data from an *in situ* Differential Geospatial Positioning System (dGPS) dam site survey (Mohammed, 2018). The SRTM elevation data (EROS, 2018c) was selected as it is open-access, and the scale of the existing dam is far greater than a single 3 arc-second grid cell. The site is characterised by low-to-medium relief and SRTM products are considered to have small vertical errors in such circumstances. For example, Falorni et al. (2005) describe a low-relief site as having a mean vertical error of 0.36 m when SRTM elevations were compared with GPS elevations.

Before starting the processing, a comparison of elevations between the SRTM data (**Figure 4.3b**) and the dGPS survey points was undertaken to establish the presence of any systematic vertical offset. A plot of SRTM elevation against the corresponding elevation from the dGPS survey (**Figure B1**,

**Appendix B)** confirmed the presence of such an offset. The linear regression formula derived from this plot was applied to all dGPS points. The reduced vertical offset produced by this adjustment of the dGPS data can be observed by comparing the SRTM and adjusted dGPS contour lines (**Figure B2, Appendix B**).

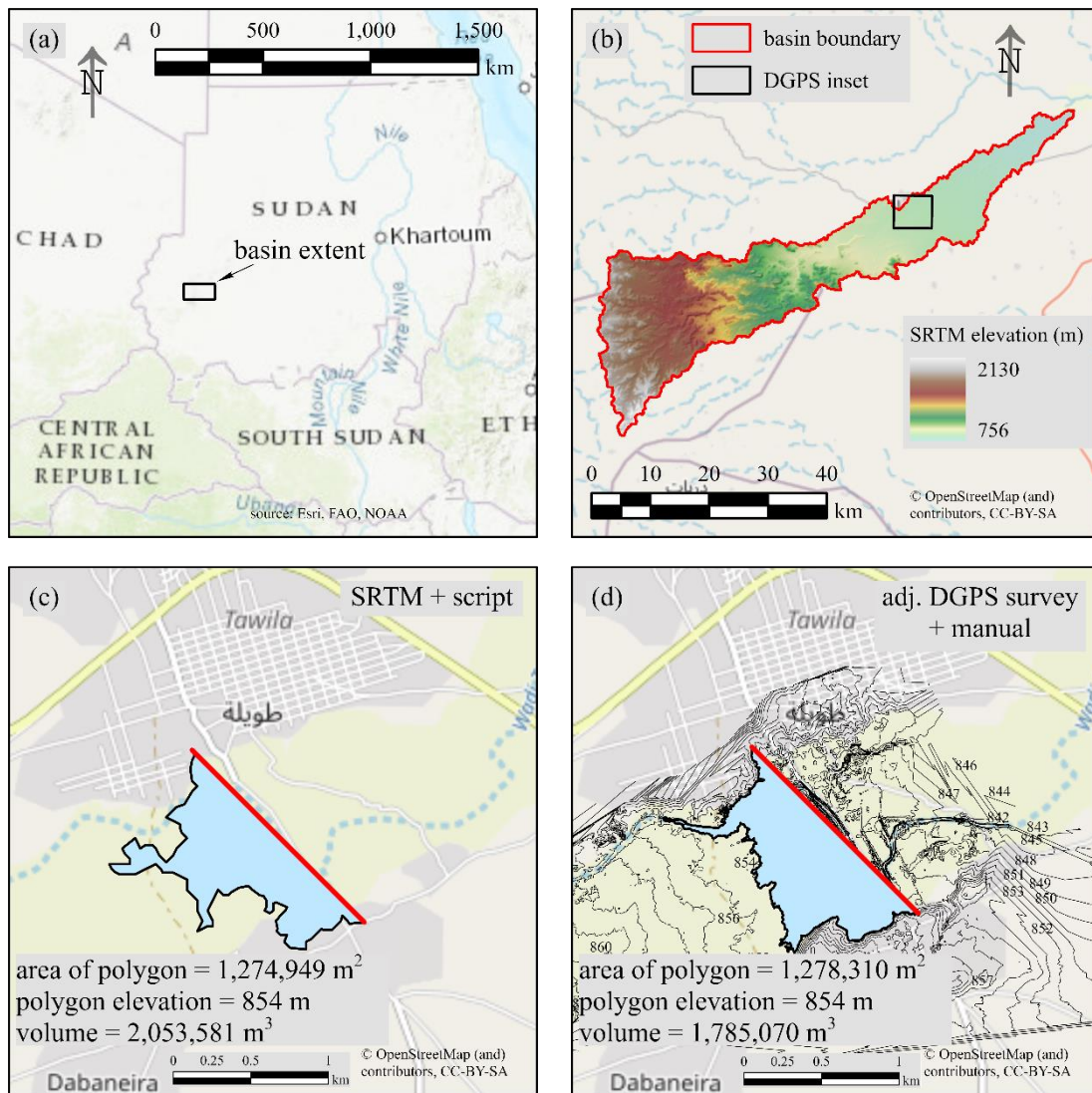


**Figure 4.3. Validation of the geometrical process: (a) country map with inset of basin extent, (b) Shuttle Radar Topography Mission (SRTM) 3 arc-second elevation of basin, (c) script outputs of barrier at 854 m based on SRTM DSM input, (d) barrier and polygon created manually using differential Global Positioning System (dGPS) ground survey.**

A check was carried out to verify that the SiteFinder script was producing realistic measurements, for the polygon (area of influence) and volume (storage capacity). This was done by first selecting a barrier along with its associated polygon created by the script with the SRTM input (**Figure 4.3c**) located

within the boundary of the dGPS survey. A comparator barrier (and its associated polygon) was then created (**Figure 4.3d**) manually by forming a barrier at the same elevation and orientation as the SRTM-derived barrier and intersecting it with the adjusted dGPS contours. The storage volume that would be impounded by these two barriers were calculated. The SRTM/SiteFinder method gave a polygon area of 1,274,949 m<sup>2</sup> and a storage volume of 2,053,581 m<sup>3</sup>, and the corresponding dGPS/manual process values were 1,278,310 m<sup>2</sup> and 1,785,070 m<sup>3</sup> respectively. This is a less than 1.0 % difference for area and an approximately 15.0 % difference for volume. In terms of area, at least, this difference demonstrates a strong level of consistency between the SRTM and dGPS-derived results. The 15 % difference encountered when comparing the volumes may be explained by several factors including the period of 18 years between the SRTM and dGPS data acquisition. The SRTM survey is a Digital Surface Model (Gallant et al., 2012) which may have picked up the top of any vegetation or buildings rather than the ground, while the elevation points for the dGPS survey are of the dam structure and the ground surrounding the embankment only. Finally, the distance between the survey points for the dGPS ranged between 10 and 20 m and thus were better suited to capture relief features of the site compared to the 3 arc-seconds SRTM elevation product which resulted in a grid size of 92 m × 92 m.

### **4.3.3 Application and validation to water harvesting scenarios**

To assess its performance in a previously unexamined context, SiteFinder was applied to a different study area with the intention of identifying locations within it that have favourable characteristics for siting water harvesting structures. Three scenarios were explored, each one defined by constraints on the input parameters that resulted in a different scale of water harvesting structure being identified.

The study area used for this application is in central Ethiopia between latitudes 8.155 N to 8.206 N and longitudes 38.937 E to 39.046 E. It covers an area of 68.4 km<sup>2</sup> (12 km × 5.7 km) and has an elevation range of slightly over 600 m (**Figure 4.4**) and is representative of the arid to semi-arid regions where water harvesting techniques are most commonly implemented. The digital elevation data to which the process was applied was taken from the 1-arc second global digital elevation product from the NASA Space Shuttle Radar Topography Mission (SRTM), which is freely available via the US Geological Survey (EROS, 2018c). This is a digital surface model (DSM) rather than a digital terrain model (DTM) but offers good coverage of arid and semi-arid regions and is often used for water harvesting site selection (Vema et al., 2019; Mugo and Odera, 2019).

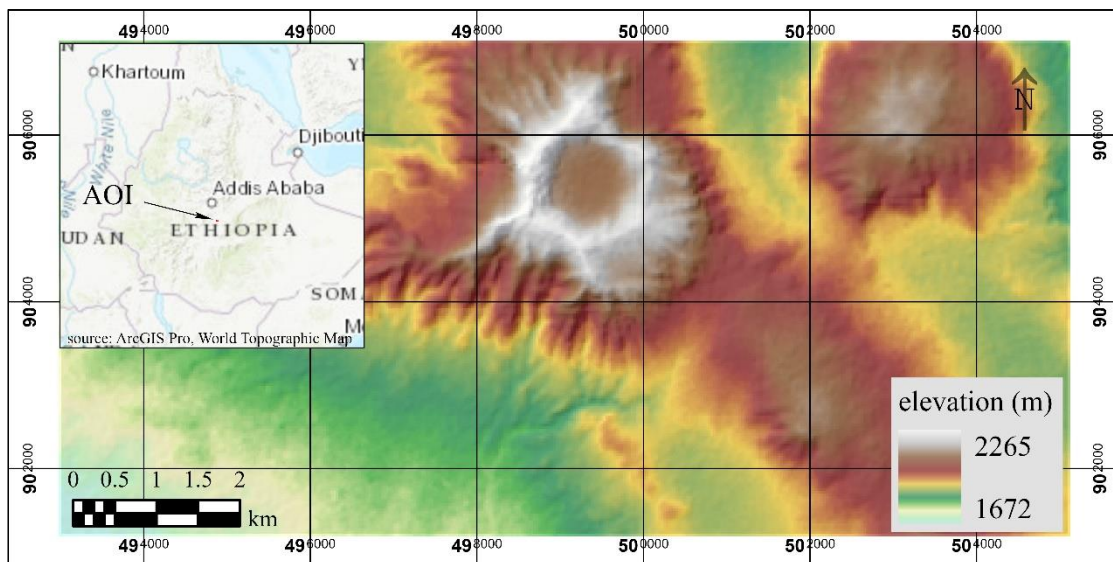


**Figure 4.4. Ethiopia: area of interest (AOI) showing Shuttle Radar Topography Mission (SRTM) elevation data with country level map (inset).**

In Scenario 1, the rationale was to imitate a national governmental department tasked with finding sites suitable for large dams with the primary purpose of creating water supply reservoirs. Candidate sites were sought that would be able to accommodate structures with a barrier height of over 15 m – to meet a definition of a large dam (ICOLD, 2011) but not greater than 25 m. Other defined criteria included storage capacity in excess of 1,000,000 m<sup>3</sup> and a storage volume to barrier volume ratio of at

least ten, the latter acting as an indicator of value-for-money. Finally, the dam length was constrained to be no greater than 2,000 m. The minimum and maximum catchment areas were set to 2,000,000 m<sup>2</sup> and 9,000,000 m<sup>2</sup> respectively following analysis of a flow accumulation raster to identify the most significant drainage channels within the AOI. The search parameters are summarised in **Table 4.2**.

Scenario 2 aimed to replicate the implementation of a water harvesting techniques at a scale of interest to planners at a regional level. SiteFinder was therefore used to search for sites suitable for large gully erosion control check dams, classified when the gully depth is more than 5 m (Geyik, 1986). The search parameters are summarised in **Table 4.3**.

Scenario 3 was intended to resemble a community-based project, possibly supported by a non-governmental organisation, whose goal is to increase crop productivity by placing more agricultural land under flood. The water harvesting structure considered therefore is in the form of earth embankment, no more than 2 m in height, intended to hold back runoff, and as the dry season advances water loss through evaporation causes more land to become available for planting, similar to some earth embankment dams in Sudan (Zumrawi, 2015) and comparable in purpose to the traditional *Teras* system (Van Dijk and Ahmed, 1993; Niemeijer, 1998) also found in Sudan. In this scenario embankments should be no more 400 m in length. Since the aim of project is to bring land under irrigation the desired feature of any site is the area of influence (the saturated zone upstream of the barrier) which should be a minimum of 10,000 m<sup>2</sup>. To identify locations that offer acceptable value-for-money barriers would only be considered viable if the area of influence to barrier volume ratio is equal or greater than one hundred. The search parameters are summarised in **Table 4.4**.

#### **4.3.4 High-resolution DEM**

To test the accuracy of the process using the 1 arc-second resolution DSM, it was repeated for each of the three scenarios using a higher resolution DEM and the results compared. The higher resolution DEM was found using an open topography website (OpenTopography, 2008) and consisted of a 1 m × 1 m resolution product (Airborne Research and Survey Facility, 2009) obtained using a LiDAR instrument by the UK Natural Environment Research Council Airborne Research and Survey Facility.

The comparison of results from the two elevation data products was carried out using a modified version of SiteFinder, so that while the siting points and axis directions were derived from the SRTM DSM the actual barriers and storage volumes were created on a LiDAR DTM elevation surface. This approach allowed a comparison of barriers and impoundments to be made for barriers formed at the same location, in the same direction and of a similar height, but using elevation models of different resolutions, thereby isolating the effects of the resolution change.

From the matching pairs of barrier data, three parameters were analysed to assess the comparison of the SRTM-based results and the LiDAR-based results. Barrier length, area of influence and storage volume were chosen since these metrics play a significant role in the water harvesting site selection, either directly or indirectly, and they cover dimensions of length, area, and volume. Comparisons of these parameters from the two elevation data products were carried out using Spearman's rank correlation tests and Root Mean Square Error (RMSE) analysis.

### **4.4 Results**

#### **4.4.1 High-resolution DEM**

The modified version of SiteFinder identified 903 barriers in the LiDAR DTM. These were compared against barriers identified in the SRTM DSM. However, since there is a difference between the two

elevation models not all barriers (with a shared siting point and contour reference) formed on the LiDAR DTM model were also formed on the SRTM DSM surface. Barriers sharing the same siting point, the same contour reference and formed on both elevation models were matched. The results of the statistical comparisons of parameters derived from each DEM are presented in **Table 4.1**. Charts of each metric are provided in **Appendix B (Figure B3 and Figure B4)**.

**Table 4.1. Analysis of results from all case study scenarios comparing barrier length (L), polygon area (A), and storage volume (V) using Shuttle Radar Topography Mission (SRTM) elevation data against high-resolution Airborne Research and Survey Facility LiDAR data.**

		LSRTM - LLiDAR	ASRTM - ALiDAR	VSRTM - VLiDAR
Spearman's rho	Correlation Coefficient	.568**	.683**	.721**
	Sig. (1-tailed)	<0.001	<0.001	<0.001
	N	685	685	685
Root Mean Square Error		188 m	78,887 m <sup>2</sup>	552,018 m <sup>3</sup>
Normalised Root Mean Square Error (RMSE divided by LiDAR mean)		0.91	1.15	1.16

\*\* . Correlation is significant at the 0.01 level (1-tailed).

#### 4.4.2 Scenario 1 Case Study - Large Dam

The results for Scenario 1 are presented in **Table 4.2**. In total, SiteFinder identified 383 siting points and created 376 barriers. The initial desired minimum storage volume was set at  $1 \times 10^6$  m<sup>3</sup> while SiteFinder outputted barriers with a maximum storage volume  $13.9 \times 10^6$  m<sup>3</sup> and since storage volume was considered to be an important metric it was decided to increase the minimum storage volume, so a filter was applied resulting in only barriers with a storage volume equal or greater than  $10 \times 10^6$  m<sup>3</sup> were included in the final barrier list.

The storage to barrier volume ratio (SBVR) for some barriers fell well below the desired ratio of ten, so these were removed by applying a filter, resulting in the filtered barriers having a SBVR not less than 15.4. Consequently, only five barriers remained. Although these were all associated with different siting points, those points were all clustered together, thus effectively, a single site was identified (**Figure 4.5**).

**Table 4.2. Case study Scenario 1: desired parameters, search parameters, tool output parameters, filter limits and parameter range of filtered barriers.**

scenario reference	Scenario 1					
implementation level	national					
structure type	large dam					
primary purpose	water supply					
<b>parameter</b>	<b>limit</b>	<b>desired</b>	<b>search</b>	<b>output</b>	<b>filter</b>	<b>range</b>
barrier height (m)	min.	15	10	10		20
	max.	25	30	30		23
barrier length (m)	min.			68		1,004
	max.	2,000	2,000	1,427		1,216
area of influence (10 <sup>6</sup> m <sup>2</sup> )	min.					1.0
	max.					1.2
catchment area (10 <sup>6</sup> m <sup>2</sup> )	min.		2			3.6
	max.		9			6.1
storage volume (10 <sup>6</sup> m <sup>3</sup> )	min.	1		0.1	10.0	10.5
	max.			13.9		13.9
storage to barrier volume ratio (-)	min.	10		0.0	10.0	15.4
	max.			33		23.9
catchment area to storage volume ratio (m <sup>-1</sup> )	min.					0.3
	max.					0.5
siting points (№)				383		5
barriers (№)				376		5

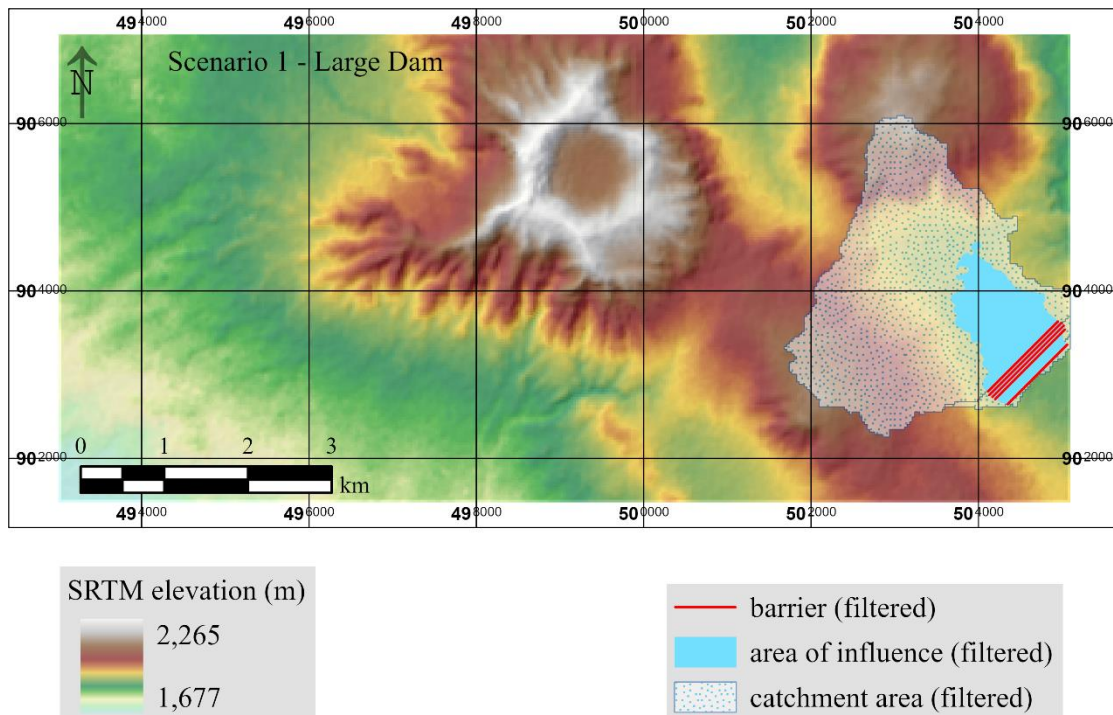


**Figure 4.5. Scenario 1 (Large Dam) results using Shuttle Radar Topography Mission (SRTM) elevation data.**

The ranges of values of parameters defining the identified barriers and impoundments are shown in **Table 4.2**. This information could be used to inform decisions as to whether it would be worthwhile investigating sites as potential water harvesting locations. In this scenario, planners would observe that the catchment area to storage volume ratio is no greater than  $0.5 \text{ m}^2\text{m}^{-3}$  for any of the identified barrier locations and may conclude this is insufficient to generate the inflows needed to fill the dam and hence decide not to pursue the site as a location for a large dam. For comparison, Papenfus (2003) describes three potential dams with catchment area to storage volume ratio ranging from 69 to  $122 \text{ m}^2\text{m}^{-3}$ , drought reserve dams should have a catchment area to storage volume ratio from  $50\text{--}100 \text{ m}^2\text{m}^{-3}$  (Agriculture Victoria, 2020) and Nissen-Petersen (2006) details a dam design with a catchment area to water storage volume of  $333 \text{ m}^2\text{m}^{-3}$ .

#### **4.4.3 Scenario 2 Case Study - Gully Check Dam**

The results from Scenario 2 are presented in **Table 4.3**. SiteFinder identified only 23 barriers from a total of 4,586 siting points analysed. Of these, some had very low SBVRs. A filter was applied that removed all those with  $\text{SBVR} < 2.5$ , resulting in six barriers at different siting points across the study area, although two barriers are located in the same gully separated by only 30 m. While the filtered barriers met the desired parameter ranges for barrier length and catchment area, they all fell outside the desired range for the parameters of catchment area to storage volume ratio ( $< 15 \text{ m}^{-1}$ ) and barrier height (5–7 m). From the results of the filtered barriers the ranges of storage volume, catchment area and barrier height were  $900,000\text{--}2,300,000 \text{ m}^3$ ,  $60,000\text{--}200,000 \text{ m}^2$ , and 3–3.6 m respectively. Ettazarini (2021) describes small check dams having a storage volume up to  $500,000 \text{ m}^3$ , while Geyik (1986) defines medium sized gully dams having a catchment area range of  $20,000\text{--}200,000 \text{ m}^2$  and a range of gully depth of 1–5 m, so while the intention was to locate large gully check dams SiteFinder results appear to show that sites for medium sized check dams have been identified.

The six filtered barriers, located in a total of five gullies, together with the respective area of influence and catchment area of each barrier are shown in **Figure 4.6**.

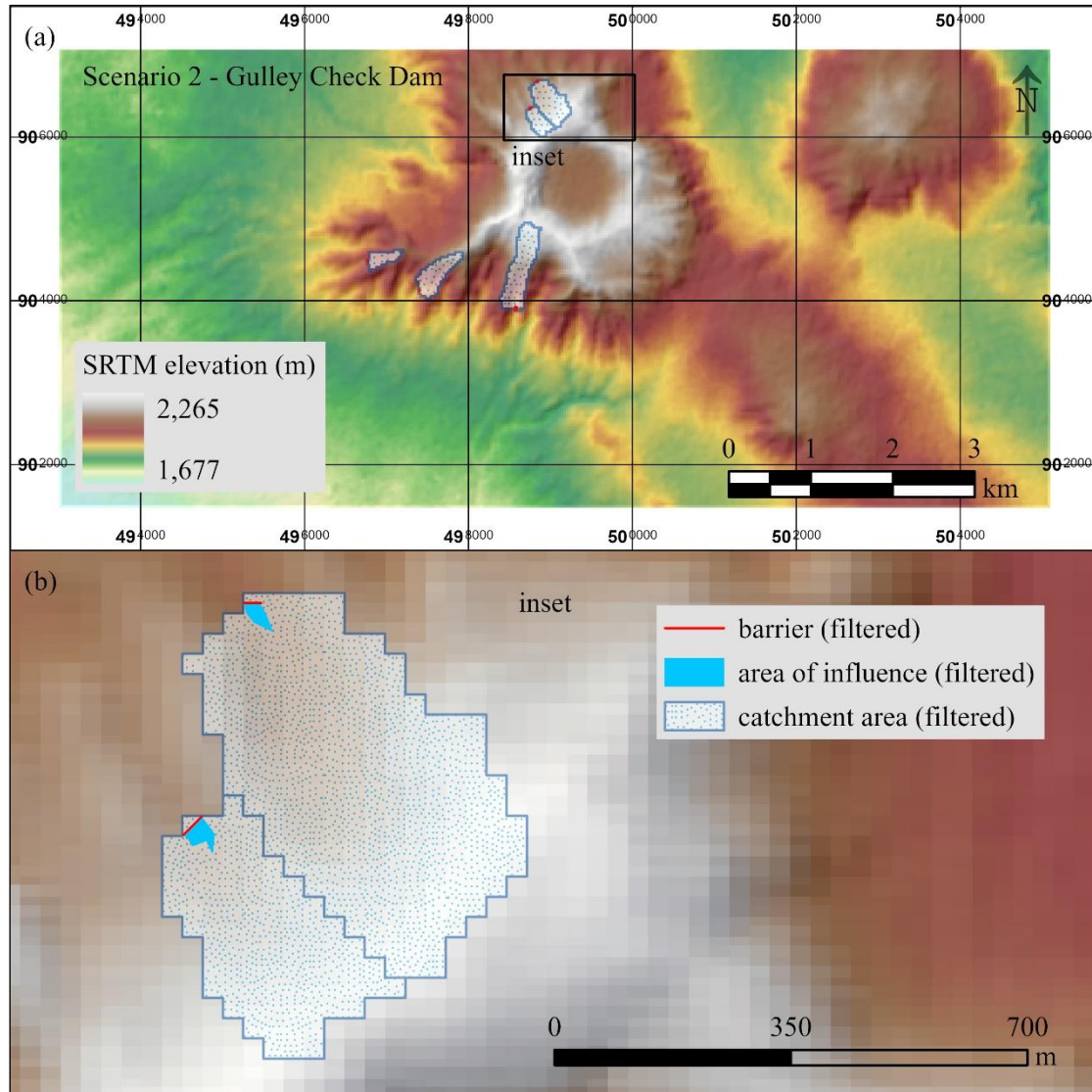


**Figure 4.6.** (a) Scenario 2 (Gully Check Dam) results using Shuttle Radar Topography Mission (SRTM) elevation data with inset box, (b) inset of two filtered barriers with their respective area of influence and catchment area.

#### 4.4.4 Scenario 3 Case Study - Earth Embankment

The results for Scenario 3 are presented in **Table 4.4**. In total 801 siting points were analysed as potential sites for earth embankments resulting in 1,771 potential barriers.

A barrier height filter was applied so that all barriers would be at least 1 m and no greater than 2 m. Placing a maximum limit on the height of filtered barriers of just 2 m increases the prospect that the construction could be accomplished using local oversight and labour as the work is technically less demanding than constructing higher embankments.

**Table 4.3. Case study Scenario 2: desired parameters, search parameters, tool output parameters, filter limits and parameter range of filtered barriers.**

scenario reference	Scenario 2					
implementation level	regional					
structure type	gully check dam					
primary purpose	erosion control					
<b>parameter</b>	<b>limit</b>	<b>desired</b>	<b>search</b>	<b>output</b>	<b>filter</b>	<b>range</b>
barrier height (m)	min.	5	3	3		3
	max.	7	9	6.5		3.6
barrier length (m)	min.			19		24
	max.	40	40	39		39
area of influence (10 <sup>6</sup> m <sup>2</sup> )	min.					0.7
	max.					1.6
catchment area (10 <sup>6</sup> m <sup>2</sup> )	min.	0.05	0.05	0.04		0.06
	max.	0.4	0.4	0.4		0.2
storage volume (10 <sup>6</sup> m <sup>3</sup> )	min.					0.9
	max.					2.3
storage to barrier volume ratio (-)	min.			0.4	2.5	2.8
	max.			7.8		7.8
catchment area to storage volume ratio (m <sup>-1</sup> )	min.	5		35		35
	max.	15		2,467		170
siting points (№)				4,586		6
barriers (№)				23		6

A high proportion (508 from a total 1,771) of outputted barriers had a SBVR ranging from zero to almost three, so a filter (equal or greater than 3) was applied to ensure these barriers were not included in the final list selected barriers.

In this scenario the purpose of the water harvesting structure is to provide irrigated land immediately upstream of the barrier (i.e. the area of influence) so a condition was applied to ensure that all filtered barriers provided at least 100 m<sup>2</sup> of irrigated land for every cubic metre of embankment constructed. This demonstrates the capacity of SiteFinder to output a ‘socio-economic’ criterion, since the area of influence to barrier volume ratio is an indicator of value-for-money.

A catchment area to storage volume ratio filter was applied that set an upper limit of  $15 \text{ m}^{-1}$  as a way of controlling the amount of runoff a water harvesting site would receive. The rationale behind such a filter is that planners may wish to avoid sites where excess runoff might require expensive technical solutions and focus on sites where excess runoff is less problematic.

Of the seven barriers filtered from the initial 1,771 barriers the SBVR was found to range from 234 to 1,374 (**Table 4.4**). SiteFinder calculates the storage to include the volume of any natural depressions (i.e. pools) should they occur within the area of influence, together with storage created as a direct result of the barrier. SiteFinder is able to compute the volume of natural depressions as it computes site geometry based on a TIN surface (**Figure 4.1**) created using a DEM that has not been ‘filled’ to remove ‘sinks’.

**Table 4.4** shows the range of parameter values for both the total unfiltered 1,771 barriers and the seven filtered barriers. The final filtered barriers, all of which meet the ‘desired’ criteria (**Table 4.4**) are distributed in three distinct clusters (**Figure 4.7**).

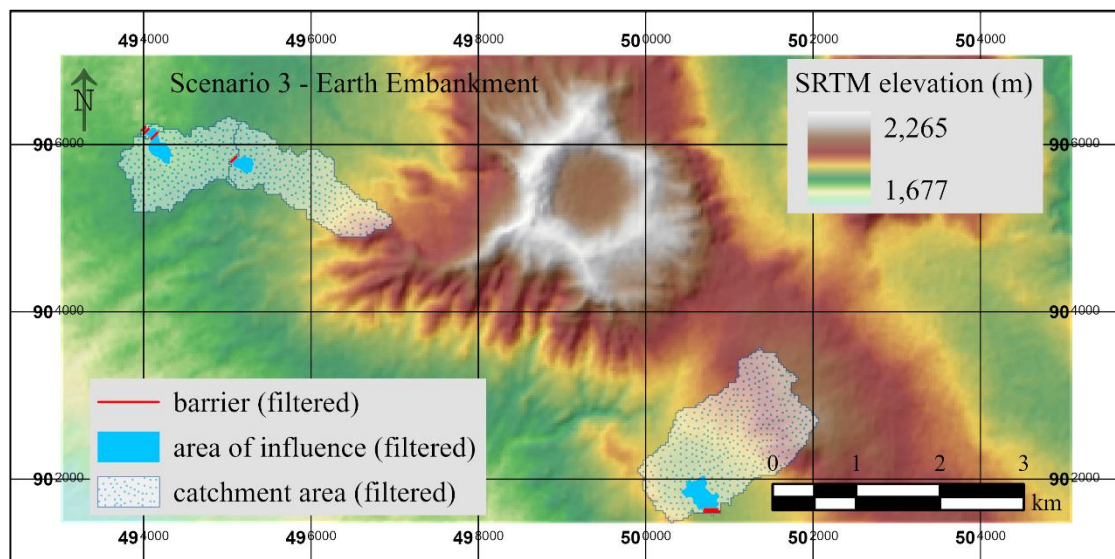


Figure 4.7. Scenario 3 (Earth Embankment) results using Shuttle Radar Topography Mission (SRTM) elevation data.

**Table 4.4. Case study Scenario 3: desired parameters, search parameters, tool output parameters, filter limits and parameter range of filtered barriers.**

scenario reference	Scenario 3					
implementation level	community					
structure type	earth embankment dam					
primary purpose	irrigation (flood recession)					
<b>parameter</b>	<b>limit</b>	<b>desired</b>	<b>search</b>	<b>output</b>	<b>filter</b>	<b>range</b>
barrier height (m)	min.	1	0	0	1	1
	max.	2	3	8	2	2
barrier length (m)	min.		0	0.4		55
	max.	400	400	377		180
area of influence ( $10^6$ m <sup>2</sup> )	min.	0.01				0.04
	max.					0.1
catchment area ( $10^6$ m <sup>2</sup> )	min.	1	1	0.5		0.9
	max.	5	5	6.9		2.0
storage volume ( $10^6$ m <sup>3</sup> )	min.					0.1
	max.					0.2
storage to barrier volume ratio (-)	min.			0	3	234
	max.			1,374		1,374
area of influence to barrier volume ratio (m <sup>-1</sup> )	min.	100		0.2	100	114
	max.			837		717
catchment area to storage volume ratio (m <sup>-1</sup> )	min.			4.7		8
	max.			$28 \times 10^9$	15	13
catchment area to cultivation area ratio (-)	min.			12		16
	max.			$112 \times 10^6$		33
siting points (N <sup>o</sup> )				801		6
barriers (N <sup>o</sup> )				1,771		7

## 4.5 Discussion

The case studies demonstrate how SiteFinder can analyse automatically thousands of potential external water harvesting sites within a GIS environment and provide useful information (e.g. barrier volume and storage capacity) using a digital elevation raster as the primary data source. The automated method runs entirely within the GIS environment and provides information for site selection purposes (e.g. barrier dimensions and storage geometry) which cannot be obtained from a slope raster, which is most the common type of dataset currently used by researchers for water harvesting site selection (Adham et al., 2016a). Bespoke software and tools (Petheram et al., 2017; Wimmer et al., 2019; Teschemacher et al., 2020), described earlier in this chapter, do exist to automate the process of extracting dam details for potential sites. but all function outside a GIS environment.

The SiteFinder tool described here does not aim to provide the answer to where the best water harvesting sites are but rather provides relevant barrier characteristics, calculated within the GIS environment, allowing the possibility of readily incorporating results into a multi-criteria decision-making process, again using the GIS environment, which would allow the consideration of other biophysical, socio-economic, and environmental factors.

Integral to the functioning of SiteFinder is the use of flow direction to determine the orientation of the barrier (set perpendicular to flow direction), which is an innovative feature for an automated water harvesting site selection process. This has the benefit of allowing SiteFinder to scan a higher number of locations as processing time required to optimise barrier orientation is avoided. Unlike some site selection tools (Wimmer et al., 2019; Teschemacher et al., 2020) SiteFinder considers catchment area. Catchment area is related to runoff efficiency (Karnieli et al., 1988) and the volume of runoff a water harvesting site will receive. SiteFinder calculates catchment area and uses it to search for potential sites and outputs water harvesting site characteristics including catchment area to cultivation area (Critchley and Siegert, 1991). This implies that if data on annual catchment runoff were available, SiteFinder would readily be able to output the site selection criterion of inflow to storage volume ratio (Papenfus, 2003) using the catchment area to storage volume ratio that it already calculates.

Often the choice of which locations should be reviewed for potential water harvesting sites involves an amount of human interpretation of maps to judge the best spots or “narrows” (Forzieri et al., 2008) as places to be analysed for suitability. SiteFinder offers an objective and repeatable alternative to identify sites with favourable characteristics. For the siting of large water harvesting structures there is an argument that human interpretation alone can identify sites of interest that warrant further analysis. For example, in Scenario 1 (**Figure 4.5**) there are only a few places that a large dam could be sited, and these locations could possibly be ascertained using visual interpretation of maps alone.

However, the same task becomes extraordinarily difficult for smaller water harvesting structures like those described in Scenario 2 (**Figure 4.6**) and Scenario 3 (**Figure 4.7**).

For a small dam the volume of material required to construct the barrier itself can represent approximately sixty percent of the Bill of Quantities (Nissen-Petersen, 2006). The barrier volume therefore can be used as a proxy for capital cost. SiteFinder calculates the barrier volume based on the barrier length and barrier height. However, planners invariably want to establish the cost-benefit of any proposed scheme in the initial stages of the project cycle. To address this, SiteFinder provides the storage volume to barrier volume ratio and area of influence to barrier volume ratio (**Table 4.2**), either of which could aid a decision-making process on site suitability. Of the forty-eight papers reviewed by Adham et al. (2016a) only four refer to cost. One uses a fixed cost for the water harvesting solution (Jothiprakash and Sathe, 2009), two use price-of-land (Banai-Kashani, 1989; Sekar and Randhir, 2007), and only one (Forzieri et al., 2008) considers the water storage volume against the volume of the dam (or barrier volume) but in a process that requires visual interpretation of satellite imagery to estimate the width of “narrows”. SiteFinder provides an automated process that bridges biophysical criteria (e.g. area of influence) with socio-economic criteria, e.g. cost-benefit information in the form of storage volume to barrier volume ratio.

SiteFinder calculates the barrier height based on the elevation profile along the entire barrier crest and similarly the catchment area of the site is based on flow accumulation associated with the barrier crest line. This method is therefore arguably more sophisticated than other site selection methods that establish site suitability using single raster cell values, e.g. slope. SiteFinder considers potential water harvesting sites in full, extracting and using values from any number of raster cells and so represents a shift away from a single cell approach to one whereby the water harvesting structure is considered as a complete entity. A problem with using values obtained at single raster cells to support a site

suitability assessment is that as the cell size decreases (due to the use of a higher resolution dataset) the size of the raster cell becomes smaller in proportion to the water harvesting structure, although it is possible to calculate surface parameters (including slope) using windows greater than the normal default size of  $3 \times 3$  cells. Better elevation data, in terms of vertical accuracy and spatial resolution, is associated with regional and local scale data (Schumann and Bates, 2018) and since it has been demonstrated that SiteFinder can be successfully used with high resolution datasets such as LiDAR (**Table 4.1**) it therefore can exploit the increased detail these DEMs offer in a way that techniques that assess site suitability based on values at individual raster cells cannot.

For every barrier created by SiteFinder, a polygon is also created that represents the area of influence (saturated zone) upstream of the water harvesting structure. These polygons represent the area affected by the barrier in a more realistic way compared to representing a water harvesting structure by a single point (or raster cell) or just the barrier alone. As part of a site selection process these area of influence polygons could be overlaid with land use and land cover maps. For example, if the purpose of the water harvesting structure is to facilitate artificial groundwater recharge (Zaidi et al., 2015) the polygons defining the area of influence could be overlaid with soil texture and vadose zone thickness maps to enable the hydrological response to be more realistically assessed. Selection criteria have been presented in the case studies presented (**Table 4.2**, **Table 4.3**, **Table 4.4**) but SiteFinder outputs allow users to formulate other criteria that they may consider useful in a site selection process. For example, it may be useful to know the area of influence to storage volume ratio as a way of limiting evaporation (Reseigh, 2021) and this could simply be obtained since both parameters (area of influence and volume) are contained within the barrier database. As SiteFinder works within a GIS environment combining its results with other parameters is straightforward, requiring no additional software. For instance, the catchment area calculated by SiteFinder in case study Scenario 2 could be used together

with the slope (calculated using GIS but not with SiteFinder) to ascertain the runoff energy which is strongly associated with erosion control check dam collapse (Castillo et al., 2007).

The case studies presented above utilised a 1 arc-second (30 m x 30m) SRTM DSM. The resulting barriers locations were compared against the equivalent barriers locations based on the high-resolution (1 m × 1 m) DTM and show a higher degree of agreement for water harvesting structures longer in length. The implication is that using a high-resolution DEM will give more accurate results. That said, SiteFinder is intended for use in scoping, so all potential sites will require detailed, ground-based survey at a later stage. The risk however, especially when using a 1 arc-second DSM as here, is that when identifying smaller water harvesting structures (e.g. Scenarios 2 and 3), selected sites may have quite different parameters that those predicted by the tool and possibly some locations that would make suitable sites for water harvesting structures are missed.

SiteFinder calculates the barrier crest width as being fixed at just 0.25 m. This is somewhat less than the 3 m proposed by Nissen-Petersen (2006), so the tool could be used for low standing water harvesting structures without significantly overestimating the barrier volume. A future refinement of the tool could set the crest width as a function of the height of the barrier (Stephens, 2010) as well as allowing the user more control over the design of the barrier structure to match the water harvesting technique.

For the three scenarios presented in the case study, SiteFinder was only used to find potential locations for water harvesting structures. In the locations identified, runoff from the outer limits of the catchment area would need to flow some distance before reaching the area of influence where it would be impounded (**Figure 4.5, Figure 4.6, Figure 4.7**). No analysis was undertaken to test the functionality of the SiteFinder in finding sites suitable for *in situ* water harvesting. GIS-based decision support

systems have been used to identify areas suitable for *in situ* water harvesting (Mahmoud and Alazba, 2015) and this is a potential further application of the tool. A feature of SiteFinder is that the barrier axis is set perpendicular to the flow direction, calculated using the D8 procedure, described by Jenson and Domingue (1988). This D8 flow direction is also the basis for siting point identification since the flow accumulation raster is created with the D8 flow direction raster as the input. Other flow direction methods do exist such as multi-flow-direction (MFD) (Qin et al., 2007) and D-Infinity (Tarboton, 1997). Future research could investigate if these flow direction methods would be preferable to the D8 method in setting the barrier axis direction. Similarly, it would be interesting to determine if some flow direction methods offer advantages to others for siting point identification, especially if SiteFinder is to be used for both external and *in situ* water harvesting. Orlandini and Moretti (2009) concluded that the choice of using non-dispersive methods over dispersive methods is dependent on the need to delineate flow paths or to focus on divergent terrains. This tentatively suggests that dispersive flow direction methods would be more applicable for *in situ* water harvesting and non-dispersive methods (e.g. D8) better for external water harvesting.

None of the filtered barriers (**Table 4.2, Table 4.3, Table 4.4**) are presented as recommendations for water harvesting sites since some criteria typically incorporated into a site selection process were not considered. SiteFinder does however demonstrate its capacity to generate pertinent site characteristics within a GIS environment that could form part of a multi-criteria analysis (MCA) approach to water harvesting site identification. Therefore, a future development would be to use SiteFinder as part of a ‘real-world’ MCA water harvesting site selection process considering a range of biophysical, socio-economic, and environmental criteria, with the aim of identifying suitable locations prior to any site visit.

## 4.6 Conclusions

A novel methodology has been presented for automatically obtaining the characteristics of potential external water harvesting sites using a script-based tool operating entirely within a GIS environment using a digital elevation product as the primary source of information. Using an automated process, a total of 5,770 sites were analysed, the characteristics of barriers computed, resulting in the selection of sites based on water harvesting site selection parameters. To our knowledge, this is the first time that details of potential sites, including details of the barrier (height, length, and volume) and storage geometry, have been automatically calculated within a GIS environment. Outputs are provided in geospatial formats including barriers represented by lines, and polygons representing the area of influence linked to each barrier. The tool functions using low-to-high resolution elevation datasets and can find site characteristics for any size water harvesting structure.

Since GIS is used extensively by researchers as part of water harvesting site selection processes it is envisaged that SiteFinder could be readily assimilated into decision-making methods, enabling combination of outputs created by this tool with other biophysical, socio-economic, and environmental criteria to aid the identification of potential water harvesting sites.

It is suggested that SiteFinder is best suited for scoping, prior to any field-visits, automatically calculating the catchment area, storage capacity, and barrier dimensions for potential *ex situ* water harvesting earth embankments with a 0.25 m crest width and fixed slope but with future refinements the tool could offer greater control over the barrier specifications (e.g. shape, slope, and crest width) allowing a wider range of water harvesting structures to be analysed. It is recommended that further research is undertaken to ascertain the quality of the digital elevation products (e.g. in relation to spatial resolution and vertical accuracy) required to compute the geometry of potential water harvesting structures to within acceptable levels of uncertainty.

HRRTLE (High Resolution Runoff and Transmission Loss Estimator): a novel tool for mapping connectivity of runoff in ephemeral stream networks to aid the siting of water harvesting structures

# **5 HRRTLE (High Resolution Runoff and Transmission Loss Estimator): a novel tool for mapping connectivity of runoff in ephemeral stream networks to aid the siting of water harvesting structures**

## **5.1 Abstract**

Water harvesting is predominantly carried out in arid and semi-arid regions. Site selection studies often rely on a methodology that calculates runoff using curve numbers to generate runoff maps. These maps, typically used as part of a multi-criteria selection process, identify areas conducive to the siting of water harvesting structures. However, traditional runoff maps do not account for transmission losses that occur along the surface flow path to the catchment outlet, and these losses can be significant in arid and semi-arid regions. Here we introduce a methodology that incorporates a curve number runoff method while also addressing transmission losses.

Our approach, utilising three global datasets, was validated against observed runoff data from 28 catchments worldwide, and infers hydraulic characteristics of both overland and channel flow from curve number values. This involves leveraging the curve number dataset twice: initially for calculating runoff and subsequently for forecasting transmission losses. The outcomes include a runoff connectivity map, at a spatial resolution of  $250\text{ m} \times 250\text{ m}$ , presenting the runoff depth (in mm) for

HRRTLE (High Resolution Runoff and Transmission Loss Estimator): a novel tool for mapping connectivity of runoff in ephemeral stream networks to aid the siting of water harvesting structures

each pixel based on the direct runoff generated at that pixel and reaching the catchment outlet. This connectivity map aids planners in comprehending the dynamics of surface runoff towards a catchment outlet, assisting in identifying potential locations for future water harvesting structures.

The process integrates 38 years of precipitation data, enabling predictions not only for average annual runoff but also for the return periods of various annual runoff volumes. Despite the simplicity of the model, a positive Nash-Sutcliffe efficiency value was observed in 11 out of the 28 catchments.

## 5.2 Introduction

Water harvesting – the collection of runoff water for productive purposes (Critchley and Siegert, 1991) – is a common practice in arid and semi-arid regions. Beyond their primary role of collecting and storing water for domestic, agricultural or industrial use, water harvesting structures can have many other benefits, including increased plant biomass production, recharge of aquifers, reduced soil erosion, and flood mitigation (Gupta, 1994; Abdeldayem et al., 2020; Parimalarenganayaki, 2021; Strohmeier et al., 2021). There are many factors that need to be considered when deciding whether a location is appropriate for development as a water harvesting site, and several different methodologies have been deployed to identify sites. These include methods applicable to different types of water harvesting systems, including check dams (Patel et al., 2015, Ettazarini, 2021), structures located in gullies (Li et al., 2020), and small dams located on the surface or underground (Forzieri et al., 2008). Surprisingly, the prediction of runoff (i.e. water volume inflow to a water harvesting storage site from its catchment) is not routinely used in site selection. Adham et al. (2016a) reviewed water harvesting site selection studies and found only 13 of 48 included runoff as a site suitability criterion, while the most frequently used biophysical criterion was slope (40 of 48 studies). Quantifying runoff volume to

HRRTLE (High Resolution Runoff and Transmission Loss Estimator): a novel tool for mapping connectivity of runoff in ephemeral stream networks to aid the siting of water harvesting structures

a potential site is crucial to determine whether a scheme will receive sufficient water on an annual basis to fulfil its intended purpose; help determine the height of the storage structure that needs to be constructed (Stephens, 2010); and ascertain if excessive inflows will be problematic. Locations where the ratio of total volume of inflow to storage capacity is close to one are optimal for siting water harvesting structures (Adham et al., 2016a). Hence, an important principle on which the work reported here is based is that the ratio of mean annual inflow volume to water harvesting storage volume is a key design metric and should be incorporated as one of the most important biophysical criteria in any water harvesting siting methodology.

Predicting the harvested water volume at a potential site requires knowledge of its catchment's area, rainfall, and rainfall-runoff relationship (Critchley and Siegert, 1991). Because catchments differ in terms of size, topography, geology, and land cover, the rainfall-runoff relationship will vary between them. Rainfall patterns can also change significantly, even between nearby catchments. Moreover, climate change is affecting mean precipitation and evaporation with "seasonally variable regimes becoming more variable" (Konapala et al., 2020, p. 1). Therefore, prediction of harvested water volumes for proposed storage sites requires contemporary data specific to the catchment in question.

Several methods have been used to quantify runoff in water harvesting site selection studies. These include the empirical formula of Tixeront (Mechlia et al., 2009), the Finkel method (Elewa et al., 2012), the Watershed Modeling System conceptual model (Jabr and El-Awar, 2004) and the Soil Conservation Service Curve Number (SCS-CN) methodology (Gupta et al., 1997; Senay and Verdin, 2004; Kadam et al., 2012; Mugo and Odera, 2019; Shalamzari et al., 2019). Their outputs typically comprise of runoff maps (Senay and Verdin, 2004), predictions of total catchment runoff (e.g. Gupta et al., 1997) and runoff coefficients (e.g. Ramakrishnan et al., 2009). Runoff maps allow the ratio of

HRRTLE (High Resolution Runoff and Transmission Loss Estimator): a novel tool for mapping connectivity of runoff in ephemeral stream networks to aid the siting of water harvesting structures

annual runoff to available storage volume to be calculated for potential water harvesting sites (Sayl et al., 2019). Presented as a thematic layer, with runoff classified ordinally (e.g. low, moderate, or high) or fully quantitatively (e.g. depth, annual flood volume) they have been incorporated into GIS-based site selection methodologies in various ways. For example, De Winnaar et al. (2007) and Nagarajan et al. (2015) created maps showing zones of low, moderate, and high runoff potential. Sayl et al. (2019) and Al-Ghobari et al. (2020) created maps of annual flood volume and potential runoff depth. Haile and Suryabhagavan (2019) incorporated a thematic map of runoff depth into a Fuzzy Logic model as part of a GIS-based approach for identifying potential rainwater harvesting sites. To improve the effectiveness of simulating the final runoff map of the watershed Karimi and Zeinivand (2021) used a distributed spatial-physical based model with 594 “subwatersheds” to create an annual runoff depth map to locate potential rainwater harvesting sites whilst accounting for daily temperature and evapotranspiration.

The method used most commonly for runoff calculation in water harvesting site selection is the SCS-CN methodology, which was first introduced in 1956 (Mishra et al., 2012). It can be described as a conceptual model supported by empirical data, which is used to estimate the volume of direct runoff (i.e. runoff generated by rainfall, rather than from baseflow) generated at locations within a catchment from rainfall depth, using an empirical parameter known as a “curve number” (CN), values of which are determined based on soil type and soil cover (e.g. vegetation or crops, vegetative debris, built environment surface materials) (Ponce and Hawkins, 1996). CN is essentially a measure of land surface permeability and therefore of sub-surface potential moisture retention capacity, and by extension the potential for runoff to be generated by precipitation. The SCS-CN methodology calculates runoff using a CN value by first finding the soil water retention capacity,  $S$ , using:

HRRTLE (High Resolution Runoff and Transmission Loss Estimator): a novel tool for mapping connectivity of runoff in ephemeral stream networks to aid the siting of water harvesting structures

$$S = 25.4 \left( \frac{1000}{CN} - 10 \right) \quad (5.1)$$

where  $S$  is the maximum soil water retention (mm), and  $CN$  is the curve number (dimensionless). From this, runoff generated is computed using:

$$Q = \frac{(P - 0.2S)^2}{(P + 0.8S)} \quad \text{if } P > 0.2S$$

$$Q = 0 \quad \text{if } P \leq 0.2S \quad (5.2)$$

where  $Q$  is the direct runoff (mm), and  $P$  is the storm rainfall (mm). Curve number rainfall-runoff models are best used for ungauged catchments when runoff is the only output needed (Sitterson et al., 2017). As water harvesting site selection planners typically deal with ungauged catchments it is not surprising that so many water harvesting selection studies use the SCS-CN methodology to compute runoff. While this method is appropriate for such purposes, difficulties do remain. Notably, as it was formulated for use on small agricultural catchments (Soulis, 2021), its application to larger catchments needs to take into account the tendency for runoff efficiency to decrease as catchment area increases (Karnieli et al., 1988).

To predict the water storage yield at a particular location from precipitation in its catchment, in addition to knowledge of catchment area, rainfall and rainfall-runoff relationships, understanding is also required of the transmission losses – to infiltration, evaporation or other processes – experienced by the runoff as it travels from its points of creation (where the precipitation falls) to the proposed storage location. These losses are typically high in arid regions, where water harvesting is commonly practised (McMahon and Nathan, 2021). Hughes and Sami (1992) estimated total transmission losses of 22 %

HRRTLE (High Resolution Runoff and Transmission Loss Estimator): a novel tool for mapping connectivity of runoff in ephemeral stream networks to aid the siting of water harvesting structures

and 75 % for two rainfall events in a semi-arid ephemeral channel system located in Africa with transmission losses largely taking the form of infiltration of water into the ground. For a semi-arid basin in Brazil, Toledo et al. (2020) stated that transmission losses accrued at a rate of 2.7 % for every kilometre of river system. Consequently, runoff maps that do not include an allowance for transmission losses cannot be verified against observed flow data, should they exist. Thus, another difficulty in using the SCS-CN method in larger catchments is obtaining data quantifying the land surface conditions over which transmission losses occur at sufficient spatial resolution. Typically, modelling a catchment to incorporate such transmission losses involves aggregating land into sub-catchments with uniform runoff-loss characteristics. This “lumped” approach reduces spatial variability. Remote sensing offers an ever-increasing availability of high spatial resolution data products that can address this problem. The method described in this paper aims to exploit this to create high-spatial resolution runoff maps whilst incorporating transmission losses.

The aim of this study is to develop and test a novel procedure to create maps showing the mean annual runoff from locations within arid and semi-arid catchments to collection points that takes into account transmission losses at high spatial resolution, i.e. at the pixel resolution of currently available remote sensing data, rather than at the much coarser sub-catchment scale that has typically been used to date. The intention is that this procedure can be used to aid the siting of water harvesting structures in regions where on-the-ground data is sparse. This aim is addressed through the following objectives:

- 1 Create a model to compute generated runoff using global precipitation and curve number datasets.
- 2 Model flowpaths from points where runoff is generated to the catchment outlet.

HRRTLE (High Resolution Runoff and Transmission Loss Estimator): a novel tool for mapping connectivity of runoff in ephemeral stream networks to aid the siting of water harvesting structures

- 3 Develop a transmission loss model to determine the proportion of runoff reaching the outlet.
- 4 Evaluate model results against observed runoff data, including evaluating the effect of incorporating transmission losses by comparing results for model runs with and without them incorporated.
- 5 Examine the characteristics of catchments best modelled by the procedures developed.

The novel contributions of this work lie in the use of fully distributed data sets, rather than the lumped approach taken previously, and in the novel method put forward for calculation of transmission losses. The approach taken to calculating transmission losses is based on the following argument. In arid and semi-arid regions, there are far fewer rainy days than in humid regions. Only some rainy days create direct runoff. Even fewer rainy days are responsible for runoff reaching a collection point. So, in these regions, where water harvesting is largely practised, there are only brief periods when runoff is being generated and transferred to a candidate water harvesting site downstream. Within such ephemeral systems, baseflow is less significant, or largely absent, compared to more humid regions. The method described here exploits these characteristics of arid zone hydrology, generating runoff using daily precipitation data, while surface flow (and hence transmission loss) is modelled as a singular annual event. Such an approach eliminates the need for hydrograph routing, allowing catchments to be modelled at relatively high spatial resolution without requiring the creation of sub-basins.

The rainfall–runoff yield model effectively consists of two components. The first component generates direct runoff from daily precipitation data using the SCS-CN method with curve number values extracted from a global dataset (Jaafar et al., 2019). The second component calculates transmission losses over flowpaths from cells where the runoff is generated to the candidate water harvesting storage

HRRTLE (High Resolution Runoff and Transmission Loss Estimator): a novel tool for mapping connectivity of runoff in ephemeral stream networks to aid the siting of water harvesting structures

site, at high spatial resolution. Outputs include a runoff connectivity map (RCM) of annual runoff depth reaching the storage site, and the predicted mean annual runoff volume. These two components are combined in the “High Resolution Runoff and Transmission Loss Estimation” tool, or HRRTLE (pronounced “hurtle”).

## **5.3 Materials and methods**

### **5.3.1 Method summary**

A set of catchments in arid or semi-arid climate zones were identified for which the necessary data sets – elevation (as a digital elevation model, DEM), curve number, rainfall, and discharge – were available. The position of the gauging station used to gather discharge data determined the outlet of each catchment, hence catchments became proxies for candidate water harvesting catchments for model development purposes, with their outlets (gauging station location) acting as places for potential collection and storage sites for the harvested water. Each catchment in turn was represented as an array of 250 m × 250 m cells and characterised in terms of its size, shape, and elevation. Using a long-term precipitation dataset and a global curve number dataset, runoff generated directly by precipitation was calculated for all cells within each catchment at a daily resolution using the SCS-CN procedure. These were summed to give an annual value of runoff (in mm) generated at each cell. This was followed by the calculation of transmission losses – quantified as transferral ratios, the fraction of generated runoff reaching the catchment outlet on an annual time scale – which involved several stages. Firstly, analysis of pixel-scale flow accumulation, derived from the catchment’s DEM, was used to define the catchment’s stream network, and distinguish it from the rest of the catchment, where water fluxes were assumed to occur via overland flow. Flowpaths were then defined between each cell and the catchment outlet and classified into sections of in-stream and overland flow. Transferral ratios for the in-stream

HRRTLE (High Resolution Runoff and Transmission Loss Estimator): a novel tool for mapping connectivity of runoff in ephemeral stream networks to aid the siting of water harvesting structures

segment of each flow pathway were determined by considering the curve number and flow transit time. The transit time was derived from the length of the in-stream flow path and the velocity of the flow. The flow velocity was computed using Manning's equation, utilising proxies for hydraulic radii and roughness coefficients, which were determined based on available data and a set of assumptions and approximations. For the overland section of each flow path, transferral ratios were again calculated as a function of curve number and flow transit time, of the same form as that for in-stream flow, but with different values of the curve number power law index and travel time constant. Overland flow transit time was calculated from overland flow path length and flow speed, and flow speed was calculated as a function of curve number and topographic slope, again based on the available data and a set of assumptions and approximations. The overall transferral ratio was then calculated as the product of the in-stream and overland flow section transferral ratios. This was multiplied by the annual runoff value for each cell, and the total modelled discharge at the catchment outlet calculated by:

$$Q_a = \left( \frac{\sum_{i=1, j=1}^{i=m, j=n} (Q_c(i, j) TR_c(i, j))}{1000N} \right) A_c \quad (5.3)$$

where  $Q_a$  is the annual discharge ( $\text{m}^3 \text{y}^{-1}$ );  $i$  and  $j$  are cells in the X and Y directions respectively in the catchment,  $i$  running from 1 to  $m$ , and  $j$  running from 1 to  $n$ ;  $Q_c(i, j)$  is the annual direct runoff (expressed in rainfall depth equivalent,  $\text{mm y}^{-1}$ ) generated at cell  $(i, j)$ ;  $TR_c(i, j)$  is the overall transferral ratio for cell  $(i, j)$ ;  $N$  is the total number of cells in the catchment; and  $A_c$  is the total catchment area ( $\text{m}^2$ ). A schematic diagram of the main stages of the HRRTLE tool is presented (**Figure 5.1**).

HRRTLE (High Resolution Runoff and Transmission Loss Estimator): a novel tool for mapping connectivity of runoff in ephemeral stream networks to aid the siting of water harvesting structures

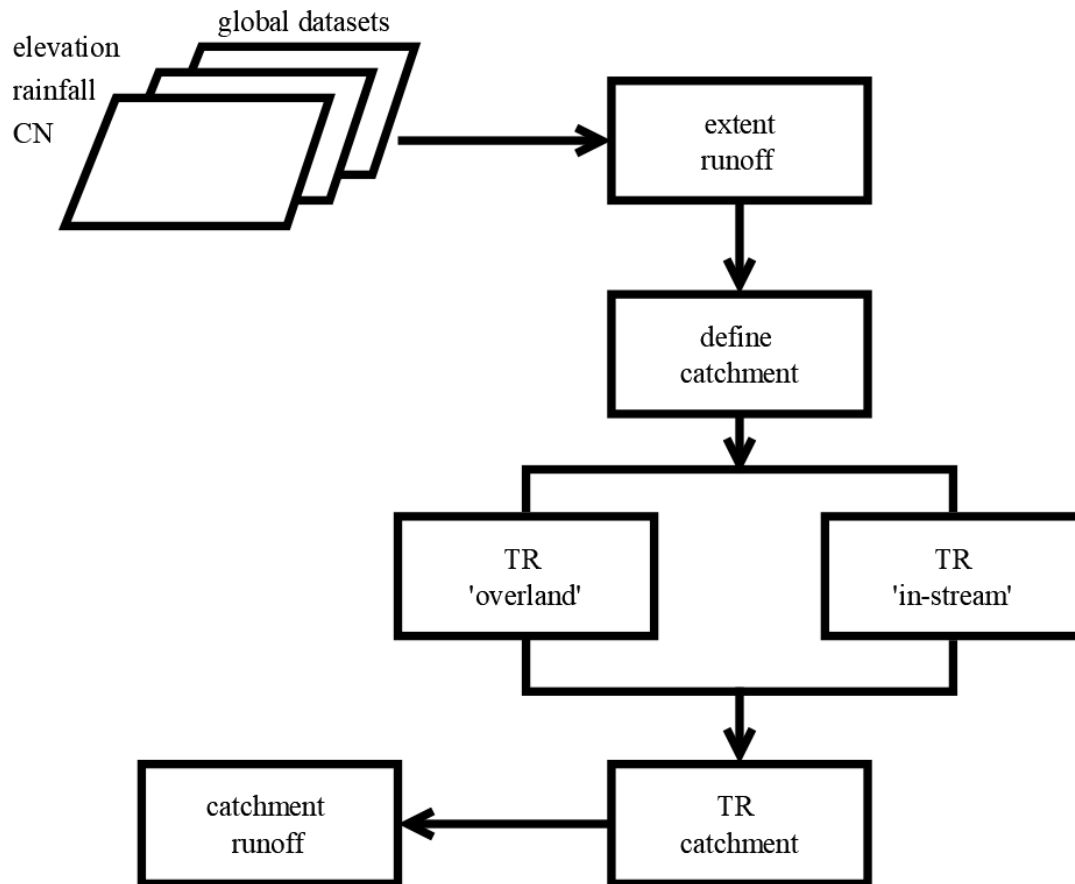


Figure 5.1. Schematic of the main stages of the HRRTLE process [CN = Curve Number; TR = Transferral Ratio].

The model was calibrated by comparing its outputs with the outflow data available for each catchment and adjusting the values of the power law index and time constant in the transferral ratio equations to optimise the model results' fit to the observed data. An assessment was then made of which types of catchments the model worked best for, why, and how the model might therefore be applied in practice, and improved in future research.

HRRTLE (High Resolution Runoff and Transmission Loss Estimator): a novel tool for mapping connectivity of runoff in ephemeral stream networks to aid the siting of water harvesting structures

### 5.3.2 Methods in detail

#### Catchment area selection and characterisation

Observed catchment outflow records from the Global Runoff Data Center database (GRDC, 2020) were scrutinised to identify catchments located primarily in arid or semi-arid regions with records spanning four decades from the early 1980's and missing <3 % daily values. Once a catchment was identified as a potential study area, three catchment morphometric parameters were computed. A GIS was used to define the catchment area from a DEM (EROS, 2018c), with a spatial resolution of 3 arc-seconds for global coverage. The catchment form factor (CFF), defined as the ratio of catchment area to the square of the basin length (Patel et al., 2015), and the Height Above Nearest Drainage (HAND) were then computed from the DEM – see Sect. 0 below for details of how the drainage network was identified. Each catchment was classified based on its area, CFF and HAND (**Table C1, Appendix C**). A subset of 28 catchments (**Figure 5.2**) that offered a range of permutations of area (large, intermediate or small), shape (CFF), and elevation (HAND) were then selected for the purposes of model development (**Table C2, Appendix C**). Of these, 15 are in South Africa, 7 in Australia, 3 in the USA, 2 in Brazil and 1 in Israel.

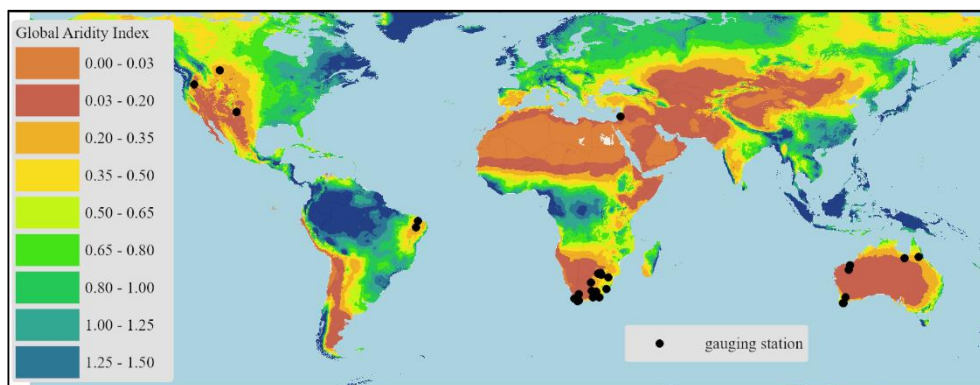


Figure 5.2. Map showing locations of runoff gauging stations used. Each station represents the outlet of a modelled catchment. Basemap of Global Aridity Index (Zomer and Trabucco, 2022).

HRRTLE (High Resolution Runoff and Transmission Loss Estimator): a novel tool for mapping connectivity of runoff in ephemeral stream networks to aid the siting of water harvesting structures

To further characterise the selected catchments, additional datasets were obtained. The mean aridity index was found for each catchment using a global aridity dataset (Zomer and Trabucco, 2022). Mean rainfall was derived from a Global Precipitation Climatology Centre (GPCC) 1° resolution dataset (Ziese et al., 2022). The baseflow percentage (i.e. the proportion of runoff at the catchment outlet that is derived from baseflow, rather than direct runoff generated by precipitation) was computed for each catchment by inputting the GRDC daily runoff data into a baseflow index calculator (U.S. Geological Survey, 2016). The runoff efficiency was calculated for each catchment by taking the ratio of the long-term runoff depth (mm) from the GRDC records to the mean depth (mm) obtained from the precipitation dataset. The mean peak runoff month was found by analysing observed runoff data. Land cover (spatial resolution ~1 km) for each catchment was obtained from global land cover datasets for the year 2000 (Eva et al., 2003; Latifovic et al., 2003; Mayaux et al., 2003; Mayaux and Bossard, 2003; Tateishi et al., 2003).

### **Direct runoff calculation**

The spatial resolution of the GPCC precipitation data was enhanced from 1° (approximately 110 km on a great circle) to 250 m using linear interpolation, to create a precipitation dataset,  $P$  (mm) that matched the spatial resolution of the CN dataset used (see below). Antecedent precipitation values,  $P\Sigma 5$  (mm), were then calculated for each day at each 250 m cell by summing the precipitation from the five preceding days. The antecedent moisture condition (AMC) was then assigned to each cell for each day based on the value of  $P\Sigma 5$  for that day and the season (**Table 5.1**), following Silveira et al. (2000).

HRRTLE (High Resolution Runoff and Transmission Loss Estimator): a novel tool for mapping connectivity of runoff in ephemeral stream networks to aid the siting of water harvesting structures

**Table 5.1. Selection of antecedent moisture condition (AMC) using antecedent precipitation (PΣ5) and season.**

AMC	dormant season PΣ5 (mm)	growing season PΣ5 (mm)
I (dry)	<13	36
II (normal)	13 to 28	36 to 53
III (wet)	>28	>53

Curve number values were taken from a global curve number dataset with a spatial resolution of 250 m (Jaafar et al., 2019), which provided CN values for the three AMC groups defined in **Table 5.1**. The appropriate CN value was selected according to the AMC value derived from **Table 5.1** and assigned to each cell in the extent. The daily direct runoff was then calculated from CN and  $P$  for each cell using the SCS-CN equations Eq. (5.1) and Eq. (5.2).

### **Transferral ratio calculations**

To determine catchment outflow from the direct runoff values for each cell in the catchment, knowledge of transmission losses is needed. These quantify how much of the direct runoff is lost – primarily to infiltration but also to evaporation and other processes (e.g. uptake by plants or animals) – on its journey from its source cell to the catchment outlet. Here, this is quantified in the form of transferral ratios – the fraction of the runoff that makes it to the catchment outlet. The transferral ratios are calculated by dividing the catchment into cells that form its drainage stream network (where fluxes are denoted “in-stream flow”) and the rest of the catchment (where fluxes are denoted “overland flow”). For runoff from each cell, partial transferral ratios are calculated for both that part of its journey that occurs as overland flow ( $TR_o$ ), and that part that occurs as in-stream flow ( $TR_n$ ). The overall transferral ratio ( $TR_c$ ) is then calculated as the product of  $TR_o$  and  $TR_n$ .

HRRTLE (High Resolution Runoff and Transmission Loss Estimator): a novel tool for mapping connectivity of runoff in ephemeral stream networks to aid the siting of water harvesting structures

### Stream network identification and parameterisation

To identify the cells that formed the catchment's stream network, the spatial resolution of the DEM was increased from 3 arc-seconds to 250 m by unifying and filling its tiles in a GIS environment (ArcGIS Pro 2.8) effectively matching its spatial resolution to that of the curve number and precipitation data. D8 flow direction value for each cell was then derived by identifying the neighbouring cell whose elevation was lowest. The D8 flow direction values were then used to calculate an unweighted flow accumulation value for each cell, defined as the total number of cells flowing into it.

Having calculated the flow accumulation value for each cell, the catchment's stream network was defined as being made up of all cells with a flow accumulation value greater than 65. This was based on the assumption that the threshold drainage area required to initiate stream formation and maintenance in arid or semi-arid zones is 4.05 km<sup>2</sup> (Gao et al., 2019), which approximates to 65 cells of size 250 m × 250 m, to the nearest whole number. Rasters of the following variables covering all cells in the stream network were then created within the GIS: the height above the catchment outlet, HACO<sub>n</sub> (m); the horizontal distance to the catchment outlet along the stream network, HFD<sub>n</sub> (m); the mean downstream slope of stream network cells,  $S_n$  (m m<sup>-1</sup>), found by dividing HACO<sub>n</sub> by HFD<sub>n</sub>, and the stream network mean downstream length, L<sub>n</sub> (m), calculated by taking the square root of the sum of the squares of HACO<sub>n</sub> and HFD<sub>n</sub>.

### In-stream flow transferral ratio calculation

The transferral ratio for that part of a cell's runoff's journey to the catchment outlet that travels down the stream network,  $TR_n$ , was calculated as:

HRRTLE (High Resolution Runoff and Transmission Loss Estimator): a novel tool for mapping connectivity of runoff in ephemeral stream networks to aid the siting of water harvesting structures

$$TR_n = \left( \frac{CN_{fd,n}}{100} \right)^{p_n} e^{k_n T_n} \quad (5.4)$$

Of the terms on the right hand side,  $CN_{fd,n}$  – the stream network mean annual curve number value for flood-days (dimensionless) – and  $T_n$  – the stream network travel time (days) are calculated, whereas  $p_n$  – the “curve number power law index” (dimensionless) – and  $k_n$  – the “travel time constant” (dimensionless) – are parameters whose values are adjusted in the calibration process whereby the calculated outflow is compared with observed outflow data for each catchment. Thus, Eq. (5.4) encapsulates the assumptions that more runoff will reach the outlet as curve number increases (which follows from the definition of curve number), and the longer the runoff takes to reach the outlet, the more of it will be lost along the way. Mathematically, these effects are hypothetically assumed to follow power law and exponential relationships, respectively.

Of the two calculated terms on the right hand side, the stream network mean annual curve number value for flood-days ( $CN_{fd,n}$ ) was calculated as the mean CN value for stream network cells in the runoff’s path for all days in the year when direct runoff occurred (i.e. when  $P\Sigma5 > 0.2S$ ). The calculation of the stream network travel time is more complex and is described in the following section.

#### Stream network travel time calculation

The stream network travel time to the catchment outlet was calculated using:

$$T_n = L_n / (86400V_n) \quad (5.5)$$

where  $T_n$  is the network mean downstream transit time (days),  $L_n$  is the stream network mean downstream length (m), and  $V_n$  is the stream network mean downstream velocity ( $m\ s^{-1}$ ). Calculation

HRRTLE (High Resolution Runoff and Transmission Loss Estimator): a novel tool for mapping connectivity of runoff in ephemeral stream networks to aid the siting of water harvesting structures

of  $L_n$  is described above. Calculation of  $V_n$  is based on Mannings equation for open channel flow (e.g. Chow et al., 1988) shown by:

$$V_n = \frac{1}{n} R^{2/3} S_f^{1/2} \quad (5.6)$$

where  $n$  is Manning's roughness coefficient ( $m^{-1/3}s$ ),  $R$  is the hydraulic radius (m), and  $S_f$  is the friction slope (dimensionless). Here,  $S_f$  is assumed to be equal to the mean downstream slope of stream network cells,  $S_n$  (see above), and the – more complex – procedures for calculating  $n$  and  $R$  are as follows.

To calculate values for  $n$ , it is first noted that there is a relationship between land use, CN and Manning's  $n$ . For example, natural forests have relatively low CN values and relatively high Manning's  $n$  values, whereas bare land has relatively high CN values and relatively low Manning's  $n$  values (Schwab et al., 1981 cited in Tarigan, 2016). Using this principle, that higher CN values are associated with lower hydraulic resistance to surface flow, a proxy for Manning's  $n$  was established by creating a linear relationship between it and CN. This was done by noting that the maximal Manning's  $n$  value is approximately 0.15, which is associated with “very weedy reaches, deep pools, or floodways with heavy stand of timber and underbrush”, while its minimal value is approximately 0.025, associated with “clean, straight, full stage, no rifts or deep pools” (Das, 2016). Similarly, CN values vary from a minimum of approximately 20 to a maximum of 100. By associating the maximal Manning's  $n$  with the minimal CN, and vice versa, and determining the equation of a line between these two points, the relationship

$$n = -0.0018CN + 0.185 \quad (5.7)$$

HRRTLE (High Resolution Runoff and Transmission Loss Estimator): a novel tool for mapping connectivity of runoff in ephemeral stream networks to aid the siting of water harvesting structures

was derived. Using the stream network mean annual curve number value for flood-days ( $CN_{fd,n}$ ), values of Manning's  $n$  can thus be estimated and used in Eq. (5.6) to calculate flow speed and thus stream network travel time.

The final element of Manning's equation, the hydraulic radius,  $R$ , is defined as  $A/P$ , the ratio of the stream flow cross-sectional area,  $A$ , to its wetted perimeter,  $P$ . These stream parameters cannot be determined directly from a DEM, or from any of the other input data sets that are commonly available. The parameter most closely related to  $A$  and  $P$  that may be derived from the available data is stream channel width,  $W$ . The precise relationship between  $W$  and  $A$  and  $P$  will vary, but for small streams in arid or semi-arid zones, we assumed that the channels would be approximately triangular and have depth  $W/12$ . The decision to select a depth of  $W/12$  was influenced by the common use of a width-to-depth ratio of 12 when delineating natural rivers (Rosgen, 1994). This choice was anticipated to accommodate a diverse range of river types. Thus, we estimated the hydraulic radius using:

$$R = \frac{\frac{W}{2} \times \frac{W}{12}}{2 \left( \left( \frac{W}{2} \right)^2 + \left( \frac{W}{12} \right)^2 \right)^{0.5}} = \frac{W}{2\sqrt{148}} \approx \frac{W}{24} \quad (5.8)$$

We derived channel widths by assuming that they were linearly related to the flow accumulation value for each stream network pixel, the calculation of which is described in this section, above. Thus:

$$W_n = aFA_n + b \quad (5.9)$$

where  $a$  and  $b$  are empirical constants that require determination. This was carried out by manually measuring 20 stream widths using an ArcGIS Pro World Imagery basemap (Source: Esri, Maxar, Earthstar Geographic, and the GIS User Community) from locations within each catchment selected

HRRTLE (High Resolution Runoff and Transmission Loss Estimator): a novel tool for mapping connectivity of runoff in ephemeral stream networks to aid the siting of water harvesting structures

to cover a range of flow accumulation values. These widths were regressed against their locations' flow accumulation values, to give catchment specific values for  $a$  and  $b$ . A list of catchment codes alongside the values of these constants is provided in **Appendix C (Table C3)**.

### **Overland flow transferral ratio calculation**

All catchment cells not designated as stream network cells, i.e. all cells with a flow accumulation value of 65 or less, were classified as “overland flow” cells. The calculation of the transferral ratio for runoff flowing through these cells followed the same general approach as that laid out above for in-stream cells, but required some different assumptions and approximations to be made to reflect the different nature of the conditions. Using the same assumptions as those represented in Eq. (5.4) for stream network cells, the overland transferral ratio,  $TR_o$ , was calculated as:

$$TR_o = \left( \frac{CN_{fd,o}}{100} \right)^{p_o} e^{k_o T_o} \quad (5.10)$$

where  $CN_{fd,o}$  is the mean CN value along the overland flow path for flood days;  $p_o$  is the overland curve number power law index;  $k_o$  is the overland travel time constant; and  $T_o$  is the overland travel time (days). For each overland cell, the travel time for runoff to reach the catchment outlet,  $T_o$ , was calculated, analogously to Eq. (5.5), as:

$$T_o = L_o / (86400 V_o) \quad (5.11)$$

where  $L_o$  is the mean downstream overland length (m), and  $V_o$  is the mean downstream overland velocity ( $m\ s^{-1}$ ).  $L_o$  was calculated as the square root of the sum of the squares of  $HAND_o$  and  $HFD_o$ , whose definition and derivation are described previously in this section.  $V_o$  was calculated using a method based on the shallow concentrated flow equations. For unpaved (grassed waterway) and paved

HRRTLE (High Resolution Runoff and Transmission Loss Estimator): a novel tool for mapping connectivity of runoff in ephemeral stream networks to aid the siting of water harvesting structures

surfaces, respectively, these give the relationships between flow speed,  $V$ , and along-flow slope,  $S_f$ , as (Cronshey et al., 1985) by:

$$V = 4.9178S_f^{0.5} \quad (5.12)$$

and

$$V = 6.1960S_f^{0.5} \quad (5.13)$$

By adopting a similar principle to that used for relating CN to Manning's coefficient in Eq. (5.7) above, a linear relationship was assumed between  $CN_{fd,o}$  and the coefficients in Eq. (5.12) and Eq. (5.13). The coefficient for the rough, unpaved surface, 4.9178 in Eq. (5.12), was given an equivalent  $CN_{fd,o}$  value of 60, while that for the smoother, paved surface, 6.1960 in Eq. (5.13), was given an equivalent  $CN_{fd,o}$  value of 100. This recasts Eq. (5.12) and Eq. (5.13) as:

$$V_o = (0.0325CN_{fd,o} + 2.95)S_o^{0.5} \quad (5.14)$$

where  $V_o$  is the mean downstream overland velocity ( $\text{m s}^{-1}$ ),  $CN_{fd,o}$  is the overland mean downstream annual curve number for flood-days (dimensionless), and  $S_o$  is the mean downstream overland slope ( $\text{m m}^{-1}$ ).

### **Overall transferral ratio**

For each cell within the catchment, the overall transferral ratio, i.e. the proportion of rainfall running off from that cell that reached the catchment outlet, was calculated as:

$$TR_c = TR_n \times TR_o \quad (5.15)$$

HRRTLE (High Resolution Runoff and Transmission Loss Estimator): a novel tool for mapping connectivity of runoff in ephemeral stream networks to aid the siting of water harvesting structures

where  $TR_c$  is the catchment transferral ratio;  $TR_n$  is the in-stream transferral ratio; and  $TR_o$  is the overland transferral ratio (which is defined as 1 if the cell in question is part of the stream network). This was then multiplied by the (annual) direct runoff for the cell to give the model's estimate of that cell's contribution to the annual runoff at the catchment outlet (i.e. the harvested water if the catchment outlet represents a potential water harvesting location).

### 5.3.3 Model performance

The performance of the HRRTLE tool was evaluated using two commonly used measures, the Nash-Sutcliffe simulation efficiency (NSE) and percentage bias (Pbias), which were calculated, respectively, as:

$$NSE = 1 - \frac{\sum_{i=1}^n (Q_{i,obs} - Q_{i,cal})^2}{\sum_{i=1}^n (Q_{i,obs} - \overline{Q_{obs}})^2} \quad (5.16)$$

and

$$Pbias = \left[ \frac{\sum_{i=1}^n (Q_{i,cal} - Q_{i,obs})}{\sum_{i=1}^n (Q_{i,obs})} \right] \times 100 \% \quad (5.17)$$

where  $n$  is the total number of events,  $Q_{i,obs}$  is the observed flow,  $Q_{i,cal}$  is the calculated flow, both at time  $i$ , and  $\overline{Q_{obs}}$  is the average observed flow (Cirilo et al., 2020). NSE is commonly used to assess the predictive abilities of hydrological models, and generates values that can range from  $-\infty$  to 1. An NSE value of 1 indicates a perfect model, with zero mean difference between observed and calculated flows.  $NSE = 0$  implies that the model has no greater predictive power than simply assuming constant flow equal to the observed mean.  $NSE < 0$  means that the model has worse predictive power than the

HRRTLE (High Resolution Runoff and Transmission Loss Estimator): a novel tool for mapping connectivity of runoff in ephemeral stream networks to aid the siting of water harvesting structures

observed mean flow (Knoben et al., 2019). Pbias (see Eq. 5.17) measures the tendency of the calculated flows to be either larger or smaller than their observed counterparts (Yapo et al., 1996). A Pbias greater than zero indicates that the model underestimates observed flows, while a negative value suggests overestimation (Carlos Mendoza et al., 2021). While achieving a bias of zero would be an ideal target for a model for the sake of scoping potential water harvesting (especially for ungauged catchments), Moriasi et al. (2007) and Abbaspour et al. (2015) suggest that an absolute value of Pbias less than 25 % indicates good model performance. Here, as we are working with ungauged catchments, we argue that this criterion for good performance should be somewhat relaxed, and thus take an absolute value of Pbias less than 50 % to indicate a threshold between adequate and inadequate performance.

HRRTLE was applied to each of the 28 catchments and the calculated flows evaluated against observed runoff records. In each case, in order to assess the value of applying the transferral ratio calculations described above, the model was run both with and without transmission losses,  $TR_c$ . If the values of NSE and Pbias improved when  $TR_c$  was applied, this would imply that its use was beneficial for model accuracy. Four parameters ( $k_n$ ,  $p_n$ ,  $k_o$ ,  $p_o$ ) from the stream network and overland transferral ratio equations, Eq. (5.4) and Eq. (5.10), were adjusted during the calibration stage. Each time one of these parameters was adjusted, the model was re-run and the NSE recorded. Once the NSE could not be increased by adjusting a particular parameter, the next parameter was used. Once a combination of parameter values was found through this process, for which the NSE value could not be further improved, it was recorded and subsequently used in the model validation stage. Observed runoff data from even years was used in the calibration stage, while odd years' data was used for validation. The number of years of data used for the calibration and validation stages, together with the optimum

HRRTLE (High Resolution Runoff and Transmission Loss Estimator): a novel tool for mapping connectivity of runoff in ephemeral stream networks to aid the siting of water harvesting structures

transferral ratio parameter values used in the validation stage for each catchment are presented in **Appendix C (Table C4)**.

## **5.4 Results**

### **5.4.1 Model output**

Runoff connectivity maps (RCMs) were generated by the HRRTLE modelling process to visually communicate the distribution of runoff contributions to the catchment outlets. An example of these maps is presented in **Figure 5.3** for catchment AUNP, which has its outlet at a gauging station on the Shaw River in northern Western Australia. In this case, 18 years of validation model outputs were used to create the RCM, which shows the annual runoff depth (mm) for each cell that reaches the catchment outlet, taking transmission losses into account. The spatial resolution of the map is 250 m × 250 m. The map shows the importance of proximity to both the outlet and the stream network for maximising outlet runoff contributions.

HRRTLE (High Resolution Runoff and Transmission Loss Estimator): a novel tool for mapping connectivity of runoff in ephemeral stream networks to aid the siting of water harvesting structures

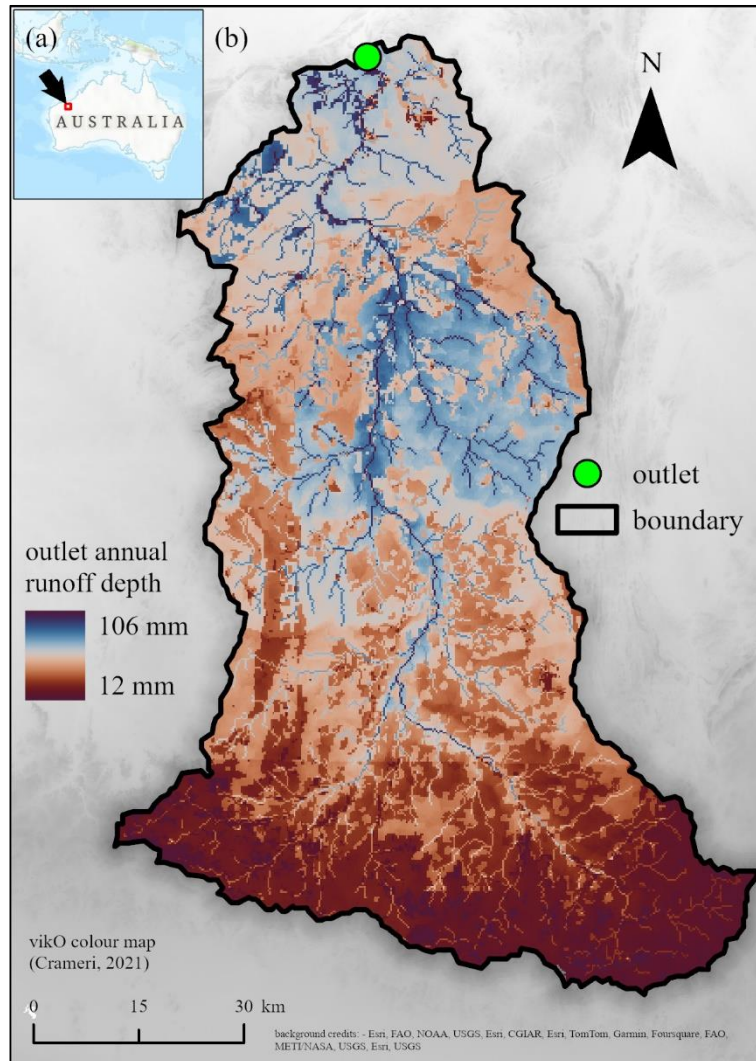


**Figure 5.3.** (a) location of AUNP catchment; (b) runoff connectivity map (RCM) for the catchment of a gauging station located on the Shaw River, showing mean annual runoff reaching catchment outlet taking transmission losses into account, created using validation data.

### 5.4.2 Assessment of model performance

**Table 5.2** summarises the optimum NSE and Pbias values for each catchment in the calibration and validation stages, for both the runoff-only ('ro') and runoff-and-transferral-ratio ('tr') versions of the model.

HRRTLE (High Resolution Runoff and Transmission Loss Estimator): a novel tool for mapping connectivity of runoff in ephemeral stream networks to aid the siting of water harvesting structures

**Table 5.2. Values of the Nash-Sutcliffe efficiency (NSE) and percentage of average tendency (Pbias) for calibration (cal) and validation (val) runs of the runoff-only (ro) and runoff-and-transferral-ratio (tr) versions of the model, for each of the 28 test catchments. The first two letters of the catchment code indicate country: Australia (AU), Brazil (BR), Israel (IR), USA (US) or South Africa (ZA).**

catchment code	calibration				validation			
	NSE <sub>ro,cal</sub> (-)	NSE <sub>tr,cal</sub> (-)	Pbias <sub>ro,cal</sub> (%)	Pbias <sub>tr,cal</sub> (%)	NSE <sub>ro,val</sub> (-)	NSE <sub>tr,val</sub> (-)	Pbias <sub>ro,val</sub> (%)	Pbias <sub>tr,val</sub> (%)
AUFR	-305.564	0.039	1158.3	-35.0	-185.942	-0.209	1382.6	-3.2
AUGD	-1.966	0.705	130.0	20.0	0.668	0.609	42.9	-26.7
AULT	-92.259	0.105	1064.0	16.5	-1.310	0.058	324.9	-62.9
AUMF	-0.629	-0.835	-52.8	-63.4	0.193	0.009	-34.3	-48.7
AUMS	-8.442	0.240	199.0	7.4	-0.407	0.672	136.7	-13.1
AUNP	-0.903	0.353	183.8	-6.5	-8.376	0.410	312.6	56.0
AUSJ	-0.327	-0.407	-51.8	-54.4	-0.764	-1.875	-35.5	-38.8
BRMN	0.281	0.265	12.7	-17.9	0.283	0.199	-2.7	-28.9
BRPR	-5.280	0.648	206.9	-3.9	-0.964	0.328	228.0	6.4
ILOB	-3.110	-3.155	-96.5	-97.1	-5.055	-5.138	-96.4	-97.0
USMH	-4.046	-6.209	-67.6	-82.2	-1.899	-2.092	-64.0	-66.7
USNP	-8.220	-8.501	-57.0	-62.8	-12.502	-10.082	-10.8	-22.0
USSC	-4.646	-4.688	-97.3	-97.7	-6.489	-6.540	-97.6	-98.0
ZAAN	-0.440	-0.663	-45.6	-50.5	-0.027	-0.109	-35.5	-41.2
ZABT	-8.615	0.044	314.1	-11.7	-30.761	-0.387	388.9	26.4
ZADE	-31.513	0.186	1175.7	4.5	-37.383	0.125	1006.1	-22.4
ZADK	-0.082	0.129	10.6	-16.8	-3.608	-1.415	108.5	64.0
ZAHE	-1.467	0.129	121.2	-27.9	-14.182	-1.712	328.0	101.7
ZAHH	0.077	0.100	4.7	-18.4	0.014	0.011	-23.3	-42.0
ZAKK	-20.469	-0.404	331.3	-12.6	-18.204	-0.117	283.7	-24.3
ZAMB	-1.951	-1.972	-88.9	-90.3	-0.882	-0.926	-91.3	-92.4
ZAMK	0.096	0.057	-44.1	-47.5	-0.036	-0.052	-11.9	-17.1
ZAO	-0.866	-0.061	76.6	24.6	-6.524	-1.319	165.1	64.7
ZAOS	-28.792	-0.274	527.9	-4.1	-0.353	-0.442	61.3	-73.8
ZASD	-1.661	-1.890	-61.9	-66.6	-1.512	-1.755	-56.0	-64.9
ZAT	-50.187	0.186	961.6	-20.5	-301.272	0.148	1646.3	43.8
ZAUL	-0.546	0.012	59.9	4.0	-0.870	0.441	77.1	14.4
ZAW	-0.378	0.527	62.3	2.0	-3.170	-0.423	87.5	19.9

A first assessment of these results suggests that the use of transferral ratios improves the performance of the model (i.e. moves the NSE closer to 1 and Pbias closer to zero) as demonstrated in **Table 5.3**. However, it also indicates that there is a significant proportion of the 28 test catchments used where it does not lead to satisfactory performance by any of the measures.

HRRTLE (High Resolution Runoff and Transmission Loss Estimator): a novel tool for mapping connectivity of runoff in ephemeral stream networks to aid the siting of water harvesting structures

**Table 5.3. Number (out of 28) catchments which show satisfactory values ( $NSE > 0$ ;  $-50\% < Pbias < 50\%$ ) for the NSE and Pbias performance metrics at the calibration (cal) and validation (val) stage of model development.**

performance measure	number of satisfactory catchments runoff only	number of satisfactory catchments with transferral ratio	improved (yes/no)
$NSE_{cal}$	3	16	yes
$Pbias_{cal}$	5	19	yes
$NSE_{val}$	4	11	yes
$Pbias_{val}$	8	17	yes

The sensitivity of the NSE to the transferral ratio equation parameters ( $k_n, p_n, k_o, p_o$  – see equations (5.4) and (5.10)) that were adjusted to calibrate the model is shown in **Figure 5.4**, for an example test catchment (code AULT), which shows typical behaviour for this analysis. It indicates that the NSE was most sensitive to the stream network flow travel time constant, and least sensitive to the overland flow travel time constant, and had intermediate sensitivity to the two curve number power law indices.

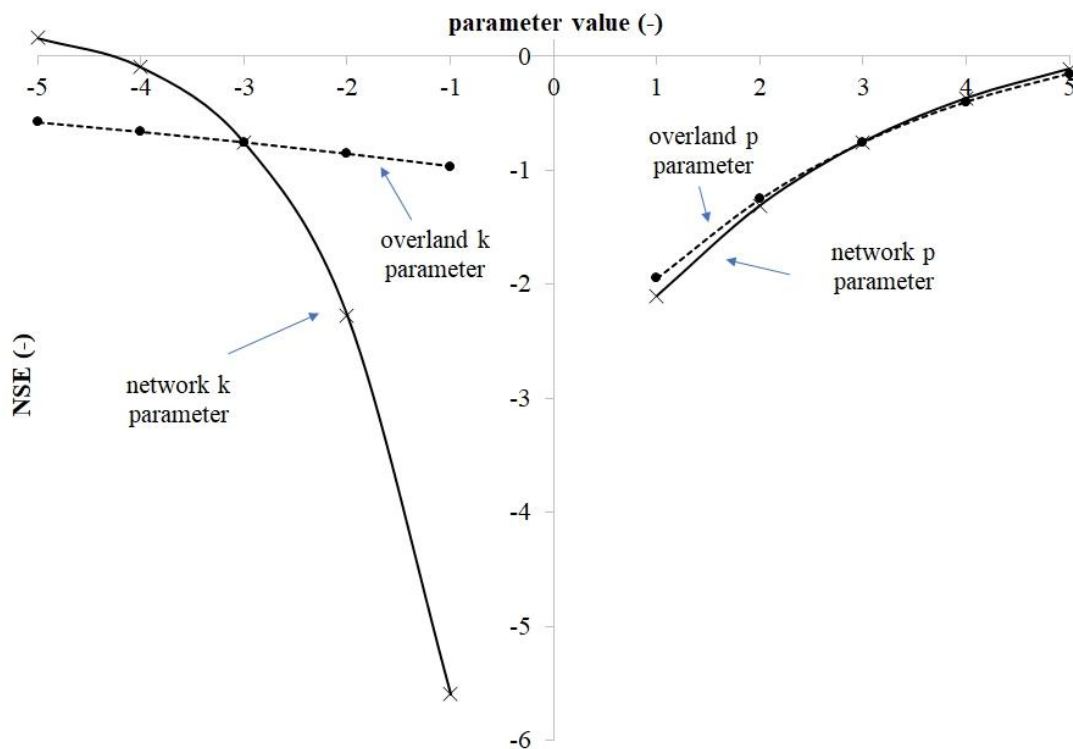


**Figure 5.4. Sensitivity of Nash-Sutcliffe efficiency (NSE) to variation in transmission loss parameters (catchment code AULT) for calibration data.**

HRRTLE (High Resolution Runoff and Transmission Loss Estimator): a novel tool for mapping connectivity of runoff in ephemeral stream networks to aid the siting of water harvesting structures

### 5.4.3 Determination of catchment types for best model performance

To determine which types of catchments the model performs best upon we focus on the results from the validation stage of the modelling (since this is a test of model performance, c.f. the calibration stage, which is an exercise in optimising the model performance) and on the results for model runs where transferral ratios are incorporated (since this is the main novel contribution of this work). On this basis, 11 of the 28 catchments have satisfactory NSE values ( $>0$ ) and 17 have satisfactory Pbias values (absolute values  $<50\%$ ), with 9 having both. These nine are listed in **Table 5.4**, with their predominant land cover characteristics.

**Table 5.4. Catchments with NSE  $> 0$  and absolute Pbias values  $<50\%$  for validation models with transferral ratio effects incorporated, with the predominant land cover characteristics.**

catchment code	predominant land cover (classification and percentage of coverage)
AUGD	grasslands with sparse shrubs 77 %
AUMS	closed shrublands 80 %
BRMN	mosaic agriculture / degraded vegetation 34 %; open deciduous forest 27 %; Montane forests 500–1000 m - open deciduous 15 %
BRPR	open shrublands 32 %; Montane forests 500–1000 m - open deciduous 18 %; Montane forests 500–1000 m - open semi-humid 10 %; mosaic agriculture / degraded vegetation 9 %; agriculture – intensive 8 %
ZADE	open grassland with sparse shrubs 85 %
ZAHH	open grassland 47 %; open grassland with sparse shrubs 38 %
ZAT	open grassland with sparse shrubs 63 %; closed grassland 34 %
ZAUL	deciduous woodland 40 %; croplands ( $>50\%$ ) 32 %

**Table 5.5. Proportion of catchments of different dominant landcover type for which the model performed satisfactorily in the validation stage with transferral ratios incorporated.**

dominant landcover type	total number of catchments / 28	# of catchments with NSE $>0$ ; -50 % $<$ Pbias $<$ 50 %	% of total catchments with NSE $>0$ ; -50 % $<$ Pbias $<$ 50 %
grassland	4	4	100
agriculture	1	1	100
woodland	2	1	50
shrubland	9	3	33
croplands	7	0	0
forest	5	0	0
	28	9	

HRRTLE (High Resolution Runoff and Transmission Loss Estimator): a novel tool for mapping connectivity of runoff in ephemeral stream networks to aid the siting of water harvesting structures

Their ranges of values, in the context of the ranges for all 28 catchments, for seven other biophysical catchment parameters are shown in **Table 5.5**. The full set of values of these parameters are provided in tabular format in the Supplementary Materials. The nine catchments with a positive NSE value and absolute Pbias values less than 50 % (**Table 5.4**) are compared to all 28 catchments in a summarised format (**Table 5.5**). **Table 5.5** shows that while seven of the 28 catchments have a dominant landcover type of ‘croplands’ none of these catchments are amongst of the nine catchments that demonstrated superior model performance (**Table 5.4**). The same situation is repeated for five catchments with a dominant landcover type of ‘forest’. All four ‘grassland’ catchments (**Table 5.5**) provided model results that fell into the top nine catchments (**Table 5.4**) as did the single catchment with a dominant landcover type of agriculture. Taken as a whole, this suggests that the model works best in catchments where there is low-growing vegetation (grassland or (pastoral) agriculture), and not well in catchments where the vegetation is tall and/or dense (croplands and forests).

HRRTLE (High Resolution Runoff and Transmission Loss Estimator): a novel tool for mapping connectivity of runoff in ephemeral stream networks to aid the siting of water harvesting structures

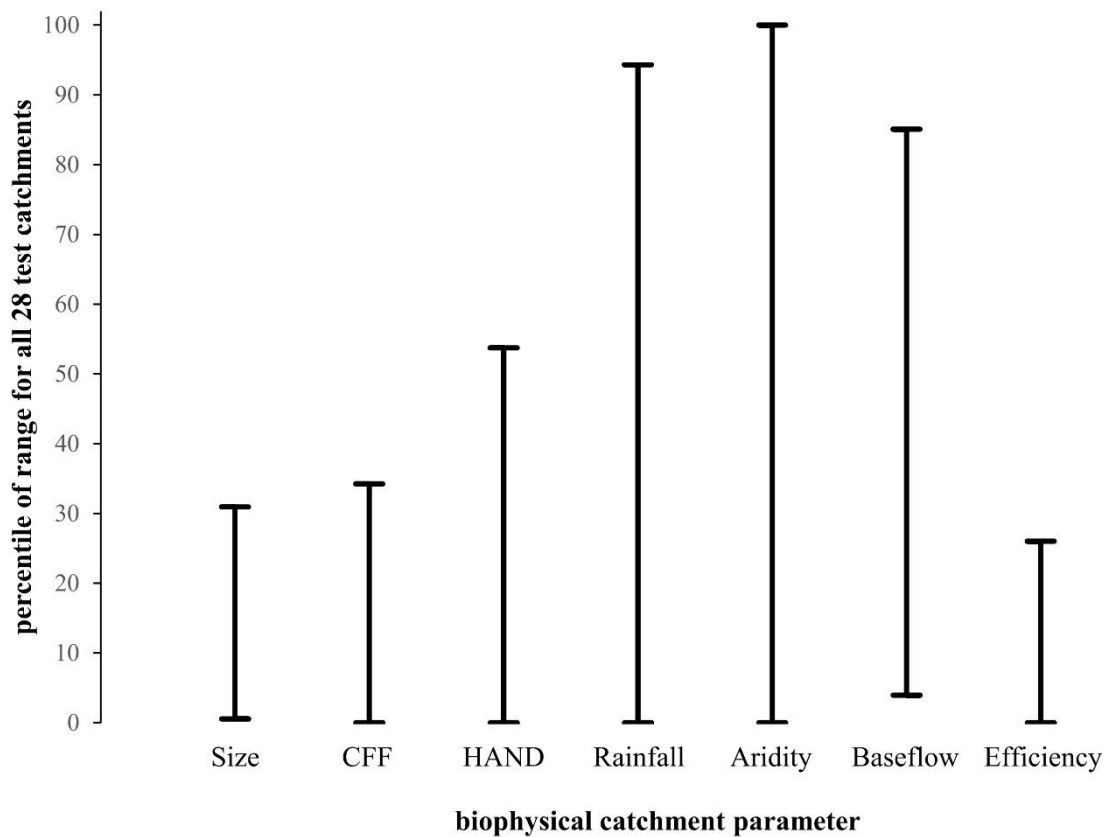


**Figure 5.5.** Range of values of seven biophysical catchment parameters for 9 catchments with  $NSE > 0$  and absolute  $Pbias < 50\%$ , in the context of the full range of values for all 28 catchments for each parameter. Size: catchment area; CFF: catchment form factor; HAND: height above nearest drainage; Rainfall: mean annual rainfall; Aridity: mean aridity index; Baseflow: % of runoff from baseflow; Efficiency: runoff efficiency

Turning next to **Figure 5.5**, the group of nine catchments for which the model performed satisfactorily are distinguished amongst the full set of 28 by their (a) relatively small size ( $<17,027 \text{ km}^2$ ); (b) relatively low ( $<0.147$ ) catchment form factor (i.e. lack of elongation in any direction); (c) low ( $<12.4\%$ ) runoff efficiency (proportion of rainfall that becomes runoff at the catchment outlet); and to a lesser extent (d) height ( $<90 \text{ m}$ ) above nearest drainage (i.e. mean elevation). The appearance of runoff efficiency in this list suggests the effect of our transferral ratio calculation method being incorporated into the model. The hydrological parameters considered – mean rainfall, aridity index and percentage of runoff from baseflow, do not distinguish the nine catchments from the full set of 28 at all. Considered together, therefore, the results shown in **Table 5.4**, **Table 5.5** and **Figure 5.5** suggest

HRRTLE (High Resolution Runoff and Transmission Loss Estimator): a novel tool for mapping connectivity of runoff in ephemeral stream networks to aid the siting of water harvesting structures

that the model works best in catchments that are relatively small; of approximately equal length in all directions; of relatively low topography; have high levels of transmission losses of runoff on its journey to the catchment outlet; and have predominantly low-growing vegetation.

## **5.5 Discussion**

### **5.5.1 Methodology**

HRRTLE employs three global datasets, one being the SRTM void filled elevation product, encompassing 80 % of the Earth's land surface between 60° north and 56° south. This dataset offers a spatial resolution of 3 arc-seconds, approximately 90 m spatial resolution, based on radar data acquired in 2000. The suitability of the elevation dataset for the HRRTLE process relies on the assumption that the elevation data from the year 2000 adequately represents in-stream networks for all modelled years, disregarding changes in morphology. The SRTM void filled elevation data, has previously been applied in hydrologic analyses for water harvesting studies (Sreedevi et al., 2009; Grum et al., 2016; Salih and Hamid, 2017; Ahmed and Diab, 2018; Abdekareem et al., 2022). The HRRTLE process adjusts the spatial resolution of the SRTM dataset to 250 m to match the curve number dataset. Consequently, some degree of diminished hydrological model performance might be anticipated compared to using the process with the original 90 m × 90 m data. Yang et al. (2001) investigated the sensitivity of hydrological models to spatial resolution changes, exploring resolutions up to 1,000 m × 1,000 m. They found that the hydrological response is sensitive to changes in the spatial resolution of the DEM, but the significance is greater for hourly response over daily response. Since the HRRTLE process employs a daily temporal resolution for runoff computation then this would suggest that the downgrade in spatial resolution from 90 m to 250 m is not expected to significantly affect runoff computation. Nevertheless, it should be noted that the HRRTLE process goes beyond mere direct

HRRTLE (High Resolution Runoff and Transmission Loss Estimator): a novel tool for mapping connectivity of runoff in ephemeral stream networks to aid the siting of water harvesting structures

runoff computation at individual cells or pixels. Instead, it models the runoff path to the designated catchment outlet and, for the modelled pathways, acquires curve number data to predict transmission losses. Hence, when a DEM is not adequately suited for modelling in-stream networks, there is a greater probability that the curve number data acquired through the HRRTLE process for cells identified as part of the 'network' does not accurately reflect channelised flow.

The HRRTLE modelling process consists essentially of two components. The first component utilises the GPCC precipitation data to predict runoff from each  $250 \text{ m} \times 250 \text{ m}$  gridded cell using curve number maps (Jaafar et al., 2019) based on the SCS-CN method. The second (novel) component predicts the amount of runoff reaching the catchment outlet from the cell where runoff occurs, accounting for transmission losses. The journey from the runoff cell to the outlet, is modelled as 'overland' flow followed by in-stream 'network' flow. This process makes a universal assumption that, regardless of actual catchment characteristics, overland flow transitions to network flow when the catchment area reaches approximately  $4 \text{ km}^2$ . One of the simplifying assumptions in the HRRTLE process involves maintaining a consistent relationship between flow accumulation (and consequently catchment area) and stream width across the entire catchment. The HRRTLE process assumes that curve number values along the overland and network flowpaths can be used to infer channel properties (i.e. Manning's roughness coefficient). To our knowledge, HRRTLE is the first rainfall-runoff model that utilises such an assumption, although Soni et al. (2022) did estimate equivalent runoff coefficients based on the colour of Google Earth pixels to predict runoff. Associating curve number with hydraulic roughness relies on the presumption that flowpaths characterised by a higher average curve number are prone to greater wetness or saturation compared to those with lower curve number values. Consequently, these paths pose reduced resistance to open channel flow and, simultaneously, result in

HRRTLE (High Resolution Runoff and Transmission Loss Estimator): a novel tool for mapping connectivity of runoff in ephemeral stream networks to aid the siting of water harvesting structures

fewer transmission losses due to the relatively higher saturation of the ground. Employing curve number values in this manner eliminates the necessity of incorporating extra datasets to define hydraulic roughness. The curve number dataset, utilised for calculating transmission losses along flowpaths, is the same dataset employed in the initial component of the model for runoff computation using the SCN-CN method. As a result, this approach restricts the number of datasets, each carrying its own uncertainties, to three.

### **5.5.2 Performance**

Out of the 28 catchments simulated with HRRTLE, nine demonstrate a positive NSE value and a Pbias within the range of -50 % to 50 % during the validation stage. Additionally, by expanding the Pbias to  $\pm 65$  %, eleven catchments show a positive NSE value in the validation results. It is thus worthwhile to examine the potential factors contributing to the superior performance of HRRTLE in certain situations and its poorer performance in others. The findings suggest that HRRTLE exhibits improved performance with smaller catchment sizes, although some larger catchments still produced reasonable results. Among the ten catchments categorised as the largest in size, four (AUGD; AUNP; ZADE; ZAT) yielded a positive NSE value during the calibration stage. One plausible explanation could be that the contributing factor to suboptimal results may not be the size of the catchment, but rather the potential for larger catchments to be more diverse and complex. This complexity, which may include engineered structures, could pose challenges for HRRTLE in achieving satisfactory modelling results. None of three large catchments located in North America (USMH; USNP; USSC) gave a positive NSE value for the validation stage.

Certain catchments exhibit relatively high runoff efficiencies, as determined through the calculation using GPCC precipitation and observed discharge data. For instance, one catchment (ILOB) has a

HRRTLE (High Resolution Runoff and Transmission Loss Estimator): a novel tool for mapping connectivity of runoff in ephemeral stream networks to aid the siting of water harvesting structures

runoff efficiency value of 47.7 %. One possible explanation for this is that the observed discharge data incorporates flows beyond those generated solely by precipitation within the catchment boundary — suggesting potential external introduction of water in some manner. Six of the 28 catchments tested in this study had a runoff efficiency greater than 16 %, none of which produced a positive NSE value in the validation stage.

The results suggest a tendency of superior model performance for catchments characterised by low-lying vegetation. One potential rationale is that the radar technology employed to generate the SRTM product encounters difficulties in penetrating vegetation. As a result, digital elevation models (DEMs) for catchments with sparse or low-lying vegetation might be more advantageous for hydrological modelling processes compared to catchments with dense canopy cover. For this study HRRTLE was used to analyse 28 catchments, five of which can be classified by a dominant ‘forest’ cover yet none of these five catchments are included in the group of nine catchments that performed better than others in terms of NSE and absolute Pbias (**Table 5.5**).

Several test catchments (coded as AUFR, ZADE, ZAT) exhibited Pbias values exceeding 1,000 % during the validation stage (**Table 5.2**) when transmission losses were not taken into account. The calculated baseflows for these catchments are 3.8 %, 7.1 %, and 14.1 %, respectively (see **Table C5** in **Appendix C**) which aligns closely with existing literature on this topic. Pilgrim et al. (1988) proposed that the rainfall-runoff modelling approach for arid and semi-arid regions may differ from that for humid zones, as baseflow is essentially absent in arid zone hydrology, while channel transmission losses are crucial. Transmission losses have been documented to surpass 75 % in arid regions (Knighton and Nanson, 1994) and up to ~70 % in semi-arid regions (Abboushi et al., 2015). Studies based in arid and semi-arid regions have generated runoff maps without incorporating

HRRTLE (High Resolution Runoff and Transmission Loss Estimator): a novel tool for mapping connectivity of runoff in ephemeral stream networks to aid the siting of water harvesting structures

transmission losses (Al-Ghobari et al., 2020; Karimi and Zeinivand 2021; Alataway, 2023; Radwan and Alazba, 2022). Such maps, if used to compute inflows for potential *ex situ* water harvesting structures, run the risk of overestimating runoff (or runoff potential) as they do not allow for transmission losses which in dryland regions can be considerable as previously noted. Sayl et al. (2019) created a runoff volume map linking infiltration losses with drainage frequency density. The concept of a connectivity map is not new, as D'Haen et al. (2013) previously developed a connectivity map of geomorphic coupling for points within a catchment in relation to the catchment outlet. Current rainfall-runoff models exhibit limitations in certain aspects. According to Shanafield et al. (2021, p. 12), rainfall-runoff models "...tell us little of the physical processes and dominant hydrologic flowpaths by which water migrates from its landing place within the catchment to become streamflow". The HRRTLE process addresses this criticism in part, as the connectivity runoff map (e.g. **Figure 5.3**) provides information on flowpaths and quantifies (in mm) the annual runoff reaching the catchment outlet (which theoretically could be a potential water harvesting location) for every pixel at a high spatial resolution allowing planners to understand the relative significance of various parts of the catchment with respect to outlet discharge.

### **5.5.3 Application**

The development of the HRRTLE process was geared towards aiding the assessment of potential water harvesting sites within a designated area. This involves a comprehensive examination of numerous locations to pinpoint areas where water harvesting offers the most advantages. The primary phase where HRRTLE is anticipated to deliver valuable applications is during the initial scoping phase of a project cycle. Several characteristics of HRRTLE make it attractive to planners and specialists in the water harvesting sector. Firstly, it relies on freely available global datasets, eliminating the costs and

HRRTLE (High Resolution Runoff and Transmission Loss Estimator): a novel tool for mapping connectivity of runoff in ephemeral stream networks to aid the siting of water harvesting structures

delays associated with acquiring national data. Secondly, it utilises commonly available software such as MATLAB and ArcGIS Pro, as opposed to specialised hydrologic modelling software. Thirdly, HRRTLE is a relatively straightforward in terms of model construction, requiring only the catchment output and the extent boundaries to be defined by the modeller.

Numerous rainfall-runoff models exist, and some of them have been applied in water harvesting research. As previously mentioned in this paper, the SCS-CN model is frequently utilised in such studies (Ramakrishnan et al., 2009; Kadam et al., 2012; Moawad, 2013; Mahmoud, 2014; Pathak et al., 2020; Aghad, 2021; Manaouch et al., 2022). However, none of these studies address transmission losses. In contrast, the HRRTLE process, while also employing the SCS-CN method, takes transmission losses into account. The well-known Hydrologic Modelling System software (HEC-HMS) has also been utilised by researchers in the field of water harvesting (El Osta et al., 2021; Ghanem et al., 2021; Ndeketeya and Dundu, 2021; Ramadan et al., 2022; Soomro et al., 2022) and offers hydrologic modelling features such as runoff hydrographs, something that the HRRTLE process does not. The Soil and Water Assessment Tool (SWAT) model has also been used in water harvesting studies, as demonstrated by Ouessar et al. (2009), Al-wadaey et al. (2016), Doulabian et al. (2021) and Umugwaneza et al. (2022). Ouessar et al. (2009) expressed a preference for a cell-based routing procedure over SWAT's semi-distributed approach at the subbasin level when modelling flows in arid environments. While the HRRTLE process does not route hydrographs it does provide a runoff connectivity map at cell-level.

There are various ways in which HRRTLE could be employed in the context of water harvesting site suitability. If a specific location has been identified for siting a water harvesting structure, HRRTLE could be configured with the catchment outlet designated as the proposed structure's location. To

HRRTLE (High Resolution Runoff and Transmission Loss Estimator): a novel tool for mapping connectivity of runoff in ephemeral stream networks to aid the siting of water harvesting structures

provide planners with a diverse set of information including a high spatial resolution runoff connectivity map (e.g. **Figure 5.3**) which would enable planners to visualise parts of the catchment that contribute varying amounts of runoff to the outlet. The tool uses almost 40 years of precipitation data, allowing the return period of annual discharge to be determined.

Assuming a consistent relationship between stream width and flow accumulation, the HRRTLE process could be automated for multiple points, each representing an outlet (i.e. a potential location for a water harvesting structure), by repeating the transferral ratio elements of HRRTLE (**Figure 5.1**) without the need to re-process the SCS-CN computations over the 'extent'. Should the outlets points be sufficiently varied in terms of location and catchment area it would be possible to establish a regression relationship between catchment area and annual runoff discharge, allowing a prediction of annual runoff for every pixel within an area of interest. HRRTLE does not route hydrographs, resulting in the absence of peak flow estimations. Estimating peak inflows in response to a single flood event is essential when designing a water harvesting structure so excess inflows can bypass safely. Here we suggest that during the initial scoping phase of water harvesting sites, considering the ratio of annual runoff to the size of the water harvesting reservoir can aid the selection process. This approach would help streamline site options, allowing modelling efforts for individual events to focus on a reduced number of potential water harvesting sites. Potentially HRRTLE results could be combined with automated tools that compute water harvesting reservoir metrics (Petheram et al., 2017; Wimmer et al., 2019; Teschemacher et al., 2020; Delaney et al., 2022) so the site selection criteria such as reservoir storage volume to annual inflow volume ratio could be computed. The HRRTLE process does not serve as a substitute for established rainfall-runoff models (such as SWAT and HEC-HMS), but such models could be utilised after HRRTLE has been used to narrow down the number of possible sites or to reinforce the findings from the HRRTLE process.

HRRTLE (High Resolution Runoff and Transmission Loss Estimator): a novel tool for mapping connectivity of runoff in ephemeral stream networks to aid the siting of water harvesting structures

In cases where observed runoff data is available, HRRTLE can undergo calibration against these data. However, in practical terms, water harvesting scoping studies often occur in regions where obtaining observed runoff data is unavailable (i.e. ungauged catchments). The absence of observed discharge data presents challenges. As Beven (2012, p. 329) notes, "One of the great unsolved challenges in hydrology is the accurate simulation of a catchment without any observational data with which to calibrate a hydrological model, i.e. an ungauged basin." Despite this obstacle, HRRTLE does possess potential uses in ungauged catchments. Results could be sensitivity-based, with calibration performed for a range of runoff efficiencies. Alternatively, by matching catchment characteristics from gauged catchments where HRRTLE has been successfully calibrated and verified with observed discharge data to another ungauged catchment with the same essential characteristics, HRRTLE parameters could be applied to the ungauged catchment.

#### **5.5.4 Future work**

The GPCC precipitation dataset (Ziese et al., 2022) used in the HRRTLE process has a temporal range of 39 years (1982–2020) and a spatial resolution of 1.0 degree  $\times$  1.0 degree. The dataset is based on precipitation data provided by national meteorological and hydrological services, regional and global data collections as well as the World Meteorological Organization Global Telecommunication System data. GPCC offers full global coverage of the Earth's surface. Basheer and Elagib (2019) evaluated this for the Nile Basin, along with another five long-term rainfall products, and ranked the GPCC project the best performing based on monthly, maximum monthly and annual scales. Nevertheless, the spatial resolution of this dataset is rather coarse in comparison to the sizes of most of the 28 catchments examined in this study. To illustrate this point, a precipitation tile with a spatial resolution of 1.0 degree (~110 km on the equator) encompasses an area of about 12,000 km<sup>2</sup>, whereas only 5 of the catchments

HRRTLE (High Resolution Runoff and Transmission Loss Estimator): a novel tool for mapping connectivity of runoff in ephemeral stream networks to aid the siting of water harvesting structures

studied exceed this size. Therefore, future efforts could explore the sensitivity of HRRTLE to precipitation from higher resolution datasets.

In this investigation, the SCS-CN component of the HRRTLE process incorporated an initial abstraction ratio of 0.2, aligning with earlier studies (Sekar and Randhir, 2007; Elewa et al., 2012; Shalamzari et al., 2019). Nevertheless, other studies have utilised different ratio values (Liu et al., 2021; Weerasinghe et al., 2011). Subsequent research could investigate the consequences of altering the initial abstraction ratio. In this version of HRRTLE the SCS-CN component assumes a permanent dormant season so additional work could investigate how to distinguish between the dormant and growing season especially if this can be achieved without the need to introduce additional datasets. The HRRTLE modelling process computes annual runoff based on the calendar year, presuming that the entirety of annual discharge stems exclusively from precipitation occurring within the same calendar year. Future work could explore the effects of re-designing the modelling process, so the annual discharge calculations begin at the end of the dry season for example.

To model the 28 catchments using the HRRTLE process and establish the relationship between stream width and flow accumulation, a manual and subjective approach was employed, relying on individual judgment to delineate the riverbank. Introducing an objective and automated process to determine the relationship between stream width and flow accumulation would likely be advantageous. Flow width rasters can be created using SAGA-GIS (Conrad, 2009) based on the work by Gruber and Peckham (2009) and Quinn et al. (1991) yet flow widths are limited by the spatial resolution of the raster pixels. Automated tools based on remote sensing products have been developed such as RivWidthCloud (Yang et al., 2020) and GrabRiver (Wang et al., 2022b), while Mengen et al., 2020 created an automated process using Sentinel-1 products. These tools and processes could potentially automate

HRRTLE (High Resolution Runoff and Transmission Loss Estimator): a novel tool for mapping connectivity of runoff in ephemeral stream networks to aid the siting of water harvesting structures

the stream width measurement stage in future iterations of HRRTLE. However, the effectiveness of these tools to measure river widths for non-perennial river systems (typically associated with water harvesting) may be diminished compared to perennial rivers.

The HRRTLE process utilises in-stream network cells to extract CN values as a component of its methodology for calculating the transferral ratio. It is preferable therefore for an accurate alignment between the modelled in-stream cells and the actual stream network. The underlying assumption is that the current version of HRRTLE adequately maps genuine in-stream networks. Nonetheless, future work could assess the sensitivity of network modelling accuracy and explore ways to enhance the modelling process by using other elevation products than the SRTM void filled used in this study. HydroSHEDS is modified SRTM elevation data that integrates hydrographic baseline data (Lehner and Grill, 2013), is freely available, and could be more appropriate for the HRRTLE process should it offer superior modelling of stream networks so allowing the extraction of more pertinent values from the Curve Number dataset. Alternatively, it is possible to transform a Digital Surface Model (DSM) to a Digital Terrain Model (DTM) by eliminating forest canopy height so making it more preferable for hydrologic modelling performance. Such a procedure has been carried out on a Copernicus DEM with a land cover dataset (Potapov et al., 2021) creating a DTM dataset (Strahlendorff, 2024).

The HRRTLE process uses gridded maps of curve numbers (Jaafar et al., 2019) the development of which was based on the USDA Soil Conservation Service (SCS) Runoff Curve Number (CN) method. Sujud and Jaafar (2022) conducted runoff computations using this dataset in conjunction with the SCS-CN method, revealing that model performance was influenced by factors such as climate, soil permeability, and bedrock permeability. A potential area for future investigation could examine of the influence of permeability, particularly bedrock permeability, on the accuracy of HRRTLE results.

HRRTLE (High Resolution Runoff and Transmission Loss Estimator): a novel tool for mapping connectivity of runoff in ephemeral stream networks to aid the siting of water harvesting structures

In arid and semi-arid regions, the primary source of groundwater recharge is often considered to be transmission losses in ephemeral river systems (Shanafield et al., 2021). Although HRRTLE does not explicitly distinguish between losses attributed to evapotranspiration and those due to infiltration, in certain catchments, infiltration (representing groundwater recharge) can account for as much as 95 % of all transmission losses (McMahon and Nathan, 2021). Therefore, while HRRTLE was developed to quantify runoff, there exists the potential for HRRTLE outputs to be utilised to estimate groundwater recharge.

Model outputs for all catchments underwent verification against observed runoff data, yet acquiring these data from arid and semi-arid regions, crucial for validating runoff models, poses a considerable challenge. The scarcity of observed data stands out as a major issue for runoff modelling in arid regions (Pilgrim et al., 1988). While modelling can complement measurements, it cannot serve as a substitute for them (Silberstein, 2006). The limited availability of observed runoff data in arid and semi-arid regions, particularly in regions where water harvesting is practised, impedes the development of rainfall-runoff models, including the advancement of the HRRTLE process. Therefore, future efforts to enhance discharge measurement techniques, enabling the verification of models against actual flow data, would be valuable.

## **5.6 Conclusion**

Relying on three global datasets in conjunction with satellite imagery, a rainfall-runoff modelling process has been developed to compute annual catchment runoff and provide a high spatial resolution runoff connectivity map at 250 m × 250 m. The outcomes of this process, referred to as High Resolution Runoff and Transmission Loss Estimator (HRRTLE) tool, underwent validation against

HRRTLE (High Resolution Runoff and Transmission Loss Estimator): a novel tool for mapping connectivity of runoff in ephemeral stream networks to aid the siting of water harvesting structures

observed runoff data, achieving satisfactory results in some instances but not universally. HRRTLE integrates and tests the hypothesis that curve number values can be indicative of the hydraulic properties of surface flow. It is anticipated that HRRTLE could prove valuable for specialists engaged in water harvesting site selection, particularly those seeking to employ the SCS-CN method for runoff prediction but wish to account for transmission losses, a capability offered by the HRRTLE process. Further efforts (e.g. using a more hydrologically accurate DEM) are recommended to refine and enhance the HRRTLE process and deepen the understanding of which catchment characteristics (e.g. connectivity) are more likely to yield acceptable results. The scarcity of suitable observed discharge data poses a challenge in the development of rainfall-runoff modelling procedures like HRRTLE.

# **6 Utilising remote sensing products to scope dam locations factoring topographical characteristics, annual runoff, and storage loss due to sedimentation — Port Sudan case study**

## **6.1 Abstract**

When assessing sites for water harvesting structures like dams, it is common to evaluate multiple locations using Earth observation datasets before committing to detailed assessments. Traditionally, this practice relies on limited metrics, primarily topographic slope or wetness index. In this study, we present a comprehensive approach tailored to Port Sudan, a city urgently needing sustainable water resources. We defined the area of interest and used satellite-derived terrain data to identify over 25,000 potential dam sites, filtering locations based on Strahler stream order. The geospatial tool SiteFinder was then used to determine dam sizes and reservoir dimensions for potential schemes, ranked for suitability using an Analytical Hierarchy Process (AHP) based on five local topographic characteristics. Next, we applied a rainfall-runoff model that integrates transmission losses to estimate runoff at each potential site. Schemes were filtered to retain only those predicted to receive sufficient runoff, based on the ratio of annual runoff volume to storage capacity. We then modelled storage capacity loss due to sediment retention to retain schemes with less than 2 % per year volume loss to

sedimentation. This resulted in 55 favourable schemes being identified. This approach may interest planners involved in water harvesting site selection studies, considering criteria such as storage volume, dam size, runoff, and sediment retention. Results are presented within a GIS environment, enabling the inclusion of additional criteria in the final decision-making process.

## 6.2 Introduction

There are numerous examples of Earth observation (EO) products, hydrological modelling (HM) and GIS being used in water harvesting site selection studies (see Adham et al., 2016a, for an overview). When assessing potential locations for water harvesting structures, it is vital to consider a wide variety of bio-physical, socio-economic, and environmental factors. Some factors can be evaluated by analysing the immediate local environment of a potential water harvesting site, for example slope, soil type, and storage capacity. Other factors, however, require analysis of areas often some distance away from the potential site, for example, proximity to a main road or populated area, or precipitation. Therefore, a broader catchment-based approach to site selection is necessary.

The use of Digital Elevation Models (DEMs) created from data captured by sensors on satellites enables analyses of far greater areas of land in the search for suitable locations for water harvesting structures than traditional ground-based topographic surveys. However, satellite-derived DEMs exhibit significantly lower accuracy and precision compared to those attainable through most ground-based survey methods. Consequently, these DEMs cannot serve as a viable replacement for the ground-based topographic surveys that are essential during the feasibility and detailed design phases of a project. They can, however, be used in assessments of catchments prior to ground-based surveys, to identify potentially suitable sites for water harvesting. These assessments typically use various

parameters derived from satellite data-based DEMs, including slope metrics (Ziadat et al., 2012; Mahmoud et al., 2015a; Saha et al., 2018; Ahmed et al., 2022) and the Topographic Wetness Index (TWI) (e.g. Tsiko and Haile, 2011; Bisrat and Berhanu, 2018; Ettazarini, 2021; Ezzeldin et al., 2022). However, while these metrics can provide information on the potential suitability of a location for a water harvesting structure, they do not provide information on its potential storage volume or the required size of the structure. This information is vital for planning.

There are a number of models and methods that do compute storage volume to aid the siting of water harvesting structures. Most of these operate outside GIS environments (Petheram et al., 2017; Wimmer et al., 2019; Teschemacher et al., 2020). Techniques that compute storage volume within GIS environments have the advantage that they allow results from DEM analyses to be combined easily with information from other sources as part of a multi-criteria decision-making process. For example, Walsh et al. (2015) created a web-based GIS system designed to assist in the basic screening of potential dam sites in North Carolina. However, this system requires the user to input the location of each potential dam, assessing one location at a time, which limits its application for the automatic scanning of numerous potential sites. Delaney et al. (2022) presented the geospatial tool 'SiteFinder,' which utilises a DEM to analyse the surrounding topography of potential water harvesting sites. It calculates various metrics such as storage volume and barrier dimensions that cannot be obtained directly from slope and TWI layers. While the Delaney et al. (2022) study included some ground-truthing by comparing SiteFinder outputs based on EO products against measurements from a ground survey, it did not demonstrate the efficacy of the SiteFinder tool in real-world applications.

It is important to estimate the annual runoff to a potential water harvesting site in order to obtain the ratio of annual inflow to the storage capacity of the scheme. Should runoff volumes be too low then

the reservoir will only fill partially or infrequently. Alternatively, should runoff volumes be too high then dealing with excess flows will be problematic. Despite water harvesting being defined as “the collection of runoff for productive purposes” (Critchley and Siegert, 1991, p. 6), runoff to potential sites is not routinely quantified when water harvesting site suitability assessments are conducted. Adham et al. (2016a) reviewed 48 such assessments and found that only 13 included runoff as a site selection criterion. While numerous hydrological models exist, water harvesting site selection studies that consider runoff frequently rely on the creation of runoff maps (Al-Ghobari et al., 2020; Karimi and Zeinivand, 2021; Radwan and Alazba, 2022; Alataway, 2023), often as part of a multi-themed approach. These provide information on the runoff potential at each location within the catchment of a potential site (Weerasinghe et al., 2011; Ibrahim et al., 2019; Shalamzari et al., 2019; Sayl et al., 2020a). They do not, however, compute the cumulative runoff (i.e. the volume of water that would be available for harvesting) at the potential water harvesting site. In other studies rainfall-runoff models, such as the Hydrologic Modeling System (HEC-HMS), have been employed to evaluate the potential for water harvesting (e.g. Ndeketeya and Dundu, 2021) and to provide cumulative runoff volumes at basin or sub-basin exits. However, such approaches fail to predict the runoff volume generated at every location within the study area, thereby limiting the number of potential sites that could be assessed as suitable for water harvesting. Moreover, traditional runoff maps do not allow for transmission losses, which can be significant in drylands where the implementation of water harvesting techniques is most important. They are likely therefore to over-estimate cumulative runoff volumes (Simanton et al., 1973 cited in Senay and Verdin, 2004).

Delaney et al. (2024) presented a rainfall-runoff model named ‘HRRTLE’ aimed at improving the estimation of annual runoff volumes at catchment outlets in arid and semi-arid regions. Utilising three

Utilising remote sensing products to scope dam locations factoring topographical characteristics, annual runoff, and storage loss due to sedimentation — Port Sudan case study

datasets that quantified catchment topography, curve number (rainfall-runoff relationship), and precipitation, HRRTLE estimates catchment discharge while accounting for transmission losses that would occur between where runoff is generated and a proposed water harvesting schemes are located. While Delaney et al. (2024) validated HRRTLE outputs against observed runoff data, they did not apply this in a ‘planning context’ to identify potential water harvesting locations.

For some *in situ* water harvesting techniques, such as contour bunds, the capture of sediment is a positive element leading to increased crop production (Critchley and Siegert, 1991). However, for *ex situ* water harvesting techniques such as water supply dams, the accumulation of sediment within reservoirs is regarded as disadvantageous as it reduces storage capacity. As water flows into a reservoir, the stream depth increases and mean flow speed decreases, creating a reduction in the transport capacity of the stream, resulting in the deposition of at least some of the waterborne sediments (Vanoni, 2006). Schleiss et al. (2016) questioned the sustainability of dams, citing studies that claim 0.5–1.0 % of global reservoir storage is lost each year to sedimentation, which equates to a volume greater than that created by the construction of new dams. Despite the significance of this issue, to our knowledge, other researchers have not attempted to quantify the degree of sediment retention in potential reservoirs when evaluating numerous sites using automated processes.

As previously stated, water harvesting site selection studies invariably consider more than one criterion to differentiate sites. Researchers, working within a GIS environment, typically create a thematic layer for each criterion deemed pertinent when evaluating the relative merits of sites. For example, one thematic layer may be a slope raster while another layer may be a land use / land cover (LULC) raster. There are several approaches that allow an assortment of thematic layers to be evaluated as part of decision-making process. The Analytical Hierarchy Process (AHP) has been used extensively in this

regard (e.g. Assefa et al., 2018; Li et al., 2020; Forzini et al., 2022). Other approaches include fuzzy membership/logic (e.g. Ildoromi et al., 2019; Vema et al., 2019; Nabit et al., 2023) and Boolean logic (e.g. Zaidi et al., 2015; Dile et al., 2016; Terêncio et al., 2017). It is possible to utilise more than one approach within a single study. For example, Al-Abadi et al., (2017) combined fuzzy logic and AHP, while Jamali and Kalkhajeh (2020) combined fuzzy logic and Boolean logic.

This study aims to integrate innovative and established techniques to enhance the efficiency of identifying suitable sites for water harvesting structures. The objective is to apply this methodology in a practical scenario where there is an urgent demand for water harvesting and uncertainty about optimal locations. By integrating EO products, hydrological modelling (HM), and GIS, the study assesses favourable sites and schemes for water harvesting near Port Sudan, Sudan. The study introduces a ranking method based on local topography, with provisions for incorporating additional criteria in later stages of assessment, ensuring flexibility and adaptability as the project evolves. Each scheme undergoes analysis and filtering based on the ratio of annual inflow to storage capacity volume to prevent 'under-filling' and 'over-filling'. An additional filter considers the degree of sedimentation. This methodology is designed to be flexible, allowing for iterative refinement of site selection by adjusting criteria importance and filter thresholds. Initially screening thousands of potential sites, the goal is to present a methodology that narrows down options to a manageable number of promising sites and schemes. This smaller, more favourable set of sites can then undergo further scrutiny using criteria beyond this study's scope, such as continued use of remote sensing products or field surveys. This study is expected to interest planners in dryland regions who are tasked with identifying suitable locations for constructing new water harvesting structures, such as dams.

## 6.3 Materials and methods

### Study area

The provision of water to Port Sudan (**Figure 6.1**), a commercially important city with an estimated population of approximately 850,000 people (Grant et. al., 2016) located on Sudan's Red Sea coastline, is challenging and complex. Over the past century, there have been various interventions, initiatives, and announcements, aimed at improving access to water.

In 2005, Al-Khaleej newspaper reported (Info-Prod (Middle East) Ltd., 2005) an agreement to create a trunk water main from Atbarah (Atbara District, River Nile State) to Port Sudan. By 2013, water shortages persisted, with many relying on water tankers, undermining the then President's vision for Port Sudan (BBC Worldwide Limited, 2013). The crisis, exacerbated by power outages, led to soaring water prices and protests. Allegations of corruption and further price increases followed, with many relying on artificial ponds for water. In 2016, the Red Sea State Governor prioritised resolving the water issues (AllAfrica Global Media, 2016) and a \$20 million project was subsequently announced to address water needs (States News Service, 2016), however little progress has been made. In 2023, activists welcomed an agreement to supply Port Sudan with River Nile water (AllAfrica Global Media, 2023).

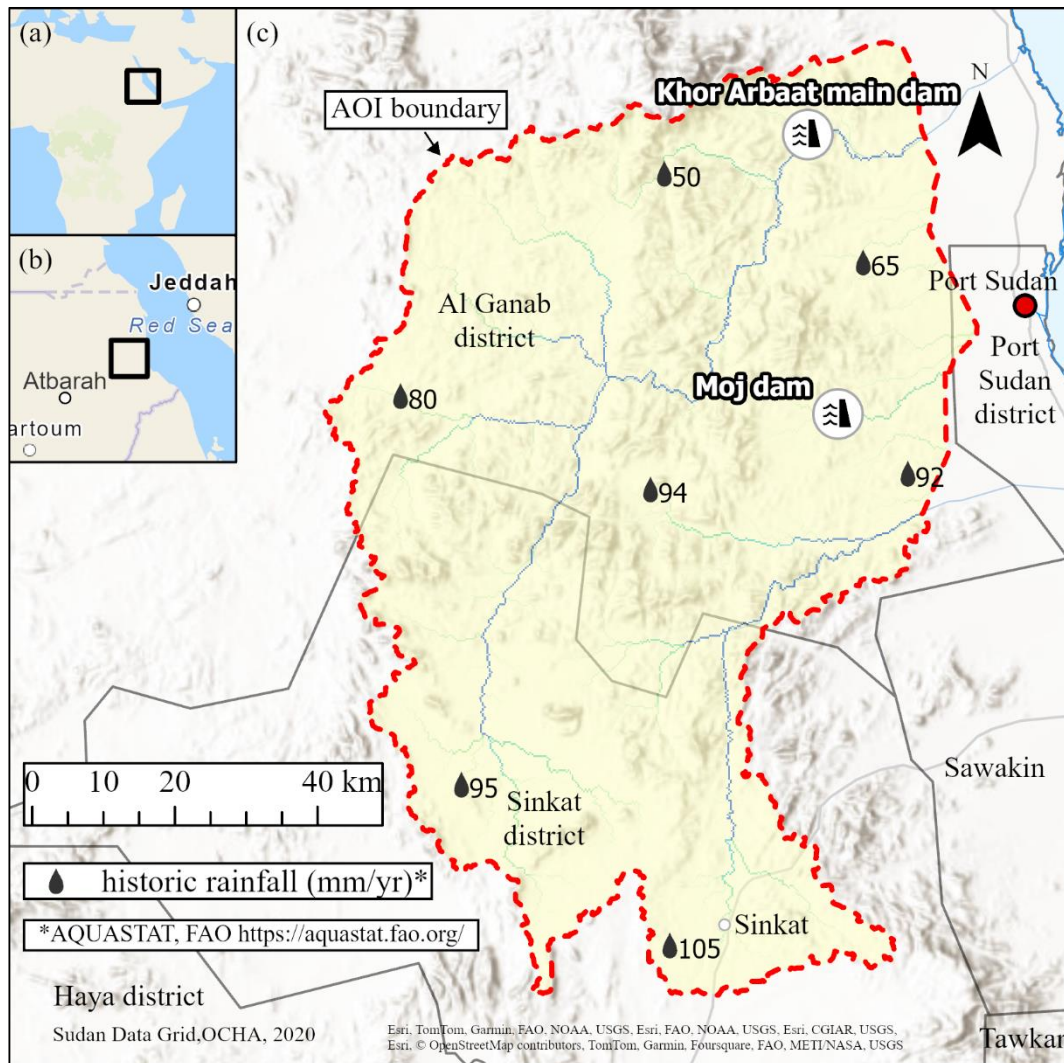


**Figure 6.1.** Map of area of interest (AOI) showing significant watercourses together with locations of Khor Arbaat main dam and Moj dam. Study area = 7,385 km<sup>2</sup>.

Regardless of plans to supply Port Sudan with water from the River Nile, the Port Sudan water supply is dependent on an array of well fields and dams with water reaching Port Sudan via either buried pipelines or by water truck. Some dams and weirs are no longer operational or have been removed but two significant sites remain (**Figure 6.1**). One is to the north-west of Port Sudan where the ‘Khor Arbaat main dam’ (also known as ‘Danfudo dam’ or ‘Arbaat dam’) and well field is located, while the other is the Moj dam and its well field located to the south-west of Port Sudan (Cattarossi et al., 2018).

The main reservoir located on the Khor Arbaat watercourse is under threat from sedimentation, having had its storage volume of 16 million cubic metres at the time of construction halved to 8.3 million cubic metres ten years later in 2013 when a bathymetric survey was undertaken (Cattarossi et al., 2018). The threat of sedimentation affecting dams situated along the Khor Arbaat ravine has been recognised for a considerable time: reservoir sedimentation was a point of contention when construction of the dam was originally discussed (Hebbert, 1935).

Dams could be rehabilitated by de-silting, removing sediments deposited in the reservoir, although the cost implications often discourage such an approach. Alternatively, new dams could be built, which raises the issue of how many potential sites were considered before deciding on the locations of existing dams. The Shora Consult (2003) report on the Khor Arbaat main dam design does not mention whether alternative sites were considered. Similarly, a consultancy report by Sinohydro Corporation Limited (2010) assessed the suitability of ten dams, both built and unbuilt, in the Red Sea State. This report states that these dam site locations were provided by the “owner” and gives no indication that these ten sites were selected from a larger pool of candidate sites.

The area of interest (AOI) for the present study was delineated by taking the catchment boundaries of existing known dams important in supplying water for Port Sudan as well as additional catchments in the vicinity of Port Sudan that may be of interest to planners. AOI delineation was achieved by identifying points on major riverbeds downstream of existing dams, and on major riverbeds along the Red Sea State hills, located to the west of Port Sudan. For each identified point the catchment boundary was computed using tools from a GIS hydrology toolset using a Shuttle Radar Topographic Mission (SRTM) void-filled DEM (**Table 6.1**) set at a spatial resolution of 90 m × 90 m. The individual catchments were then amalgamated, creating an AOI of 7,385 km<sup>2</sup>. To put this figure into perspective

Utilising remote sensing products to scope dam locations factoring topographical characteristics, annual runoff, and storage loss due to sedimentation — Port Sudan case study

the catchment areas of Khor Arbaat main dam and Moj dam are 4,201 km<sup>2</sup> and 180 km<sup>2</sup> respectively (Cattarossi et al., 2018). Locations of prominent dams, both in-service and out-of-service, located within the AOI are shown in **Figure 6.1**. This figure also shows the AOI boundary and locations of major settlements. Co-ordinates of dams shown in **Figure 6.1**, together with details of three other dams, are listed in **Appendix D (Table D1)**.



**Figure 6.2.** Image of Moj dam reservoir. Stone-armoured upstream dam batter wall can be observed in the bottom-right. The presence of vegetation in the reservoir is attributed to sedimentation [Photographed by Mohammed M. Salih in 2024].

Historic rainfall data indicate that areas in the southern part of the AOI receive approximately twice as much annual precipitation as those in the northern part (**Figure 6.1**). Based on a global database (Zomer and Trabucco, 2022), the northern region of the AOI is labelled as ‘hyper-arid’, while the southern region is labelled as ‘arid’.

Utilising remote sensing products to scope dam locations factoring topographical characteristics, annual runoff, and storage loss due to sedimentation — Port Sudan case study

**Table 6.1. Details of datasets.**

#	datasets	product name	structure	spatial resolution	source	reference
1	elevation	SRTM void-filled DEM	raster	3"	USGS ( <a href="https://earthexplorer.usgs.gov">https://earthexplorer.usgs.gov</a> )	EROS, 2018c
2	precipitation	GPCC Full Data Daily Version 2022 at 1.0°	raster	1.0°	Deutscher Wetterdiens ( <a href="https://opendata.dwd.de">https://opendata.dwd.de</a> )	Ziese et al., 2022
3	curve number	GCN250, global curve number datasets for hydrologic modelling and design	raster	250 m	FIGSHARE <a href="https://figshare.com/">https://figshare.com/</a>	Jaafar et al., 2019

### 6.3.1 Methodology synopsis

The methodology to identify the most favourable sites for dam construction consisted of several distinct steps. Firstly, the AOI boundary was defined as a polygon. Thousands of DEM cells within the AOI were then identified as potential dam sites based on a stream ordering-based search. Each site was assessed using the SiteFinder geospatial tool (Delaney et al., 2022) using five criteria which captured the local topographic characteristics (LTCs) that defined the dimensions of the potential dams and their water storage capabilities. Each potential scheme was then scored using a weighted combination of these criteria, the weighting being determined by an analytical hierarchy process (AHP). The HRRTLE rainfall-runoff model (Delaney et al., 2024) was then used in order to determine the ratio of annual inflow to reservoir storage capacity for each scheme. The potential schemes were filtered using this ratio to ensure that selected schemes would be neither underfilled nor overfilled. Finally, using outputs from both the SiteFinder and HRRTLE steps, a GIS script was used to calculate the storage loss due to sedimentation for each scheme. A final filter was then applied using the results of the sedimentation loss analysis, leaving only those schemes predicted to be largely unaffected by sedimentation. The major stages of the methodology are presented schematically in **Figure 6.3**.

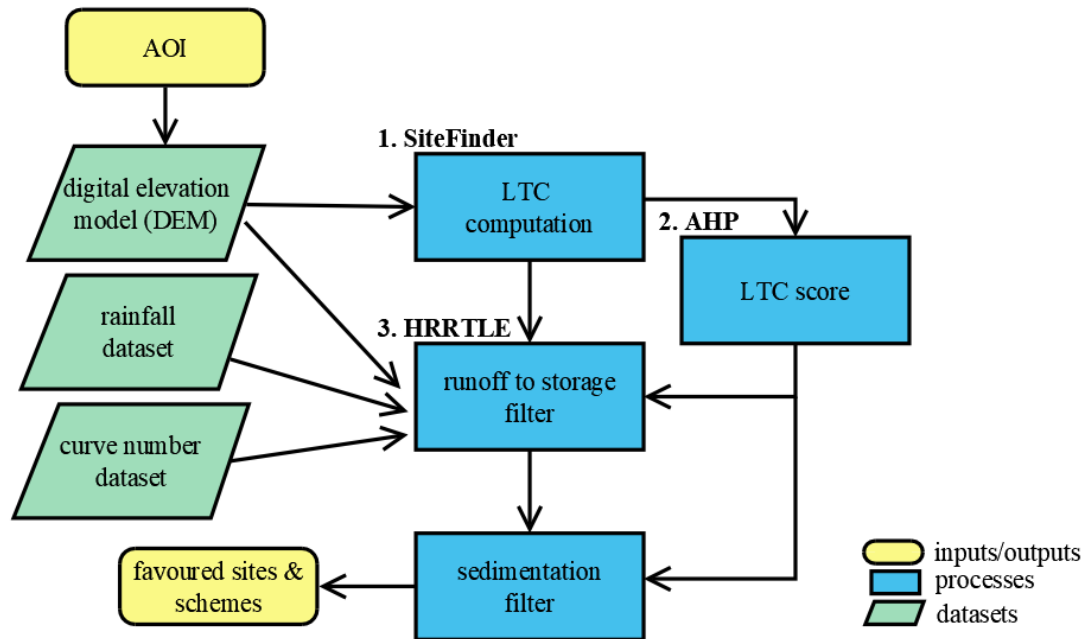


Figure 6.3. Schematic of input datasets and processing chain [AOI, area of interest; AHP, Analytical Hierarchy Process; LTC, local topographic characteristics].

### 6.3.2 Step 1: Initial identification of potential sites based on stream ordering

Elevation data for all cells within the AOI were retrieved from mosaiced SRTM elevation tiles resampled to a spatial resolution of 90 m × 90 m (Table 6.1). A sink-filling algorithm was then used to eliminate minor imperfections on the DEM surface, ensuring that no cell was lower than any of its eight surrounding neighbours. A flow directional tool was then applied to the sink-filled DEM to create a D8 flow direction raster, identifying the steepest downslope neighbouring cell. From this a stream order raster was derived, using the standard Strahler method (Tarboton et al., 1991). The number of cells within the AOI assigned to each stream order is shown in Table 6.2. Potential dam sites were identified as cells with a stream order of five or higher. This reduced the number of cells needing to be analysed by subsequent steps from 623,684 to 25,025 – approximately 4 % of the total.

Utilising remote sensing products to scope dam locations factoring topographical characteristics, annual runoff, and storage loss due to sedimentation — Port Sudan case study

**Table 6.2. Number of raster cells within the AOI assigned each stream order (Strahler method), derived from elevation data with a spatial resolution of 90 m × 90 m.**

stream order	number of cells	% of cells assigned stream order
1	416,842	66.8
2	103,817	16.6
3	50,314	8.1
4	27,686	4.4
5	13,309	2.1
6	6,212	1.0
7	2,558	0.4
8	1,505	0.2
9	1,441	0.2
total	623,684	100.0

### 6.3.3 Step 2: Ranking schemes based on scoring of local topographic characteristics

The SiteFinder geo-spatial tool (Delaney et al., 2022) was used to compute basic reservoir characteristics (e.g. storage volume) and dam characteristics (e.g. barrier height) – collectively termed as local topographic characteristics (LTCs) – at each of the stream order  $\geq 5$  cells, using the DEM described in the previous section. The maximum barrier height (i.e. height of dam above elevation surface) was set at 10 m, and the maximum barrier length (i.e. maximum length of dam crest) was set to 1000 m. The SiteFinder tool then attempts to construct up to three water harvesting schemes for each site analysed, each with a different barrier height. Therefore, every site may be associated with up to three distinct schemes.

The results generated by the SiteFinder tool comprised of local topographic characteristics (LTCs) of each potential site expressed in terms of five criteria describing the dimensions of the potential dam (barrier) and its associated water storage capacity:

Utilising remote sensing products to scope dam locations factoring topographical characteristics, annual runoff, and storage loss due to sedimentation — Port Sudan case study

- barrier height (BH)
- barrier volume (BV)
- area of influence or reservoir boundary (AI)
- water storage volume (SV)
- water storage volume to barrier volume ratio (SBVR)

The LTCs were analysed using the Analytical Hierarchy Process (AHP) to compute weights by determining priorities (Saaty, 1987; Saaty, 1994; Saaty, 2008) to rank water harvesting schemes. AHP involves creating a matrix to evaluate the relative importance of each component against all others. The process consists of two main stages: first, calculating the component 'weights'; second, checking the consistency ratio (CR) of the matrix. If the consistency is insufficient, the pairwise comparison matrix is adjusted, and the weights are recalculated. This process is repeated until an acceptable consistency is achieved. The practical interpretation and implementation of Saaty's computing priorities and AHP processes were guided by Mathew (2018).

### **Computation of weights**

Each paired component in the matrix represents either a criterion (e.g. barrier volume) or a sub-criterion. A criterion weight indicates the importance of that criterion relative to others. For example, the criterion weight for water storage volume (SV) shows its importance compared to other criteria (i.e. BH, BV, AI, and SBVR). The sum of all criteria weights equals 1.000.

For each criterion, there are five sub-criterion weights. For instance, the barrier volume (BV) criterion, is sub-divided into five classes, with each class assigned its own specific weight. This allows

favourable barrier volumes to be given a higher weight than schemes with less favourable barrier volumes.

In total, six pairwise comparison matrices were produced: one for each of the five main criteria (BH, BV, AI, SV, and SBVR) and one for each set of sub-criterion weights. Like the criterion weights, the sum of all sub-criterion weights for a specific parent criterion equals 1.000. A worked example illustrating the implementation of the AHP in this study to obtain weights for criteria and sub-criteria is provided in **Figure D1 (Appendix D)**.

**Table 6.3. The fundamental scale (Saaty, 1987).**

intensity of importance on an absolute scale	definition
1	equal importance
3	moderate importance of one over another
5	essential or strong importance
7	very strong importance
9	extreme importance
2, 4, 6, 8	intermediate values between the adjacent judgements

### **Consistency check**

A consistency ratio below 0.10 was used as an indication that the pairwise comparison matrix had been completed satisfactorily since a CR of 0.10 or less is considered “positive evidence for informed judgment” (Saaty, 1994, p. 104). To obtain the CR value, the principal eigenvalue ( $\lambda_{max}$ ) must first be known and can be computed after the weights have been calculated. The procedure to obtain  $\lambda_{max}$  for each pairwise matrix is outlined in **Appendix D (Figure D1)**. With  $\lambda_{max}$  known, the consistency index (CI) can be found using:

$$CI = (\lambda_{max} - n)/(n - 1) \tag{6.1}$$

where  $n$  is the number of pairs in the pairwise table. The number of pairs is equal to the number of components being evaluated in the pairwise comparison matrix. The size of pairwise matrix may vary, however throughout this study, all pairwise comparison matrices contained five paired components, hence  $n = 5$ . With  $n$  known, the random consistency index (RI) was obtained from a table provided by Saaty (1994), which lists RI values for  $n$  ranging from 1 to 10. When  $n$  equals 5 the random consistency index is 1.11. The consistency ratio (CR), the ratio of CI to RI, was subsequently computed, and if found to be less than 0.1, adjustments were made to the pairwise comparison matrix, and the CR re-calculated.

**Final pairwise comparison matrices and weights**

The final pairwise comparison matrix used to compute weights for each of the five main criteria is provided in **Table 6.4**, while equivalent matrices used to find sub-criterion weights are provided **Appendix D (Table D2 to Table D6)**.

**Table 6.4. Final pairwise comparison matrix used to compute weights for five main criteria [BH, barrier height (m); BV, barrier volume (m<sup>3</sup>); AI, area of influence (m<sup>2</sup>); SV, storage volume (m<sup>3</sup>); SBVR, storage volume to barrier volume ratio (-)].**

	BH	BV	AI	SV	SBVR
BH	1.00	0.5	3.00	0.14	0.33
BV	2.00	1.00	2.00	1.00	1.00
AI	0.33	0.50	1.00	0.11	0.20
SV	7.00	1.00	9.00	1.00	3.00
SBVR	3.00	1.00	5.00	0.33	1.00

### **LTC score**

A ‘total weight’  $w_t$  for each potential dam site was calculated using:

$$w_t = (w_{c,i} \times w_{sc,i}) + \dots + (w_{c,n} \times w_{sc,n}) \quad (6.2)$$

where  $w_{c,i}$  and  $w_{sc,i}$  are the criterion weight and the sub-criterion weight of the  $i^{\text{th}}$  criterion respectively, and  $n = 5$  is the number of components of the pairwise comparison matrix.

The total weight ( $w_t$ ) is used as a quantitative measure to rank schemes based on their local topographic characteristics score ( $LTC_{\text{score}}$ ). For this site selection study, we have defined the total weight to be equal to the score, thus  $LTC_{\text{score}} = w_t$ . This notation makes the relationship between the score and the ranking criterion more descriptive and clearer.

Weights for all five main criteria, along with their respective sub-criterion weights, are summarised in **Table 6.5**. This table also includes a column named ‘sub-criterion range’. For each potential water harvesting scheme, this range determines the sub-criterion weight assigned to its respective criterion.

An illustration of how an  $LTC_{\text{score}}$  is determined is now provided. Starting with Eq. (6.2), then setting the total weight equal to the score (i.e.  $LTC_{\text{score}} = w_t$ ), and using the criteria weights and the maximum sub-criterion weight for each criterion (**Table 6.5**), a scheme with a *theoretical* maximum  $LTC_{\text{score}}$  (= 0.4363) is obtained as follows:

$$\begin{aligned} LTC_{\text{score}} = & (0.093 \times 0.412) + (0.213 \times 0.503) + (0.056 \times 0.416) + (0.431 \times 0.416) \\ & + (0.207 \times 0.416) \end{aligned} \quad (6.3)$$

Utilising remote sensing products to scope dam locations factoring topographical characteristics, annual runoff, and storage

loss due to sedimentation — Port Sudan case study

Thus, by using the SiteFinder results along with the weights from **Table 6.5** and Eq. (6.2), an  $LTC_{score}$  was calculated for each potential water harvesting scheme. A higher  $LTC_{score}$  indicates a more favourable scheme.

**Table 6.5. Criterion weights and sub-criterion weights used to calculate local topographic characteristics (LTC) scores [“max” sub-script refers to the maximum corresponding criterion value outputted from all SiteFinder runs].**

criteria	criteria weight	sub-criterion range	sub-criterion weight	consistency ratio
barrier height (BH), m	0.093	> 10 m	0.074	
		> 8 m – ≤ 10 m	0.412	
		> 6 m – ≤ 8 m	0.311	
		> 4 m – ≤ 6 m	0.154	
		≤ 4 m	0.049	
		$\Sigma$	<b>1.000</b>	
barrier volume (BV), m <sup>3</sup>	0.213	> 0.8BV <sub>max</sub>	0.035	
		> 0.6BV <sub>max</sub> – ≤ 0.8BV <sub>max</sub>	0.068	
		> 0.4BV <sub>max</sub> – ≤ 0.6BV <sub>max</sub>	0.134	
		> 0.2BV <sub>max</sub> – ≤ 0.4BV <sub>max</sub>	0.260	
		≤ 0.2BV <sub>max</sub>	0.503	
$\Sigma$	<b>1.000</b>	0.054		
area of influence (AI), m <sup>2</sup>	0.056	> 0.8AI <sub>max</sub>	0.416	
		> 0.6AI <sub>max</sub> – ≤ 0.8AI <sub>max</sub>	0.262	
		> 0.4AI <sub>max</sub> – ≤ 0.6AI <sub>max</sub>	0.161	
		> 0.2AI <sub>max</sub> – ≤ 0.4AI <sub>max</sub>	0.099	
		≤ 0.2AI <sub>max</sub>	0.062	
$\Sigma$	<b>1.000</b>	0.015		
storage volume (SV), m <sup>3</sup>	0.431	> 0.8SV <sub>max</sub>	0.416	
		> 0.6SV <sub>max</sub> – ≤ 0.8SV <sub>max</sub>	0.262	
		> 0.4SV <sub>max</sub> – ≤ 0.6SV <sub>max</sub>	0.161	
		> 0.2SV <sub>max</sub> – ≤ 0.4SV <sub>max</sub>	0.099	
		≤ 0.2SV <sub>max</sub>	0.062	
$\Sigma$	<b>1.000</b>	0.015		
storage volume to barrier volume ratio (SBVR), (-)	0.207	> 0.8SBVR <sub>max</sub>	0.416	
		> 0.6SBVR <sub>max</sub> – ≤ 0.8SBVR <sub>max</sub>	0.262	
		> 0.4SBVR <sub>max</sub> – ≤ 0.6SBVR <sub>max</sub>	0.161	
		> 0.2SBVR <sub>max</sub> – ≤ 0.4SBVR <sub>max</sub>	0.099	
		≤ 0.2 × SBVR <sub>max</sub>	0.062	
$\Sigma$	<b>1.000</b>	0.015		
$\Sigma$	<b>1.000</b>			
<b>consistency ratio</b>	0.083			

### **6.3.4 Step 3: Filtering of schemes based on ratio of annual inflow to potential storage capacity**

The potential storage capacity (SV) of each scheme has already been calculated as one of the five criteria in the previous section. To quantify the other element of this ratio, the annual inflow predicted runoff reaching each potential dam site was calculated. HRRTLE (Delaney et al., 2024) is a high-resolution runoff and transmission loss estimator tool for mapping connectivity of runoff in ephemeral stream networks and was developed to aid the siting of water harvesting structures. Three datasets were used to create the HRRTLE models, namely, precipitation from 1982–2020 (Ziese et al., 2022), a curve number dataset at a spatial resolution of 250 m × 250 m (Jaafar et al., 2019) and the SRTM void-filled DEM (**Table 6.1**) resampled from a spatial resolution 3 arc-seconds to 250 m × 250 m. Stream widths were manually extracted from Google Earth satellite imagery at 100 locations spread throughout the AOI to produce regression relationships between stream width and flow accumulation, a procedure required by the HRRTLE modelling process. Due to the absence of observed runoff data, adjustments were made to the HRRTLE calibration parameters to achieve a runoff coefficient close to 0.1, consistent with two previously developed hydrological models located within the AOI (Cattarossi et al., 2018). Twenty HRRTLE models, located throughout the AOI, were then created using the calibration parameters and stream width equation constants. A regression relationship was established between the catchment area and annual runoff volumes based on the outputs of these 20 models. Given the known pixel size, the catchment area for each pixel was calculated using a flow accumulation raster. This approach enabled the prediction of annual runoff volumes ( $\text{m}^3 \text{y}^{-1}$ ) for all potential dam sites across 39 years of precipitation data. These predictions were then used to estimate the 2-year return period volumes for each site, which were subsequently employed in assessing the annual inflow to storage capacity ratio. Due to the high variability in annual discharge, with the HRRTLE models

often predicting zero annual runoff, a 2-year return period was chosen as a reasonable level of service for this context. Using return periods shorter than 2 years can result in very low runoff volumes, and a 1-year return period can produce unrealistic predicted discharge volumes, including negative values.

In order to estimate the 2-year return period annual runoff volume, return periods were calculated from the 39 years of annual runoff volume data using a methodology originally developed for predicting flood flows by Gumbel (1941). This assumes that the annual runoff volume that has a given probability of occurrence of return period can be expressed as:

$$x = u + y/\alpha \quad (6.4)$$

where  $x$  is the annual runoff volume,  $y$  is a variable related to the probability of occurrence and therefore the return period, and both  $u$  and  $\alpha$  are constants to be determined using the available data. The variable  $y$  is related to the probability of occurrence  $B(y)$  by:

$$B(y) = e^{-e^{-y}} \quad (6.5)$$

The constants  $u$  and  $\alpha$  are calculated by first determining the mean and mean square annual runoff volumes using:

$$\bar{u} = \frac{1}{n} \sum_{m=1}^n x_m \quad (6.6)$$

and

$$\overline{u^2} = \frac{1}{n} \sum_{m=1}^n x_m^2 \quad (6.7)$$

Utilising remote sensing products to scope dam locations factoring topographical characteristics, annual runoff, and storage loss due to sedimentation — Port Sudan case study

where  $n$  is the number of years of available annual runoff volume data (39 in this case). The standard deviation  $s$  of the annual runoff volumes is then found by assuming they are samples from a normal distribution, using the Gaussian formula:

$$s = \sqrt{\left(1 + \frac{1}{n-1}\right)(\overline{u^2} - \bar{u}^2)} \quad (6.8)$$

Then, following Gumbel (1941) the inverse of the constant  $\alpha$  is found using:

$$\frac{1}{\alpha} = 0.7796968s \quad (6.9)$$

and the remaining constant  $u$  found using:

$$u = \bar{u} - \frac{0.5772157}{\alpha} \quad (6.10)$$

To obtain the catchment runoff that could be expected to occur with 50 % probability (i.e.  $B(y) = 0.5$ ) in any given year, i.e. a runoff value with a return period of 2 years, the value of  $y$  was found that gave  $B(y) = 0.5$  via Eq. (6.5). In this case, through a process of iteration,  $y$  was found to be 0.3665. Denoting the annual runoff volume as  $Q$  rather than  $x$  in Eq. (6.4) then enables the annual runoff volume with a 2-year return period,  $Q_{T=2}$ , to be expressed as:

$$Q_{T=2} = u + 0.3665/\alpha \quad (6.11)$$

Since runoff models were created for 20 catchment outlets, a method was needed to determine annual runoff for the thousands of pixels analysed using SiteFinder. This was achieved through regression analysis, plotting catchment area against HRRTLE annual runoff results, resulting in the equation:

Utilising remote sensing products to scope dam locations factoring topographical characteristics, annual runoff, and storage loss due to sedimentation — Port Sudan case study

$$Q_{T=2} = 0.0031A_c + 17485 \quad (6.12)$$

where  $A_c$  is the catchment area ( $m^2$ ), for which  $r^2 = 0.997$ .

The ratio of the annual runoff volume ( $Q_{T=2}$ ) to the calculated available storage volume (SV) was then determined and used to filter out schemes based on the degree of inundation. This filter serves two purposes. First, it eliminates schemes that would fill infrequently due to insufficient runoff, making dam construction economically unfeasible and providing inadequate environmental flows. Second, it removes schemes that are frequently inundated to a high extent, indicating potential difficulties in managing excess water, which could necessitate costly spillway construction.

Similarly to Eq. (6.12), another expression was created by linear regression of the average runoff volume ( $Q_{ave}$ ,  $m^3 y^{-1}$ ) against the catchment area ( $A_c$ ,  $m^2$ ), which is necessary for sedimentation loss modelling:

$$Q_{ave} = 0.0044A_c + 3048 \quad (6.13)$$

for which  $r^2 = 0.996$ .

#### **6.3.5 Step 4: Filtering of schemes where sedimentation would be excessive**

In order to estimate the amount of sedimentation that might be expected in a dammed reservoir in the Port Sudan area, we first need to estimate the sediment yield of its catchment.

This was done by assuming (following Pandey et al., 2016) a power law relationship between the catchment sediment yield  $S_y$  ( $m^3 y^{-1}$ ), and the annual runoff of water into the reservoir  $Q$  ( $m^3 y^{-1}$ ):

Utilising remote sensing products to scope dam locations factoring topographical characteristics, annual runoff, and storage loss due to sedimentation — Port Sudan case study

$$S_y = aQ^b \quad (6.14)$$

where  $a$  and  $b$  are constants.  $Q$  can be calculated for the catchment of any proposed dam site using HRRTLE, as above. To calculate appropriate values of  $a$  and  $b$ , the only available information on reservoir sedimentation from the Port Sudan area was used. This came from a report that found that the Khor Arbaat main dam reservoir had lost 60 % of its storage capacity due to sedimentation between 2003 and May 2018 (Cattarossi et al., 2018). The process of obtaining values for  $a$  and  $b$  used the following steps.

Firstly, we assumed a relationship between sediment yield of the catchment and the volume of sediment retained in the reservoir,  $S_r$ , of the form:

$$S = \frac{T_e}{100} S_y \quad (6.15)$$

where  $T_e$  is the trap efficiency (%). The trap efficiency was calculated using the formula:

$$T_e = 100 - (1600k^{-0.2} - 12) \quad (6.16)$$

where  $k$  is a dimensionless sedimentation index found by multiplying gravitational acceleration ( $g = 9.81 \text{ m s}^{-2}$ ) by the Sedimentation Index,  $SI$  ( $\text{s}^2 \text{ m}^{-1}$ ) (Morris et al., 2008), which is defined as:

$$SI = RP/V_I \quad (6.17)$$

where  $RP$  is the residence time (retention period) of the reservoir (s), and  $V_I$  is mean flow speed in the reservoir ( $\text{m s}^{-1}$ ). The residence time of the reservoir is calculated as:

Utilising remote sensing products to scope dam locations factoring topographical characteristics, annual runoff, and storage loss due to sedimentation — Port Sudan case study

$$RP = SV/I \quad (6.18)$$

where  $SV$  is the reservoir storage's volume capacity (as defined above), and  $I$  is the rate of inflow into the reservoir ( $\text{m}^3 \text{s}^{-1}$ ), which is calculated using:

$$I = \frac{Q}{T_Q \times 24 \times 3600} \quad (6.19)$$

where  $Q$  is the annual runoff volume into the reservoir ( $\text{m}^3 \text{y}^{-1}$ ), and  $T_Q$  is the mean number of days inflow occurs per year. Both  $Q$  and  $T_Q$  are estimated by running the HRRTLE model for the Khor Arbaat main dam reservoir catchment.

The mean flow speed in the reservoir was calculated using:

$$V_I = I/A_{cs} \quad (6.20)$$

where  $A_{cs}$  is the cross-sectional area of the reservoir ( $\text{m}^2$ ).

Given that the storage volume of the potential reservoir basin ( $SV$ ) has already been calculated, to obtain the mean cross-sectional area,  $A_{cs}$ , its length  $L$  (m) needs to be known. Then

$$A_{cs} = SV/L \quad (6.21)$$

The length of the reservoir was determined by obtaining the elevations of a set of points covering the reservoir and its surroundings, using Google Earth and the Schneider (2019) web-based portal. In a GIS environment, through a kriging surface interpolation, these elevation data were utilised to generate an elevation raster with a spatial resolution of 15 m. This was converted into elevation contours, and the contour corresponding to the maximum level of 231 m asl (the height of the top of the dam,

according to Cattarossi et al., 2018) was selected. The reservoir length was then measured from the middle of the dam to the furthest point on this contour.

Having obtained all the necessary parameter values and relationships, the appropriate values for  $a$  and  $b$  in the power law relationship in Eq. (6.14), were calculated by applying the above equations. The objective was to determine values of  $a$  and  $b$  that give a value of  $S_y$  calculated using Eq. (6.14) that matches that calculated using Eq. (6.15) and the known extent of sedimentation in the reservoir (60 % from 2003–2018). To achieve the latter, the volume of runoff ( $Q$ ) into the reservoir and the number days inflows occurred ( $T_Q$ ) was simulated for each year 2003–2018 using the HRRTLE model, and the values of  $a$  and  $b$  adjusted until the retained sediment  $S_r$  matched the reported 60 % of the effective storage volume reported by Cattarossi et al. (2018). See **Table D7 (Appendix D)**.

Thus, the simple model in Eq. (6.15) was calibrated for the conditions in the Port Sudan area and was used to estimate volumetric losses of reservoir capacity due to sedimentation for the potential schemes remaining after the filtering process described in the sections above. To achieve this, the runoff ( $Q$ ) was calculated for all potential sites using the regression equation Eq. (6.13) developed for catchment area against runoff. The inflow period ( $T_Q$ ) was found not to be sensitive to catchments area and was hence approximated as  $0.8 \text{ d y}^{-1}$  for all sites.

With the annual runoff ( $Q$ ), inflow period ( $T_Q$ ) and dam and reservoir dimensions obtained for each potential dam scheme, the trap efficiency ( $T_e$ ) was computed using Eq. (6.16) based on mean annual runoff over the 39 years for which precipitation data was available (1982–2000). The sediment yield ( $S_y$ ) was calculated using Eq. (6.14) and the retained sediment ( $S_r$ ) calculated using Eq. (6.15) allowing the reduction in storage volume due to sedimentation,  $SV_L$  (%), to be calculated as:

Utilising remote sensing products to scope dam locations factoring topographical characteristics, annual runoff, and storage loss due to sedimentation — Port Sudan case study

$$SV_L = \frac{S_r}{SV} \times 100 \quad (6.22)$$

This information was then used to carry out a final filter of potential schemes, removing those that had an unacceptably high predicted level of sedimentation losses.

## 6.4 Results

### 6.4.1 Local topographic characteristics

Five SiteFinder runs were performed, each corresponding to a stream order from fifth to ninth. The number of cells analysed as potential siting points for dams in each of the five runs were 13,309, 6,212, 2,588, 1,505, and 1,441, respectively — 25,025 points in total (**Table 6.2**). SiteFinder sought to place dam schemes with three different barrier heights for each siting point. However, in some locations, that was not possible due to the nature of the topography. Therefore, the number of dam schemes for each siting point varies from zero to three. Across the entire set of 25,025 analysed siting points, 14,755 were found theoretically suitable for a water harvesting structure and thus passed to the next step of the selection process. As some sites possess the potential for multiple barrier heights, the overall count of potential water harvesting schemes was 19,562.

A summary of the SiteFinder results is presented in **Table 6.6**. The largest barrier volume (151,000 m<sup>3</sup>), storage volume (37,846,000 m<sup>3</sup>), and the maximum LTC<sub>score</sub> were all found at stream order 7 sites. A stream order 6 site produced the maximum storage volume to barrier volume ratio (13,793), and a stream order 8 site produced the greatest area of influence (reservoir boundary) of the entire set of results, 6,601,000 m<sup>2</sup>.

Utilising remote sensing products to scope dam locations factoring topographical characteristics, annual runoff, and storage loss due to sedimentation — Port Sudan case study

SiteFinder produced 19,562 schemes, with only one falling into the highest  $LTC_{score}$  range bin of 0.36–0.40 (**Table 6.10**), receiving a score of 0.3609, thus making it the most favourable based solely on  $LTC_{score}$ . Conversely, the lowest  $LTC_{score}$  identified was 0.0574, shared among four schemes. The scheme with the highest  $LTC_{score}$  is associated with a stream order 7 site, whereas the lowest scoring schemes are at stream order 5, 7, and 9 sites. **Figure 6.4** illustrates the barriers and their respective areas of influence (reservoir boundary) generated by SiteFinder for the highest  $LTC_{score}$  scheme and one of the lowest  $LTC_{score}$  schemes.

**Table 6.6. Summary of SiteFinder results. [BV, barrier volume; AI, area of influence; SV, storage volume; SBVR, storage volume to barrier volume ratio; LTC, local topographic characteristic].**

stream order	sites analysed	sites	potential schemes	max. BV	max. AI	max. SV	max. SBVR	max. $LTC_{score}$
	#	#	#	( $m^3$ )	( $m^2$ )	( $m^3$ )	(-)	(-)
5	13,309	8,083	8,746	124,000	2,208,000	12,500,000	5,310	0.1971
6	6,212	3,668	4,278	82,000	1,860,000	7,338,000	13,793	0.2280
7	2,588	1,151	2,394	151,000	5,532,000	37,846,000	10,656	0.3609
8	1,505	952	2,099	146,000	6,601,000	28,142,000	3,300	0.2859
9	1,441	901	2,045	130,000	2,681,000	10,296,000	4,124	0.1906
5–9	$\Sigma 25,055$	$\Sigma 14,755$	$\Sigma 19,562$	151,000	6,601,000	37,846,000	13,793	0.3609

**Table 6.7. SiteFinder results showing the scheme with the maximum  $LTC_{score}$  and the four schemes with the minimum  $LTC_{score}$ , together with respective metrics [SBVR, storage volume to barrier volume ratio; LTC, local topographic characteristic].**

$LTC_{score}$	barrier length	barrier volume	barrier height	storage volume	area of influence	SBVR
(-)	(m)	( $m^3$ )	(m)	( $m^3$ )	( $m^2$ )	(-)
0.3609*	203	21,968	9.2	37,846,000	5,532,000	1,720
0.0574*	537	123,772	13.4	4,906,000	1,180,000	40
0.0574	832	147,085	11.8	1,858,000	425,000	13
0.0574	856	151,286	11.8	2,608,000	688,000	17
0.0574	612	129,569	12.9	5,019,000	990,000	39

\* presented in **Figure 6.4**

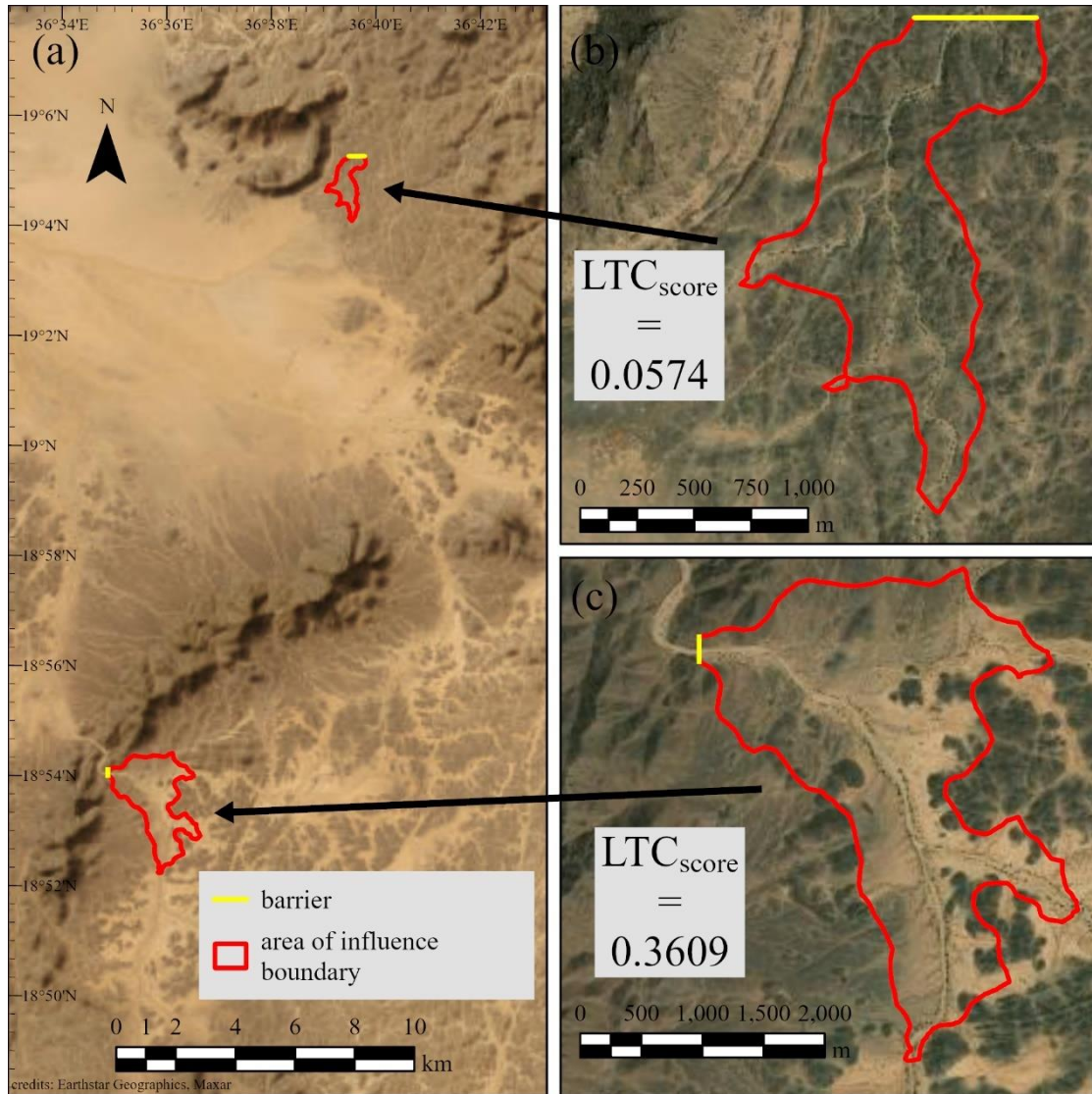


Figure 6.4. SiteFinder results: (a) scheme with the highest LTC<sub>score</sub> (0.3609) and one of four schemes with the lowest LTC<sub>score</sub> (0.0574), (b) higher resolution details of low LTC<sub>score</sub> scheme, (c) higher resolution details of highest LTC<sub>score</sub> scheme [LTC, local topographic characteristic].

Table 6.7 provides a summary of metrics for both the highest ranked LTC<sub>score</sub> scheme and the four lowest ranked schemes. This summary underscores how SiteFinder, in conjunction with its weighting methodology, identifies schemes based on various metrics, i.e. barrier volume, barrier height, storage volume, area of influence, and storage volume to barrier volume ratio (SBVR). Notably, the highest

Utilising remote sensing products to scope dam locations factoring topographical characteristics, annual runoff, and storage loss due to sedimentation — Port Sudan case study

ranked scheme based on  $LTC_{score}$  not only exhibits a relatively large storage volume but also demonstrates a significantly higher SBVR compared to the other four schemes. This suggests potentially better value for money, as for every unit of barrier volume 1,723 units of storage capacity are provided, whereas for the other schemes, SBVRs are significantly lower at 40, 13, 17, and 39 respectively.

**Table 6.8.** All schemes outputted by SiteFinder with a storage volume greater than the Khor Arbaat main dam immediately after construction and before storage loss to sedimentation (i.e. 16 million cubic metres), along with their corresponding local topographic characteristics score ( $LTC_{score}$ ) and stream order.

storage volume ( $\times 10^6 \text{ m}^3$ )	$LTC_{score}$ (-)	stream order
37.8	0.3609	7
32.6	0.3005	7
27.2	0.1548	7
23.4	0.2841	7
19.5	0.2273	7
28.1	0.2427	8
26.7	0.1704	8
23.8	0.2859	8
21.2	0.1409	8
20.4	0.1992	8
17.4	0.2367	8
16.8	0.2367	8
16.6	0.1323	8

Of all the sites analysed, only 13 schemes were identified as having a reservoir storage volume greater than the storage capacity of the Khor Arbaat main dam at the time of construction (i.e. 16 million cubic metres) before storage loss to sedimentation. **Table 6.8** gives the storage volume of all these 13 schemes alongside the scheme’s respective  $LTC_{score}$ , and stream order number.

### 6.4.2 Runoff volume to reservoir capacity ratio

In this stage, the 19,562 schemes identified in the previous section were assessed to filter out those predicted to be underfilled (insufficient runoff to justify creating an impoundment of the predicted size) or overfilled (runoff volume far exceeds reservoir capacity). Schemes with an annual runoff volume (2-year return period,  $Q_{T=2}$ , probability of occurrence) to storage volume ratio below one were

classified as 'underfilling' and were excluded. These schemes are considered economically poor value due to under-utilised storage volume and insufficient regular excess flows, which limit environmental flows (ecodeficit). Conversely, schemes where the ratio exceeded ten were classified as 'overfilling' and also excluded. While some degree of overfilling is desirable, as uncontrolled spills provide water for downstream users and ecological flows (ecosurplus), excessive overfilling indicates significant challenges in safely managing uncontrolled spills (excess flows). Therefore, a cut-off ratio is used to exclude these schemes. This approach is consistent with the study by Vogel et al. (2007), who introduced the concept of ecodeficit/ecosurplus and the ratio of reservoir storage to annual inflow to evaluate reservoir performance.

A breakdown of schemes identified as under-filling, over-filling, and those passing the filter for further consideration is presented (**Table 6.9**). Of the 19,562 schemes assigned an LTC score, a total of 6,733 schemes were removed as predicted to be under-filling, and 3,820 schemes were removed as predicted to be over-filling, leaving 9,009 schemes for further consideration. Of the original 19,562 schemes, only 29 schemes — stream orders 6, 7, and 8, with 1, 12, and 16 schemes respectively (**Table 6.9**) — were assigned an  $LTC_{score}$  greater than 0.2. All these 29 schemes were removed from further consideration by the under-filling element of the annual runoff to storage capacity ratio filter. **Figure 6.5a** shows all 19,562 schemes assigned an LTC score whilst **Figure 6.5b** shows the 9,009 schemes remaining after applying the filtering process.

Utilising remote sensing products to scope dam locations factoring topographical characteristics, annual runoff, and storage

loss due to sedimentation — Port Sudan case study

**Table 6.9. Results showing breakdown of schemes based on annual runoff (2-yr return period) to storage volume ratio. Schemes removed due to under-filling ratio (column “<1”), schemes removed due to over-filling ratio (column “>10”), & schemes passing the filter (column “1–10”). Schemes grouped by local topographic characteristics score (LTC<sub>score</sub>).**

stream order	number of potential schemes																	
	5			6			7			8			9			5-9		
LTC <sub>score</sub>	<1	>10	1-10	<1	>10	1-10	<1	>10	1-10	<1	>10	1-10	<1	>10	1-10	<1	>10	1-10
>0.04–0.08	11	0	0	7	0	0	7	0	1	6	0	0	0	1	4	31	1	5
>0.08–0.12	17	0	0	16	0	2	183	0	27	88	1	108	0	9	149	304	10	286
>0.12–0.16	3283	877	3621	925	516	2093	396	302	806	108	629	499	1	897	258	4713	3221	7277
>0.16–0.20	775	1	161	531	16	171	272	10	378	78	103	463	0	458	268	1656	588	1441
>0.20–0.24	0	0	0	1	0	0	9	0	0	14	0	0	0	0	0	24	0	0
>0.24–0.28	0	0	0	0	0	0	0	0	0	1	0	0	0	0	0	1	0	0
>0.28–0.32	0	0	0	0	0	0	2	0	0	1	0	0	0	0	0	3	0	0
>0.32–0.36	0	0	0	0	0	0	0	0	0	0	0	0	0	0	0	0	0	0
>0.36–0.40	0	0	0	0	0	0	1	0	0	0	0	0	0	0	0	1	0	0
Σ	4086	878	3782	1480	532	2266	870	312	1212	296	733	1070	1	1365	679	<b>6733</b>	<b>3820</b>	<b>9009</b>

### 6.4.3 Sedimentation

The storage capacity loss in reservoirs due to sedimentation was calculated for 19,562 schemes identified through SiteFinder runs, following the methodology described above. A chart in **Appendix D (Figure D2)** depicts the reservoir storage capacity loss due to sedimentation based on an average annual runoff) for all schemes. Only those schemes with sedimentation loss below 2 % y<sup>-1</sup> were retained, a total of 371 schemes. The locations of these 371 potential dam schemes are presented in **Figure 6.5c**. Among these schemes, a variety of LTC scores exist, with the highest score being 0.1885, shared by 55 schemes. These 55 schemes, categorised by storage volume, are shown in **Figure 6.5d**. Among these, the scheme with the greatest volume (2.6 million cubic metres) is highlighted in **Figure 6.6**, along with its respective runoff connectivity map created using the HRRTLE modelling process. The runoff depths indicated in the figure represent the mean annual runoff depth for pixels relative to the catchment outlet, which is the location of the scheme. This highlights the parts of the catchment that are most significant in terms of runoff reaching the potential location of the scheme.

loss due to sedimentation — Port Sudan case study

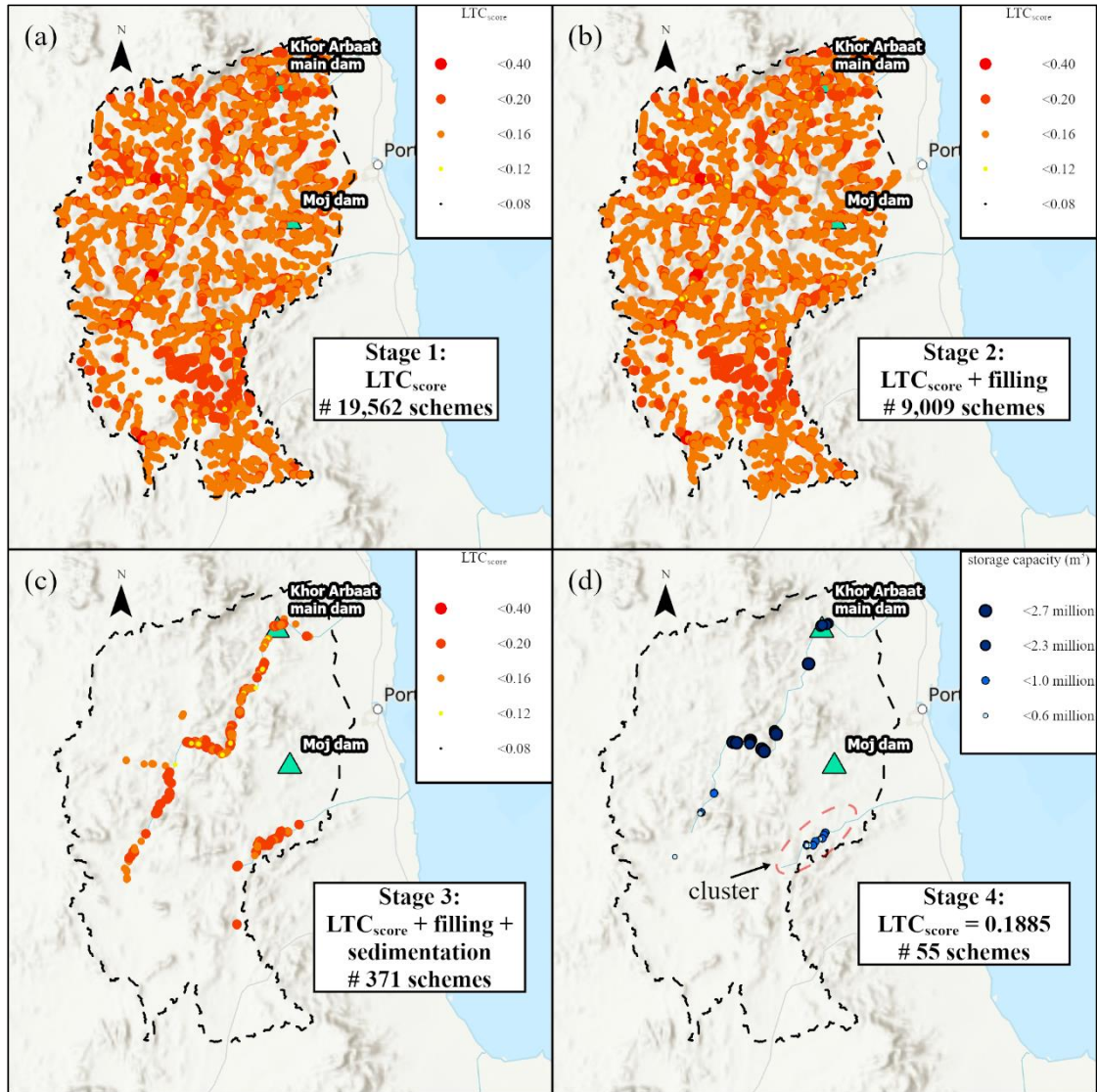


Figure 6.5. Results, (a) LTC<sub>score</sub>, (b) filtered by ‘filling’, (c) filtered by storage loss due to sedimentation, (d) highest LTC<sub>score</sub> schemes from final filter stage, segregated by storage volume.

Utilising remote sensing products to scope dam locations factoring topographical characteristics, annual runoff, and storage

loss due to sedimentation — Port Sudan case study

**Table 6.10. Number of potential schemes grouped by local topographic characteristic score (LTCscore). Columns “a” refers to all schemes found using SiteFinder while columns “b” excludes schemes with a predicted annual runoff (50 % probability) to storage volume ratio below parity and greater than 10. Columns “c” excludes schemes with sedimentation loss greater or equal to 2 %. Results segregated by stream order.**

stream order	number of potential schemes																	
	5			6			7			8			9			5-9		
LTC <sub>score</sub>	a	b	c	a	b	c	a	b	c	a	b	c	a	b	c	a	b	c
>0.04–0.08	11	0	0	7	0	0	8	1	0	6	0	0	5	4	0	37	5	0
>0.08–0.12	17	0	0	18	2	1	210	27	0	197	108	2	158	149	56	600	286	59
>0.12–0.16	7,781	3,621	0	3,534	2,093	1	1,504	806	6	1,236	499	26	1,156	258	112	15,211	7,277	145
>0.16–0.20	937	161	1	718	171	1	660	378	0	644	463	38	726	268	127	3,685	1,441	167
>0.20–0.24	0	0	0	1	0	0	9	0	0	14	0	0	0	0	0	24	0	0
>0.24–0.28	0	0	0	0	0	0	0	0	0	1	0	0	0	0	0	1	0	0
>0.28–0.32	0	0	0	0	0	0	2	0	0	1	0	0	0	0	0	3	0	0
>0.32–0.36	0	0	0	0	0	0	0	0	0	0	0	0	0	0	0	0	0	0
>0.36–0.40	0	0	0	0	0	0	1	0	0	0	0	0	0	0	0	1	0	0
Σ	8,746	3,782	1	4,278	2,266	3	2,394	1,212	6	2,099	1,070	66	2,045	679	295	19,562	9,009	371

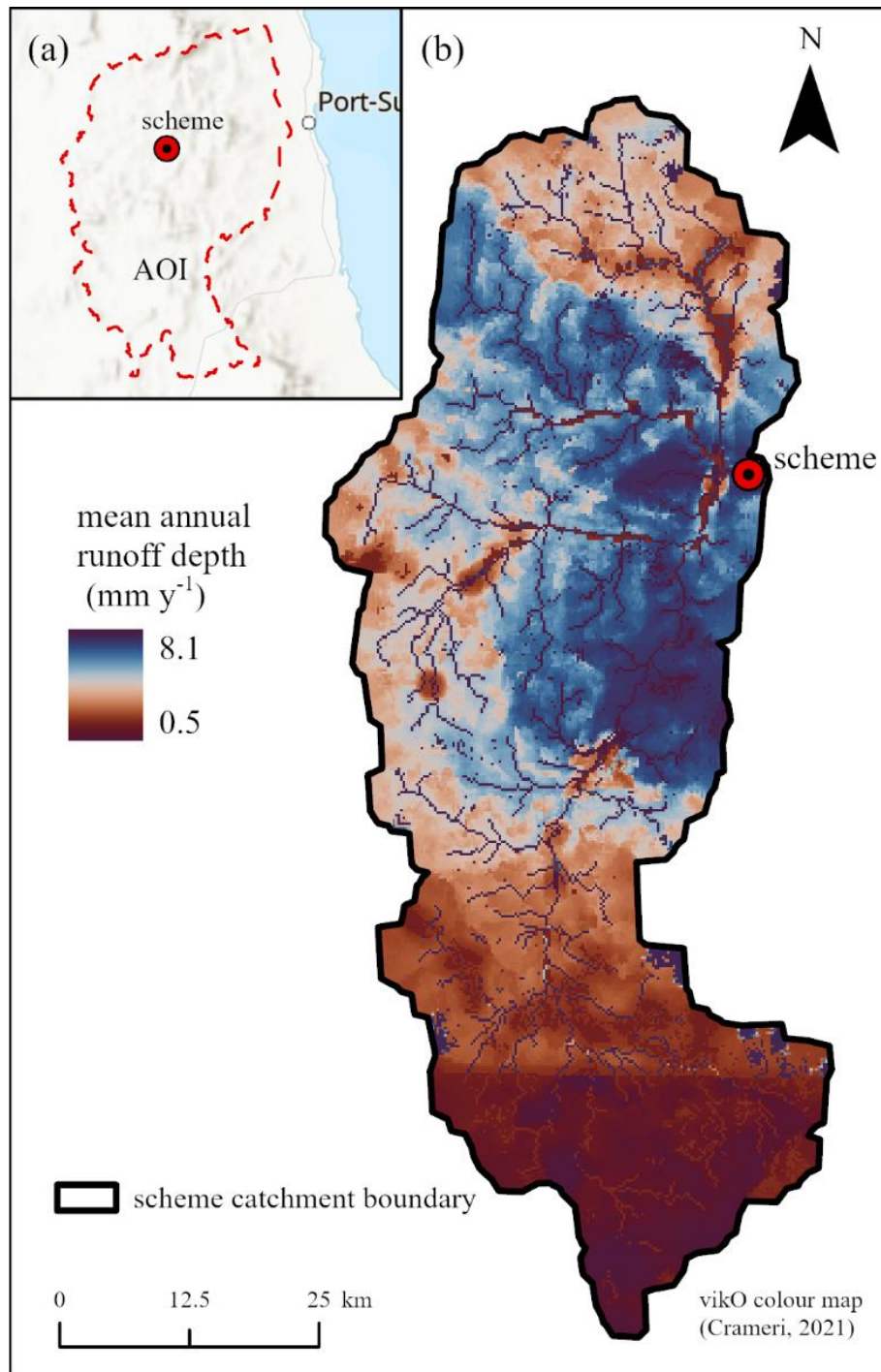


Figure 6.6. (a) Location of the scheme with the largest storage volume among the 55 favoured schemes found within the area of interest (AOI), and (b) HRRTLE model connectivity map showing the mean annual runoff reaching the scheme.

## 6.5 Discussion

### 6.5.1 Selection via filtering by stream order and LTCs

The process described above, of assigning a stream order to each cell within the AOI, and filtering out all those with stream order  $<5$  greatly reduced the number of cells of potential interest, by approximately 96 % in a single step. This begs the question of whether the retained range of stream orders (5–9) captures all the optimal locations for potential dam sites, or if there are any desirable sites at cells with lower stream orders. Considering the  $LTC_{score}$  of potential schemes, there were no stream order 5 cells with a score greater than 0.2 (columns ‘a’, **Table 6.10**), whereas this threshold was exceeded by cells of stream orders 6, 7 and 8. This suggests that lower stream order sites will tend not to be associated with schemes with a higher  $LTC_{score}$ , and that the greatly increased amount of processing time required for SiteFinder to analyse the much larger number of lower stream order cells is not justified.

The study demonstrated the capability of SiteFinder to carry out analysis of a large number of potential dam sites without requiring excessive time or computational resource: in total, 25,005 cells were analysed over five separate runs, with the largest single run analysing 13,309 cells. To our knowledge, SiteFinder is the only GIS-based tool that is capable of analysing such a large number of potential water harvesting sites in a single autonomous process to calculate barrier and reservoir metrics. Moreover, it provides site specific information on potential water harvesting locations including storage capacity and barrier volume. Commonly such information is not available to planners at the scoping stage of a project cycle. Of the 48 papers reviewed by Adham et al. (2016a) none used barrier dimensions or reservoir metrics as a selection criterion, whereas slope was the most widely used biophysical criterion, with 40 out of the 48 studies adopting it as a site selection criterion. Slope has

often been considered alongside various factors when determining suitable sites for dam construction. For example, Tsiko and Haile (2011) used six criteria to identify suitable reservoir locations, including slope. Sites with a slope of  $\leq 12^\circ$  were given the highest ranking for this criterion. Similarly, Alrawi et al. (2023) applied eight criteria to find appropriate dam locations, also considering slope. In their study, sites with a slope of  $< 2^\circ$  received the highest ranking for the slope criterion.

The application of the AHP procedure for scoring potential sites identified by the stream order filter and SiteFinder demonstrates a method for assessing sites on the basis of a combination of multiple criteria, which can be compared to a large volume of sites.

In this study five criteria, all associated with the immediate topography of a potential dam site, were used in the AHP pairwise weighting methodology. However, the number of criteria applied to the AHP methodology varies amongst water harvesting studies. Some use four criteria (e.g. Munyao, 2010), some five (e.g. Jabr and El-Awar, 2004; Hameed, 2013; Mahmoud, 2014; Mahmoud and Alazba, 2015) and some seven (e.g. Ramakrishnan et al., 2009). Tsiko and Haile (2011) ranked 14 criteria grouped under the headings ‘environmental’, ‘hydrological’, ‘economic’ and ‘institutional’. While the selection of suitable sites for water harvesting structures requires many different types of factors to be taken into account, there is also a limit to the number of criteria that can be considered within a pairwise matrix before the process becomes cumbersome to complete in a meaningful way, especially for non-expert stakeholders who may be the key decision makers regarding site selection. Furthermore, judgement needs to be applied to limit the number of factors included, as some might be better suited for exclusion rather than being included with a low ranking, as this could lead to unfeasible schemes being retained as potential options.

Water harvesting site selection studies using multicriteria decision analysis have been criticized for being subjective (Sayl al et., 2020b). While the methodology used to create the  $LTC_{score}$  here is mathematical and repeatable, this is a valid criticism. The use of the fundamental scale (**Table 6.3**) requires judgements to be made on the relative importance of criteria to create the numeric values in the pairwise matrix (e.g. **Table 6.4**). At present, this is necessarily the case, as no objective method for weighting the criteria is available. To optimise its validity, it has been based on the expert judgement of stakeholders with extensive experience of the landscape and hydrology of the Port Sudan region (two of the authors). Nevertheless, this criticism points to a possible avenue of further work that would consult within the water harvesting sector more widely to establish a set of common criteria and AHP weightings for a range of environments.

### **6.5.2 Filtering by runoff inflow to reservoir capacity ratio**

After applying LTC scores to 19,562 potential schemes, located at 14,755 separate sites, the assessment process continued by evaluating the ratio of inflow volume to storage capacity. It is pertinent to discuss whether the cutoff ratios used in this filtering process ( $<1$  for underfilling, and  $>10$  for overfilling) are appropriate. Of these 19,562 schemes, 9,009 schemes (~46 %) passed through the filter into the next stage of analysis, while 6,733 schemes (~34 %) were eliminated due to the underfilling component of the filter, and 3,820 schemes (~20 %) were eliminated due to the overfilling component.

However, as detailed in the **Results (Section 6.4)**, the underfilling component of this filtering process removed every scheme with an LTC score greater than 0.2 (29 schemes in total). The AHP was designed to assign more desirable potential schemes with higher LTC scores. Hence, the implication is that in further work, the underfilling ratio threshold (i.e.  $<1$ ) could be adjusted (lowered) to

potentially allow schemes with an LTC score greater than 0.2 into the next stage of the site selection process. However, lowering the underfilling ratio will reduce the water available for downstream users and amplify the ecodeficit. There may be circumstances where planners would be willing to accept such a compromise, especially if a water harvesting scheme's principal purpose was to offer flood-recession farming and/or the creation of a wetland.

This methodology presented in this study does not negate the requirement to consider a design-flood hydrograph for water-control and conveyance structures (USDA, 1987). However, it would be impracticable to carry out such design work and associated costings for thousands of potential dam sites, and the methodology presented in this study offers a way to disregard more problematic schemes, leaving a reduced number to be costed using a design-flood hydrograph. This approach may also reduce scenarios where a dam site is selected but the excess water conveyance structure (e.g. spillway) is down-sized due to high predicted capital costs, resulting in the increased risk of catastrophic dam failure.

The assessment of the risk of underfilling or overfilling schemes being selected for dam construction is complicated by the nature of precipitation in arid environments, which is characterised by low rainfall with high temporal and spatial variability (Nicholson, 2011). According to the taxonomy of Jorgensen and Fath (2008), the average precipitation in the dataset used for the AOI of this study ( $45 \text{ mm y}^{-1}$ ) categorizes it as an 'extreme arid desert', while the annual precipitation values ( $60 \text{ mm y}^{-1}$  and  $73 \text{ mm y}^{-1}$ ) used in a previous hydrologic study of the region (Cattarossi et al., 2018) place it in the 'arid desert' category. The runoff model used in this paper to compute the discharge volumes at catchments outlets utilises a precipitation dataset (Ziese et al., 2022) with a relatively coarse spatial resolution of 1 degree ( $\sim 110 \text{ km}$  at the equator) relative to the size of the study area. Hence, a single

precipitation grid cell covers an area greater than the entire AOI (**Figure 6.1**), thus there is no information in this dataset regarding spatial variability of rainfall within the AOI. In terms of temporal variability, the runoff modelling work undertaken using HRRTLE predicted that it was not uncommon, despite periods of rainfall, for there to be no catchment discharge for entire years at a time. This may accurately reflect actual runoff patterns, or it may be a result of the simplistic nature of the rainfall-runoff model or the low spatial resolution of the precipitation dataset.

In general, annual rainfall data in arid zones displays a positive skew, in contrast to temperate zone data that typically conforms to a normal distribution, and is thus characterized by a greater frequency of annual values falling below the mean than above it (Jones, 1981). Consequently, for arid catchments it is preferable to use frequency of occurrence, for example the 2-year return period values employed in this study, rather than employing mean precipitation data to forecast runoff. Nevertheless, there are significant limitations with regards to both the spatial and temporal resolution of the datasets used to underpin the analyses reported here, and this remains an area in which both further studies are likely to be fruitful and more highly resolved data is urgently required.

### **6.5.3 Sedimentation**

Vanmaercke et al. (2014) reviewed reports of sediment yield in 36 African countries and found that the maximum reported sediment yield in Sudan was  $3,422 \text{ t km}^{-2} \text{ y}^{-1}$ , implying that Sudanese sediment yields are high compared to those in other countries in Africa. It is therefore not surprising that reservoir sedimentation is a significant issue for dams constructed in the AOI, as evidenced by consultancy reports (e.g. Cattarossi et al., 2018) and field trips undertaken by the authors (e.g. **Figure 6.2**). The retained sediment modelling procedure carried in this study assumed that there are no ‘active’ sediment management schemes undertaken and that the degree of retained sediment is therefore solely

a consequence of the shape and size of the reservoir, combined with the nature of the water and sediment flowing into the reservoir. Strategies for active sedimentation management do exist and could be considered by planners. For example, Emamgholizadeh et al. (2018) investigated watershed management, sluicing, flushing, density current venting, and bypass as ways of managing sedimentation for the Dez Reservoir in Iran, a similarly arid context.

The methodology for dam site selection in this study excluded projects with an annual storage loss due to sedimentation equal to or greater than 2 %  $y^{-1}$ . Records from the Cattarossi et al. (2018) report show that the Khor Arbaat main dam has an average sedimentation rate of approximately 7.4 %  $y^{-1}$ , which is significantly higher than the average rates of 0.84 %  $y^{-1}$  and 1.02 %  $y^{-1}$  for reservoirs in Africa and the Middle East, respectively (Schleiss et al., 2016). Therefore, the 2 %  $y^{-1}$  sedimentation loss rate threshold used in this study is relatively high compared to global norms but is still well below the historic loss rates of documented reservoirs within the AOI. The significant storage loss due to sedimentation observed at the dam projects within this study's AOI underscores the critical need for an effective sedimentation management strategy. Without such a strategy, sedimentation rates similar to those at the Khor Arbaat main dam reservoir could drastically reduce the storage capacities of new dams within a few years.

Despite the potential impact on the operational longevity of a water harvesting scheme site, suitability studies tend not to include sedimentation as a selection criterion. Of the 48 site suitability studies reviewed by Adham et al. (2016a) 'sedimentation' is not listed in any of the classification groups. Only one study (Salih and Al-Tarif, 2012) does consider sedimentation by calculating a 'reflecting factor' based on basin length but this method relates to basin geomorphology (river deposits and erosion) and not specifically to reservoir sedimentation. To our knowledge, therefore, this is the first study to

compute reservoir sedimentation for numerous potential dam schemes using automated processes. The processes presented could allow planners to consider reservoir sedimentation at the scoping stage of a planning process when numerous potential locations need to be analysed. It also demonstrates the value of SiteFinder outputs for not only indicating the dimensions of potential water harvesting schemes, but also for helping to predict the loss of storage capacity due to sedimentation.

#### **6.5.4 Favoured schemes**

The 55 schemes identified and described as the most favourable (**Table D8, Appendix D**) using the methodology outlined in this study vary in terms of location and storage volume capacity. The scheme with the largest storage capacity has a predicted storage capacity of 2.6 million cubic metres, significantly less than the storage capacity of the Khor Arbaat main dam at the time of construction (i.e. 16 million cubic metres). A significant proportion of the 55 most favourable schemes (**Figure 6.5d**) are located upstream of the existing Khor Arbaat main dam and its well field. Hence, construction of a dam will affect the yield of any built dam located downstream. Additionally, many are in less desirable locations, being further away from Port Sudan (following the route dictated by valley bottoms). It may be concluded, therefore, that none of the schemes identified as “favoured” by this study compare positively with the existing Khor Arbaat main dam in terms of storage capacity and location.

Of the 55 schemes identified, 20 are located relatively close to each other in the same ravine (see the cluster labelled in **Figure 6.5d**). In reality, it would not be possible to construct all 20 schemes due to interference between schemes given their proximity. Additionally, the storage volumes of these schemes are all less than 1 million cubic metres. Despite these issues, the ravine where these 20 schemes are located is potentially interesting, as it might be possible (subject to further studies) to

construct a series of dams together with well-fields all within this ravine. Another aspect is that there appears to be no existing downstream dam, and the distance from the ravine to Port Sudan (~47 km) is not dissimilar to that of the Khor Arbaat main dam to Port Sudan (~44 km).

### 6.5.5 Future work

The reservoir storage loss modelling in this study utilised data from a consultancy report (Cattarossi et al., 2018) to calibrate the HRRTLE model for runoff prediction and to establish the relationship between runoff and sediment yield. While the Cattarossi et al. (2018) report focuses on dams within the AOI and is therefore relevant to this study, its relevance would diminish if the methodology were applied elsewhere in Sudan or beyond. The methodology presented in this study utilises global datasets (DEM, precipitation, and curve number) and could theoretically be applied to a study in any arid region. However, this study has demonstrated the importance of local expertise to contextualise the problem statement, contribute to the AHP, and access data and reports not readily available through traditional academic sources. Therefore, any future work would also require similar local expertise.

This study utilised five features, extracted from a DEM through an automated process, to establish LTC scores for potential water harvesting schemes. Runoff was modelled to forecast the extent of filling for each potential scheme. Similarly, storage loss due to retained sediment was predicted for each scheme. While these criteria ( $LTC_{score}$ , filling, sedimentation) are relevant for use in a water harvesting site selection study adopting a multi-criteria decision-making process they cannot be considered as exhaustive. Hence the short-listed schemes in the **Results (Section 6.4)** are not recommendations for water harvesting structures but rather should be considered as locations that may merit further investigation. Future work could involve generating additional thematic layers within a GIS environment, with each layer representing a site selection criterion not addressed in the scope of

this study. This would potentially enhance the comprehensiveness of the site selection methodology. Examples of criteria not covered in this study but have been used in similar studies include geological (Yousif and Sracek, 2016), land cover (Sajikumar and Remya, 2015), soil type (Patel and Chaudhari, 2023), and normalised difference vegetation index (Bisrat and Berhanu, 2018). Subsequent research could concentrate on integrating additional criteria into a multi-criteria decision-making process, potentially utilising established methodologies like the AHP pairwise matrix (e.g. Adem et al., 2023; Vázquez et al., 2023), Boolean (e.g. Gavhane et al., 2023; Odeh et al., 2023), or fuzzy logic (e.g. Aghaloo and Sharifi, 2023; Debebe et al., 2023), or alternatively exploring less-established methodologies.

## 6.6 Conclusions

Globally, the sustainability of water supply reservoirs is affected by sedimentation, which reduces yield and shortens the lifespan of investments. Reservoirs in drylands tend to be more severely affected due to higher levels of sediment yield. This study offers a methodology to evaluate numerous potential dam sites based on crucial selection criteria, including storage loss due to sedimentation, appropriateness of local topography, and the ratio of reservoir inflows to storage capacity. Applying this methodology to a Port Sudan case study we conclude:

- By categorising pixels according to stream order and executing SiteFinder (Delaney et al., 2022), we analysed over 25,000 potential locations, obtaining five topographic-based characteristics for 19,562 potential dam schemes. Utilising the in-country water harvesting experience of several authors of this study, along with an established Analytical Hierarchy Process weighting method, we were able to score schemes based on their local topographic suitability.
- Utilising almost four decades of precipitation data from a global climate dataset, the probability of occurrence for annual runoff was modelled, allowing a relationship to be established

between catchment area and annual runoff for all potential locations. Of the 19,562 schemes, 6,733 were eliminated due to insufficient annual inflows, while 3,820 were eliminated due to excessive annual inflows, leaving 9,009 schemes for further consideration.

- Using a combination of SiteFinder and runoff modelling outputs, the degree of sedimentation was computed for all potential schemes. Applying a filter, retaining only schemes with a predicted storage loss to sedimentation of less than 2 %  $y^{-1}$ , resulted in 371 schemes of interest. Of these schemes, a total of 55 schemes all have been assigned the same local topographic score.

The methodology presented in this study has the potential to be valuable during the first stage of water harvesting site selection, enabling more detailed studies to be carried out at a relatively small number of locations with confidence that they represent the best options available within the area of interest.

# 7 Synopsis and recommendations

## 7.1 Synopsis

The overarching aim of this thesis, as outlined in **Chapter 1**, was to develop, test, and assess novel methods for extracting hydro-morphological information from remote sensing products to support more effective site selection in the water harvesting sector. To achieve this overarching aim, four objectives were identified. This chapter reviews all four objectives and identifies the stages in the thesis where each was successfully addressed.

**Chapter 2** provided an overview of water harvesting, including clear definitions and illustrative examples of various water harvesting technologies. It explored the classification of these technologies, along with their applications and benefits. The chapter also examined the role of water harvesting in the context of global development goals, highlighting how different water harvesting technologies could contribute to achieving specific Sustainable Development Goals. Additionally, this chapter identified the range of biophysical criteria used to determine if a site is suitable for a particular type of water harvesting technology. A wide range of techniques were identified, each appropriate to different hydro-meteorological, morphological, and social contexts. A summary of the different methodological approaches used to identify optimal locations for potential water harvesting projects was also included. **Chapter 2** also presented a range of biophysical criteria used by researchers to determine the suitability of sites for water harvesting technologies. The most common biophysical criterion for site selection was found to be slope. Problems with this choice of criterion are addressed in subsequent chapters, particularly **Chapter 4**.

As water harvesting projects are often implemented in regions where ground-based data are sparse and difficult to collect, remote sensing provides a solution for gathering valuable data. However, **Chapter 2** risks giving the impression that water harvesting relates primarily to issues centred on biophysical factors. This is not the case. A wide range of non-biophysical factors must be considered during the planning stage for a water harvesting project to be successful.

Although these additional considerations are not covered in significant detail within this thesis, they remain important. Key factors include land tenure, environmental impact, administrative procedures, risk assessments, and financial viability. Since the focus of this thesis is on extracting hydro-morphological site selection characteristics from remote sensing products, it intentionally avoids exploring some less technical, yet nonetheless crucial, factors. However, relevant literature exists on these topics. For example, Bot et al. (2000) highlight how the “participatory approach” places particular emphasis on social factors in development planning, particularly in rural settings.

**Chapter 3** presented a systematic literature review investigating the role of remote sensing in water harvesting research. While peer-reviewed articles on water harvesting existed, none had previously focused specifically on remote sensing applications within this field. Using targeted search terms, research literature was gathered from two bibliographic search engines, which, after filtering, yielded a pool of 290 peer-reviewed articles. This collection of articles was subsequently studied and analysed. The most frequently used remote sensing products were identified and classified, and their applications were assessed, with notable trends reported and evidence-based recommendations offered. The evaluation of these articles demonstrated that remote sensing products, alongside hydrological modelling and GIS tools, played a significant role in many water harvesting studies. For example, freely available global Digital Elevation Model (DEM) products were widely used to compute slope

at potential water harvesting sites. However, tools enabling a more comprehensive morphological analysis of potential sites were generally found to be lacking or operating outside a GIS environment.

While **Chapter 3** provides clear evidence that remote sensing products are now extensively used in water harvesting site selection studies, it largely fails to establish an objective relationship between remote sensing product specifications and the type of water harvesting system being investigated.

**Chapter 2** makes it clear that water harvesting systems vary significantly in scale, both in terms of the water harvesting structure and the catchment area, while **Chapter 3** identifies the remote sensing products commonly used by researchers for site selection studies. However, the resolution of remote sensing products — whether spatial, temporal, or spectral — varies considerably.

The implication from **Chapter 3** is that researchers are selecting remote sensing products for a particular water harvesting study based on ease of accessibility rather than the product's suitability for the task at hand. A more reasoned approach would be to first consider the scale of the water-harvesting system being studied and then use this information to determine the minimum specifications required for remote sensing products to achieve the objectives of a particular study within an acceptable degree of uncertainty.

In **Chapter 4**, a novel GIS-based tool (“SiteFinder”) was presented. This tool was designed to support the process of water harvesting site selection, addressing a research gap recognised in **Chapters 2** and **3**. While researchers regularly utilise remote sensing products, the predominant use of slope as a criterion indicated a demand for a GIS tool capable of providing more comprehensive information on potential sites. Starting with a DEM, the tool produced a flow direction raster and subsequently created virtual barriers perpendicular to the direction of the modelled stream flow. The tool accounted for the surrounding topography by intersecting each barrier with a contour layer, also derived from the DEM,

and, through an automated procedure, provided details of potential water harvesting schemes. These details included the barrier size and the dimensions of the flooded zone upstream of the barrier. To verify the accuracy of the tool's outputs (including dimensions of length, area, and volume), results were cross-checked against equivalent outputs derived from LiDAR data. The analysis showed Spearman's rho correlation coefficients of 0.568, 0.683, and 0.721 for length, area, and volume, respectively, indicating a stronger correlation for volume compared to area and length. This comparison also revealed that using a global DEM produced less accurate outputs relative to those based on LiDAR data, a difference attributed to the global DEM's lower horizontal and vertical resolutions compared to the LiDAR-derived DEM. This observation led to the conclusion that SiteFinder results obtained using a global DEM are likely to yield greater inaccuracies when assessing smaller water harvesting structures. Consequently, it was determined that a global DEM is not suitable for assessing certain water harvesting structures, and DEMs with higher spatial resolutions should be preferred. Despite this recognition, a key critique of **Chapter 4** is that it did not sufficiently explore the broader implications of using global DEMs for water harvesting site selection. Water harvesting technologies range from small-scale microcatchments to large-scale macrocatchments, each with distinct site selection requirements. Hence, the work in **Chapter 4** could be extended by expanding on the relationship between freely available datasets and their suitability for evaluating water-harvesting systems, relative to system scale. Crucially, researchers must assess whether a given DEM dataset has sufficient resolution and accuracy to capture — within an acceptable degree of uncertainty — the topographic characteristics of potential water-harvesting sites and their associated catchments.

For instance, while global DEMs may suffice for the preliminary identification of large-scale water-harvesting systems, they are likely to prove unreliable for selecting microcatchment systems, where finer topographic detail is essential. **Chapter 4** acknowledged that lower-resolution global DEMs

introduced inaccuracies in estimating length, area, and volume. However, it did not explore in detail how these inaccuracies might inform decision-making for water-harvesting technologies across different scales.

While acknowledging shortcomings related to the lack of guidance on the limitations of commonly used DEM datasets (e.g. SRTM DEM, ASTER GDEM) for site selection, the development of the SiteFinder tool was significant. It represented an automated process operating entirely within the GIS environment and offered more relevant site selection characteristics compared to slope, which was the most commonly established biophysical criterion used by researchers. The SiteFinder tool met the first objective of this thesis, which was to develop and evaluate an automated tool designed to provide more comprehensive and practical information on potential water harvesting sites, extending beyond the biophysical criterion of slope. Researchers working in the water harvesting sector have shown interest in this approach and in the methodology employed by the SiteFinder tool. Masi et al. (2024) recreated the Delaney et al. (2022) SiteFinder tool for a study on the optimal siting of artificial reservoirs, modifying the barrier orientation to allow for more possibilities rather than restricting it to being perpendicular to the flow direction.

**Chapter 5** presented a modelling tool (“HRRTLE”) inspired by runoff maps (frequently used in the water harvesting sector), to predict runoff in drylands. The methodology combined an established method for computing runoff at each pixel with an innovative procedure for calculating transmission losses, producing a high spatial resolution (250 m × 250 m) connectivity map. The connectivity map allowed the runoff volume reaching the catchment outlet to be predicted. The outlet could be the location of a potential water harvesting site. The computational process involved using the global curve number twice: first, as part of an established process to compute runoff, and secondly, in a novel approach to estimate the surface roughness coefficient, which helped establish surface and channel

flow behaviours. This parsimonious methodology, which did not require the creation of sub-basins, relied solely on three global datasets: DEM, curve number, and precipitation. The use of only three datasets formed part of a deliberate simplification strategy. The rationale behind this decision was to minimise potential sources of input uncertainty that may propagate through the model, while still capturing the principal uncertainties associated with hydrological runoff processes in dryland regions. Predicted runoff volumes were compared to observed runoff data obtained from a global runoff database, covering a total of 28 catchments. The Nash–Sutcliffe efficiency (NSE) coefficient to be used to evaluate the predictive performance of the model. For the validated model results, there was a marked range in NSE values, from -10.082 to 0.672, with  $NSE = 0$  indicating that the model had no predictive power beyond assuming constant flow equal to the observed mean, and  $NSE = 1$  indicating a perfect model. Similarly, percentage bias (Pbias) was used to measure the tendency of the calculated runoff volumes to be larger or smaller than observed runoff volumes. Again, for the validated model results, the range of absolute Pbias varied from 101.7 % to 3.2 %. Satisfactory model results were obtained for nine of the 28 catchments, which had an  $NSE > 0$  and an absolute Pbias  $< 50$  %, indicating that the developed rainfall-runoff model did not perform well for all catchments tested and highlighted limitations with the model.

The second objective of this thesis was to explore ways to improve traditional runoff mapping by accounting for transmission losses, thereby providing more accurate estimates of runoff at catchment outlets, and to quantitatively evaluate model performance. The HRRTLE tool, presented in **Chapter 5**, serves as evidence that this objective has been successfully achieved. Notably, **Table 5.2** presents results demonstrating that the HRRTLE model offers substantially superior performance compared to results obtained without accounting for transmission losses.

A critical evaluation of the HRRTLE tool suggests that the choice of equation used to estimate transmission losses may have been unnecessarily complex. The concept employed by the HRRTLE tool — specifically, the use of curve number values as a proxy for surface roughness — is novel; therefore, very little literature was available to express losses as a function of the curve number. Given this, it may have been beneficial to begin testing the HRRTLE tool methodology with simpler equations and fewer parameters. This approach could have made the methodology easier to communicate and the sensitivity analysis more straightforward due to the reduced number of parameters. Once the HRRTLE tool had been demonstrated to be sound, there would then have been an opportunity to develop more sophisticated equations to express transmission losses.

The model performance results were presented in **Chapter 5**, as outlined above. While this chapter offers valuable insights (e.g. **Table 5.2**) into the performance of both the runoff-only model (excluding transmission losses) and the full HRRTLE tool (including transmission losses), the analysis could be further strengthened with a more structured and detailed comparison to other widely used rainfall-runoff models, particularly those commonly applied in the water harvesting sector. Expanding on the advantages of the HRRTLE tool in relation to these models would enhance the understanding of its relative benefits and potential applications. For example, a comparative analysis of HRRTLE alongside other established approaches (e.g. runoff potential maps, HEC-HMS, SWAT) could enhance the evaluation of the tool's benefits and relevance. Such a comparison would be especially valuable in the context of identifying multiple potential water harvesting sites within ungauged catchments.

Biophysical parameters were analysed to identify commonalities between catchment characteristics and satisfactory model results, indicating that the model performed best for catchments that were relatively small, approximately equal in length in all directions, with low topography, high transmission losses, and predominantly low-growing vegetation. Poor model performance was

attributed to human-induced hydrological disturbances, such as irrigation, dams, and urbanisation). A key limitation was quantifying catchment characteristics without assessing hydrologic connectivity. Evaluating this could have revealed objective hydrological disturbance indicators, providing stronger evidence for understanding HRRTLE model performance.

**Chapter 6** demonstrated the value of the SiteFinder tool as part of water harvesting site selection study. The development and testing of the tool (see **Chapter 4**) covered a relatively small number of sites whereas the use of SiteFinder in this chapter demonstrated that the tool can be used to analyse thousands of potential water harvesting sites. This was achieved by disaggregating the study area into pixels based on stream order. The rainfall-runoff model developed and tested (see **Chapter 5**) was utilised to predict the probability of occurrence of annual runoff volumes at sites throughout the study area. By combining site-specific data produced by the SiteFinder tool with catchment runoff data produced by the rainfall-runoff model the ratio of annual inflows to storage capacity was obtained for thousands of potential water harvesting schemes. It was the first time such an analysis had been performed on such a sizeable number of schemes and represented a step forward in improving the operational safety of water harvesting structures as it provided information on the extent of inundation. Similarly, outputs from the SiteFinder tool's computational runs, including polygons representing the flooded area of water harvesting schemes, were combined with runoff data produced by the rainfall-runoff model to predict the severity of reservoir sedimentation. The third objective of this thesis was to address the issue of reservoir sedimentation by developing and assessing an automated method for evaluating the susceptibility of potential reservoirs to future storage loss. This section of **Chapter 6** demonstrates how the third thesis objective was successfully met.

Water harvesting experts based in Sudan were requested to contribute to the process by quantifying the relative importance of selection criteria. This tested the appropriateness of the decision-making element of the study for use in actual site selection studies. One limitation of **Chapter 6** relates to difficulties in carrying out in-person field validations of identified potential water harvesting sites. While on-the-ground assessments were constrained — primarily due to site accessibility issues and security concerns — a preliminary review of several sites was still carried out. These real-world challenges highlight the practical complexities of fieldwork in some dryland regions and underscore the value of remote assessment tools such as SiteFinder and HRRTLE, which offer a viable approach to evaluating water harvesting sites in logistically challenging environments.

**Chapter 6** presented metrics for potential water harvesting schemes, including barrier volume, storage volume, annual inflow volume, and reservoir sedimentation. The fourth and final objective of this thesis was to devise a site selection methodology that incorporates tools developed in the previously stated objectives, and to test its usability through a case study in a dryland region. As the metrics presented and methodology outlined in **Chapter 6** incorporated novel tools (namely SiteFinder and HRRTLE) for assessing dam sites in Sudan, this demonstrates successful fulfilment of the fourth thesis objective.

However, since these computed metrics are presented without a specified level of confidence, there is a risk that the chapter conveys an unwarranted sense of accuracy. This could lead to confusion if sites identified as having greater potential are later evaluated using more precise methodologies, revealing discrepancies between these results and the metrics presented in **Chapter 6**. Presenting the metrics of water harvesting schemes in a manner that explicitly highlights the inherent uncertainties of the approach used would have added value to this chapter.

This issue raises a broader debate about water harvesting scoping tools and methodologies. Allocating human, financial, and technical resources to a smaller number of potential water harvesting schemes would allow for more accurate site-specific assessments, rather than distributing the same resources across multiple sites. Scoping studies for water harvesting sites, therefore, involve a trade-off between resource availability, the accuracy and breadth of data obtained, and the number of sites assessed.

It is reasonable to conclude that, by their very nature, scoping studies — designed to assess a relatively large number of potential sites — will inevitably provide less detailed and less certain information compared to assessments focused on a smaller number of selected sites. This is a crucial message for planners and stakeholders involved in water harvesting site selection studies. However, it remains unclear what level of accuracy is acceptable for scoping studies, or whether it is preferable to prioritise identifying the most promising sites within a study area while accepting a higher degree of inaccuracy in the site selection metrics.

## **7.2 Future research recommendations**

The development of the SiteFinder tool (see **Chapter 4**) and its application in a case study (see **Chapter 6**) demonstrated how a remote sensing product (i.e. DEM) can be utilised to extract biophysical information (e.g. storage capacity) for potential water harvesting structures. Testing and assessing the performance of the SiteFinder tool showed that there are limitations to what can be accurately achieved using global DEMs. Therefore, an interesting direction for further research would be to obtain or commission a high-resolution DEM of an entire watershed in an arid or semi-arid region. Such a DEM could serve as the basis for determining the specifications needed for a DEM that accurately identifies water harvesting structures of a particular size. For example, researchers may

benefit from guidelines specifying the attributes required of a DEM to reliably extract relevant information on potential water harvesting structures to a reasonable degree of accuracy.

While some countries (e.g. Australia) with extensive arid and semi-arid regions provide LiDAR-derived DEM datasets covering their entire territory (Australian Government, 2015), the same cannot be said for many low-income countries, where water harvesting has significant potential to improve livelihoods. LiDAR-derived DEMs not only offer higher spatial resolution and accuracy compared to existing free global DEMs but also enable the creation of terrain elevation models rather than surface elevation models.

Until LiDAR-derived DEMs become more widely available to a greater number of countries, researchers will need to rely on global DEMs or alternative methods. One such alternative is generating DEMs from remote sensing datasets, such as interferometric synthetic aperture radar (InSAR). While producing high-quality DEMs using InSAR is particularly challenging in mountainous regions (Yan et al., 2025), it remains an area of active research.

Notably, drylands have less vegetation cover compared to humid regions, meaning that elevation models created using InSAR may provide a more accurate representation of bare-earth terrain. This is because radar signals often struggle to penetrate dense vegetation and tree cover, making InSAR less effective in heavily forested regions. Given the strong association between water harvesting and drylands, InSAR-derived DEMs remain a promising avenue for future research, with potential benefits for the water harvesting sector.

While the SiteFinder tool meets the requirements of the first objective of the thesis (see **Thesis aim and objectives, Section 1.1**), it is specifically designed to identify technologies within the ‘macrocatchment’ classification group of water harvesting. Macrocatchment water harvesting

technologies typically involve structures built across the path of a stream or river, with runoff often reaching the structure from a considerable distance. Future research could focus on improving site selection methodologies using remote sensing and GIS tools to identify suitable locations for microcatchment and floodwater harvesting technologies. Both groups present challenges in terms of site selection using remote sensing products. Microcatchment areas, by definition, are small, so global DEMs with spatial resolutions around 30 m are unlikely to capture the topography of potential sites in sufficient detail. Technologies in the floodwater harvesting group often have cultivation zones located away from the channel network, adding complexity to identifying suitable sites.

There is potential to expand the role of the SiteFinder tool in further research, particularly regarding the tool's area of influence output. This area delineates, via a polygon, the region that would be flooded if a water harvesting structure were constructed. Consequently, an exciting avenue for further research would be to explore how the area of influence polygon could be used to extract data from other datasets (e.g. soil moisture, contours) and examine the interconnections between these data elements and the suitability of the locality for siting water harvesting structures.

The case study undertaken (see **Chapter 6**) demonstrated that it is possible to score potential water harvesting schemes based on several characteristics, which could be of interest to planning agencies seeking objective methods for allocating resources across multiple projects. Further research into developing standardised scoring systems could therefore be beneficial and support the water harvesting sector.

Currently, anyone wishing to use the SiteFinder tool faces two obstacles. Firstly, the code for the SiteFinder tool is not open, and secondly, it operates solely within a proprietary GIS environment (ArcGIS Pro), which excludes a considerable proportion of researchers in the water harvesting sector.

The issue of proprietary software also affects those wishing to use the rainfall-runoff model developed and tested (see **Chapter 5**). Future research could investigate demand, and if this proves significant, it could inform the preferred method of access. Options might include continuing with proprietary GIS software, creating a plugin for open-source GIS software (e.g. QGIS), developing a web-based portal, offering a consultancy service, or a combination of these approaches. Before publicly releasing the tools developed and presented in this thesis, it would be beneficial to optimise the coding. This would enable the SiteFinder tool, for example, to analyse a greater number of siting points within a given time frame for a specified computational processing capacity.

The rainfall-runoff model in **Chapter 5**, and its use in conjunction with a water harvesting site selection study in **Chapter 6**, fulfils the second thesis objective. As emphasised previously in this chapter, model outputs were cross-checked against actual runoff; however, access to a broader range of observed runoff data would be advantageous. Runoff gauging stations in drylands are often situated on rivers with a significant baseflow, whereas much of the water harvesting occurs on or near short-lived (ephemeral) streams and rivers. Therefore, there is a need for improved access to runoff data specific to these short-lived streams and rivers with negligible baseflow. This could be achieved through enhanced access to existing runoff data or by conducting novel research to collect new, original data. Greater access to short-lived flow data in drylands would complement further research using remote sensing imagery to estimate such flow regimes. *In situ* measurements are crucial for verifying runoff models, yet there is a paucity of suitable data from drylands, as highlighted in **Chapter 5**. While remote sensing products are improving in terms of temporal resolution, spectral resolution, and spatial resolution, the same cannot be said for the gathering of field measurements in drylands. This issue needs to be addressed to fully capitalise on the advancements in remote sensing.

Although the case study presented in **Chapter 6** benefited from in-country expertise, it could be criticised as somewhat of an academic exercise in that it lacked input from key planning agencies. Water harvesting projects typically involve multiple stakeholders at local, regional, national, and international levels. These stakeholders may represent government departments, non-governmental organisations, and community groups. Hence, further research could involve conducting a water harvesting site selection study that includes a broader range of stakeholders and has the potential for actual implementation of identified water harvesting schemes. Such a study would therefore combine biophysical criteria, aided by the analysis of remote sensing datasets, with socio-economic considerations and constraints. As outlined in **Chapter 2**, water harvesting technologies offer a range of benefits and serve multiple purposes, presenting numerous opportunities for building on the approaches discussed in **Chapters 4, 5, and 6**.

In 2016, the first conference on the Great Green Wall for the Sahara and the Sahel Initiative was held in Senegal (M2 Presswire, 2016), almost a decade after the initiative was originally launched. The objective of this sustainable land management programme — the largest of its kind in Africa — is to grow a continuous belt of trees and vegetation spanning over 8,000 km across the Sahel, from the coast of Senegal in the west to the coast of Djibouti in the east. This ambitious project seeks to combat desertification and establish a vast green corridor across the African continent (United Nations Climate Change, 2015). Concerns have been raised in recent years over the slow pace of progress towards the Great Green Wall's 2030 goals (Bizcommunity.com, 2024).

While satellite remote sensing has been employed to monitor and assess progress — providing data on factors such as land cover type, vegetation index, precipitation rates, land surface temperature, and surface soil moisture (Deng et al., 2024) — there could be value in expanding the use of remote sensing to assist in establishing water harvesting systems to support the growth of trees along this trans-African

“highway”. A similar approach could be taken to the traditional *Jessour* water harvesting system used in Tunisia (see **Table 2.5**), where trees are planted in the upstream zone of the water harvesting structure. Using remote sensing products in combination with methodologies, or modified methodologies, presented in this thesis (particularly in Chapters **4**, **5**, and **6**) could aid the identification of suitable locations for constructing *Jessours*.

While the overarching focus of this study was the evaluation of scoping tools to aid water harvesting site selection in drylands, there may be potential to adapt the tools developed in this thesis for applications in humid regions. Nicholson et al. (2012) state that modern land use practices in the United Kingdom increase runoff volumes, leading to flooding in towns and villages downstream. They further propose that soft-engineered runoff attenuation features (RAFs) — such as storage ponds, barriers, and bunds — strategically located within a catchment, can be used to attenuate runoff and reduce the severity of flooding. Hence, a GIS tool like SiteFinder (see Chapter **4** and **6**) may potentially be helpful in identifying appropriate locations, particularly if it demonstrates effectiveness when used with DEMs of higher spatial resolution than those applied in this thesis.

The research presented in this thesis demonstrated the potential to shift from traditional pixel-based selection criteria to an approach that considers entire water harvesting schemes (see **Chapter 4**). Future research should continue in this direction, as this approach provides a more accurate representation of actual water harvesting schemes compared to a pixel-based approach. The rainfall-runoff model developed and tested (see **Chapter 5**) introduced novel elements, including the use of curve number data as a proxy for Manning’s roughness coefficient. Additional research into the relationship between curve numbers and surface roughness would therefore be valuable. **Chapter 6** showed that it was possible to compute, for multiple potential water harvesting schemes, the volume of annual runoff in relation to storage volume, which was useful in identifying the most viable schemes. Future research

could build on this work by focusing on hydro-meteorological data from remote sensing products to compute maximum probable flood events and assess the morphological limitations of potential water harvesting schemes in safely managing such events.

This thesis established a foundation for scoping water harvesting sites using remote sensing products and geospatial tools by presenting novel methods. Notably, there is evidence that researchers have already begun to adopt at least one of these approaches in their work. This suggests that the techniques introduced in this thesis could serve as a valuable resource for future research or to support the work of planners. Future work should build on this by focusing on defining the minimum remote sensing product specifications required for the scale of water harvesting systems being selected. Tools should ideally be made accessible and open-source. Ground-truthing should be expanded in scope to improve the validation of tools. New tools should be developed to evaluate sites for a broader range and scale of water harvesting technologies. Additionally, decision-making methodologies should integrate socio-economic criteria alongside technical considerations.

# References

- Abbaspour, K.C., Rouholahnejad, E., Vaghefi, S., Srinivasan, R., Yang, H. and Kløve, B. (2015) ‘A continental-scale hydrology and water quality model for Europe: Calibration and uncertainty of a high-resolution large-scale SWAT model’, *Journal of hydrology*, 524, pp. 733–752. Available at: <https://www.sciencedirect.com/science/article/pii/S0022169415001985>.
- Abboushi, A.M.E., Almasri, M.N. and Shadeed, S.M. (2015) ‘A preliminary investigation of wadi-aquifer interaction in the semi-arid watershed of Faria, Palestine using tracer-based methodology’, *Environmental Earth Sciences*, 73(12), pp. 7861–7872. Available at: <https://doi.org/10.1007/s12665-014-3944-8>.
- Abdalla, O.A.E. and Al-Rawahi, A.S. (2013) ‘Groundwater recharge dams in arid areas as tools for aquifer replenishment and mitigating seawater intrusion: Example of AlKhod, Oman’, *Environmental Earth Sciences*, 69(6), pp. 1951–1962. Available at: <https://doi.org/10.1007/s12665-012-2028-x>.
- Abdekareem, M., Al-Arifi, N., Abdalla, F., Mansour, A. and El-Baz, F. (2022) ‘Fusion of Remote Sensing Data Using GIS-Based AHP-Weighted Overlay Techniques for Groundwater Sustainability in Arid Regions’, *Sustainability*, 14(13), p. 7871. Available at: <https://doi.org/10.3390/su14137871>.

Abdeldayem, O.M., Eldaghar, O., Mostafa, M.K., Habashy, M.M., Hassan, A.A., Mahmoud, H., Morsy, K.M., Abdelrady, A. and Peters, R.W. (2020) 'Mitigation plan and water harvesting of flashflood in arid rural communities using modelling approach: A case study in Afouna village, Egypt', *Water (Basel)*, 12(9), p. 2565. Available at: <https://doi.org/10.3390/W12092565>.

Abdelkebir, B., Maoui, A., Mokhtari, E., Engel, B., Chen, J. and Aboelnour, M. (2021) 'Evaluating Low-Impact Development practice performance to reduce runoff volume in an urban watershed in Algeria', *Arabian Journal of Geosciences*, 14(9), p. 814. Available at: <https://doi.org/10.1007/s12517-021-07178-0>.

Abdullah, M., Al-Ansari, N. and Laue, J. (2020) 'Water Harvesting in Iraq: Status and Opportunities', *Journal of Earth Sciences and Geotechnical Engineering*, 10(1), pp. 1792–9660.

Abualtayef, M., Rahman, G.A., Snounu, I., Qahman, K., Sirhan, H. and Seif, A.K. (2017) 'Evaluation of the effect of water management interventions on water level of Gaza coastal aquifer', *Arabian Journal of Geosciences*, 10(24), p. 555. Available at: <https://doi.org/10.1007/s12517-017-3329-x>.

Addisu, S. and Mekonnen, M. (2019) 'Check dams and storages beyond trapping sediment, carbon sequestration for climate change mitigation, Northwest Ethiopia', *Geoenvironmental Disasters*, 6(1), p. 4. Available at: <https://doi.org/10.1186/s40677-019-0120-1>.

- Adem, A.A., Yibeltal, M., Mhired, D.A., Tilahun, S.A., Zimale, F.A., Worqlul, A.W., Enku, T. and Teferi, E.T. (2023) 'Identification of suitable land for supplemental surface irrigation in semi-arid areas of North-western Ethiopia', *Remote Sensing Applications: Society and Environment*, 29, p. 100899. Available at: <https://doi.org/10.1016/j.rsase.2022.100899>.
- Adham, A., Riksen, M., Ouessar, M. and Coen, R. (2016a) 'Identification of suitable sites for rainwater harvesting structures in arid and semi-arid regions: A review', *International Soil and Water Conservation Research*, 4(2), pp. 108–120. Available at: <https://doi.org/10.1016/j.iswcr.2016.03.001>.
- Adham, A., Riksen, M., Ouessar, M. and Ritsema, C. (2016b) 'A Methodology to Assess and Evaluate Rainwater Harvesting Techniques in (Semi-) Arid Regions', *Water*, 8(5), p. 198. Available at: <https://doi.org/10.3390/w8050198>.
- Adham, A., Sayl, K.N., Abed, R., Abdeladhim, M.A., Wesseling, J.G., Riksen, M., Fleskens, L., Karim, U. and Ritsema, C.J. (2018) 'A GIS-based approach for identifying potential sites for harvesting rainwater in the Western Desert of Iraq', *International Soil and Water Conservation Research*, 6(4), pp. 297–304. Available at: <https://doi.org/10.1016/j.iswcr.2018.07.003>.
- Adham, A., Wesseling, J.G., Abed, R., Riksen, M., Ouessar, M. and Ritsema, C.J. (2019) 'Assessing the impact of climate change on rainwater harvesting in the Oum Zessar watershed in Southeastern Tunisia', *Agricultural Water Management*, 221, pp. 131–140. Available at: <https://doi.org/10.1016/j.agwat.2019.05.006>.

Aghad, M., Manaouch, M., Sadiki, M., Batchi, M. and Al Karkouri, J. (2021) 'Identifying suitable sites for rainwater harvesting using runoff model (SCS-CN), remote sensing and GIS based fuzzy analytical hierarchy process (FAHP) in Kenitra province, NW Morocco', *Geographia Technica*, 16(Special Issue), pp. 111–127. Available at:  
[https://doi.org/10.21163/GT\\_2021.163.09](https://doi.org/10.21163/GT_2021.163.09).

Aghaloo, K. and Sharifi, A. (2023) 'A GIS-based agroecological model for sustainable agricultural production in arid and semi-arid areas: The case of Kerman Province, Iran', *Current Research in Environmental Sustainability*, 6, p. 100230. Available at:  
<https://doi.org/10.1016/j.crsust.2023.100230>.

Agriculture Victoria (2020) Drought Reserve Dams, Agriculture Victoria. Available at:  
<https://agriculture.vic.gov.au/farm-management/water/managing-dams/drought-reserve-dams> (Accessed: 24 March 2022).

Ahirwar, S., Malik, M.S., Ahirwar, R. and Shukla, J.P. (2020) 'Identification of suitable sites and structures for artificial groundwater recharge for sustainable groundwater resource development and management', *Groundwater for Sustainable Development*, 11, p. 100388. Available at: <https://doi.org/10.1016/j.gsd.2020.100388>.

Ahmed, A., Valyrakis, M., Ghumman, A.R., Arshad, M., Pasha, G.A., Farooq, R. and Janjua, S. (2022) 'Assessing the rainfall water harvesting potential using Geographical Information Systems (GIS)', *CivilEng*, 3(4), pp. 895–908. Available at:  
<https://doi.org/10.3390/civileng3040051>.

- Ahmed, A.A. and Diab, M.S. (2018) 'Hydrologic analysis of the challenges facing water resources and sustainable development of Wadi Feiran basin, southern Sinai, Egypt', *Hydrogeology Journal*, 26(7), pp. 2475–2493. Available at: <https://doi.org/10.1007/s10040-018-1764-8>.
- Airborne Research and Survey Facility (ARSF) (2009) 'Data from the Photographic Camera, Optech LIDAR and AISA Eagle and Hawk Instruments on-board the Dornier Do228-101 D-CALM Aircraft during Flight ET07/03 over the Alem Tena Area, Ethiopia'. NERC Earth Observation Data Centre. Available at: <https://catalogue.ceda.ac.uk/uuid/b30490c666dd23b43789412183602a5c> (Accessed: 30 July 2020).
- Ajibade, T.F., Nwogwu, N.A., Ajibade, F.O., Adelodun, B., Idowu, T.E., Ojo, A.O., Iji, J.O., Olajire, O.O. and Akinmusere, O.K. (2020) 'Potential dam sites selection using integrated techniques of remote sensing and GIS in Imo State, Southeastern, Nigeria', *Sustainable Water Resources Management*, 6(4), p. 57. Available at: <https://doi.org/10.1007/s40899-020-00416-5>.
- Al-Abadi, A.M., Shahid, S., Ghalib, H.B. and Handhal, A.M. (2017) 'A GIS-Based Integrated Fuzzy Logic and Analytic Hierarchy Process Model for Assessing Water-Harvesting Zones in Northeastern Maysan Governorate, Iraq', *Arabian Journal for Science and Engineering*, 42(6), pp. 2487–2499. Available at: <https://doi.org/10.1007/s13369-017-2487-1>.
- Al-Adamat, R. (2008) 'GIS as a decision support system for siting water harvesting ponds in the basalt aquifer/NE Jordan', *Journal of Environmental Assessment Policy and Management*, 10(02), pp. 189–206. Available at: <https://doi.org/10.1142/S1464333208003020>.

Alaska Satellite Facility (2023) PALSAR RTC DEM Information, Alaska Satellite Facility (ASF).

Available at: <https://asf.alaska.edu/information/palsar-rtc-dem-information> (Accessed: 24 July 2023).

Alataway, A. (2023) ‘SCS-CN and GIS-Based Approach for Estimating Runoff in Western Region of Saudi Arabia’, *Journal of Geoscience and Environment Protection*, 11(3), pp. 30–43.

Alem, F., Abebe, B.A., Degu, A.M., Goitom, H. and Grum, B. (2022) ‘Assessment of water harvesting potential sites using GIS-based MCA and a hydrological model: case of Werie catchment, northern Ethiopia’, *Sustainable Water Resources Management*, 8(3), p. 70.

Available at: <https://doi.org/10.1007/s40899-022-00652-x>.

Al-Ghobari, H., Dewidar, A. and Alataway, A. (2020) ‘Estimation of surface water runoff for a semi-arid area using RS and GIS-Based SCS-CN method’, *Water (Switzerland)*, 12(7), p. 1924.

Available at: <https://doi.org/10.3390/w12071924>.

Al-Hasani, B., Abdellatif, M., Carnacina, I., Harris, C., Al-Quraishi, A., Maarroof, B.F. and Zubaidi, S.L. (2023) ‘Integrated geospatial approach for adaptive rainwater harvesting site selection under the impact of climate change’, *Stochastic Environmental Research and Risk Assessment*, 38(3), pp. 1009–1033.

Available at: <https://doi.org/10.1007/s00477-023-02611-0>.

Ali, A., Oweis, T., Rashid, M., El-Naggar, S. and Aal, A.A. (2007) ‘Water harvesting options in the drylands at different spatial scales’, *Land Use and Water Resources Research*, 7, p. 13.

Available at: <https://ageconsearch.umn.edu/record/48065?v=pdf>.

- Al-Kakey, O., Othman, A.A., Al-Mukhtar, M. and Dunger, V. (2023) 'Proposing Optimal Locations for Runoff Harvesting and Water Management Structures in the Hami Qeshan Watershed, Iraq', *ISPRS International Journal of Geo-Information*, 12(8), p. 312. Available at: <https://doi.org/10.3390/ijgi12080312>.
- Al-Khuzaei, M.M., Janna, H. and Al-Ansari, N. (2020) 'Assessment model of water harvesting and storage location using GIS and remote sensing in Al-Qadisiyah, Iraq', *Arabian Journal of Geosciences*, 13(21), p. 1154. Available at: <https://doi.org/10.1007/s12517-020-06154-4>.
- AllAfrica Global Media (2016) 'Port Sudan's Water Shortage Worsening', *allAfrica.com* (English).
- AllAfrica Global Media (2023) 'Sudan: Drinking Water Agreement Welcomed in Port Sudan, but Activists Question Govt Commitment', *allAfrica.com* (English).
- Almasalmeh, O., Adel, A. and Mourad, K.A. (2022) 'Floodwater harvesting within Wadi Billi, Egypt', *Water Science*, 36(1), pp. 98–112. Available at: <https://doi.org/10.1080/23570008.2022.2129150>.
- Alrawi, I., Chen, J.P., Othman, A.A., Ali, S.S. and Harash, F. (2023) 'Insights of dam site selection for rainwater harvesting using GIS: A case study in the Al- Qalamoun Basin, Syria', *HELIYON*, 9(9). Available at: <https://doi.org/10.1016/j.heliyon.2023.e19795>.
- Al-wadaey, A., Ziadat, F., Oweis, T., Elkhboli, M. and Alboueichi, A. (2016) 'Targeting Sub-Watersheds with Conservation Practices Using SWAT model and GIS Techniques in Libya', *Biosciences, Biotechnology Research Asia*, 13(3), pp. 1353–1362. Available at: <https://doi.org/10.13005/bbra/2276>.

- Alwan, I.A., Aziz, N.A. and Hamoodi, M.N. (2020) 'Potential Water Harvesting Sites Identification Using Spatial Multi-Criteria Evaluation in Maysan Province, Iraq', ISPRS International Journal of Geo-Information, 9(4), p. 235. Available at: <https://doi.org/10.3390/ijgi9040235>.
- American Water Works Association (AWWA) (2006) Water Chlorination/Chloramination Practices and Principles - AWWA Manual M20. 2nd edn. American Water Works Association (AWWA). Available at: <https://app.knovel.com/hotlink/toc/id:kpWCCPPMW5/water-chlorination-chloramination/water-chlorination-chloramination>.
- Anschuetz, J., Kome, A., Nederlof, M., de Neef, R. and van de Ven, T. (2003) 'Water Harvesting and Soil Moisture Retention'. Wageningen: Agromisa Foundation. Available at: <https://www.agromisa.org/product-category/series-agrodok/>.
- Asmar, N.F., Sim, J.O.L., Ghodieh, A. and Fauzi, R. (2021) 'Effect of Land Use\Land Cover Changes on Estimated Potential Runoff in the Nablus Mountains Watersheds of Palestine: A Case Study', Journal of the Indian Society of Remote Sensing, 49(5), pp. 1067–1080. Available at: <https://doi.org/10.1007/s12524-020-01278-2>.
- Assefa, T., Jha, M., Reyes, M., Srinivasan, R. and Worqlul, A. (2018) 'Assessment of Suitable Areas for Home Gardens for Irrigation Potential, Water Availability, and Water-Lifting Technologies', Water, 10(4), p. 495. Available at: <https://doi.org/10.3390/w10040495>.
- Australian Government (2015) Digital Elevation Model (DEM) of Australia derived from LiDAR 5 Metre Grid, Commonwealth of Australia (Geoscience Australia). Available at: <https://doi.org/https://doi.org/10.26186/89644>.

Babker, Z., Elagib, N.A., Al Zayed, I.S. and Sulieman, R. (2020) 'Floodwater harvesting to manage irrigation water and mesquite encroachment in a data-sparse river basin: an eco-hydrological approach', *River Research and Applications*, 36(9), pp. 1852–1867. Available at:

<https://doi.org/10.1002/rra.3703>.

Badan Informasi Geospasial (2018) DEMNAS Seamless Digital Elevation Model (DEM), Badan Informasi Geospasial. Available at: <https://tanahair.indonesia.go.id/demnas/#/demnas> (Accessed: 3 August 2023).

Baek, C.W. and Coles, N.A. (2013) 'An artificial catchment rainfall-runoff collecting system: Design efficiency and reliability potential considering climate change in Western Australia', *Agricultural Water Management*, 121, p. 124.

Bajabaa, S., Masoud, M. and Al-Amri, N. (2014) 'Flash flood hazard mapping based on quantitative hydrology, geomorphology and GIS techniques (case study of Wadi Al Lith, Saudi Arabia)', *Arabian Journal of Geosciences*, 7(6), pp. 2469–2481. Available at:

<https://doi.org/10.1007/s12517-013-0941-2>.

Balasubramanian, A., Duraisamy, K., Thirumalaisamy, S., Krishnaraj, S. and Yatheendradasan, R.K. (2017) 'Prioritization of subwatersheds based on quantitative morphometric analysis in lower Bhavani basin, Tamil Nadu, India using DEM and GIS techniques', *Arabian Journal of Geosciences*, 10(24), p. 552. Available at: <https://doi.org/10.1007/s12517-017-3312-6>.

- Bañados, J.H. and Quijano, I.P. (2022) ‘Rainwater Retention Site Assessment For Urban Flood Risk Reduction And Flood Defence In Mandaue City, Philippines’, *ISPRS Annals of the Photogrammetry, Remote Sensing and Spatial Information Sciences*, X-3/W1-202(3/W1-2022), pp. 1–7. Available at: <https://doi.org/10.5194/isprs-annals-X-3-W1-2022-1-2022>.
- Banai-Kashani, R. (1989) ‘A new method for site suitability analysis: The analytic hierarchy process’, *Environmental Management*, 13(6), pp. 685–693. Available at: <https://doi.org/10.1007/BF01868308>.
- Basheer, M. and Elagib, N.A. (2019) ‘Performance of satellite-based and GPCC 7.0 rainfall products in an extremely data-scarce country in the Nile Basin’, *Atmospheric Research*, 215, pp. 128–140. Available at: <https://doi.org/10.1016/j.atmosres.2018.08.028>.
- BBC Worldwide Limited (2013) ‘Severe water shortage hits Port Sudan’, *BBC Monitoring Middle East*. Available at: <https://www.proquest.com/wire-feeds/severe-water-shortage-hits-port-sudan/docview/1365975531/se-2?accountid=11979>.
- Behera, M.D., Biradar, C., Das, P. and Chowdary, V.M. (2019) ‘Developing quantifiable approaches for delineating suitable options for irrigating fallow areas during dry season—a case study from Eastern India’, *Environmental Monitoring and Assessment*, 191(S3), p. 805. Available at: <https://doi.org/10.1007/s10661-019-7697-4>.
- Bera, A. and Mukhopadhyay, B.P. (2023) ‘Identification of suitable sites for surface rainwater harvesting in the drought prone Kumari River basin, India in the context of irrigation water management’, *Journal of Hydrology*, 621, p. 129655. Available at: <https://doi.org/10.1016/j.jhydrol.2023.129655>.

- Beven, K. (2012) *Rainfall-Runoff Modelling: The Primer: Second Edition*. 2nd ed., Rainfall-Runoff Modelling: The Primer: Second Edition. 2nd ed. Hoboken: Wiley. Available at: <https://doi.org/10.1002/9781119951001>.
- Bhuvan: ISRO/NRSC (2023) Bhuvan Indian Geo-Platform of ISRO, National Remote Sensing Centre. Available at: <https://bhuvan.nrsc.gov.in/> (Accessed: 11 August 2023).
- Binnie, C., Kimber, M. and Thomas, H. (2018) *Basic Water Treatment*. 6th ed. London: ICE Publishing.
- Bisrat, E. and Berhanu, B. (2018) ‘Identification of Surface Water Storing Sites Using Topographic Wetness Index (TWI) and Normalized Difference Vegetation Index (NDVI)’, *Journal of Natural Resources and Development*, 08, pp. 91–100. Available at: <https://doi.org/10.5027/jnrd.v8i0.09>.
- Biswas, B. (2009) ‘Changing water resources study using GIS and spatial model — A case study of Bhatar Block, district Burdwan, West Bengal, India’, *Journal of the Indian Society of Remote Sensing*, 37(4), pp. 705–717. Available at: <https://doi.org/10.1007/s12524-009-0049-z>.
- Bizcommunity.com (2024) ‘Will Africa’s Great Green Wall hit 2030 goal?’, Cape Town: Disco Digital Media, Inc. Available at: <https://www.proquest.com/other-sources/will-africa-amp-a-pos-s-great-green-wall-hit-2030/docview/3067560268/se-2?accountid=11979> (Accessed: 19 March 2025).
- Boers, T.M. (1994) *Rainwater harvesting in arid and semi-arid zones*. Int. Inst. for Land Reclamation.

- Boers, T.M., Zondervan, K. and Ben-Asher, J. (1986) 'Micro-catchment-water-harvesting (MCWH) for arid zone development', *Agricultural Water Management*, 12(1–2), p. 21. Available at: [https://doi.org/10.1016/0378-3774\(86\)90003-X](https://doi.org/10.1016/0378-3774(86)90003-X).
- Boers, T.M. and Ben-Asher, J. (1982) 'A review of rainwater harvesting', *Agricultural Water Management*, 5(2), pp. 145–158. Available at: [https://doi.org/10.1016/0378-3774\(82\)90003-8](https://doi.org/10.1016/0378-3774(82)90003-8).
- Bossio, D., Geheb, K. and Critchley, W. (2010) 'Managing water by managing land: Addressing land degradation to improve water productivity and rural livelihoods', *Agricultural Water Management*, 97(4), p. 536. Available at: <https://doi.org/10.1016/j.agwat.2008.12.001>.
- Bot, A.J., Nachtergaele, F.O. and Young, A. (2000) *Land Resource Potential and Constraints at Regional and Country Levels*. Rome: Food & Agriculture Organization of the United Nations.
- Bretas, E.M., Lemos, J. V and Lourenço, P.B. (2012) 'Masonry Dams: Analysis of the Historical Profiles of Sazilly, Delocre, and Rankine', *International Journal of Architectural Heritage*, 6(1), pp. 19–45. Available at: <https://doi.org/10.1080/15583058.2010.501399>.
- Bruins, H.J., Evenari, M. and Nessler, U. (1986) 'Rainwater-harvesting agriculture for food production in arid zones: the challenge of the African famine', *Applied Geography*, 6(1), pp. 13–32. Available at: [https://doi.org/10.1016/0143-6228\(86\)90026-3](https://doi.org/10.1016/0143-6228(86)90026-3).

- Bruins, H.J., Bithan-Guedj, H. and Svoray, T. (2019) 'GIS-based hydrological modelling to assess runoff yields in ancient-agricultural terraced wadi fields (central Negev desert)', *Journal of Arid Environments*, 166, pp. 91–107. Available at: <https://doi.org/10.1016/j.jaridenv.2019.02.010>.
- Buraihi, F.H. and Shariff, A.R.M. (2015) 'Selection of Rainwater Harvesting Sites by Using Remote Sensing and GIS Techniques: A Case Study of Kirkuk, Iraq, *Jurnal Teknologi*, 76(15), pp. 75–81. Available at: <https://doi.org/10.11113/jt.v76.5955>.
- Büyüksalih, G., Koçak, G., Topan, H., Oruç, M. and Marangoz, A. (2005) 'Spot revisited: Accuracy assessment, DEM generation and validation from stereo spot 5 HRG images', *Photogrammetric Record*, 20(110), pp. 130–146. Available at: <https://doi.org/10.1111/j.1477-9730.2005.00314.x>.
- Cairncross, S. and Feachem, R.G. (1993) *Environmental health engineering in the tropics: an introductory text*. 2nd ed. Chichester: J. Wiley.
- Carlos Mendoza, J.A., Chavez Alcazar, T.A. and Zuñiga Medina, S.A. (2021) 'Calibration and Uncertainty Analysis for Modelling Runoff in the Tambo River Basin, Peru, Using Sequential Uncertainty Fitting Ver-2 (SUFI-2) Algorithm', *Air, Soil and Water Research*, 14, p. 1178622120988707. Available at: <https://doi.org/10.1177/1178622120988707>.
- Castillo, V.M., Mosch, W.M., García, C.C., Barberá, G.G., Cano, J.A.N. and López-Bermúdez, F (2007) 'Effectiveness and geomorphological impacts of check dams for soil erosion control in a semiarid Mediterranean catchment: El Cárcavo (Murcia, Spain)', *Catena* (Giessen), 70(3), pp. 416–427. Available at: <https://doi.org/10.1016/j.catena.2006.11.009>.

- Cattarossi, A., Polo, P., Mastrocola, P., Ouechtati, E.F.S., Isotton, G., Fileccia, A. and Walther, C. (2018) Management of Critical Water Supply Sources near Port Sudan, Sudan: Arbaat Dam and Well Fields at Arbaat and Moj. Treviso, Italy.
- Cherlet, M., Hutchinson, C., Reynolds, J., Hill, J., Sommer, S. and von Maltitz, G. (2018) ‘World Atlas of Desertification’. Luxembourg: Publication Office of the European Union. Available at: <https://wad.jrc.ec.europa.eu/>.
- Chow, V. Te, Maidment, D.R. and Mays, L.W. (1988) Applied hydrology. New York: McGraw-Hill.
- Chunhong, H., Deyi, W., Jayakumar, R. and Shingo, A. (2004) Warping Dams: Construction and its Effects on Environment, Economy, and Society in Loess Plateau Region of China. Beijing: UNESCO.
- Cirilo, J.A., Verçosa, L.F. de M., Gomes, M.M. de A., Feitoza, M.A.B., Ferraz, G. de F. and Silva, B. de M. (2020) ‘Development and application of a rainfall-runoff model for semi-arid regions’, RBRH, 25. Available at: <https://doi.org/10.1590/2318-0331.252020190106>.
- CNES (2023) SPOT Earth seen from space, CNES Projects Library. Available at: <https://spot.cnes.fr/en/SPOT/index.htm> (Accessed: 29 July 2023).
- Congalton, R., Gu, J., Yadav, K., Thenkabail, P. and Ozdogan, M. (2014) ‘Global Land Cover Mapping: A Review and Uncertainty Analysis’, Remote Sensing, 6(12), pp. 12070–12093. Available at: <https://doi.org/10.3390/rs61212070>.

Conrad, O. (2009) 'SAGA-GIS Module Library Documentation (v2.2.1) Module Flow Width and Specific Catchment Area'. Available at: [https://saga-gis.sourceforge.io/saga\\_tool\\_doc/2.2.1/ta\\_hydrology\\_19.html](https://saga-gis.sourceforge.io/saga_tool_doc/2.2.1/ta_hydrology_19.html).

Crameri, F. (2021) 'Scientific colour maps'. Available at: <https://doi.org/https://doi.org/10.5281/zenodo.1243862>.

Critchley, W. and Siegert, K. (1991) A Manual for the Design and Construction of Water Harvesting Schemes for Plant Production. Food and Agriculture Organisation of the United Nations, Rome, Italy. Rome, Italy: Food and Agriculture Organization of The United Nations. Available at: <http://www.fao.org/docrep/U3160E/u3160e00.HTM>.

Critchley, W., Gowing, J.W. and Mollee, E. (2012) Water Harvesting in Sub-Saharan Africa. Routledge.

Cronshey, R.G., Roberts, R.T. and Miller, N. (1985) Urban Hydrology for Small Watersheds (Tr-55 Rev.). US Department of Agriculture, Soil Conservation Service, Engineering Division.

Dabiri, D., Alipor, A., Azad, B. and Fatahi, A. (2016) 'Site selection of in-situ and ex-situ methods of rain water harvesting in the arid regions of Iran', International Research Journal of Engineering and Technology, 3(4), pp. 270–276.

Das, G.P. (2016) Hydrology and Storm Sewer Design. First edit. New York, [New York] (222 East 46th Street, New York, NY 10017). Available at: <http://a.cloud.igpublish.com/iglibrary/public/MPB0000315.html?1>.

- de Winnaar, G., Jewitt, G.P.W. and Horan, M. (2007) ‘A GIS-based approach for identifying potential runoff harvesting sites in the Thukela River basin, South Africa’, *Physics and Chemistry of the Earth, Parts A/B/C*, 32(15–18), pp. 1058–1067. Available at: <https://doi.org/10.1016/j.pce.2007.07.009>.
- Debebe, D., Seyoum, T., Tessema, N. and Ayele, G.T. (2023) ‘Modeling rainfall-runoff estimation and assessing water harvesting zone for irrigation practices in Keleta watershed, Awash river basin, Ethiopia’, *Geocarto International*, 38(1). Available at: <https://doi.org/10.1080/10106049.2023.2236582>.
- Debebe, Y., Otterpohl, R. and Islam, Z. (2022) ‘Remote sensing and multi-criterion analysis for identifying suitable rainwater harvesting areas’, *Acta Geophysica*, 71(2), pp. 855–872. Available at: <https://doi.org/10.1007/s11600-022-00910-8>.
- Delaney, R.G., Blackburn, G.A., Whyatt, J.D. and Folkard, A.M. (2022) ‘SiteFinder: A geospatial scoping tool to assist the siting of external water harvesting structures’, *Agricultural Water Management*, 272, p. 107836. Available at: <https://doi.org/10.1016/j.agwat.2022.107836>.
- Delaney, R.G., Blackburn, G.A., Folkard, A.M. and Whyatt, J.D. (2024) ‘HRRTLE (High Resolution Runoff and Transmission Loss Estimator): a novel tool for mapping connectivity of runoff in ephemeral stream networks to aid the siting of water harvesting structures’, *Hydrol. Earth Syst. Sci. Discuss.* [preprint]. Available at: <https://doi.org/10.5194/hess-2024-97>.
- Deng, A., Hao, X. and Qu, J.J. (2024) ‘A Preliminary Assessment of Land Restoration Progress in the Great Green Wall Initiative Region Using Satellite Remote Sensing Measurements’, *Remote Sensing*, 16(23), p. 4461. Available at: <https://doi.org/10.3390/rs16234461>.

- D'Haen, K., Dugar, B., Verstraeten, G., Degryse, P. and De Brue, H. (2013) 'A sediment fingerprinting approach to understand the geomorphic coupling in an eastern Mediterranean mountainous river catchment', *Geomorphology*, 197, pp. 64–75.
- Dile, Y.T., Rockström, J. and Karlberg, L. (2016) 'Suitability of Water Harvesting in the Upper Blue Nile Basin, Ethiopia: A First Step towards a Mesoscale Hydrological Modeling Framework', *Advances in Meteorology*, 2016, pp. 1–12. Available at: <https://doi.org/10.1155/2016/5935430>.
- Dile, Y.T., Karlberg, L., Temesgen, M. and Rockström, J. (2013) 'The role of water harvesting to achieve sustainable agricultural intensification and resilience against water related shocks in sub-Saharan Africa', *Agriculture, Ecosystems & Environment*, 181(C), pp. 69–79. Available at: <https://doi.org/10.1016/j.agee.2013.09.014>.
- Doherty, D. (2000) 'A Primer on Dam Design, Design and Construction of Earth Dams', *The Permaculture Activist: Earthworks and Energy*, p. 7. Available at: <https://www.permaculturedesignmagazine.com/product-page/44-nov-2000-6-earthworks-and-energy>.
- Doulabian, S., Ghasemi Tousi, E., Aghlmand, R., Alizadeh, B., Ghaderi Bafti, A. and Abbasi, A. (2021) 'Evaluation of Integrating SWAT Model into a Multi-Criteria Decision Analysis towards Reliable Rainwater Harvesting Systems', *Water*, 13(14), p. 1935. Available at: <https://doi.org/10.3390/w13141935>.

- Duan, W.L., Maskey, S., Chaffe, P.L.B., Luo, P., He, B., Wu, Y. and Hou, J. (2021) 'Recent Advancement in Remote Sensing Technology for Hydrology Analysis and Water Resources Management', *Remote Sensing*, 13(6), p. 1097. Available at:  
<https://doi.org/10.3390/rs13061097>.
- Durga Rao, K.H.V. and Bhaumik, M.K. (2003) 'Spatial Expert Support System in Selecting Suitable Sites for Water Harvesting Structures — A Case Study of Song Watershed, Uttaranchal, India', *Geocarto International*, 18(4), pp. 43–50. Available at:  
<https://doi.org/10.1080/10106040308542288>.
- Dwiatmojo, H.R., Komariah, Ramelan, A.H. and Priyanto, E. (2021) 'Mapping of rain water harvesting potential at Keduang Sub-watershed, Central Java, Indonesia', *IOP Conference Series: Earth and Environmental Science*, 824(1), p. 012029. Available at:  
<https://doi.org/10.1088/1755-1315/824/1/012029>.
- Eekhout, J.P.C. and de Vente, J. (2022) 'Global impact of climate change on soil erosion and potential for adaptation through soil conservation', *Earth-Science Reviews*, 226, p. 103921. Available at: <https://doi.org/https://doi.org/10.1016/j.earscirev.2022.103921>.
- Earth Resources Observation and Science (EROS) Center (2018a) USGS EROS Archive - Commercial Satellites - SPOT Historical, USGS. Available at:  
<https://doi.org/10.5066/P9CBCJGZ>.

Earth Resources Observation and Science (EROS) Center (2018b) Shuttle Radar Topography

Mission (SRTM) - Mission Summary, USGS EROS Archive. Available at:

<https://www.usgs.gov/centers/eros/science/usgs-eros-archive-digital-elevation-srtm-mission-summary> (Accessed: 25 July 2023).

Earth Resources Observation and Science (EROS) Center (2018c) USGS EROS Archive - Digital

Elevation - Shuttle Radar Topography Mission (SRTM) Void Filled, USGS. Available at:

<https://doi.org/10.5066/F7F76B1X> (Accessed: 15 November 2022).

Earth Resources Observation and Science (EROS) Center (2018d) USGS EROS Archive - Digital

Elevation - Shuttle Radar Topography Mission (SRTM) 1 Arc-Second Global, USGS.

Available at: <https://doi.org/10.5066/F7PR7TFT> (Accessed: 18 November 2020).

El Osta, M., El Sabri, M. and Masoud, M. (2021) ‘Environmental sensitivity of flash flood hazard

based on surface water model and GIS techniques in Wadi El Azariq, Sinai, Egypt’,

Environmental Technology & Innovation, 22, p. 101522. Available at:

<https://doi.org/10.1016/j.eti.2021.101522>.

Elewa, H.H., Qaddah, A.A. and El-Feel, A.A. (2012) ‘Determining Potential Sites for Runoff Water

Harvesting using Remote Sensing and Geographic Information Systems-Based Modeling in

Sinai’, American Journal of Environmental Sciences, 8(1), pp. 42–55.

Elewa, H.H., Nosair, A.M., Zelenakova, M., Mikita, V., Abdel Moneam, N.A. and Ramadan, E.M.

(2023) ‘Environmental Sustainability of Water Resources in Coastal Aquifers, Case Study:

El-Qaa Plain, South Sinai, Egypt’, Water, 15(6), p. 1118. Available at:

<https://doi.org/10.3390/w15061118>.

Emamgholizadeh, S., Bateni, S.M. and Nielson, J.R. (2018) 'Evaluation of different strategies for management of reservoir sedimentation in semi-arid regions: a case study (Dez Reservoir)', *Lake and Reservoir Management*, 34(3), pp. 270–282. Available at: <https://doi.org/10.1080/10402381.2018.1436624>.

eoPortal (2012) IRS (Indian Remote Sensing Satellites). Available at:

<https://www.eoportal.org/satellite-missions/irs#eop-additional-articles-section> (Accessed: 1 August 2023).

Ettazarini, S. (2021) 'GIS-based land suitability assessment for check dam site location, using topography and drainage information: a case study from Morocco', *Environmental earth sciences*, 80(17), p. 567. Available at: <https://doi.org/10.1007/s12665-021-09881-3>.

Eva, H.D., de Miranda, E.E., Di Bella, C.M., Gond, V., Huber, O., Sgrenzaroli, M., Jones, S., Coutinho, A., Dorado, A., Guimar, M., Elvidge, C., Achard, F., Belward, A.S., Bartholom, E., Baraldi, A., Grandi, G., De Vogt, P., Fritz, S. and Hartley, A. (2003) 'The Land Cover Map for South America in the Year 2000'. GLC2000 database, European Commission Joint Research Centre. Available at: <https://forobs.jrc.ec.europa.eu/products/glc2000/products.php>.

Ezzeldin, M., Konstantinovich, Evgeny, S., Igorevich and Ilya, G. (2022) 'Determining the suitability of rainwater harvesting for the achievement of sustainable development goals in Wadi Watir, Egypt using GIS techniques', *Journal of Environmental Management*, 313, p. 114990. Available at: <https://doi.org/10.1016/j.jenvman.2022.114990>.

- Falorni, G., Teles, V., Vivoni, E.R., Bras, R.L. and Amaratunga, K.S. (2005) 'Analysis and characterization of the vertical accuracy of digital elevation models from the Shuttle Radar Topography Mission', *Journal of Geophysical Research: Earth Surface*. Falorni, G, 110(2), pp. F02005-n/a. Available at: <https://doi.org/10.1029/2003JF000113>.
- Fang, N., Zeng, Y., Ran, L., Wang, Zhen, Lu, X., Wang, Zhengang, Yang, X., Jian, J., Yu, Q., Ni, L., Liu, C., Yue, C. and Shi, Z. (2023) 'Substantial role of check dams in sediment trapping and carbon sequestration on the Chinese Loess Plateau', *Communications Earth & Environment*, 4(1), p. 65. Available at: <https://doi.org/10.1038/s43247-023-00728-2>.
- Farswan, S., Vishwakarma, C.A., Mina, U., Kumar, V. and Mukherjee, S. (2019) 'Assessment of rainwater harvesting sites in a part of North-West Delhi, India using geomatic tools', *Environmental Earth Sciences*, 78(11), p. 329. Available at: <https://doi.org/10.1007/s12665-019-8332-y>.
- Ferguson, J. (2015) *Permaculture as Farming Practice and International Grassroots Network: A Multidisciplinary Study*, Graduate College. University of Illinois at Urbana-Champaign. Available at: <https://www.ideals.illinois.edu/handle/2142/89037>.
- Forzieri, G., Gardenti, M., Caparrini, F. and Castelli, F. (2008) 'A methodology for the pre-selection of suitable sites for surface and underground small dams in arid areas: A case study in the region of Kidal, Mali', *Physics and Chemistry of the Earth*, 33(1–2), pp. 74–85. Available at: <https://doi.org/10.1016/j.pce.2007.04.014>.

- Forzini, E., Piemontese, L., Bresci, E., Barthod, B., Bielser, F., Sylvestre, M., Adhikari, N., Pun, S. and Castelli, G. (2022) 'Identification of suitable sites for traditional *pokhari* water harvesting in mountain rural communities of the Himalaya', *Hydrology Research*, 53(11), pp. 1340–1356. Available at: <https://doi.org/10.2166/nh.2022.027>.
- Freeman, M.C., Pringle, C.M. and Jackson, C.R. (2007) 'Hydrologic Connectivity and the Contribution of Stream Headwaters to Ecological Integrity at Regional Scales 1', *JAWRA Journal of the American Water Resources Association*, 43(1), pp. 5–14. Available at: <https://doi.org/10.1111/j.1752-1688.2007.00002.x>.
- Gallant, J.C., Read, A.M. and Dowling, T.I. (2012) 'Removal of tree offsets from SRTM and other Digital Surface Models', *The International Archives of the Photogrammetry, Remote Sensing and Spatial Information Sciences*, pp. 275–280. Available at: <https://doi.org/10.5194/isprsarchives-xxxix-b4-275-2012>.
- Gao, H., Birkel, C., Hrachowitz, M., Tetzlaff, D., Soulsby, C. and Savenije, H.H.G. (2019) 'A simple topography-driven and calibration-free runoff generation module', *Hydrology and Earth System Sciences*, 23(2), pp. 787–809. Available at: <https://doi.org/10.5194/hess-23-787-2019>.
- Gavhane, K.P., Mishra, A.K., Sarangi, A., Singh, D.K. and Sudhishri, S. (2023) 'Targeting of rainwater harvesting structures using geospatial tools and analytical hierarchy process (AHP) in the semi-arid region of Rajasthan (India)', *Environmental Science and Pollution Research*, 30(22), pp. 61682–61709. Available at: <https://doi.org/10.1007/s11356-023-26289-7>.

- Gebrernichael, D., Nyssen, J., Poesen, J., Deckers, J., Haile, M., Govers, G. and Moeyersons, J. (2005) 'Effectiveness of stone bunds in controlling soil erosion on cropland in the Tigray Highlands, northern Ethiopia', *Soil use and management*, 21(3), pp. 287–297.
- Geyik, M.P. (1986) *FAO watershed management field manual Gully control* FAO Conservation Guide 13/2. Rome, Italy: Food and Agricultural Organization of the United Nations. Available at: <http://www.fao.org/docrep/006/AD082E/AD082e00.htm#cont>.
- Ghanem, M., Abu Sadah, M. and Keilani, Y. (2021) 'Watershed modelling development for generating runoff estimation of Sarida Catchment/Central West Bank', *Environmental Monitoring and Assessment*, 193(10), p. 672. Available at: <https://doi.org/10.1007/s10661-021-09468-2>.
- Gilić, F., Gasparovic, M. and Baucic, M. (2023) 'Current state and challenges in producing large-scale land cover maps: review based on recent land cover products', *GEOCARTO INTERNATIONAL*, 38(1). Available at: <https://doi.org/10.1080/10106049.2023.2242693>.
- Gontia, N.K. and Patil, P.Y. (2012) 'Assessment of Groundwater Recharge Through Rainfall and Water Harvesting Structures in Jamka Microwatershed Using Remote Sensing and GIS', *Journal of the Indian Society of Remote Sensing*, 40(4), pp. 639–648. Available at: <https://doi.org/10.1007/s12524-011-0176-1>.
- Grant, D., Hadzic, D., Pasupaleti, P., Meijden, G. van der, Osmaston, N., Goes, B. and Knightbridge, J. (2016) *Master Plan Report Volume 2: Water Supply - Port Sudan Water and Sanitation Programme*. Cambridge, United Kingdom.

GRDC (2020): GRDC Major River Basins. Global Runoff Data Centre. 2nd, rev. ed. Koblenz: Federal Institute of Hydrology (BfG).

Gruber, S. and Peckham, S. (2009) 'Chapter 7 Land-Surface Parameters and Objects in Hydrology', in. Elsevier Science & Technology, pp. 171–194. Available at:  
[https://doi.org/10.1016/S0166-2481\(08\)00007-X](https://doi.org/10.1016/S0166-2481(08)00007-X).

Grum, B., Hessel, R., Kessler, A., Woldearegay, K., Yazew, E., Ritsema, C. and Geissen, V. (2016) 'A decision support approach for the selection and implementation of water harvesting techniques in arid and semi-arid regions', *Agricultural Water Management*, 173, pp. 35–47. Available at: <https://doi.org/10.1016/j.agwat.2016.04.018>.

Gumbel, E.J. (1941) 'The return period of flood flows', *The annals of mathematical statistics*, 12(2), pp. 163–190.

Gupta, G.N. (1994) 'Influence of rain water harvesting and conservation practices on growth and biomass production of *Azadirachta indica* in the Indian desert', *Forest Ecology and Management*, 70(1), pp. 329–339. Available at:  
[https://doi.org/https://doi.org/10.1016/0378-1127\(94\)90098-1](https://doi.org/https://doi.org/10.1016/0378-1127(94)90098-1).

Gupta, K.K., Deelstra, J. and Sharma, K.D. (1997) 'Estimation of water harvesting potential for a semiarid area using GIS and remote sensing', *IAHS Publications-Series of Proceedings and Reports-Intern Assoc Hydrological Sciences*, 242(63), p. 63.

- Gutierrez Caloir, B.E., Abebe, Y.A., Vojinovic, Z., Sanchez, A., Mubeen, A., Ruangpan, L., Manojlovic, N., Plavsic, J. and Djordjevic, S. (2023) ‘Combining machine learning and spatial data processing techniques for allocation of large-scale nature-based solutions’, *Blue-Green Systems*, 5(2), pp. 186–199. Available at: <https://doi.org/10.2166/bgs.2023.040>.
- Gyasi-Agyei, Y., Willgoose, G. and de Troch, F.P. (1995) ‘Effects of Vertical Resolution and Map Scale of Digital Elevation Models on Geomorphological Parameters Used in Hydrology’, *Hydrological processes*, 9(3-4), pp. 363–382.
- Haile, G. and Suryabhagavan, K.V. (2019) ‘GIS-based approach for identification of potential rainwater harvesting sites in Arsi Zone, Central Ethiopia’, *Modeling Earth Systems and Environment*, 5(1), pp. 353–367. Available at: <https://doi.org/10.1007/s40808-018-0537-7>.
- Hameed, H.M. (2013) *Water Harvesting in Erbil Governorate, Kurdistan region, Iraq: Detection of Suitable Sites Using Geographic Information System and Remote Sensing*, Department of Physical Geography and Ecosystems Science. Lund University S- 223 62 Lund Sweden.
- Hebbert, M.H.E. (1935) ‘The Port Sudan water supply’, *Sudan Notes and Records*, 18(1), pp. 89–101. Available at: <https://www.jstor.org/stable/41716097>.
- Helmreich, B. and Horn, H. (2009) ‘Opportunities in rainwater harvesting’, *Desalination*, 248(1–3), pp. 118–124. Available at: <https://doi.org/10.1016/j.desal.2008.05.046>.
- Hirano, A., Welch, R. and Lang, H. (2003) ‘Mapping from ASTER stereo image data: DEM validation and accuracy assessment’, *ISPRS JOURNAL OF PHOTOGRAMMETRY AND REMOTE SENSING*, 57 (Joint Workshop on Challenges in Geospatial Analysis and Visualization), pp. 356–370. Available at: [https://doi.org/10.1016/S0924-2716\(02\)00164-8](https://doi.org/10.1016/S0924-2716(02)00164-8).

- Hirt, C., Filmer, M.S. and Featherstone, W.E. (2010) ‘Comparison and validation of the recent freely available ASTER-GDEM ver1, SRTM ver4.1 and GEODATA DEM-9S ver3 digital elevation models over Australia’, *Australian Journal of Earth Sciences*, pp. 337–347.  
Available at: <https://doi.org/10.1080/08120091003677553>.
- Horton, R.E. (1933) ‘The role of infiltration in the hydrologic cycle’, *Eos, Transactions American Geophysical Union*, 14(1), pp. 446–460.
- Hughes, D.A. and Sami, K. (1992) ‘Transmission losses to alluvium and associated moisture dynamics in a semiarid ephemeral channel system in Southern Africa’, *Hydrological Processes*, 6(1), pp. 45–53. Available at: <https://doi.org/10.1002/hyp.3360060105>.
- Hurni, H. (2008) ‘Review of 15 years WOCAT-Achievements, global issues, synergies and challenges for the future: Sustainable land management in response to global challenges’.  
Available at: [https://boris.unibe.ch/34423/1/WCOATSymposium\\_2008.pdf](https://boris.unibe.ch/34423/1/WCOATSymposium_2008.pdf).
- Ibrahim, G.R.F., Rasul, A., Ali Hamid, A., Ali, Z.F. and Dewana, A.A. (2019) ‘Suitable Site Selection for Rainwater Harvesting and Storage Case Study Using Dohuk Governorate’, *Water*, 11(4), p. 864. Available at: <https://doi.org/10.3390/w11040864>.
- ICARDA (2023) ICARDA - About us. International Center for Agricultural Research in the Dry Areas (ICARDA). Available at: <https://www.icarda.org/about-us> (Accessed: 1 June 2023).
- ICOLD (2011) Constitution of ICOLD, International Commission on Large Dams. ICOLD / CIGB.  
Available at: [http://www.icold-cigb.org/userfiles/files/CIGB/INSTITUTIONAL\\_FILES/Constitution2011.pdf](http://www.icold-cigb.org/userfiles/files/CIGB/INSTITUTIONAL_FILES/Constitution2011.pdf)  
(Accessed: 9 August 2021).

- Ildoromi, A.R., Sepehri, M., Malekinezhad, H., Kiani-Harchegani, M., Ghahramani, A., Hosseini, S.Z. and Artimani, M.M. (2019) 'Application of multi-criteria decision making and GIS for check dam layout in the Ilanlu basin, northwest of Hamadan Province, Iran', *Physics and Chemistry of the Earth, Parts A/B/C*, 114, p. 102803. Available at:  
<https://doi.org/10.1016/j.pce.2019.10.002>.
- Inamdar, P.M., Cook, S., Sharma, A.K., Corby, N., O'Connor, J. and Perera, B.J.C. (2013) 'A GIS based screening tool for locating and ranking of suitable stormwater harvesting sites in urban areas', *Journal of Environmental Management*, 128, pp. 363–370. Available at:  
<https://doi.org/10.1016/j.jenvman.2013.05.023>.
- Info-Prod (Middle East) Ltd. (2005) 'Sudan: Agreement to Create a Water Distribution Truck Line to the City of Port Sudan', IPR Strategic Business Information Database.
- Jaafar, H.H., Ahmad, F.A. and El Beyrouthy, N. (2019) 'GCN250, new global gridded curve numbers for hydrologic modeling and design', *Scientific Data*, 6(1), p. 145. Available at:  
<https://doi.org/10.1038/s41597-019-0155-x>.
- Jabr, W.M. and El-Awar, F.A. (2004) 'GIS and analytic hierarchy process for siting water harvesting reservoirs', Beirut: The Department of Land and Water Resources at the Faculty of Agriculture and Food Sciences of the American University of Beirut-Lebanon.
- Jamali, A.A. and Ghorbani Kalkhajeh, R. (2020) 'Spatial Modeling Considering valley's Shape and Rural Satisfaction in Check Dams Site Selection and Water Harvesting in the Watershed', *Water Resources Management*, 34(10), pp. 3331–3344. Available at:  
<https://doi.org/10.1007/s11269-020-02616-2>.

- Jenson, S.K. and Domingue, J.O. (1988) 'Extracting topographic structure from digital elevation data for geographic information system analysis', *Photogrammetric Engineering and Remote Sensing*, 54(11), pp. 1593–1600.
- Jha, M.K., Chowdary, V.M., Kulkarni, Y. and Mal, B.C. (2014) 'Rainwater harvesting planning using geospatial techniques and multicriteria decision analysis', *Resources, Conservation and Recycling*, 83, pp. 96–111. Available at: <https://doi.org/10.1016/j.resconrec.2013.12.003>.
- Jones, K.R. (1981) *Arid zone hydrology for agricultural development*. Rome, Italy: FAO.
- Jorgensen, S.E. and Fath, B.D. (2008) *Encyclopedia of Ecology*. Amsterdam, The Netherlands: Elsevier BV. Available at: <https://pure.iiasa.ac.at/id/eprint/8658/>.
- Jothiprakash, V. and Sathe, M. V. (2009) 'Evaluation of Rainwater Harvesting Methods and Structures Using Analytical Hierarchy Process for a Large Scale Industrial Area', *Journal of Water Resource and Protection*, 01(06), pp. 427–438. Available at: <https://doi.org/10.4236/jwarp.2009.16052>.
- Kadam, A.K., Kale, S.S., Pande, N.N., Pawar, N.J. and Sankhua, R.N. (2012) 'Identifying Potential Rainwater Harvesting Sites of a Semi-arid, Basaltic Region of Western India, Using SCS-CN Method', *Water Resources Management*, 26(9), pp. 2537–2554. Available at: <https://doi.org/10.1007/s11269-012-0031-3>.
- Kahinda, J.M., Lillie, E.S.B., Taigbenu, A.E., Taute, M. and Boroto, R.J. (2008) 'Developing suitability maps for rainwater harvesting in South Africa', *Physics and Chemistry of the Earth, Parts A/B/C*, 33(8–13), pp. 788–799.

Kar, G., Patra, P.K., Raychaudhuri, M., Anand, P.S.B., Alam, N.M., Panigrahi, S., Sahoo, H. and Chaudhari, S.K. (2021) 'Land Resources Evaluation and Drainage Network Analysis of Watershed for Site Specific Crop Planning Using GIS', *Current Science*, 121(11), p. 1470. Available at: <https://doi.org/10.18520/cs/v121/i11/1470-1479>.

Karimi, H. and Zeinivand, H. (2021) 'Integrating runoff map of a spatially distributed model and thematic layers for identifying potential rainwater harvesting suitability sites using GIS techniques', *Geocarto International*, 36(3), pp. 320–339. Available at: <https://doi.org/10.1080/10106049.2019.1608590>.

Karmakar, M. and Ghosh, D. (2022) 'A GIS-based approach for identification of optimum runoff harvesting sites and storage estimation: a study from Subarnarekha-Kangsabati Interfluve, India', *Applied Geomatics*, 14(2), pp. 253–266. Available at: <https://doi.org/10.1007/s12518-022-00433-3>.

Karnieli, A., Ben-Asher, J., Dodi, A., Issar, A. and Oron, G. (1988) 'An empirical approach for predicting runoff yield under desert conditions', *Agricultural Water Management*, 14(1–4), pp. 243–252. Available at: [https://doi.org/10.1016/0378-3774\(88\)90078-9](https://doi.org/10.1016/0378-3774(88)90078-9).

Keys, R. (1981) 'Cubic convolution interpolation for digital image processing', *IEEE Transactions on Acoustics, Speech, and Signal Processing*, 29(6), pp. 1153–1160. Available at: <https://doi.org/10.1109/TASSP.1981.1163711>.

- Khetkratok, N., Akama, K., Suzuki, K. and Sriboonlue, V. (2010) 'Evaluation of Appropriate Locations and Capacities of On-farm Ponds in Northeast Thailand', *Japan Agricultural Research Quarterly: JARQ*, 44(2), pp. 207–215. Available at: <https://doi.org/10.6090/jarq.44.207>.
- Kibret, S., McCartney, M., Lautze, J., Nhamo, L. and Yan, G. (2021) 'The impact of large and small dams on malaria transmission in four basins in Africa', *Scientific Reports*, 11(1), p. 13355. Available at: <https://doi.org/10.1038/s41598-021-92924-3>.
- Kiggundu, N., Wanyama, J., Mfitumukiza, D., Twinomuhangi, R., Barasa, B., Katimbo, A. and Birungi Kyazze, F. (2018) 'Rainwater harvesting knowledge and practice for agricultural production in a changing climate: A review from Uganda's perspective', *Agricultural Engineering International: CIGR Journal*, 20(2), pp. 19–34.
- Knighton, A.D. and Nanson, G.C. (1994) 'Flow Transmission Along an Arid Zone Anastomosing River, Cooper Creek, Australia', *Hydrological Processes*, 8(2), pp. 137–154. Available at: <https://doi.org/10.1002/hyp.3360080205>.
- Knoben, W.J.M., Freer, J.E. and Woods, R.A. (2019) 'Technical note: Inherent benchmark or not? Comparing Nash-Sutcliffe and Kling-Gupta efficiency scores', *Hydrology and Earth System Sciences*, 23(10), pp. 4323–4331. Available at: <https://doi.org/10.5194/hess-23-4323-2019>.
- Konapala, G., Mishra, A.K., Wada, Y. and Mann, M.E. (2020) 'Climate change will affect global water availability through compounding changes in seasonal precipitation and evaporation', *Nature Communications*, 11(1), p. 3044. Available at: <https://doi.org/10.1038/s41467-020-16757-w>.

- Koohafkan, P. and Stewart, B.A. (2012) 'Water and Cereals in Drylands', pp. 1–110. Available at: <https://doi.org/10.4324/9781849773744>.
- Krois, J. and Schulte, A. (2014) 'GIS-based multi-criteria evaluation to identify potential sites for soil and water conservation techniques in the Ronquillo watershed, northern Peru', *Applied Geography*, 51, pp. 131–142. Available at: <https://doi.org/10.1016/j.apgeog.2014.04.006>.
- Kukko, A., Kaartinen, H. and Hyyppä, J. (2019) 'Technologies for the Future: A Lidar Overview - Building the Capability for High-density 3D Data', Gim International.
- Latifovic, R., Zhu, Z., Cihlar, J., Beaubien, J. and Fraser, R. (2003) 'The Land Cover Map for North America in the Year 2000'. GLC2000 database, European Commission Joint Research Centre. Available at: <http://www-gem.jrc.it/glc2000>.
- Lehner, B. and Grill, G. (2013) 'Global river hydrography and network routing: baseline data and new approaches to study the world's large river systems', *Hydrological processes*. [Chichester, Sussex, England] :, pp. 2171–2186. Available at: <https://doi.org/10.1002/hyp.9740>.
- Lehner, B., Verdin, K. and Jarvkonis, A. (2008) 'New global hydrography derived from spaceborne elevation data', *Eos, Transactions American Geophysical Union*, 89(10), pp. 93–94.
- Li, L., Yang, J.S., Sun, W.Y. and Shen, S.S. (2018) 'Analysis of the typical small watershed of warping dams in the sand properties', *E3S Web of Conferences*. Edited by M. Mostafa, 38, p. 03052. Available at: <https://doi.org/10.1051/e3sconf/20183803052>.

- Li, Z., Zhang, W., Aikebaier, Y., Dong, T., Huang, G., Qu, T. and Zhang, H. (2020) 'Sustainable Development of Arid Rangelands and Managing Rainwater in Gullies, Central Asia', *Water*, 12(9), p. 2533. Available at: <https://doi.org/10.3390/w12092533>.
- Liu, D., Wang, D., Du, G., Yuan, S., Yu, C., Zhao, M., Fang, L., Fu, Y., Zhang, W. and Liu, H. (2022) 'Planning of Water-Saving Green Space System Based on GIS Technology and Archydrodata Model', *Water Resources*, 49(4), pp. 733–742. Available at: <https://doi.org/10.1134/S0097807822040121>.
- Liu, W., Feng, Q., Wang, R. and Chen, W. (2021) 'Effects of initial abstraction ratios in SCS-CN method on runoff prediction of green roofs in a semi-arid region', *Urban forestry & urban greening*, 65, p. 127331. Available at: <https://doi.org/10.1016/j.ufug.2021.127331>.
- Logsdon, G.S. (2008) *Water filtration practices including slow sand filters and precoat filtration*. 1st ed. Denver, Colo.: American Water Works Association.
- López-Ramos, A., Medrano-Barboza, J.P., Martínez-Acosta, L., Acuña, G.J., Remolina López, J.F. and López-Lambrano, A.A. (2022) 'Assessment of Morphometric Parameters as the Basis for Hydrological Inferences in Water Resource Management: A Case Study from the Sinú River Basin in Colombia', *ISPRS International Journal of Geo-Information*, 11(9), p. 459. Available at: <https://doi.org/10.3390/ijgi11090459>.
- M2 Presswire (2016) 'First Great Green Wall Conference'. Available at: <https://link.gale.com/apps/doc/A450601837/ITOF?u=unilanc&sid=bookmark-ITOF&xid=88e05c08> (Accessed: 19 March 2025).

- Mahato, S. and Pal, S. (2019) 'Groundwater Potential Mapping in a Rural River Basin by Union (OR) and Intersection (AND) of Four Multi-criteria Decision-Making Models', *Natural Resources Research*, 28(2), pp. 523–545. Available at: <https://doi.org/10.1007/s11053-018-9404-5>.
- Mahmoud, S.H. (2014) 'Delineation of potential sites for groundwater recharge using a GIS-based decision support system', *ENVIRONMENTAL EARTH SCIENCES*, 72(9), pp. 3429–3442. Available at: <https://doi.org/10.1007/s12665-014-3249-y>.
- Mahmoud, S.H., Mohammad, F.S. and Alazba, A.A. (2014) 'Determination of potential runoff coefficient for Al-Baha Region, Saudi Arabia using GIS', *Arabian Journal of Geosciences*, 7(5), pp. 2041–2057. Available at: <https://doi.org/10.1007/s12517-014-1303-4>.
- Mahmoud, S.H. (2014) 'Investigation of rainfall–runoff modeling for Egypt by using remote sensing and GIS integration', *CATENA*, 120, pp. 111–121. Available at: <https://doi.org/10.1016/j.catena.2014.04.011>.
- Mahmoud, S.H. and Alazba, A.A. (2015) 'The potential of in situ rainwater harvesting in arid regions: developing a methodology to identify suitable areas using GIS-based decision support system', *Arabian Journal of Geosciences*, 8(7), pp. 5167–5179. Available at: <https://doi.org/10.1007/s12517-014-1535-3>.
- Mahmoud, S.H., Adamowski, J., Alazba, A.A. and El-Gindy, A.M. (2016) 'Rainwater harvesting for the management of agricultural droughts in arid and semi-arid regions', *Paddy and Water Environment*, 14(1), pp. 231–246. Available at: <https://doi.org/10.1007/s10333-015-0493-z>.

- Mahmoud, S.H. and Alazba, A.A. (2016) 'Towards a sustainable capital city: an approach for flood management and artificial recharge in naturally water-scarce regions, Central Region of Saudi Arabia', *Arabian Journal of Geosciences*, 9(2), p. 92. Available at: <https://doi.org/10.1007/s12517-015-2021-2>.
- Mahmoud, S.H., Alazba, A.A., Adamowski, J. and El-Gindy, A.M. (2015a) 'GIS methods for sustainable stormwater harvesting and storage using remote sensing for land cover data - location assessment', *Environmental Monitoring and Assessment*, 187(9), p. 598. Available at: <https://doi.org/10.1007/s10661-015-4822-x>.
- Mahmoud, S.H., Mohammad, F.S. and Alazba, A.A. (2015b) 'Delineation of potential sites for rainwater harvesting structures using a geographic information system-based decision support system', *Hydrology Research*, 46(4), pp. 591–606. Available at: <https://doi.org/10.2166/nh.2014.054>.
- Mahmoud, S.H. and Tang, X. (2015) 'Monitoring prospective sites for rainwater harvesting and stormwater management in the United Kingdom using a GIS-based decision support system', *Environmental Earth Sciences*, 73(12), pp. 8621–8638. Available at: <https://doi.org/10.1007/s12665-015-4026-2>.
- Mallick, J., Shivhare, V., Singh, C. and Al Subih, M. (2022) 'Prioritizing Watershed Restoration, Management, and Development Based on Geo-Morphometric Analysis in Asir Region of Saudi Arabia Using Geospatial Technology', *Polish Journal of Environmental Studies*, 31(2), pp. 1201–1222. Available at: <https://doi.org/10.15244/pjoes/142158>.

Mamin, H.N. and Majeed, S.A. (2022) ‘Runoff Estimation and Dam Selection Site in the Khur khur Watershed (KHW), Using (SCS-CN) Method and (GIS & RS) Techniques’, IOP Conference Series: Earth and Environmental Science, 1120(1), p. 012019. Available at: <https://doi.org/10.1088/1755-1315/1120/1/012019>.

Manaouch, M., Sadiki, M. and Fenjiro, I. (2022) ‘Integrating GIS-based FAHP and WaTEM/SEDEM for identifying potential RWH areas in semi-arid areas’, Geocarto International, 37(25), pp. 8882–8905. Available at: <https://doi.org/10.1080/10106049.2021.2007295>.

Masi, M., Arrighi, C., Piragino, F. and Castelli, F. (2024) ‘Participatory multi-criteria decision making for optimal siting of multipurpose artificial reservoirs’, Journal of Environmental Management, 370, p. 122904. Available at: <https://doi.org/10.1016/j.jenvman.2024.122904>.

Mathew, M. (2018) Analytic Hierarchy Process (AHP), YouTube. Available at: <https://youtu.be/J4T70o8gilk?si=4bTMygDP9qNUGbT9> (Accessed: 15 June 2024).

Mati, B., Bock, T De, Bancy Mati, Bock, Tanguy De, Malesu, M., Khaka, E., Oduor, A., Nyabenge, M. and Oduor, V. (2006) Mapping the Potential of Rainwater Harvesting Technologies in Africa: A GIS overview on development domains for the continent and ten selected countries, Technical Manual No. 6. Edited by A.R. Oduor and G. Obanyi. Nairobi, Kenya: World Agroforestry Centre (ICRAF), Netherlands Ministry of Foreign Affairs. Available at: <http://worldagroforestrycentre.net/downloads/publications/PDFs/MN15297.PDF>.

MATLAB, 2020. version 9.8.0 (R2020a), Natick, Massachusetts: The MathWorks Inc.

Maxar (2019) 'QuickBird Datasheet'. Maxar. Available at:

<https://www.digitalglobe.com/products/satellite-imagery>.

Mayaux, P., Bartholom, E., Cabral, A., Cherlet, M., Defourny, P., Gregorio, A. Di, Diallo, O., Massart, M., Nonguierma, A., Pekel, J.-F., Pretorius, C., Vancutsem, C. and Vasconcelos, M. (2003) 'The Land Cover Map for Africa in the Year 2000'. GLC2000 database, European Commission Joint Research Centre.

Mayaux, P. and Bossard., K. (2003) 'The Land Cover Map for Australia in the Year 2000'. GLC2000 database, European Commission Joint Research Centre.

Mbilinyi, B.P., Tumbo, S.D., Mahoo, H.F. and Mkiramwinyi, F.O. (2007) 'GIS-based decision support system for identifying potential sites for rainwater harvesting', *Physics and Chemistry of the Earth*, 32(15), pp. 1074–1081. Available at: <https://doi.org/10.1016/j.pce.2007.07.014>.

McHugh, M.L. (2012) 'Interrater reliability: the kappa statistic', *Biochemia Medica*, 22(3), pp. 276–282. Available at: <https://doi.org/10.11613/BM.2012.031>.

McMahon, T.A. and Nathan, R.J. (2021) 'Baseflow and transmission loss: A review', *WIREs. Water*, 8(4), p. 30. Available at: <https://doi.org/10.1002/wat2.1527>.

Mechlia, N.B., Oweis, T., Masmoudi, M., Khatteli, H., Ouessar, M., Sghaier, N., Anane, M. and Sghaier, M. (2009) *Assessment of Supplemental Irrigation And Water Harvesting Potential: Methodologies and Case Studies From Tunisia*. Aleppo, Syria: International Center for Agricultural Research in the Dry Areas (ICARDA). Available at: <http://www.icarda.org>.

- Mekdaschi-Studer, R. and Liniger, H. (2013) *Water Harvesting: Guidelines to Good Practice*, Water. Centre for Development and Environment (CDE) and Institute of Geography, University of Bern Rainwater Harvesting Implementation Network (RAIN), Amsterdam MetaMeta, Wageningen The International Fund for Agricultural Development (IFAD), Rome.
- Mengen, D., Ottinger, M., Leinenkugel, P. and Ribbe, L. (2020) ‘Modeling River Discharge Using Automated River Width Measurements Derived from Sentinel-1 Time Series’, *Remote Sensing*, 12(19), p. 3236. Available at: <https://doi.org/10.3390/rs12193236>.
- Miller, M. (2011) *Using Google Maps and Google Earth*. 1st edition. Place of publication not identified.
- Mishra, S.K., Pandey, A. and Singh, V.P. (2012) ‘Special Issue on Soil Conservation Service Curve Number (SCS-CN) Methodology’, *Journal of Hydrologic Engineering*, 17(11), pp. 1157–1157. Available at: [https://doi.org/10.1061/\(ASCE\)HE.1943-5584.0000694](https://doi.org/10.1061/(ASCE)HE.1943-5584.0000694).
- Moawad, M.B. (2013) ‘Analysis of the flash flood occurred on 18 January 2010 in wadi El Arish, Egypt (a case study)’, *Geomatics, Natural Hazards and Risk*, 4(3), pp. 254–274. Available at: <https://doi.org/10.1080/19475705.2012.731657>.
- Mohammad, F.S. and Adamowski, J. (2015) ‘Interfacing the geographic information system, remote sensing, and the soil conservation service–curve number method to estimate curve number and runoff volume in the Asir region of Saudi Arabia’, *Arabian Journal of Geosciences*, 8(12), pp. 11093–11105. Available at: <https://doi.org/10.1007/s12517-015-1994-1>.
- Mohammed, H.M.H. (2018) *Topographic Survey of Tawila Dam, North Darfur State, Sudan* [unpublished raw dataset]. Khartoum.

- Moreno-Mateos, D., Mander, Ü. and Pedrocchi, C. (2010) ‘Optimal location of created and restored wetlands in Mediterranean agricultural catchments’, *Water Resources Management*, 24(11), pp. 2485–2499.
- Moriasi, D.N., Arnold, J.G., Van Liew, M.W., Bingner, R.L., Harmel, R.D. and Veith, T.L. (2007) ‘Model evaluation guidelines for systematic quantification of accuracy in watershed simulations’, *Transactions of the ASABE*, 50(3), pp. 885–900. Available at: <https://doi.org/10.13031/2013.23153>.
- Morris, G.L., Annandale, G. and Hotchkiss, R. (2008) ‘Reservoir Sedimentation’, in M. Garcia (ed.) *Sedimentation Engineering: Processes, Measurements, Modeling, and Practice*. Reston, VA: American Society of Civil Engineers, pp. 579–612. Available at: <https://doi.org/10.1061/9780784408148>.
- Mugo, G.M. and Odera, P.A. (2019) ‘Site selection for rainwater harvesting structures in Kiambu County-Kenya’, *The Egyptian Journal of Remote Sensing and Space Science*, 22(2), pp. 155–164. Available at: <https://doi.org/10.1016/j.ejrs.2018.05.003>.
- Mukherjee, I. and Singh, U.K. (2020) ‘Delineation of groundwater potential zones in a drought-prone semi-arid region of east India using GIS and analytical hierarchical process techniques’, *Catena*, 194, p. 104681. Available at: <https://doi.org/10.1016/j.catena.2020.104681>.
- Munyao, J.N. (2010) *Use Of Satellite Products To Assess Water Harvesting Potential In Remote Areas Of Africa: A Case Study Of Unguja Island Zanzibar*. International Institute for Geo-information Science and Earth Observation.

Muralikrishnan, S., Narender, B., Reddy, S. and Pillai, A. (2011) Evaluation of Indian National DEM from Cartosat-1 Data Summary Report (Ver.1). Hyderabad, India. Available at:

[https://bhuvan-app3.nrsc.gov.in/data/download/tools/document/CartoDEMReadme\\_v1\\_u1\\_23082011.pdf](https://bhuvan-app3.nrsc.gov.in/data/download/tools/document/CartoDEMReadme_v1_u1_23082011.pdf).

Murphy, P.N.C., Ogilvie, J., Castonguay, M., Zhang, C., Meng, F.-R. and Arp, P.A. (2008)

‘Improving forest operations planning through high-resolution flow-channel and wet-areas mapping’, *The Forestry Chronicle*, 84(4), pp. 568–574. Available at:

<https://doi.org/10.5558/tfc84568-4>.

Nabit, B.I., Al-Anbari, R.H. and Alwan, I.A. (2023) ‘Identifying Suitability Rainwater Harvesting

Zones in Diyala Watershed, Iraq, Using Multi-Criteria Analysis and GIS Modelling’, *IOP*

*Conference Series: Earth and Environmental Science*, 1158(2), p. 022036. Available at:

<https://doi.org/10.1088/1755-1315/1158/2/022036>.

Nadhim Al-neama, S., Yang, S. and Muneer Yahya, B. (2022) ‘Evaluation of surface run-off

potential of basins in Nineveh governorate, Iraq based on morphometric analysis, using RS and GIS’, *Materials Today: Proceedings*, 60, pp. 1753–1768. Available at:

<https://doi.org/10.1016/j.matpr.2021.12.313>.

Nagarajan, M., Seshadri, S., Vamshi, D.Y. and Madhava Prasad, N.S.S. (2015) ‘Runoff Estimation

and Identification of Water Harvesting Structures for Groundwater Recharge Using Geo-

Spatial Techniques’, *Jordan Journal of Civil Engineering*, 9(4), pp. 455–467. Available at:

<https://doi.org/10.12816/0023866>.

National Aeronautics and Space Administration Goddard Earth Science Data Information and

Services Center (GES DISC) (2017) 'README Document for the Tropical Rainfall

Measurement Mission (TRMM) Version 7'. Goddard Earth Sciences Data and Information

Services Center (GES DISC). Available at:

[https://disc2.gesdisc.eosdis.nasa.gov/data/TRMM\\_L3/TRMM\\_3B43/doc/README.TRMM\\_V7.pdf](https://disc2.gesdisc.eosdis.nasa.gov/data/TRMM_L3/TRMM_3B43/doc/README.TRMM_V7.pdf).

Ndeketeya, A. and Dundu, M. (2021) 'Application of HEC-HMS Model for Evaluation of Rainwater

Harvesting Potential in a Semi-arid City', *Water Resources Management*, 35(12), pp. 4217–

4232. Available at: <https://doi.org/10.1007/s11269-021-02941-0>.

Nicholson, A.R., Wilkinson, M.E., O'Donnell, G.M. and Quinn, P.F. (2012) 'Runoff attenuation

features: a sustainable flood mitigation strategy in the Belford catchment, UK', *Area*, 44(4),

pp. 463–469. Available at: <https://doi.org/10.1111/j.1475-4762.2012.01099.x>.

Nicholson, S.E. (2011) *Dryland Climatology*. Cambridge, United Kingdom: Cambridge University

Press. Available at:

<http://ebookcentral.proquest.com/lib/lancaster/detail.action?docID=807264>.

Niemeijer, D. (1998) 'Soil nutrient harvesting in indigenous Teras water harvesting in eastern

Sudan', *Land Degradation & Development*, 9(4), pp. 323–330. Available at:

[https://doi.org/10.1002/\(SICI\)1099-145X\(199807/08\)9:4<323::AID-LDR295>3.0.CO;2-N](https://doi.org/10.1002/(SICI)1099-145X(199807/08)9:4<323::AID-LDR295>3.0.CO;2-N).

Nissen-Petersen, E. (2006) *Water from Small Dams A handbook for technicians, farmers and others on site investigations, designs, cost estimates, construction and maintenance of small earth dams*. ASAL Consultants Ltd. for the Danish International Development Assistance (Danida) in Kenya. Available at:

[http://www.samsamwater.com/library/Book4\\_Water\\_from\\_Small\\_Dams.pdf](http://www.samsamwater.com/library/Book4_Water_from_Small_Dams.pdf).

Odeh, T., Sawaqed, R., Murshid, E.A. and Mohammad, A.H. (2023) ‘GIS-based analytical analysis for selecting potential runoff harvesting sites: the case study of Amman-Zarqa Basin’, *Sustainable Water Resources Management*, 9(3), p. 97. Available at:

<https://doi.org/10.1007/s40899-023-00879-2>.

Okeola, O.G., Sulaiman, L.T., Sholagberu, T.A. and Salami, W.A. (2023) ‘Spatial Hydrological Analysis on storm water harvesting investigation for sustainable water resources management strategy’, *International Review of Applied Sciences and Engineering*, 14(1), pp. 114–124. Available at: <https://doi.org/10.1556/1848.2022.00464>.

OpenTopography (2008) *OpenTopography High-Resolution Topography Data and Tools*, OpenTopography. Available at: <https://portal.opentopography.org/datasets> (Accessed: 3 September 2019).

Orlandini, S. and Moretti, G. (2009) ‘Determination of surface flow paths from gridded elevation data’, *Water Resources Research*, 45(3). Available at:

<https://doi.org/10.1029/2008WR007099>.

Othman, A.A., Al-Maamar, A.F., Al-Manmi, D.A.M.A., Liesenberg, V., Hasan, S.E., Obaid, A.K. and Al-Quraishi, A.M.F. (2020) ‘GIS-Based Modeling for Selection of Dam Sites in the Kurdistan Region, Iraq’, *ISPRS International Journal of Geo-Information*, 9(4), p. 244.

Available at: <https://doi.org/10.3390/ijgi9040244>.

Ouali, L., Hssaisoune, M., Kabiri, L., Slimani, M.M., El Mouquaddam, K., Namous, M., Arioua, A., Ben Moussa, A., Benqlilou, H. and Bouchaou, L. (2022) ‘Mapping of potential sites for rainwater harvesting structures using GIS and MCDM approaches: case study of the Toudgha watershed, Morocco’, *Euro-Mediterranean Journal for Environmental Integration*, 7(1), pp. 49–64.

Available at: <https://doi.org/10.1007/s41207-022-00294-7>.

Ouessar, M., Bruggeman, A., Abdelli, F., Mohtar, R.H., Gabriels, D. and Cornelis, W.M. (2009) ‘Modelling water-harvesting systems in the arid south of Tunisia using SWAT’, *Hydrology and Earth System Sciences*, 13(10), pp. 2003–2021.

Available at: <https://doi.org/10.5194/hess-13-2003-2009>.

Oweis, T. and Hachum, A. (2006) ‘Water harvesting and supplemental irrigation for improved water productivity of dry farming systems in West Asia and North Africa’, *Agricultural Water Management*, 80(1), pp. 57–73.

Available at: <https://doi.org/10.1016/j.agwat.2005.07.004>.

Oweis, T., Hachum, A. and Kijne, J. (1999) *Water harvesting and supplemental irrigation for improved water use efficiency in dry areas*. Colombo, Sri Lanka: IWMI.

Available at: <https://doi.org/10.3910/2009.372>.

Oweis, T., Prinz, D. and Hachum, A. (2001) *Water Harvesting: Indigenous Knowledge for the Future of the Drier Environments*. Aleppo, Syria: International Center for Agricultural Research in the Dry Areas (ICARDA).

Oweis, T.Y. (2017) ‘Rainwater harvesting for restoring degraded dry agro-pastoral ecosystems: a conceptual review of opportunities and constraints in a changing climate’, *Environmental Reviews*, 25(2), pp. 135–149. Available at: <https://doi.org/10.1139/er-2016-0069>.

Padmavathy, A.S., Ganesha Raj, K., Yogarajan, N., Thangavel, P. and Chandrasekhar, M.G. (1993) ‘Checkdam site selection using GIS approach’, *Advances in Space Research*, 13(11), pp. 123–127. Available at: [https://doi.org/10.1016/0273-1177\(93\)90213-U](https://doi.org/10.1016/0273-1177(93)90213-U).

Panagopoulos, A. (2021) ‘Water-energy nexus: desalination technologies and renewable energy sources’, *Environ Sci Pollut Res Int*, 28(17), pp. 21009–21022. Available at: <https://doi.org/10.1007/s11356-021-13332-8>.

Pandey, A., Himanshu, S.K., Mishra, S.K. and Singh, V.P. (2016) ‘Physically based soil erosion and sediment yield models revisited’, *Catena*, 147, pp. 595–620. Available at: <https://doi.org/https://doi.org/10.1016/j.catena.2016.08.002>.

Papenfus, N. (2003) *Criteria for Siting Dams, Dams For Africa*. Available at: <http://www.damsforafrica.com/investigations-reports-proposals.html> (Accessed: 24 March 2022).

Parimalarenganayaki, S. (2021) ‘Managed Aquifer Recharge in the Gulf Countries: A Review and Selection Criteria’, *Arabian Journal for Science and Engineering*, 46(1). Available at: <https://doi.org/10.1007/s13369-020-05060-x>.

- Park, C. and Allaby, M. (2017) *A Dictionary of Environment and Conservation*. 3rd edn. Oxford University Press. Available at: <https://doi.org/10.1093/acref/9780191826320.001.0001>.
- Parsaie, A., Ememgholizadeh, S., Haghiabi, A.H. and Moradinejad, A. (2018) ‘Investigation of trap efficiency of retention dams’, *Water science & technology. Water supply*, 18(2), pp. 450–459. Available at: <https://doi.org/10.2166/ws.2017.109>.
- Patel, A. and Chaudhari, N. (2023) ‘Enhancing water security through site selection of water harvesting structures in semi-arid regions: a GIS-based multiple criteria decision analysis’, *Water Supply*, 23(10), pp. 4149–4165. Available at: <https://doi.org/10.2166/ws.2023.257>.
- Patel, D.P., Srivastava, P.K., Gupta, M. and Nandhakumar, N. (2015) ‘Decision support system integrated with geographic information system to target restoration actions in watersheds of arid environment: A case study of Hathmati watershed, Sabarkantha District, Gujarat’, *Journal of Earth System Science*. Bangalore, India :, pp. 71–86. Available at: <https://doi.org/10.1007/s12040-014-0515-z>.
- Pathak, S., Ojha, C.S.P., Garg, R.D., Liu, M., Jato-Espino, D. and Singh, R.P. (2020) ‘Spatiotemporal Analysis of Water Resources in the Haridwar Region of Uttarakhand, India’, *Sustainability*, 12(20), p. 8449. Available at: <https://doi.org/10.3390/su12208449>.
- Patil, D. and Gupta, R. (2023) ‘GIS-based multi-criteria decision-making for ranking potential sites for centralized rainwater harvesting’, *Asian Journal of Civil Engineering*, 24(2), pp. 497–506. Available at: <https://doi.org/10.1007/s42107-022-00514-z>.

Pawattana, C. and Tripathi, N.K. (2008) 'Analytical Hierarchical Process (AHP)-Based Flood Water Retention Planning in Thailand', *GIScience & Remote Sensing*, 45(3), pp. 343–355.

Available at: <https://doi.org/10.2747/1548-1603.45.3.343>.

Petheram, C., Gallant, J. and Read, A. (2017) 'An automated and rapid method for identifying dam wall locations and estimating reservoir yield over large areas', *Environmental Modelling & Software*, 92, pp. 189–201. Available at: <https://doi.org/10.1016/j.envsoft.2017.02.016>.

Available at: <https://doi.org/10.1016/j.envsoft.2017.02.016>.

Piemontese, L., Castelli, G., Fetzer, I., Barron, J., Liniger, H., Harari, N., Bresci, E. and Jaramillo, F.

(2020) 'Estimating the global potential of water harvesting from successful case studies',

*Global Environmental Change*, 63, p. 102121. Available at:

<https://doi.org/10.1016/j.gloenvcha.2020.102121>.

Piemontese, L., Castelli, G., Limones, N., Grazio, A. and Bresci, E. (2023) 'Large-scale siting of sand dams: A participatory approach and application in Angolan drylands', *Land degradation & development*, 34(3), pp. 844–858. Available at: <https://doi.org/10.1002/ldr.4500>.

Available at: <https://doi.org/10.1002/ldr.4500>.

Pilgrim, D.H., Chapman, T.G. and Doran, D.G. (1988) 'Problems of rainfall-runoff modelling in arid and semiarid regions', *Hydrological Sciences Journal*, 33(4), pp. 379–400. Available at:

<https://doi.org/10.1080/02626668809491261>.

Pisaniello, J.D., Dam, T.T. and Tingey-Holyoak, J.L. (2015) 'International small dam safety assurance policy benchmarks to avoid dam failure flood disasters in developing countries',

*Journal of Hydrology*, 531, pp. 1141–1153. Available at:

<https://doi.org/10.1016/j.jhydrol.2015.09.077>.

Ponce, V.M. and Hawkins, R.H. (1996) 'Runoff Curve Number: Has It Reached Maturity?', *Journal of Hydrologic Engineering*, 1(1), pp. 11–19. Available at:

[https://doi.org/10.1061/\(ASCE\)1084-0699\(1996\)1:1\(11\)](https://doi.org/10.1061/(ASCE)1084-0699(1996)1:1(11)).

Potapov, P., Li, X., Hernandez-Serna, A., Tyukavina, A., Hansen, M.C., Kommareddy, A., Pickens, A., Turubanova, S., Tang, H., Silva, C.E., Armston, J., Dubayah, R., Blair, J.B. and Hofton, M. (2021) 'Mapping global forest canopy height through integration of GEDI and Landsat data', *Remote Sensing of Environment*, 253, p. 112165. Available at:

<https://doi.org/https://doi.org/10.1016/j.rse.2020.112165>.

Potere, D. (2008) 'Horizontal Positional Accuracy of Google Earth's High-Resolution Imagery Archive', *Sensors*, 8(12), pp. 7973–7981. Available at: <https://doi.org/10.3390/s8127973>.

Prinz, D. and Malik, A.H. (2002) 'Runoff farming', *Institute of Water Resources Management, Hydraulic and Rural Engineering*: Germany.

Purkis, S.J. and Klemas, V. (2011) *Remote sensing and global environmental change*. Chichester, England.

Qin, C., Zhu, A. -X., Pei, T., Li, B., Zhou, C. and Yang, L. (2007) 'An adaptive approach to selecting a flow-partition exponent for a multiple-flow-direction algorithm', *International Journal of Geographical Information Science*, 21(4), pp. 443–458. Available at:

<https://doi.org/10.1080/13658810601073240>.

Quinn, P., Beven, K., Chevallier, P. and Planchon, O. (1991) 'The prediction of hillslope flow paths for distributed hydrological modelling using digital terrain models', *Hydrol. Process*, 5(1), pp. 59–79. Available at: <https://doi.org/10.1002/hyp.3360050106>.

- Radwan, F. and Alazba, A.A. (2022) ‘Suitable sites identification for potential rainwater harvesting (PRWH) using a multi-criteria decision support system (MCDSS)’, *Acta Geophysica*, 71(1), pp. 449–468. Available at: <https://doi.org/10.1007/s11600-022-00895-4>.
- Rai, P.K., Chandel, R.S., Mishra, V.N. and Singh, P. (2018) ‘Hydrological inferences through morphometric analysis of lower Kosi river basin of India for water resource management based on remote sensing data’, *Applied Water Science*, 8(1), p. 15. Available at: <https://doi.org/10.1007/s13201-018-0660-7>.
- Ramadan, E.M, Shahin, H.A., Abd-Elhamid, H.F., Zelenakova, M. and Eldeeb, H.M. (2022) ‘Evaluation and Mitigation of Flash Flood Risks in Arid Regions: A Case Study of Wadi Sudr in Egypt’, *Water*, 14(19), p. 2945. Available at: <https://doi.org/10.3390/w14192945>.
- Ramakrishnan, D., Bandyopadhyay, A. and Kusuma, K.N. (2009) ‘SCS-CN and GIS-based approach for identifying potential water harvesting sites in the Kali Watershed, Mahi River Basin, India’, *Journal of earth system science*, 118, pp. 355–368.
- Ramakrishnan, D., Durga Rao, K.H. V and Tiwari, K.C. (2008) ‘Delineation of potential sites for water harvesting structures through remote sensing and GIS techniques: a case study of Kali watershed, Gujarat, India’, *Geocarto International*, 23(2), pp. 95–108. Available at: <https://doi.org/10.1080/10106040701417246>.
- Ray, S.K. (2023) ‘Identifying the groundwater potential zones in Jamsholaghat sub-basin by considering GIS and multi-criteria decision analysis’, *International Journal of Environmental Science and Technology*, 21(1), pp. 515–540. Available at: <https://doi.org/10.1007/s13762-023-04923-8>.

- Rejani, R., Rao, K.V., Srinivasa Rao, C.H., Osman, M., Sammi Reddy, K., George, B., Pratyusha Kranthi, G.S., Chary, G.R., Swamy, M.V. and Rao, P.J. (2017) 'Identification of Potential Rainwater-Harvesting Sites for the Sustainable Management of a Semi-Arid Watershed', *Irrigation and Drainage*, 66(2), pp. 227–237. Available at: <https://doi.org/10.1002/ird.2101>.
- Reseigh, J. (2021) Controlling Dam Evaporation, Sheep Connect South Australia. Available at: <https://www.sheepconnectsa.com.au/management/water/dams/controlling-dam-evaporation> (Accessed: 2 July 2021).
- Reuter, H.I., Neison, A., Strobl, P., Mehl, W. and Jarvis, A. (2009) 'A first assessment of Aster GDEM tiles for absolute accuracy, relative accuracy and terrain parameters', in 2009 IEEE International Geoscience and Remote Sensing Symposium, pp. V-240-V-243. Available at: <https://doi.org/10.1109/IGARSS.2009.5417688>.
- Rockström, J. and Falkenmark, M. (2015) 'Agriculture: Increase water harvesting in Africa', *Nature*, 519(7543), pp. 283–285. Available at: <https://doi.org/10.1038/519283a>.
- Rosgen, D.L. (1994) 'A classification of natural rivers', *Catena*, 22(3), pp. 169–199. Available at: [https://doi.org/10.1016/0341-8162\(94\)90001-9](https://doi.org/10.1016/0341-8162(94)90001-9).
- Roy, A., Keesari, T., Sinha, U.K. and Sabarathinam, C. (2019) 'Delineating groundwater prospect zones in a region with extreme climatic conditions using GIS and remote sensing techniques: A case study from central India', *Journal of Earth System Science*, 128(8), p. 201. Available at: <https://doi.org/10.1007/s12040-019-1205-7>.

- Saaty, R.W. (1987) 'The analytic hierarchy process - what it is and how it is used', *Mathematical Modelling*, 9(3–5), pp. 161–176. Available at: [https://doi.org/10.1016/0270-0255\(87\)90473-8](https://doi.org/10.1016/0270-0255(87)90473-8).
- Saaty, T.L. (1990) 'How to make a decision: The analytic hierarchy process', *European Journal of Operational Research*, 48(1), pp. 9–26. Available at: [https://doi.org/10.1016/0377-2217\(90\)90057-I](https://doi.org/10.1016/0377-2217(90)90057-I).
- Saaty, T.L. (2008) 'Decision making with the analytic hierarchy process', *Int. J. Services Sciences*, 1(1), pp. 83–98.
- Saaty, T.L. (1994) 'How to make a decision: the analytic hierarchy process', *Interfaces*, 24(6), pp. 19–43.
- Sacolo, S.J. and Mkhanda, S.H. (2021) 'Assessment of the potential of rainwater harvesting for maize production in the Lubombo plateau', *Physics and Chemistry of the Earth, Parts A/B/C*, 124, p. 102935. Available at: <https://doi.org/10.1016/j.pce.2020.102935>.
- Saha, A., Patil, M., Karwariya, S., Pingale, S.M., Azmi, S., Goyal, V.C. and Rathore, D.S. (2018) 'Identification of potential sites for water harvesting structures using geospatial techniques and multi-criteria decision analysis', *The International Archives of the Photogrammetry, Remote Sensing and Spatial Information Sciences*, XLII–5(5), pp. 329–334. Available at: <https://doi.org/10.5194/isprs-archives-XLII-5-329-2018>.
- Sahu, P. and Siddha, S. (2022) 'Development of a novel process to select suitable sites for establishing water harvesting structures in Central Gujarat, India', *Environmental Earth Sciences*, 81(9), p. 265. Available at: <https://doi.org/10.1007/s12665-022-10378-w>.

- Sajikumar, N. and Remya, R.S. (2015) 'Impact of land cover and land use change on runoff characteristics', *Journal of Environmental Management*, 161, pp. 460–468. Available at: <https://doi.org/10.1016/j.jenvman.2014.12.041>.
- Salar, S.G., Othman, A.A. and Hasan, S.E. (2018) 'Identification of suitable sites for groundwater recharge in Awaspi watershed using GIS and remote sensing techniques', *Environmental Earth Sciences*, 77(19), p. 701. Available at: <https://doi.org/10.1007/s12665-018-7887-3>.
- Salem, A.B., M'Nassri, S., Asma, E.A., Bouaziz, R. and Majdoub, R. (2020) 'Evaluation of Meskat System Functionality as Water Harvesting at Wadi Hamdoun Watershed (Sousse, Tunisia) Using the Geographic Information System', *Applied Environmental Research*, 42(1), pp. 58–70. Available at: <https://doi.org/10.35762/AER.2020.42.1.5>.
- Salih, A.A.M. and Hamid, A.A. (2017) 'Hydrological studies in the White Nile State in Sudan', *The Egyptian Journal of Remote Sensing and Space Science*, 20, pp. S31–S38. Available at: <https://doi.org/10.1016/j.ejrs.2016.12.004>.
- Salih, S.A. and Al-Tarif, A.S.M. (2012) 'Using of GIS Spatial Analyses to Study the Selected Location for Dam Reservoir on Wadi Al-Jirnaf, West of Shirqat Area, Iraq', *Journal of Geographic Information System*, 04(02), pp. 117–127. Available at: <https://doi.org/10.4236/jgis.2012.42016>.
- Sampson, E. (2024) 'Dam Collapse Devastates Communities in Eastern Sudan', *The New York Times*, 26 August. Available at: <https://www.nytimes.com/2024/08/26/world/africa/sudan-arbaat-dam-collapse.html>.

- Sayl, K.N., Mohammed, A.S. and Ahmed, A.D. (2020a) ‘GIS-based approach for rainwater harvesting site selection’, IOP Conference Series: Materials Science and Engineering, 737(1), p. 012246. Available at: <https://doi.org/10.1088/1757-899X/737/1/012246>.
- Sayl, K.N., Muhammad, N.S. and El-Shafie, A. (2019) ‘Identification of potential sites for runoff water harvesting’, Proceedings of the Institution of Civil Engineers - Water Management, 172(3), pp. 135–148. Available at: <https://doi.org/10.1680/jwama.16.00109>.
- Sayl, K., Adham, A. and Ritsema, C.J. (2020b) ‘A GIS-Based Multicriteria Analysis in Modeling Optimum Sites for Rainwater Harvesting’, Hydrology, 7(3), p. 51. Available at: <https://doi.org/10.3390/hydrology7030051>.
- Schleiss, A.J., Franca, M.J., Juez, C. and De Cesare, G. (2016) ‘Reservoir sedimentation’, Journal of Hydraulic Research, 54(6), pp. 595–614. Available at: <https://doi.org/10.1080/00221686.2016.1225320>.
- Schmugge, T.J., Kustas, W.P., Ritchie, J.C., Jackson, T.J. and Rango, A. (2002) ‘Remote sensing in hydrology’, Advances in Water Resources, 25(8–12), pp. 1367–1385. Available at: [https://doi.org/10.1016/S0309-1708\(02\)00065-9](https://doi.org/10.1016/S0309-1708(02)00065-9).
- Schneider, A. (2019) ‘GPS Visualizer - Find “Missing” Elevations with GPS Visualizer’, GPS Visualizer. Available at: <https://www.gpsvisualizer.com/elevation> (Accessed: 17 November 2023).
- Schumann, G.J-P. and Bates, P.D. (2018) ‘The Need for a High-Accuracy, Open-Access Global DEM’, Frontiers in Earth Science, 6, p. 225. Available at: <https://doi.org/10.3389/feart.2018.00225>.

- Schwab, G., Frevert, R.K., Edminster, T.W. and Barnes, K.K. (1981) Soil and water conservation engineering. 3d ed. New York: Wiley.
- Sekar, I. and Randhir, T.O. (2007) ‘Spatial assessment of conjunctive water harvesting potential in watershed systems’, *Journal of Hydrology*, 334(1–2), pp. 39–52. Available at: <https://doi.org/10.1016/j.jhydrol.2006.09.024>.
- Şen, Z. (2021) ‘Reservoirs for Water Supply Under Climate Change Impact-A Review’, *Water Resources Management*, 35(11), pp. 3827–3843. Available at: <https://doi.org/10.1007/s11269-021-02925-0>.
- Şen, Z., Al Alsheikh, A., Al-Turbak, A.S., Al-Bassam, A.M. and Al-Dakheel, A.M. (2013) ‘Climate change impact and runoff harvesting in arid regions’, *Arabian Journal of Geosciences*, 6(1), pp. 287–295. Available at: <https://doi.org/10.1007/s12517-011-0354-z>.
- Senay, G.B. and Verdin, J.P. (2004) ‘Developing Index Maps of Water-Harvest Potential in Africa’, *Applied Engineering in Agriculture*, pp. 789–799. Available at: <https://doi.org/10.13031/2013.17725>.
- Setiawan, O. and Nandini, R. (2022) ‘Identification of suitable sites for rainwater harvesting using GIS-based multi-criteria approach in Nusa Penida Island, Bali Province, Indonesia’, *IOP Conference Series: Earth and Environmental Science*, 1039(1), p. 012010. Available at: <https://doi.org/10.1088/1755-1315/1039/1/012010>.
- Shalamzari, J.M., Zhang, W., Gholami, A. and Zhang, Z. (2019) ‘Runoff Harvesting Site Suitability Analysis for Wildlife in Sub-Desert Regions’, *Water*, 11(9), p. 1944. Available at: <https://doi.org/10.3390/w11091944>.

- Shanafield, M., Bourke, S.A., Zimmer, M.A. and Costigan, K.H. (2021) ‘An overview of the hydrology of non-perennial rivers and streams’, *WIREs Water*, 8(2), p. e1504. Available at: <https://doi.org/10.1002/wat2.1504>.
- Shora Consult (2003) Khor Arbaat Development Study and Design Final Report. Khartoum, Sudan.
- Siabi, W.K. (2008) ‘Access to Sanitation and Safe Water: Aeration and its application in groundwater purification’, in 33rd WEDC International Conference, Accra, Ghana, 2008. Ghana: 33rd WEDC International Conference, Accra, Ghana, 2008.
- Silberstein, R.P. (2006) ‘Hydrological models are so good, do we still need data?’, *Environmental Modelling & Software*, 21(9), pp. 1340–1352. Available at: <https://doi.org/https://doi.org/10.1016/j.envsoft.2005.04.019>.
- Silveira, L., Charbonnier, F. and Genta, J.L. (2000) ‘L’humidité antérieure des sols dans la méthode “curve number”’, *Hydrological Sciences Journal*, 45(1), pp. 3–12. Available at: <https://doi.org/10.1080/02626660009492302>.
- Simanton, J.R., Sutter, N.G. and Renard, K.G. (1973) ‘Procedures for identifying parameters affecting storm runoff volumes in a semiarid environment’, *ARS-W; 1*. Available at: <https://www.tucson.ars.ag.gov/unit/publications/PDFfiles/128.pdf>.
- Singhai, A., Das, S., Kadam, A.K., Shukla, J.P., Bundela, D.S. and Kalashetty, M. (2019) ‘GIS-based multi-criteria approach for identification of rainwater harvesting zones in upper Betwa sub-basin of Madhya Pradesh, India’, *Environment, Development and Sustainability*, 21(2), pp. 777–797. Available at: <https://doi.org/10.1007/s10668-017-0060-4>.

Sinohydro Corporation Limited (2010) Sudan Water Harvesting Project - A Summary of Survey in Reservoirs of Red Sea State. Unpublished report.

Sitterson, J., Knightes, C., Parmar, R., Wolfe, K., Muche, M. and Avant, B. (2017) An Overview of Rainfall-Runoff Models Types. EPA/600/R-. Athens, US: U.S. Environmental Protection Agency, Washington, DC. Available at:

[https://cfpub.epa.gov/si/si\\_public\\_file\\_download.cfm?p\\_download\\_id=533906](https://cfpub.epa.gov/si/si_public_file_download.cfm?p_download_id=533906)

Soni, P., Medhi, H., Sagar, A., Garg, P., Singh, A. and Karna, U. (2022) ‘Runoff estimation using digital image processing for residential areas’, Journal of Water Supply: Research and Technology-Aqua, 71(8), pp. 938–948. Available at: <https://doi.org/10.2166/aqua.2022.070>.

Soomro, A.G., Shah, S.A., Memon, A.H., Alharabi, R.S., Memon, D., Panhwar, S. and Keerio, H.A. (2022) ‘Cascade Reservoirs: An Exploration of Spatial Runoff Storage Sites for Water Harvesting and Mitigation of Climate Change Impacts, Using an Integrated Approach of GIS and Hydrological Modeling’, Sustainability, 14(20), p. 13538. Available at:

<https://doi.org/10.3390/su142013538>.

Soulis, K.X. (2021) ‘Soil conservation service curve number (SCS-CN) Method: Current applications, remaining challenges, and future perspectives’, Water. MDPI, p. 192. Available at: <https://www.mdpi.com/2073-4441/13/2/192>.

Sreedevi, P.D., Owais, S., Khan, H.H. and Ahmed, S. (2009) ‘Morphometric analysis of a watershed of South India using SRTM data and GIS’, Journal of the Geological Society of India, 73(4), pp. 543–552. Available at: <https://doi.org/10.1007/s12594-009-0038-4>.

States News Service (2016) ‘African Development Bank to sink US \$20 million in Port Sudan urgent water and sanitation project’, States News Service, 15 December. Available at:

<https://link.gale.com/apps/doc/A474036901/AONE?u=unilanc&sid=bookmark-AONE&xid=8fbb720a>.

Stephens, T. (2010) Manual on small earth dams, A guide to siting, design and construction, FAO drainage and irrigation paper, Number 64. Rome, Italy: Food & Agriculture Organisation of the United Nations.

Strahlendorff, M. (2024) ‘Copernicus 10 arc second DEM and derived Topographic information’, Copernicus. Available at: <https://copernicus.data.lit.fmi.fi/dtm/index.html> (Accessed: 21 February 2024).

Strahler, A.N. (1957) ‘Quantitative analysis of watershed geomorphology’, Eos, Transactions American Geophysical Union. Strahler, 38(6), pp. 913–920. Available at: <https://doi.org/10.1029/TR038i006p00913>.

Strohmeier, S., Fukai, S., Haddad, M., AlNsour, M., Mudabber, M., Akimoto, K., Yamamoto, S., Evett, S. and Oweis, T. (2021) ‘Rehabilitation of degraded rangelands in Jordan: The effects of mechanized micro water harvesting on hill-slope scale soil water and vegetation dynamics’, Journal of Arid Environments, 185, p. 104338. Available at: <https://doi.org/https://doi.org/10.1016/j.jaridenv.2020.104338>.

Sujud, L.H. and Jaafar, H.H. (2022) ‘A global dynamic runoff application and dataset based on the assimilation of GPM, SMAP, and GCN250 curve number datasets’, SCIENTIFIC DATA, 9(1). Available at: <https://doi.org/10.1038/s41597-022-01834-0>.

- Sutradhar, S., Mondal, P. and Das, N. (2021) 'Delineation of groundwater potential zones using MIF and AHP models: A micro-level study on Suri Sadar Sub-Division, Birbhum District, West Bengal, India', *Groundwater for Sustainable Development*, 12, p. 100547. Available at: <https://doi.org/10.1016/j.gsd.2021.100547>.
- Tachikawa, T., Hato, M., Kaku, M. and Iwasaki, A. (2011) 'Characteristics of ASTER GDEM version 2', in *IGARSS. IEEE*, pp. 3657–3660. Available at: <https://doi.org/10.1109/IGARSS.2011.6050017>.
- Tang, Q.H., Gao, H.L., Lu, H. and Lettenmaier, D.P. (2009) 'Remote sensing: hydrology', *Progress in Physical Geography-Earth and Environment*, 33(4), pp. 490–509. Available at: <https://doi.org/10.1177/0309133309346650>.
- Tarboton, D.G. (1997) 'A new method for the determination of flow directions and upslope areas in grid digital elevation models', *Water Resources Research*. Tarboton, 33(2), pp. 309–319. Available at: <https://doi.org/10.1029/96WR03137>.
- Tarboton, D.G., Bras, R.L. and Rodriguez-Iturbe, I. (1991) 'On the extraction of channel networks from digital elevation data', *Hydrological processes*, 5(1), pp. 81–100.
- Tarigan, S.D. (2016) 'Modeling effectiveness of management practices for flood mitigation using GIS spatial analysis functions in Upper Cilliwung watershed', *IOP Conference Series: Earth and Environmental Science*, 31(1), p. 012030. Available at: <https://doi.org/10.1088/1755-1315/31/1/012030>.

Tateishi, R., Zhu, L. and Sato, H.P. (2003) ‘The Land Cover Map for Central Asia for the Year 2000’. GLC2000 database, European Commission Joint Research Centre. Available at:

<http://www-gem.jrc.it/glc2000>.

Tedela, N.H., Rasmussen, T.C. and McCutcheon, S.C. (2007) ‘Effects of seasonal variation on runoff curve number for selected watersheds of Georgia—preliminary study’, in Proc., Georgia Water Resources Conference.

Terêncio, D.P.S., Fernandes, L.F.S., Cortes, R.M. V, Moura, J.P. and Pacheco, F.A.L. (2018) ‘Rainwater harvesting in catchments for agro-forestry uses: A study focused on the balance between sustainability values and storage capacity’, *Science of the Total Environment*, 613, pp. 1079–1092. Available at: <https://doi.org/10.1016/j.scitotenv.2017.09.198>.

Terêncio, D.P.S., Sanches Fernandes, L.F., Cortes, R.M.V. and Pacheco, F.A.L. (2017) ‘Improved framework model to allocate optimal rainwater harvesting sites in small watersheds for agro-forestry uses’, *Journal of Hydrology*, 550, pp. 318–330. Available at:

<https://doi.org/10.1016/j.jhydrol.2017.05.003>.

Teschemacher, S., Bittner, D. and Disse, M. (2020) ‘Automated Location Detection of Retention and Detention Basins for Water Management’, *Water*, 12(5), p. 1491. Available at:

<https://doi.org/10.3390/w12051491>.

The European Space Agency (2023) Sentinel Online, Sentinel-2 MSI, Overview, The European Space Agency. Available at: <https://sentinel.esa.int/web/sentinel/user-guides/sentinel-2-msi/overview> (Accessed: 27 July 2023).

- Thomas, D.S.G. (2011) *Arid zone geomorphology: process, form, and change in drylands*. 3rd ed. Oxford: Wiley-Blackwell.
- Thornton, P., Dijkman, J., Herrero, M., Szilagyi, L. and Cramer, L. (2022) ‘Aligning vision and reality in publicly funded agricultural research for development: A case study of CGIAR’, *Food Policy*, 107, p. 102196.
- Tiwari, A., Silver, M. and Karnieli, A. (2023) ‘A deep learning approach for automatic identification of ancient agricultural water harvesting systems’, *International Journal of Applied Earth Observation and Geoinformation*, 118, p. 103270. Available at: <https://doi.org/10.1016/j.jag.2023.103270>.
- Toledo, C.E., Nogueira, J.C.M. and Camargo, A. de A. (2020) ‘Evaluation of water loss in transit and surface runoff in a Brazilian semi-arid basin’, *Rev. Ambient. Água*, 15(4), pp. 1–12. Available at: <https://doi.org/10.4136/ambi-agua.2545>.
- Traboulsi, H. and Traboulsi, M. (2017) ‘Rooftop level rainwater harvesting system’, *Applied Water Science*, 7(2), pp. 769–775. Available at: <https://doi.org/10.1007/s13201-015-0289-8>.
- Tsiko, R.G. and Haile, T.S. (2011) ‘Integrating geographical information systems, fuzzy logic and analytical hierarchy process in modelling optimum sites for locating water reservoirs. A case study of the debub district in eritrea’, *Water (Switzerland)*, 3(1), pp. 254–290. Available at: <https://doi.org/10.3390/w3010254>.
- Tuinhof, A., Van Steenberghe, F., Vos, P. and Tolck, L. (2012) *Profit from Storage. The costs and benefits of water buffering*. Edited by 3R Water Secretariat. Wageningen, The Netherlands.

Tumbo, S.D., Mbilinyi, B.P., Mahoo, H.F. and Mkilamwinyi, F.O. (2014) ‘Identification of Suitable Indices for Identification of Potential Sites for Rainwater Harvesting’, *Tanzania Journal of Agricultural Sciences*, 12(2), pp. 35–46.

U.S. Geological Survey (USGS) (2015) ‘Landsat—Earth observation satellites (ver. 1.4, August 2022): U.S. Geological Survey Fact Sheet 2015–3081’, Fact Sheet. Version 1. Reston, VA, p. 4. Available at: <https://doi.org/https://doi.org/10.3133/fs20153081>.

U.S. Geological Survey (USGS) (2016) ‘PART: A computerized method of base-flow-record estimation’. U.S. Geological Survey (USGS). Available at: <https://water.usgs.gov/software/lists/groundwater>.

Umugwaneza, A., Chen, X., Liu, T., Mind’je, R., Uwineza, A., Kayumba, P.M., Uwamahoro, S., Umuhoza, J., Gasirabo, A. and Maniraho, A.P. (2022) ‘Integrating a GIS-based approach and a SWAT model to identify potential suitable sites for rainwater harvesting in Rwanda’, *Journal of Water Supply: Research and Technology-Aqua*, 71(3), pp. 415–432. Available at: <https://doi.org/10.2166/aqua.2022.111>.

UNEP (1997) ‘World Atlas of Desertification: Second Edition’. Available at: <https://wedocs.unep.org/20.500.11822/30300>.

United Nations (2020) Global indicator framework for the Sustainable Development Goals and targets of the 2030 Agenda for Sustainable Development. United Nations (UN).

United States Department of Agriculture (USDA) (1987) *Design of Small Dams*. Rev. reprint. Washington: United States Department of the Interior.

- United States Department of Agriculture (USDA) (1997) Ponds — Planning, Design, Construction, Agriculture Handbook Number 590. US Department of Agriculture. Available at: <https://nrcspad.sc.egov.usda.gov/distributioncenter/pdf.aspx?productID=115>.
- Van Dijk, J.A. and Ahmed, M.H. (1993) Opportunities for expanding water harvesting in Sub-Saharan Africa: the case of the Teras of Kassala, Opportunities for Expanding Water Harvesting in Sub-Saharan Africa. International Institute for Environment and Development. Available at: <http://www.jstor.org/stable/resrep01678>.
- Vanmaercke, M., Poesen, J., Broeckx, J. and Nyssen, J. (2014) ‘Sediment yield in Africa’, Earth-Science Reviews, 136, pp. 350–368. Available at: <https://doi.org/10.1016/j.earscirev.2014.06.004>.
- Vanoni, V.A., Sedimentation, A.S. of C.E.T.C. for the P. of the M. on and (U.S.), E. and W.R.I. (2006) Sedimentation engineering. 2nd ed. Reston, VA: American Society of Civil Engineers.
- Vázquez, R.B.I., Salcedo Sánchez, E.R., Esquivel Martínez, J.M., Gómez Albores, M.Á., Gómez Noguez, F., Gutiérrez Flores, C. and Talavera Mendoza, O. (2023) ‘Use of Analytic Hierarchy Process Method to Identify Potential Rainwater Harvesting Sites: Design and Financial Strategies in Taxco de Alarcón, Southern Mexico’, Sustainability, 15(10), p. 8220. Available at: <https://doi.org/10.3390/su15108220>.
- Vema, V., Sudheer, K.P. and Chaubey, I. (2019) ‘Fuzzy inference system for site suitability evaluation of water harvesting structures in rainfed regions’, Agricultural Water Management, 218, pp. 82–93. Available at: <https://doi.org/10.1016/j.agwat.2019.03.028>.

- Vogel, R.M., Sieber, J., Archfield, S.A., Smith, M.P., Apse, C.D. and Huber-Lee, A. (2007) 'Relations among storage, yield, and instream flow', *Water Resources Research*, 43(5), pp. W05403-n/a. Available at: <https://doi.org/10.1029/2006WR005226>.
- Waghaye, A.M., Singh, D.K., Sarangi, A., Sena, D.R., Sahoo, R.N. and Sarkar, S.K. (2023) 'Identification of suitable zones and sites for rainwater harvesting using GIS and multicriteria decision analysis', *Environmental Monitoring and Assessment*, 195(2), p. 279. Available at: <https://doi.org/10.1007/s10661-022-10801-6>.
- Walsh, S.J., Page, P.H., McKnight, S.A., Yao, X. and Morrissey, T.P. (2015) 'A reservoir siting tool for North Carolina: System design & operations for screening and evaluation', *Applied Geography*, 60, pp. 139–149. Available at: <https://doi.org/10.1016/j.apgeog.2015.03.015>.
- Wang, L., Jiao, W., MacBean, N., Rulli, M.C., Manzoni, S., Vico, G. and D'Odorico, P. (2022a) 'Dryland productivity under a changing climate', *Nature Climate Change*, 12(11), pp. 981–994. Available at: <https://doi.org/10.1038/s41558-022-01499-y>.
- Wang, Q., Zhang, E., Li, Fengmin and Li, Fengrui (2008) 'Runoff efficiency and the technique of micro-water harvesting with ridges and furrows, for potato production in semi-arid areas', *Water Resources Management*, 22(10), pp. 1431–1443. Available at: <https://doi.org/10.1007/s11269-007-9235-3>.
- Wang, W., Straffelini, E. and Tarolli, P. (2023) 'Steep-slope viticulture: The effectiveness of micro-water storage in improving the resilience to weather extremes', *Agricultural Water Management*, 286, p. 108398. Available at: <https://doi.org/10.1016/j.agwat.2023.108398>.

- Wang, Y., Tian, Y. and Cao, Y. (2021) ‘Dam siting: A review’, *Water (Switzerland)*, 13(15), p. 2080. Available at: <https://doi.org/10.3390/w13152080>.
- Wang, Z., Li, J., Lin, Y., Meng, Y. and Liu, J. (2022b) ‘GrabRiver: Graph-Theory-Based River Width Extraction From Remote Sensing Imagery’, *IEEE Geoscience and Remote Sensing Letters*, 19, pp. 1–5. Available at: <https://doi.org/10.1109/LGRS.2020.3023043>.
- Ward, M., Poleacovschi, C. and Perez, M. (2021) ‘Using AHP and Spatial Analysis to Determine Water Surface Storage Suitability in Cambodia’, *Water*, 13(3), p. 367. Available at: <https://doi.org/10.3390/w13030367>.
- Weerasinghe, H., Schneider, U.A. and Löw, A. (2011) ‘Water harvest- and storage- location assessment model using GIS and remote sensing’, *Hydrology and Earth System Sciences Discussions*, 8(2), pp. 3353–3381. Available at: <https://doi.org/10.5194/hessd-8-3353-2011>.
- Weiss, A.D. (2001) *Topographic Position and Landforms Analysis*, The Nature Conservancy. Available at: [https://www.jennessent.com/downloads/TPI-poster-TNC\\_18x22.pdf](https://www.jennessent.com/downloads/TPI-poster-TNC_18x22.pdf) (Accessed: 31 August 2024).
- Wimmer, M.H., Pfeifer, N. and Hollaus, M. (2019) ‘Automatic detection of potential dam locations in digital terrain models’, *ISPRS International Journal of Geo-Information*, 8(4), p. 197. Available at: <https://doi.org/10.3390/ijgi8040197>.
- WMO (1990) ‘Glossary of terms used in agrometeorology. CAGM No. 40. WMO/TD-No. 391.’ Geneva: World Meteorological Organization. Available at: [https://library.wmo.int/doc\\_num.php?explnum\\_id=9537](https://library.wmo.int/doc_num.php?explnum_id=9537).

WordCloud.com (no date). Available at: <https://classic.wordclouds.com/about/> (Accessed: 22 August 2024).

Yang, D., Herath, S. and Musiak, K. (2001) 'Spatial resolution sensitivity of catchment geomorphologic properties and the effect on hydrological simulation', *Hydrol. Process*, 15(11), pp. 2085–2099. Available at: <https://doi.org/10.1002/hyp.280>.

Yan, L., Li, H., Hao, X., Wang, J., Yin, Z. and Liu, J. (2025) 'Generation and Assessment of Digital Elevation Models by Combining Sentinel-1A and Sentinel-1B Data in Mountain Glacier Area', *IEEE Journal of Selected Topics in Applied Earth Observations and Remote Sensing*, 18, pp. 642–654. Available at: <https://doi.org/10.1109/JSTARS.2024.3489576>.

Yang, X., Pavelsky, T.M., Allen, G.H. and Donchyts, G. (2020) 'RivWidthCloud: An Automated Google Earth Engine Algorithm for River Width Extraction from Remotely Sensed Imagery', *IEEE Geoscience and Remote Sensing Letters*, 17(2), pp. 217–221. Available at: <https://doi.org/10.1109/LGRS.2019.2920225>.

Yapo, P.O., Gupta, H.V. and Sorooshian, S. (1996) 'Automatic calibration of conceptual rainfall-runoff models: sensitivity to calibration data', *Journal of Hydrology*, 181(1), pp. 23–48. Available at: [https://doi.org/https://doi.org/10.1016/0022-1694\(95\)02918-4](https://doi.org/https://doi.org/10.1016/0022-1694(95)02918-4).

Yeomans, P.A. (1954) *The Keyline Plan*. Sydney, Australia: P.A. Yeomans.

Yeomans, P.A. (2008) *Water for Every Farm: Yeomans Keyline Plan*. Edited by K.B. Yeomans. Available at: <https://a.co/d/ivG50JD>.

Yousif, M. and Sracek, O. (2016) 'Integration of geological investigations with multi-GIS data layers for water resources assessment in arid regions: El Ambagi Basin, Eastern Desert, Egypt', *Environmental Earth Sciences*, 75(8), p. 684. Available at: <https://doi.org/10.1007/s12665-016-5456-1>.

Yousif, M. and Bubenzer, O. (2015) 'Geoinformatics application for assessing the potential of rainwater harvesting in arid regions. Case study: El Daba'a area, Northwestern Coast of Egypt', *Arabian Journal of Geosciences*, 8(11), pp. 9169–9191. Available at: <https://doi.org/10.1007/s12517-015-1837-0>.

Zaidi, F.K., Nazzal, Y., Ahmed, I., Naeem, M. and Jafri, M.K. (2015) 'Identification of potential artificial groundwater recharge zones in Northwestern Saudi Arabia using GIS and Boolean logic', *Journal of African Earth Sciences*, 111, pp. 156–169. Available at: <https://doi.org/10.1016/j.jafrearsci.2015.07.008>.

Ziadat, F.M., Mazahreh, S.S., Oweis, T.Y. and Bruggeman, A. (2006) 'A GIS-based Approach for Assessing Water Harvesting Suitability in a Badia Benchmark Watershed in Jordan', in 14th International Soil Conservation Organization Conference. Marrakech, Morocco.

Ziadat, F., Bruggeman, A., Oweis, T., Haddad, N., Mazahreh, S., Sartawi, W. and Syuof, M. (2012) 'A Participatory GIS Approach for Assessing Land Suitability for Rainwater Harvesting in an Arid Rangeland Environment', *Arid Land Research and Management*, 26(4), pp. 297–311. Available at: <https://doi.org/10.1080/15324982.2012.709214>.

Ziese, Markus; Rauthe-Schöch, Armin; Becker, Andreas; Finger, Peter; Rustemeier, Elke; Hänsel, Stephanie; Schneider, U. (2022) ‘GPPC Full Data Daily Version 2022 at 1.0°’. Available at: [https://doi.org/10.5676/DWD\\_GPCC/FD\\_D\\_V2022\\_100](https://doi.org/10.5676/DWD_GPCC/FD_D_V2022_100).

Zomer, R.J. and Trabucco, A. (2022) ‘Version 3 of the “Global Aridity Index and Potential Evapotranspiration (ET<sub>0</sub>) Database”’: Estimation of Penman-Monteith Reference Evapotranspiration. (In Press).’, CGIAR Consort Spat Inf. Available at: <https://doi.org/10.6084/m9.figshare.7504448.v4>.

Zumrawi, M. (2015) ‘Failure Investigation of Tawila Dam in North Darfur, Sudan’, International Journal of Science and Research (IJSR), 438(5), pp. 963–967.

# Appendix A. Supplementary material for Chapter 3

**Table A1. Review literature digital object identifiers (DOIs).**

ref.	DOI	ref.	DOI
1	10.3390/su15043337	151	10.15244/pjoes/142158
2	10.3390/su14137871	152	10.1088/1755-1315/1120/1/012019
3	10.3390/su14105754	153	10.1080/10106049.2021.2007295
4	10.1007/s11269-022-03416-6	154	10.1007/s12517-014-1404-0
5	10.3390/w15203592	155	10.1007/s40710-020-00434-7
6	10.1007/s12517-021-07178-0	156	10.1016/j.pce.2007.07.014
7	10.3390/hydrology10090183	157	10.1016/j.pce.2005.08.022
8	10.1007/s12517-017-3329-x	158	10.1007/s12517-021-08549-3
9	10.1016/j.rsase.2022.100899	159	10.17159/wsa/2023.v49.i1.3943
10	10.3390/w14132110	160	10.1080/19475705.2012.731657
11	10.3390/w8050198	161	10.1007/s12517-015-1994-1
12	10.1016/j.iswcr.2018.07.003	162	10.2166/hydro.2023.020
13	10.1007/s11269-013-0310-7	163	10.1016/j.cosust.2023.101336
14	10.21163/GT_2021.163.09	164	10.1007/s00704-023-04391-7
15	10.3390/w12071913	165	10.1016/j.ejrs.2018.05.003
16	10.1016/j.crsust.2023.100230	166	10.1016/j.catena.2020.104681
17	10.1016/j.gsd.2020.100388	167	10.5558/tfc83198-2
18	10.3923/jas.2007.2911.2917	168	10.5558/tfc84568-4
19	10.1007/s10040-018-1764-8	169	10.3390/su142114183
20	10.3390/w15234093	170	10.3390/hydrology7020028
21	10.1007/s40899-020-00416-5	171	10.1007/s11269-010-9641-9
22	10.1007/s13369-017-2487-1	172	10.1016/j.pce.2008.06.047
23	10.1142/S1464333208003020	173	10.1016/j.pce.2009.06.011
24	10.1016/j.jaridenv.2010.07.001	174	10.1088/1755-1315/1158/2/022036
25	10.1007/s40899-022-00652-x	175	10.1016/j.matpr.2021.12.313
26	10.1007/s13201-022-01756-7	176	10.1016/j.agwat.2014.04.012
27	10.3390/w13050704	177	10.1007/s11269-021-02941-0
28	10.3390/w12071924	178	10.1007/s40003-019-00430-w
29	10.1007/s00477-023-02611-0	179	10.1016/S0378-3774(02)00047-1
30	10.3390/w14071039	180	10.18280/ijstdp.150214
31	10.48129/kjs.11917	181	10.1007/s40899-023-00879-2
32	10.3390/ijgi12080312	182	10.4314/njtd.v16i2.3
33	10.1007/s11270-022-05796-2	183	10.1556/1848.2022.00464
34	10.1007/s12517-020-06154-4	184	10.1016/j.rsase.2018.10.006
35	10.1080/23570008.2022.2129150	185	10.3390/ijgi9040244
36	10.1016/j.heliyon.2023.e19795	186	10.1007/s41207-022-00294-7
37	10.1007/s12517-011-0306-7	187	10.1007/s40808-023-01720-7
38	10.52939/ijg.v19i3.2601	188	10.5194/hess-13-2003-2009
39	10.3390/su142114033	189	10.1016/0273-1177(93)90213-U

## Appendix A

40	10.1007/s11053-021-09835-3	190	10.1007/s10457-023-00863-x
41	10.13005/bbra/2276	191	10.1007/s13201-015-0298-7
42	10.3390/ijgi9040235	192	10.1080/15715124.2018.1505737
43	10.1007/s11356-020-09019-1	193	10.1007/s12594-022-2101-3
44	10.2166/wcc.2023.215	194	10.3390/su15129230
45	10.1007/s12524-020-01278-2	195	10.2166/ws.2023.257
46	10.3390/w10040495	196	10.1007/s12524-011-0147-6
47	10.3390/w15030507	197	10.1007/s12665-012-2086-0
48	10.1007/s12517-013-0941-2	198	10.1007/s12040-014-0515-z
49	10.1007/s12517-017-3312-6	199	10.1016/j.jenvman.2019.04.082
50	10.1080/10106049.2019.1608591	200	10.3390/su12208449
51	10.5194/isprs-annals-X-3-W1-2022-1-2022	201	10.3390/w9090710
52	10.1007/s12517-015-1870-z	202	10.1007/s42107-022-00514-z
53	10.1016/j.matpr.2023.04.182	203	10.1007/s11356-022-23039-z
54	10.1007/s10661-019-7697-4	204	10.26833/ijeg.1115608
55	10.1016/j.jhydrol.2023.129655	205	10.2747/1548-1603.45.3.343
56	10.1007/s40333-015-0059-3	206	10.3390/rs6098134
57	10.1007/s40899-018-0244-6	207	10.5194/isprsarchives-XL-8-1471-2014
58	10.1007/s12524-009-0049-z	208	10.1088/1755-1315/1032/1/012010
59	10.1016/j.jaridenv.2019.02.010	209	10.3390/w14213480
60	10.11113/jt.v76.5955	210	10.1007/s12517-018-4067-4
61	10.3390/w15071361	211	10.1007/s11600-018-0233-z
62	10.1080/24749508.2023.2209978	212	10.1007/s11600-022-00895-4
63	10.3390/w15183207	213	10.3390/su14073969
64	10.1016/j.pce.2007.07.009	214	10.1007/s13201-018-0660-7
65	10.1080/10106049.2023.2236582	215	10.3390/w14192945
66	10.1007/s11600-022-00910-8	216	10.1007/s12040-009-0034-5
67	10.1016/j.agwat.2022.107836	217	10.1080/10106040701417246
68	10.1007/s11269-011-9882-2	218	10.1007/s12594-019-1291-9
69	10.1155/2016/5935430	219	10.14419/ijet.v7i3.31.18208
70	10.1080/10106049.2022.2066205	220	10.1007/s12517-017-3288-2
71	10.3390/w13141935	221	10.3390/w15112042
72	10.1080/10106040308542288	222	10.1007/s13762-023-04923-8
73	10.1088/1755-1315/824/1/012029	223	10.1007/s10661-015-4772-3
74	10.1515/geo-2020-0313	224	10.1002/ird.2101
75	10.1016/j.eti.2021.101522	225	10.3390/w14223623
76	10.3390/w15061118	226	10.1002/ldr.4838
77	10.1007/s12665-016-5692-4	227	10.1080/10106049.2012.665499
78	10.3390/w13060804	228	10.1007/s12040-019-1205-7
79	10.1007/s12665-021-09881-3	229	10.1016/j.pce.2020.102935
80	10.1016/j.jenvman.2022.114990	230	10.46717/igj.55.1B.6Ms-2022-02-22
81	10.17159/wsa/2021.v47.i3.11863	231	10.5194/isprs-archives-XLII-5-329-2018
82	10.46754/jssm.2021.10.017	232	10.1007/s12665-022-10378-w
83	10.24996/ijis.2022.63.12.20	233	10.1007/s12517-018-3870-2
84	10.1007/s11269-022-03185-2	234	10.1016/j.jenvman.2014.12.041
85	10.1111/jfr3.12720	235	10.1007/s12665-018-7887-3

## Appendix A

86	10.1016/j.pce.2007.04.014	236	10.35762/AER.2020.42.1.5
87	10.2166/nh.2022.027	237	10.1016/j.ejrs.2016.12.004
88	10.1016/j.catena.2018.05.004	238	10.3390/su15065339
89	10.1080/10106049.2022.2091158	239	10.1088/1757-899X/737/1/012246
90	10.1016/j.jag.2010.09.001	240	10.1007/s12665-017-6699-1
91	10.1007/s11356-023-26289-7	241	10.1007/s12517-017-3193-8
92	10.1007/s10040-018-1845-8	242	10.1007/s11269-016-1350-6
93	10.1007/s10661-021-09468-2	243	10.1155/2021/5580286
94	10.1007/s12524-011-0176-1	244	10.3390/hydrology7030051
95	10.1016/j.agwat.2016.04.018	245	10.3390/w14213448
96	10.3390/w15223904	246	10.1016/j.ejrs.2012.07.001
97	10.2166/bgs.2023.040	247	10.1088/1755-1315/1039/1/012010
98	10.1007/s40808-018-0537-7	248	10.5194/hess-23-1581-2019
99	10.1080/23754931.2022.2051196	249	10.3390/w12020380
100	10.1504/IJENVH.2007.018582	250	10.1016/j.jhydrol.2019.124501
101	10.1007/s40899-022-00713-1	251	10.1007/s12518-021-00410-2
102	10.1007/s12518-020-00342-3	252	10.3390/w11091944
103	10.1080/24749508.2020.1846841	253	10.1007/s12665-018-7591-3
104	10.1177/11786221231160906	254	10.1007/s12524-009-0009-7
105	10.3390/w11040864	255	10.1016/j.jclepro.2016.11.163
106	10.1016/j.pce.2019.10.002	256	10.1007/s10668-017-0060-4
107	10.1016/j.jenvman.2013.05.023	257	10.2166/aqua.2022.070
108	10.1016/j.jhydrol.2018.04.066	258	10.3390/su142013538
109	10.1080/10106049.2016.1213889	259	10.1007/s12594-009-0038-4
110	10.1007/s11269-020-02616-2	260	10.1007/s12665-012-2172-3
111	10.1007/s11269-009-9422-5	261	10.1016/j.catena.2022.106085
112	10.1016/j.resconrec.2013.12.003	262	10.1371/journal.pone.0286061
113	10.3390/w10010064	263	10.1016/j.gsd.2021.100547
114	10.1007/s11269-012-0031-3	264	10.1007/s40899-021-00491-2
115	10.1007/s41748-020-00178-2	265	10.1080/09715010.2019.1660919
116	10.1007/s12665-015-4384-9	266	10.1111/j.1475-2743.2006.00066.x
117	10.1016/j.dib.2018.07.016	267	10.1016/j.sciaf.2023.e01620
118	10.18520/cs/v121/i11/1470-1479	268	10.3390/w15122258
119	10.1080/10106049.2019.1608590	269	10.1016/j.jhydrol.2017.05.003
120	10.1007/s12518-022-00433-3	270	10.2478/geosc-2023-0005
121	10.3390/rs14195008	271	10.1016/j.jag.2023.103270
122	10.6090/jarq.44.207	272	10.1007/s11269-018-1905-9
123	10.1088/1757-899X/881/1/012170	273	10.1007/s13201-016-0390-7
124	10.1515/REVEH.2011.036	274	10.2166/aqua.2022.111
125	10.1080/13658816.2016.1206202	275	10.1016/j.jas.2013.08.011
126	10.1007/s12517-021-06721-3	276	10.1007/s13201-018-0830-7
127	10.1080/02626667.2011.588604	277	10.3390/su15108220
128	10.2166/wst.2015.303	278	10.1007/s10661-022-10801-6
129	10.1007/s12665-016-5462-3	279	10.1016/j.agwat.2023.108398
130	10.1080/10106049.2016.1213772	280	10.1016/j.agwat.2004.07.002
131	10.1007/s12594-021-1794-z	281	10.1016/j.jaridenv.2016.08.010

## Appendix A

132	10.5558/tfc84338-3	282	10.1007/s11269-018-2050-1
133	10.3390/w12092533	283	10.1080/10106049.2013.868043
134	10.1134/S0097807822040121	284	10.1007/s12524-022-01528-5
135	10.3390/ijgi11090459	285	10.1016/j.sciaf.2022.e01322
136	10.1016/j.jher.2014.07.004	286	10.1007/s12517-011-0433-1
137	10.1007/s12145-012-0101-3	287	10.1007/s12517-015-1837-0
138	10.1007/s11053-018-9404-5	288	10.1007/s12665-016-5456-1
139	10.1007/s11600-020-00460-x	289	10.1016/j.agee.2020.107022
140	10.1007/s12517-014-1303-4	290	10.1080/15324982.2012.709214
141	10.1016/j.catena.2014.04.011		
142	10.1007/s12517-014-1535-3		
143	10.1007/s10333-015-0493-z		
144	10.1007/s12517-015-1927-z		
145	10.1007/s12517-015-2021-2		
146	10.1007/s12517-016-2439-1		
147	10.1007/s10661-015-4822-x		
148	10.2166/nh.2014.054		
149	10.1007/s12665-015-4026-2		
150	10.1007/s12517-020-5076-7		

---

# Appendix B. Supplementary material for Chapter 4

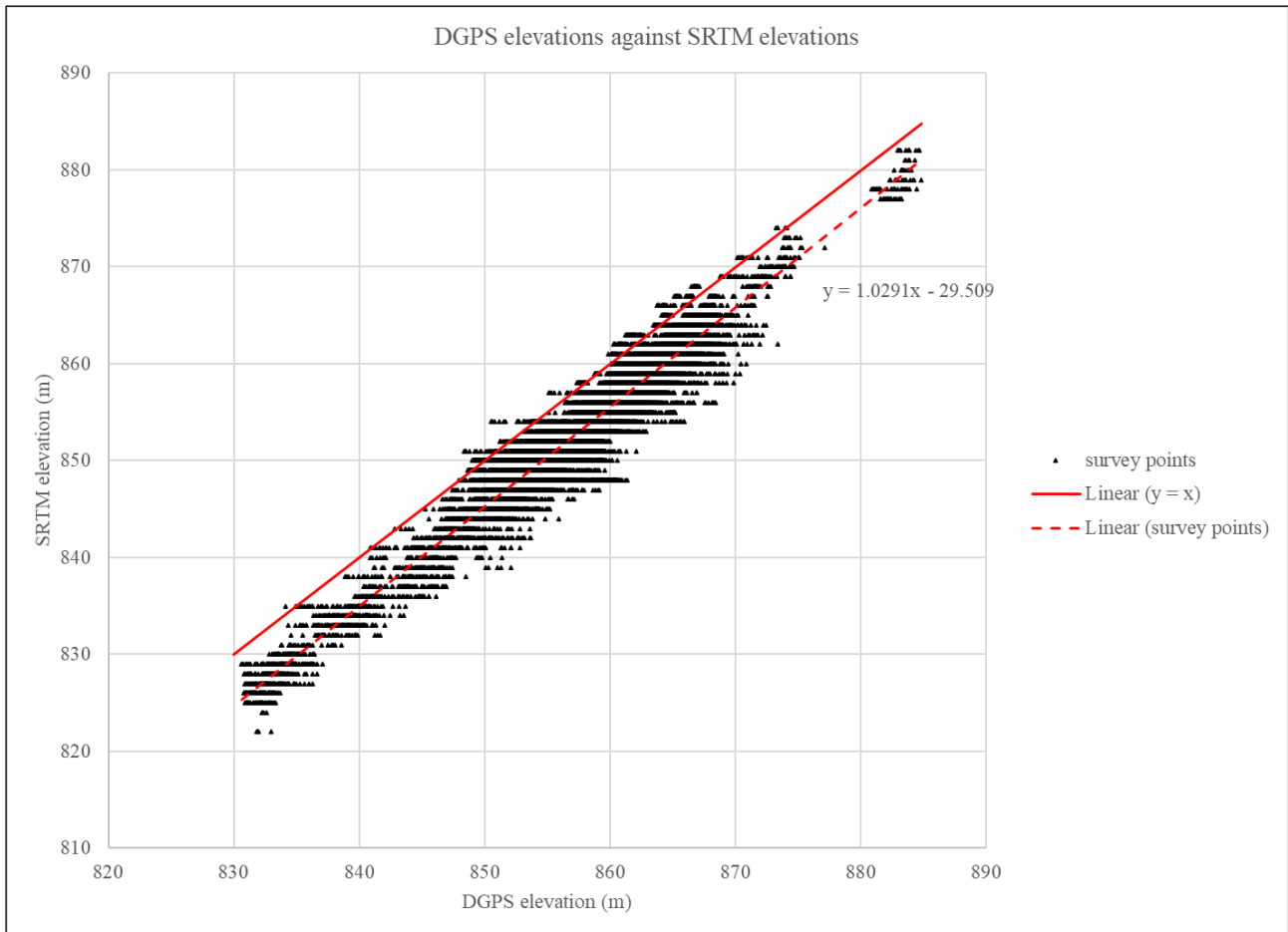


**Figure B1. Validation of the geometrical process: chart of differential Global Positioning System (dGPS) survey elevation points against Shuttle Radar Topography Mission (SRTM) elevation together with regression formula used to adjust dGPS survey data.**

Appendix B

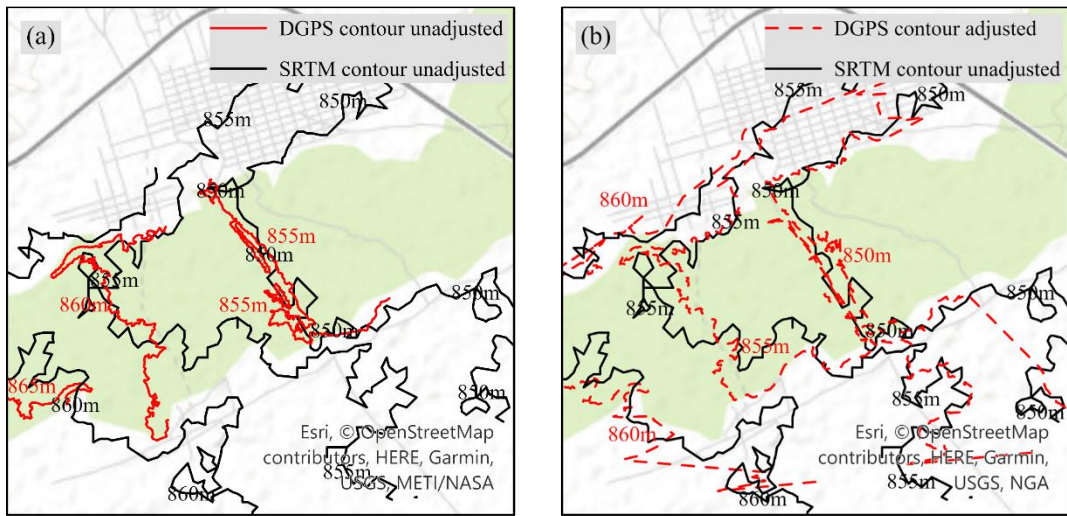


**Figure B2.** Adjustment of differential Global Positioning System (dGPS) survey data to reduce the vertical offset compared the Shuttle Radar Topography Mission (SRTM) data, (a) contours of unadjusted dGPS data and unadjusted SRTM data, (b) contours of adjusted dGPS.

## Appendix B

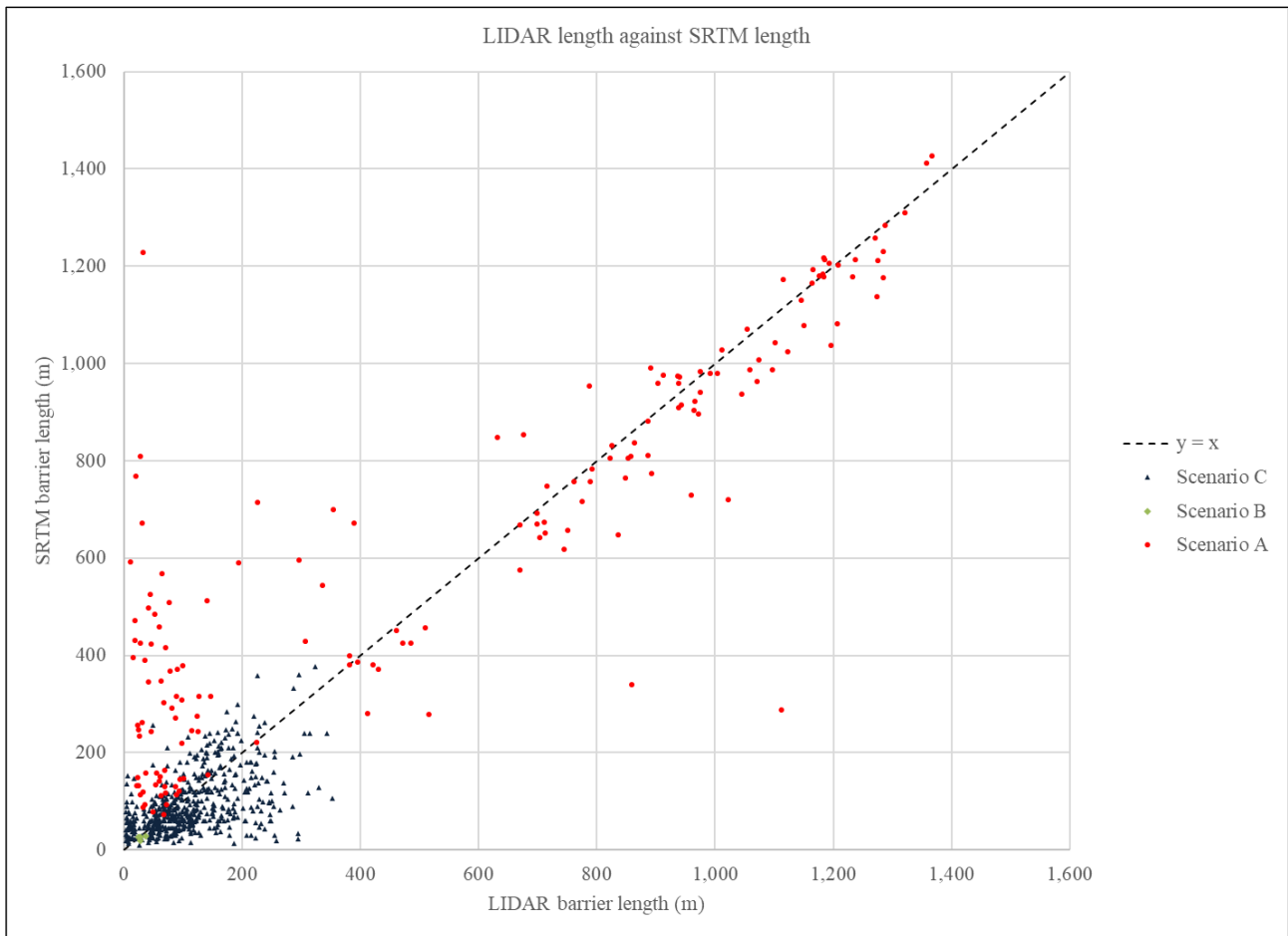


Figure B3. Barrier length comparison of LIDAR and SRTM results for all case study scenarios.

## Appendix B

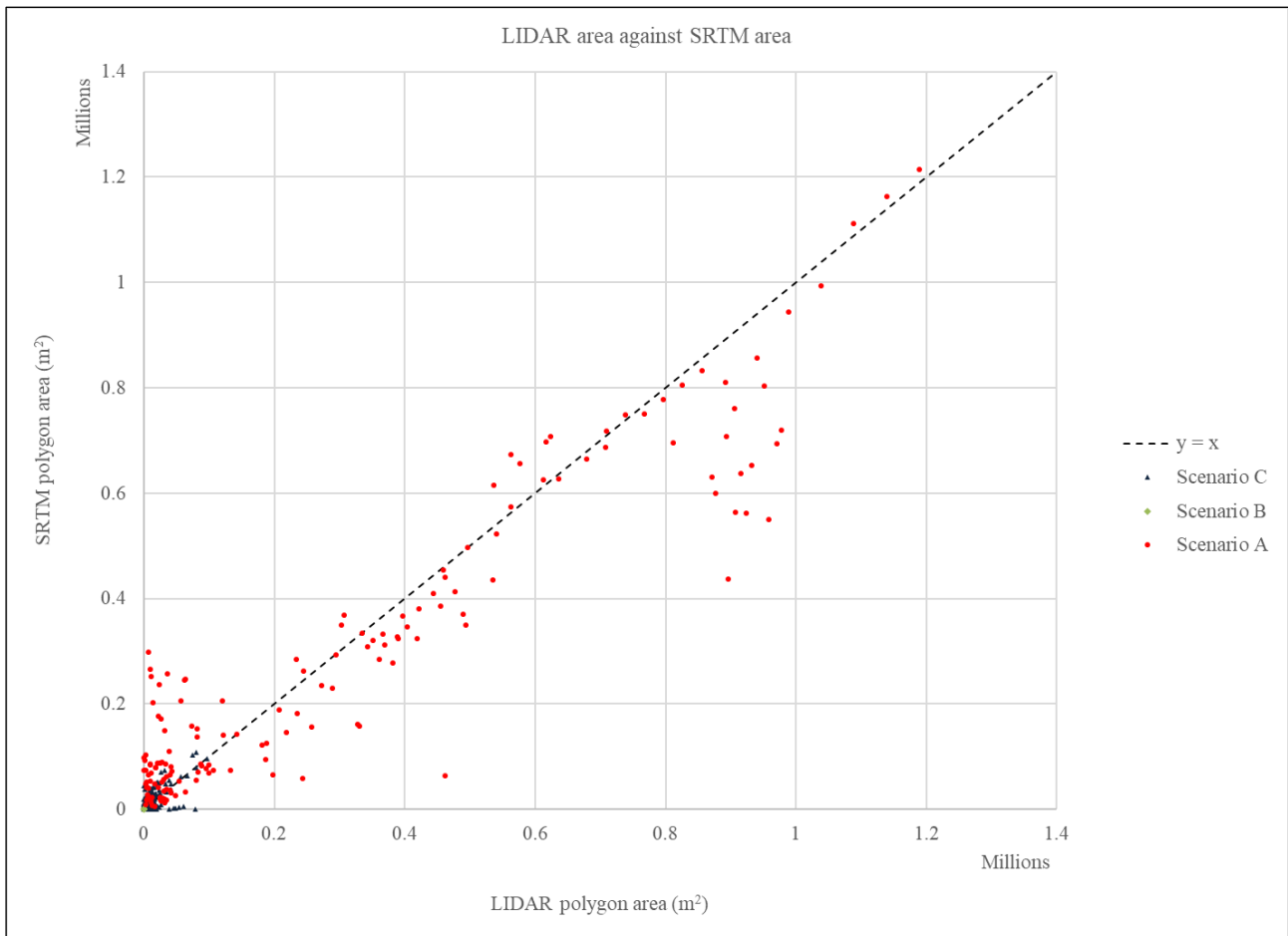


Figure B4. Polygon area comparison of LIDAR and SRTM results for all case study scenarios.

# Appendix C. Supplementary material for Chapter 5

**Table C1. Classification of catchments based on catchment size, form factor, and Height Above Nearest Drainage (HAND).**

	Class 1	Class 2	Class 3
catchment area (km <sup>2</sup> )	<= 970	> 970–<= 6000	> 6000
form factor (-)	<= 0.105	> 0.105–<= 0.150	> 0.150
HAND (m)	<= 35	> 35–<= 80	> 80

**Table C2. Summary of catchments with classifications.**

catchment code	extent code	country code	GRDC number	record start (y)	record end (y)	monthly missing values (%)	mean Aridity Index	catchment area class	form factor class	HAND class
AUMS	AUS-3	AU	5109175	1968	2019	0.0	0.37	1	1	1
ZAO	SA-3	ZA	1160660	1972	2021	0.0	0.48	1	1	2
ZAUL	SA-3	ZA	1160704	1981	2022	2.7	0.58	1	1	3
ZAKK	SA-1	ZA	1160120	1964	2022	2.6	0.31	1	2	1
ZAMK	SA-2	ZA	1196570	1955	2022	2.3	0.33	1	2	2
ZABT	SA-3	ZA	1160530	1980	2022	2.0	0.30	1	2	3
AULT	AUS-1	AU	5606097	1978	2019	0.0	0.18	1	3	1
ZAMB	SA-1	ZA	1160250	1965	2022	0.9	0.28	1	3	2
ZAOS	SA-2	ZA	1196561	1966	2021	1.7	0.33	1	3	3
AUMF	AUS-1	AU	5606042	1952	2019	0.0	0.34	2	1	1
BRPR	AS-1	BR	3650620	1973	2020	2.8	0.52	2	1	2
ZADK	SA-3	ZA	1160527	1980	2022	0.6	0.25	2	1	3
AUSJ	AUS-1	AU	5606040	1956	2019	0.0	0.47	2	2	1
ZAHH	SA-1	ZA	1159110	1927	2022	1.2	0.11	2	2	2
ZAW	SA-2	ZA	1197505	1968	2021	0.0	0.49	2	2	3
AUFR	AUS-2	AU	5607080	1967	2021	11.1	0.14	2	3	1
ZAHE	SA-2	ZA	1196300	1962	2022	2.4	0.28	2	3	2
ILOB	ME-1	IL	6594050	1970	2019	0.0	0.39	2	3	3
ZAT	SA-2	ZA	1159400	1923	2022	3.8	0.26	3	1	1
USMH	AN-1	CA	4213250	1911	2021	2.6	0.46	3	1	2
ZAAN	SA-3	ZA	1159650	1914	2022	1.4	0.46	3	1	3
AUNP	AUS-2	AU	5607520	1967	2019	0.0	0.11	3	2	1
ZADE	SA-4	ZA	1159305	1980	2022	1.6	0.18	3	2	1
USNP	AN-2	US	4151514	1938	2022	0.0	0.22	3	2	2
ZASD	SA-1	ZA	1160305	1966	2022	2.5	0.28	3	2	3
AUGD	AUS-3	AU	5109110	1969	2021	0.0	0.18	3	3	1
BRMN	AS-1	BR	3650634	1973	2020	2.9	0.42	3	3	2
USSC	AN-1	US	4115220	1929	2021	0.0	0.35	3	3	3

## Appendix C

Table C3. Stream width constants.

<b>catchment code</b>	<b>constant <i>a</i></b>	<b>constant <i>b</i></b>
AUFR	0.0040	22.7
AUGD	0.0021	48.8
AULT	0.0017	10.4
AUMF	0.0001	18.6
AUMS	-0.0011	15.7
AUNP	0.0051	79.6
AUSJ	0.0009	26.1
BRMN	0.0006	11.4
BRPR	0.0000	11.4
ILOB	0.0004	5.1
USMH	0.0003	78.6
USNP	0.0002	13.5
USSC	0.0003	13.5
ZAAN	0.0003	40.9
ZABT	0.0009	6.8
ZADE	0.0008	-48.5
ZADK	0.0011	7.1
ZAHE	0.0003	14.1
ZAHH	0.0001	21.0
ZAKK	0.0006	5.6
ZAMB	0.0050	10.2
ZAMK	0.0020	5.2
ZAO	0.0017	6.3
ZAOS	0.0001	7.6
ZASD	0.0003	20.2
ZAT	0.0000	22.8
ZAUL	0.0064	1.5
ZAW	0.0003	6.7

Appendix C

**Table C4. The number of years of data used for the calibration and validation stages, together with the optimum transferral ratio parameter values used in the validation stage for each catchment.**

catchment code	# years calibration	# years validation	validation overland	validation overland	validation network	validation network
			$k_o$	$p_o$	$k_n$	$p_n$
AUFR	20	19	-5.50	5.50	-5.50	5.50
AUGD	20	19	-4.00	2.00	-4.00	2.00
AULT	19	18	-4.00	3.50	-4.00	3.50
AUMF	19	18	-0.05	0.05	-0.05	0.05
AUMS	19	18	-3.00	3.00	-3.00	3.00
AUNP	19	18	-1.00	3.00	-2.00	3.00
AUSJ	19	17	-0.05	0.05	-0.05	0.05
BRMN	19	19	-0.20	0.20	-0.10	0.10
BRPR	19	19	-1.00	1.00	-1.00	1.00
ILOB	19	18	-0.10	0.10	-0.10	0.10
USMH	20	19	-0.05	0.05	-0.05	0.05
USNP	20	19	-0.10	0.10	-0.10	0.10
USSC	20	19	-0.10	0.10	-0.10	0.10
ZAAN	20	19	-0.05	0.05	-0.05	0.05
ZABT	20	19	-2.00	2.00	-2.50	2.50
ZADE	20	19	-0.27	0.27	-0.27	0.27
ZADK	20	19	-2.00	2.00	-2.00	2.00
ZAHE	20	19	-0.40	2.00	-0.40	2.00
ZAHH	20	19	-0.50	0.50	-0.50	0.50
ZAKK	20	19	-0.50	0.50	-0.50	0.50
ZAMB	20	19	-0.10	0.10	-0.10	0.10
ZAMK	20	19	-0.10	0.10	-0.10	0.10
ZAO	20	19	-0.50	0.50	-1.00	1.00
ZAOS	20	19	-5.50	5.50	-5.50	5.50
ZASD	20	19	-0.10	0.10	-0.10	0.10
ZAT	20	19	-1.00	1.00	-1.00	1.00
ZAUL	20	19	-0.30	1.00	-0.50	1.00
ZAW	20	19	-0.30	1.00	-0.30	1.00

Appendix C

**Table C5. Baseflow of each catchment calculated using PART software.**

<b>catchment code</b>	<b>baseflow (%)</b>	<b>daily runoff data range (years)</b>
AUFR	3.8	1982–2019
ZADE	7.1	1993–2005
ZAHH	9.3	1993–2005
AUNP	9.8	1968–2018
ZABT	14.1	2003–2011
ZAT	14.1	1989–1994
AULT	14.2	1979–2018
BRPR	20.2	1973–2013
ZAO	20.3	1973–2020
AUGD	21.7	1997–2020
ZAKK	38.2	1999–2013
AUMS	39.3	1969–2018
ZASD	39.7	2009–2021
ZAMB	41.1	1984–2021
ZAAN	43.2	1983–1998
ZADK	47.6	1995–2014
ZAHE	51.0	2015–2021
USNP	53.3	1939–2021
AUSJ	56.0	1957–2018
BRMN	59.4	1985–2019
AUMF	63.7	1952–2018
ZAW	64.1	1987–2001
USMH	64.9	1936–2021
ZAOS	66.5	1999–2020
USSC	70.0	1930–2020
ZAMK	74.6	2004–2021
ZAUL	75.0	1997–2015
ILOB	87.5	1991–2018

# Appendix D. Supplementary material for Chapter 6

## Procedure - computation of weights

Using the expert *in situ* knowledge of the Port Sudan area and water system held amongst the authors, and with reference to the AHP fundamental scale, a pairwise comparison matrix was completed by entering fundamental scales integers and computing their reciprocal values on the opposite side of the main diagonal (**STEP A**). Next the sum of each column was calculated (**STEP B**) which in turn allows elements in the array to be normalised with respect to each column (**STEP C**). The weight of each component was then found by taking the average of each row (**STEP D**).

## Procedure - consistency check

A consistency ratio (CR) below 0.10 was used as an indication that the pairwise comparison matrix had been completed satisfactorily since a CR of 0.10 or less is considered “positive evidence for informed judgment” (Saaty, 1994, p. 104).

To compute the CR, first the principal eigenvalue of the matrix ( $\lambda_{max}$ ) must first be determined. Finding  $\lambda_{max}$  involves multiplying the weight assigned to each column by the respective column elements of the original pairwise comparison matrix (**STEP A**), to obtain a new matrix (**STEP E**). Next, 'weighted sum' column values are found by summing the elements of each row (**STEP F**). For each row, dividing the weighted sum by its respective weight produces a 'ratio' (**STEP F**).  $\lambda_{max}$  is then calculated as the average of all these ratios (Saaty, 1990).

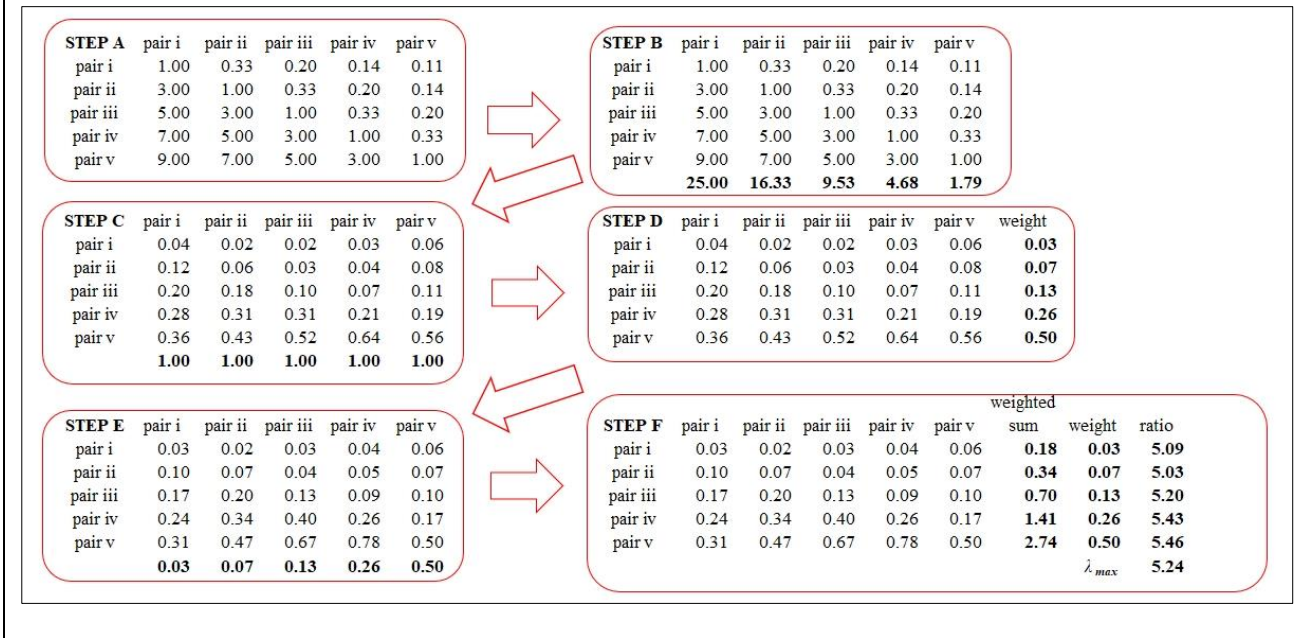


Figure D1. Worked example to illustrate how the AHP was implemented to compute weights and the principal eigenvalue.

Appendix D

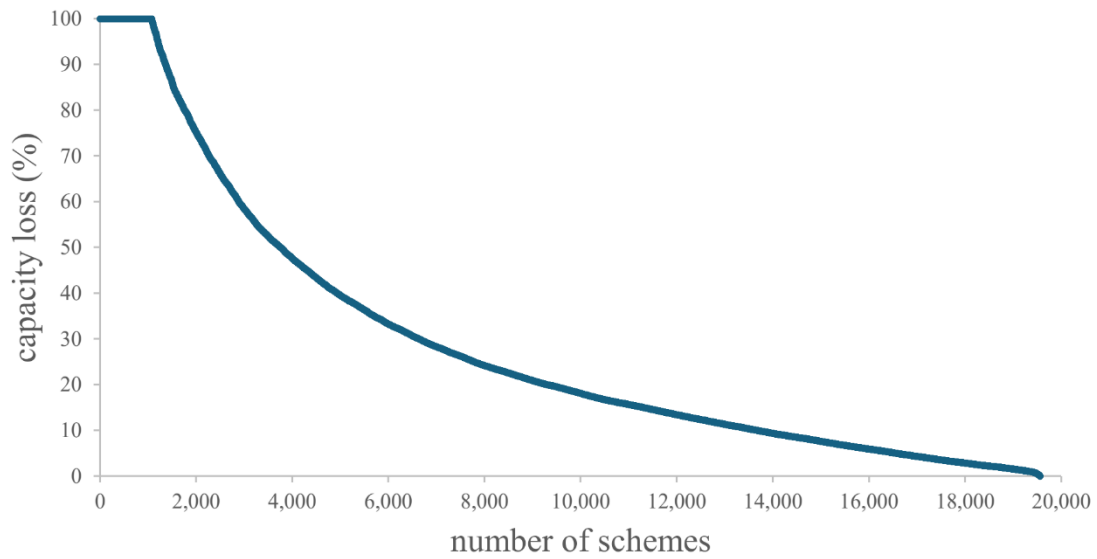


Figure D2. Annual reservoir storage capacity loss due to sedimentation for average annual runoff.

Table D1. Details of dams located within the study area.

Dam name	Latitude	Longitude	Alternative name(s)
Khor Arbaat main dam	19°50'2.88"N	36°56'19.44"E	Arbaat dam; Danfudo dam
Moj dam	19°28'55.01"N	36°58'38.06"E	
Al Fadlabi dam	19°50'23.51"N	36°58'8.28"E	
Fourth dam	19°48'9.10"N	37° 3'9.36"E	4 <sup>th</sup> dam
Gebeit dam	18°57'14.51"N	36°48'58.42"E	

Table D2. Pairwise table for barrier height (BH).

barrier height range (m)	> 10	> 8 – ≤ 10	> 6 – ≤ 8	> 4 – ≤ 6	≤ 4
> 10	1.00	0.20	0.25	0.33	2.00
> 8 – ≤ 10	5.00	1.00	2.00	2.00	9.00
> 6 – ≤ 8	4.00	0.50	1.00	3.00	7.00
> 4 – ≤ 6	3.00	0.50	0.33	1.00	2.00
≤ 4	0.50	0.11	0.14	0.50	1.00

Appendix D

**Table D3. Pairwise comparison matrix for barrier volume (BV).**

barrier volume (BV) range (m <sup>3</sup> )	> 0.8BV <sub>max</sub>	> 0.6BV <sub>max</sub> – ≤ 0.8BV <sub>max</sub>	> 0.4BV <sub>max</sub> – ≤ 0.6BV <sub>max</sub>	> 0.2BV <sub>max</sub> – ≤ 0.4BV <sub>max</sub>	≤ 0.2BV <sub>max</sub>
> 0.8BV <sub>max</sub>	1.00	0.20	0.20	0.14	0.11
> 0.6BV <sub>max</sub> – ≤ 0.8BV <sub>max</sub>	3.00	1.00	0.33	0.20	0.14
> 0.4BV <sub>max</sub> – ≤ 0.6BV <sub>max</sub>	5.00	3.00	1.00	0.33	0.20
> 0.2BV <sub>max</sub> – ≤ 0.4BV <sub>max</sub>	7.00	5.00	3.00	1.00	0.33
≤ 0.2BV <sub>max</sub>	9.00	7.00	5.00	3.00	1.00

**Table D4. Pairwise comparison matrix for area of influence (AI).**

area of influence (AI) range (m <sup>2</sup> )	> 0.8AI <sub>max</sub>	> 0.6AI <sub>max</sub> – ≤ 0.8AI <sub>max</sub>	> 0.4AI <sub>max</sub> – ≤ 0.6AI <sub>max</sub>	> 0.2AI <sub>max</sub> – ≤ 0.4AI <sub>max</sub>	≤ 0.2AI <sub>max</sub>
> 0.8AI <sub>max</sub>	1.00	2.00	3.00	4.00	5.00
> 0.6AI <sub>max</sub> – ≤ 0.8AI <sub>max</sub>	0.50	1.00	2.00	3.00	4.00
> 0.4AI <sub>max</sub> – ≤ 0.6AI <sub>max</sub>	0.33	0.50	1.00	2.00	3.00
> 0.2AI <sub>max</sub> – ≤ 0.4AI <sub>max</sub>	0.25	0.33	0.50	1.00	2.00
≤ 0.2AI <sub>max</sub>	0.20	0.25	0.33	0.50	1.00

Appendix D

**Table D5. Pairwise comparison matrix for storage volume (SV).**

storage volume (SV) range (m <sup>3</sup> )	> 0.8SV <sub>max</sub>	> 0.6SV <sub>max</sub> – ≤ 0.8SV <sub>max</sub>	> 0.4SV <sub>max</sub> – ≤ 0.6SV <sub>max</sub>	> 0.2SV <sub>max</sub> – ≤ 0.4SV <sub>max</sub>	≤ 0.2SV <sub>max</sub>
> 0.8SV <sub>max</sub>	1.00	2.00	3.00	4.00	5.00
> 0.6SV <sub>max</sub> – ≤ 0.8SV <sub>max</sub>	0.50	1.00	2.00	3.00	4.00
> 0.4SV <sub>max</sub> – ≤ 0.6SV <sub>max</sub>	0.33	0.50	1.00	2.00	3.00
> 0.2SV <sub>max</sub> – ≤ 0.4SV <sub>max</sub>	0.25	0.33	0.50	1.00	2.00
≤ 0.2SV <sub>max</sub>	0.20	0.25	0.33	0.50	1.00

**Table D6. Pairwise comparison matrix for storage volume to barrier volume ratio (SBVR).**

SBVR ratio range (-)	> 0.8SBVR <sub>max</sub>	> 0.6SBVR <sub>max</sub> – ≤ 0.8SBVR <sub>max</sub>	> 0.4SBVR <sub>max</sub> – ≤ 0.6SBVR <sub>max</sub>	> 0.2SBVR <sub>max</sub> – ≤ 0.4SBVR <sub>max</sub>	≤ 0.2SBVR <sub>max</sub>
> 0.8SBVR <sub>max</sub>	1.00	2.00	3.00	4.00	5.00
> 0.6SBVR <sub>max</sub> – ≤ 0.8SBVR <sub>max</sub>	0.50	1.00	2.00	3.00	4.00
> 0.4SBVR <sub>max</sub> – ≤ 0.6SBVR <sub>max</sub>	0.33	0.50	1.00	2.00	3.00
> 0.2SBVR <sub>max</sub> – ≤ 0.4SBVR <sub>max</sub>	0.25	0.33	0.50	1.00	2.00
≤ 0.2SBVR <sub>max</sub>	0.20	0.25	0.33	0.50	1.00

Appendix D

**Table D7. Computational table used to obtain constants for sedimentation yield equation.**

year	reservoir storage volume	runoff	inflow period	Sedimentation Index	trap efficiency	sediment yield	retained sediment	reservoir storage volume	Accumulated storage capacity loss
	$SV_s$	Q	$T_0$	SI	$T_e$	$S_y$	$S_r$	$SV_e$	
	$10^6 \text{ m}^3$	$10^6 \text{ m}^3$ $\text{y}^{-1}$	d	$\text{s}^2 \text{ m}^{-1}$	%	$10^6 \text{ m}^3 \text{ y}^{-1}$	$10^6 \text{ m}^3 \text{ y}^{-1}$	$10^6 \text{ m}^3$	%
2003	16.50	0.73	0.01	213,303	25	0.16	0.04	16.46	0.1
2004	16.46	0.42	0.10	33,485,363	80	0.10	0.08	16.38	0.7
2005	16.38	24.73	1.03	1,014,987	48	3.83	1.85	14.53	11.9
2006	14.53	1.13	0.89	286,878,882	91	0.24	0.22	14.32	13.2
2007	14.32	25.72	2.76	5,154,997	66	3.97	2.62	11.70	29.1
2008	11.70	0.42	0.10	16,914,120	76	0.10	0.07	11.62	29.5
2009	11.62	0.42	0.10	16,700,764	76	0.10	0.07	11.55	30.0
2010	11.55	126.24	2.89	152,558	19	16.61	3.13	8.42	49.0
2011	8.42	0.10	0.01	963,406	48	0.03	0.01	8.40	49.1
2012	8.40	0.42	0.10	8,726,158	71	0.10	0.07	8.33	49.5
2013	8.33	20.94	0.91	286,093	30	3.30	0.99	7.35	55.5
2014	7.35	140.82	1.03	6,286	1	18.33	0.18	7.16	56.6
2015	7.16	4.51	0.87	4,195,143	64	0.83	0.53	6.64	59.8
2016	6.64	0.42	0.10	5,441,185	66	0.10	0.06	6.57	60.2
2017	6.57	0.42	0.10	5,335,144	66	0.10	0.06	6.51	60.6
2018	6.51	11.37	1.79	2,288,830	58	1.90	1.10	5.40	67.2

Appendix D

**Table D8. Final schemes after filling and sedimentation filters applied.**

<b>Object ID</b>	<b>LTC<sub>score</sub></b>	<b>latitude (degrees)</b>	<b>longitude (degrees)</b>
1	0.1885	19.5278	19.5278
2	0.1885	19.5247	19.5247
3	0.1885	19.8339	19.8339
4	0.1885	19.8320	19.8320
5	0.1885	19.2990	19.2990
6	0.1885	19.2965	19.2965
7	0.1885	19.2900	19.2900
8	0.1885	19.2826	19.2826
9	0.1885	19.2825	19.2825
10	0.1885	19.2818	19.2818
11	0.1885	19.2821	19.2821
12	0.1885	19.2805	19.2805
13	0.1885	19.2783	19.2783
14	0.1885	19.2770	19.2770
15	0.1885	19.2737	19.2737
16	0.1885	19.2685	19.2685
17	0.1885	19.2685	19.2685
18	0.1885	19.2679	19.2679
19	0.1885	19.2661	19.2661
20	0.1885	19.2653	19.2653
21	0.1885	19.2642	19.2642
22	0.1885	19.2635	19.2635
23	0.1885	19.2637	19.2637
24	0.1885	19.2627	19.2627
25	0.1885	19.7358	19.7358
26	0.1885	19.7349	19.7349
27	0.1885	19.7341	19.7341
28	0.1885	19.5599	19.5599
29	0.1885	19.5591	19.5591
30	0.1885	19.5542	19.5542
31	0.1885	19.5534	19.5534
32	0.1885	19.5524	19.5524
33	0.1885	19.5512	19.5512
34	0.1885	19.5344	19.5344
35	0.1885	19.8388	19.8388
36	0.1885	19.5337	19.5337
37	0.1885	19.5306	19.5306
38	0.1885	19.5285	19.5285
39	0.1885	19.5283	19.5283
40	0.1885	19.5262	19.5262
41	0.1885	19.5249	19.5249
42	0.1885	19.8356	19.8356
43	0.1885	19.8345	19.8345
44	0.1885	19.5108	19.5108
45	0.1885	19.5081	19.5081
46	0.1885	19.5065	19.5065
47	0.1885	19.5053	19.5053
48	0.1885	19.3969	19.3969
49	0.1885	19.3961	19.3961
50	0.1885	19.3950	19.3950
51	0.1885	19.3945	19.3945
52	0.1885	19.3444	19.3444
53	0.1885	19.3435	19.3435
54	0.1885	19.3422	19.3422
55	0.1885	19.2281	19.2281